Normandie Université

THESE

Pour obtenir le diplôme de doctorat

Spécialité Génie Electrique
Préparée au sein de l'Université du Havre

Development of Hybridization concept for horizontal axis wind / tidal systems using functional similarities and advanced real-time emulation methods

Développement de concepts d'hybridation pour les systèmes éoliens / hydroliens à axe horizontal utilisant des similitudes fonctionnelles et méthodes d'émulation avancées en temps réel

Présentée et soutenue par

Mohmed ASHGLAF

Thèse soutenue publiquement le 26 Juin 2019 devant le jury composé de		
Prof. Seddik BACHA	Professeur des Universités - Université de Joseph Fourier	Président du jury
Mme Manuela SECHILARIU	Professeur des Universités - Université de Technologie de Compiègne	Rapporteur
M. Octavian CUREA	Professeur, Ecole Supérieure des Technologies Industrielles Avancées (ESTIA), Bidart	Rapporteur
M. Cristian NICHITA	Professeur des Universités - Université du Havre	Directeur de thèse
M. George CARAIMAN	Docteur, chef de projet EGIS Mobilité	Examinateur

Thèse dirigée par Cristian NICHITA, laboratoire GREAH

UNIVERSITÉ LE HAVRE

SPMI ECOLE DOCTORALE

GREAH Groupe de Recherche en Electrotechnique et Automatique du Havre

Acknowledgements

I wish to thank The Higher Education and Scientific Research Ministry of Libya and University of Le Havre for giving me the opportunity and facilities for research.
Thanks are also extended to **Prof. Cristian NICHITA** for his excellent supervision of the research and the writing of the thesis and the help he extended even while on vacation.

Of course that I want to thank to **Prof. Georges BARAKAT**, Director of GREAH, for his benevolence and moral support in carrying out my work.
I thank also all the staff and colleagues from GREAH for their generous help and support. Working with them during that period has been a very enriching experience.

I would also like to express my sincere gratitude to **Prof. Seddik BACHA** (Université Grenoble Alpes), who accepted to be president of the jury.

My warm gratitude is expressed to the reviewers, **Prof. Manuela SECHILARIU** (Université de Technologie de Compiègne), **Prof. Octavian CUREA** (ESTIA), who analyzed my work despite a busy schedule. I thank them very much for their availability.

I also thank to jury member, **Dr. George CARAIMAN (EGIS Mobility),** for the time spent on this event

Finally, I wish to dedicate this thesis and research to my parents, my wife Sara, my children Hazem, Morad, Annas, Yousra and Ossama, and to my sisters and brothers all of whom contributed in immeasurable ways that are too difficult to enumerate here.

Abstract

The capability of conventional wind and tidal power generation systems to supply network with reliable and stable power in all times is a new challenge due to weather fluctuating, which have a significant and direct impact on power generation. Wherefore, hybridization of wind and tidal power generation systems has been studied and investigated for achieving better the integration of wind & tidal energies on electrical grid.

Therefore, this study led me to develop contributions related to two main axes:

The first axis is focused on a new concept of **hybridization** of two different energy resources in terms of their physical properties, horizontal axis wind and tidal turbines are based on the functional similarities. These two resources are **wind energy** and **tidal energy**. In order to apply this concept "electro-mechanical coupling" practically in **real-time simulation**, a **hardware-simulator** developed at GREAH laboratory in the University of Le Havre is used. Therefore, in order to apply this concept firstly, **parameters** of the installed generator (DFIG) are **identified**; then the entire power conversion chain is **modeled** mathematically, and **simulated** in MATLAB/SIMULINK environment, and then **controlled** by two strategy modes: fixed speed control called "Direct Speed Control" ('DSC'), and variable speed control based on Maximum Power Point Tracking "Indirect Speed Control" ('ISC'). Lastly, this concept was executed practically on the **hardware-simulator** in the lab. Finally, obtained results were analyzed and discussed as described hereafter in this thesis.

The second axis is devoted for a concept of what so-called "**time-acceleration**" of simulation in **virtual time**. Subsequently, this concept was implemented on **hardware simulator** available in the laboratory **GREAH**. This concept (time-acceleration) is based on the reduction of wind profile samples. This wind profile is generated by a software program developed in **GREAH**. Anyway, this program generates a wind profile for a period of 5 hours, in other words, 18.000 samples, each time the number of samples of this profile is reduced respectively to 300 samples, 60 samples, and 30 samples, which means reducing the time of simulation. As a result, the operating time of the power generating unit will also be reduced.

The results mains are obtained firstly in MATLAB/SIMULINK and then were verified on the Real Time Emulator of the wind turbine - tidal hybrid system.

TABLE OF CONTENTS

GENERAL INTRODUCTION
CHAPTER ONE
INTRODUCTION & STATE OF THE ART

1.1 Introduction 14

1.2 Hydraulic Power Resources (Wind &Tidal) 14

1.2.1 Wind Rerource 14

1.2.2 Tidal Resource 17

1.2.3 World Large Tidal Energy Projects 18

1.3 History of Wind &Tidal Turbines 18

1.3.1 History of Wind Turbines 18

1.3.2 History of Tidal Turbines 19

1.4 Turbines Classification 20

1.4.1 Horizontal Axis Turbines (HAT) 21

1.4.2 Vertical Axis Turbines (VAWTT) 21

1.5 Wind/Tidal Turbines Construction and Operation Principle 23

1.5.1 Mechanical Parts 23

1.5.2 Electrical Parts 25

1.5.3 Operation Principle 26

1.6 Advantages & Disadvantages of Wind/Tidal Turbines 26

1.7 State of the Art-Hybrid Wind-Tidal Power Generation Systems 27

1.7.1 Current Statistics and Future Trends of Renewable Power Generation 29

1.7.2 Configurations of Hybrid Energy Systems 31

1.7.3 Integration Schemes 31

1.7.4 Unit-Sizing and Hybrid Configuration Selection 34

1.8 Hybrid Wind-Tidal Power Generation Systems - Review 35

1.8.1 Advantages and Disadvantages of Hybrid Energy Systems 42

1.9 Power Management Strategies Based on Energy Storage Technologies-Review 43

1.9.1 History of Energy Storage Systems 45

1.9.2 Role of Energy Storage Units in Power System 46

1.9.3 Basic Theory of Energy Storage Systems 48

1.9.4 Classification of Energy Storage Systems 52

1.10 Application of Energy Storage Systems....53
1.11 General Comparisons of Different Energy Storage Systems....55
1.12 Research Objectives and Contributions....56
1.13 Conclusion....57
References....58

CHAPTER TWO
MODELING OF ENERGY CONVERSION SUBSYSTEMS
FOR HORIZONTAL AXIS WIND & TIDAL TURBINES

2.1 Introduction....69
2.2 Modeling of Wind Resource....70
2.2.1 Wind Speed....70
2.2.2 Average Wind Speed (Weibull & Rayliegh)....72
2.3 Modeling of Tidal Current....74
2.4 Modeling of Wind-Tidal Turbines....75
2.5 Modeling of Doubly-Fed Induction Generator DFIG....81
2.5.1 Steady – State Modeling of DFIG....83
2.5.2 Dynamic Modeling of DFIG....87
2.5.2.1 αβ Model....88
2.5.2.2 dq Model....91
2.6 Modeling of Power Converter....93
2.6.1 Grid Side Converter Model....94
2.6..2 Rotor Side Converter Model....97
2.7 DC - Link....98
2.8 Conclusion....99
References....100

CHAPTER THREE
CONTROL METHODS FOR POWER CONVERSION SYSTEM
BASED ON WIND/TIDAL TURBINES SIMILARITIES

3.1 Introduction....104
3.2 Offshore Hybrid Wind/Tidal Power Conversion System....104
3.2.1 Concept of Electro-mechanical Coupling....104
3.2.2 Assumptions for Simulation of Electro-Mechanical Coupling....105
3.3 Turbine Control System....107

3.3.1 Control Strategies of Wind/Tidal Turbines 107
3.3.2 Operation Zones & Maximum Power Point Tracking MPPT 112
3.4 Speed Controller (ISC) Strategies 114
3.4.1 Indirect Speed Controller (ISC) Strategy 114
3.4.2 Direct Speed Controller (DSC) Strategy 116
3.5 Specific Approaches for Field - Oriented Control of DFIG.....117
3.5.1 Steady State Analysis of Doubly Fed Induction Generator (DFIG).....117
3.5.2 Control of Rotor Side Converter (AC/DC).....119
3.5.3 Power and Speed Control 122
3.5.4 Control of Gird Side Converter (Inverter) DC/AC 123
3.6 DC-Link (C-Bus).....126
3.7 Concept of "time acceleration" in Wind Turbine Power Generation.....127
3.7.1 Time Acceleration Method.....128
3.7.1.1 Wind Profile Data (18000) Samples 128
3.7.1.2 Wind Profile Data (300) Samples 130
3.8 Conclusion.....131
References 133

CHAPTER FOUR
NUMERICAL SIMULATION & EXPERIMENTAL RESULTS ON REAL TIME EMULATORS

4.1 Introduction 138
4.2 Principles of Real-Time Emulation of Actuators 138
4.2.1 Structure of Hardware Simulator.....139
4.3 Simulation and Control of Power Conversion System.....142
4.3.1 Simulation and Control of Doubly-Fed Induction Generator Based Wind Turbine 142
4.3.1.1 Control of Rotor Side Converter (RSC).....143
4.3.1.2 Control of Grid Side Converter (GSC) 149
4.3.2 Simulation and Control of Doubly-Fed Induction Generator Based Tidal Turbine.....151
4.3.2.1 Control of Rotor Side Converter (RSC).....151
4.3.2.2 Control of Grid Side Converter (Simulation Results).....153
4.4 Application of "time acceleration" Concept in Wind Turbine Power Generation.....153
4.4.1 Impact of "Time Acceleration Method" on Power Simulation 154

4.4.2 Simulation in accelerated time of 300, 60 and 30 Minutes 156
4.5 Electro-Mechanical Coupling Simulation Results 158
4.6 Electro-Mechanical Coupling Experimental Results 159
4.6.1 DFIG Modes of Operation: (Motor / Generator).....160
4.6.2 Operations modes of Simultaneous coupling of wind and tidal turbine.....161
4.7Conclusion.....163
References 164

GENERAL CONCLUSIONS

5.1 General Conclusions 166
Appendix A I
Appendix B VII
Appendix C XIV
Appendix D XVII

TABLE OF FIGURES

Figure 1 Wind Rose....15
Figure 2 Wind Distribution Curve....16
Figure 3 Weibull distribution curves....17
Figure 4 High Potential Areas for Tidal Resources....17
Figure 5 First Aerodynamic Generator Constructed by Charles F. Bruch [9]....19
Figure 6 Gedser Turbine [15]....19
Figure 7 Wind Turbine Power System [18]....21
Figure 8 Horizontal Tidal Turbine [19]....21
Figure 9 Darrieus Wind Turbine at GREAH....22
Figure 10 Drag-based wind turbine (Savonius Rotor) [21]....22
Figure 11 Swirling Turbine [22]....23
Figure 12 Wind Turbine Foundation [23]....23
Figure13 Wind Turbine Nacelle [23]....24
Figure 14 Main Mechanical Wind Turbine Components [24]....24
Figure 15 Wind Turbine Gearbox....25
Figure16 Turbine Construction [25]....25
Figure 17 Basic components of hybrid system [33]....28
Figure18 World Net Electricity Generation by Energy Source, 2012– 40....30
Figure19 World Net Electricity Generation from Renewable Resources 2012-2040....31
Figure 20 Schematic Diagram of a DC-Coupled Hybrid Energy System....32
Figure 21 Schematic of AC-Coupled Hybrid Energy System: (a) PFAC; (b) HFAC....33
Figure 22 Schematic Diagram of Hybrid-Coupled Energy System [42]....34
Figure 23 Hybrid Wind/Tidal Turbine Power Generation [46]....35
Figure 24 Configuration of Hybrid OWF and TF Connected to Power Grid Using FESS [47]....36
Figure25 Schematic Configuration of Hybrid Offshore Horizontal Axes Turbine [48]....37
Figure 26 Different Configurations of Hybrid Wind/Tidal Turbines Connected to DC-bus....38
Figure 27 Block Diagram of Hybrid Wind/Tidal Turbines....38
Figure 28 Hybrid Wind/Tidal Turbine based PMSG....39
Figure 29 Schematic of Hybrid Wind-Tidal Turbine System [56]....40
Figure 30 Hybrid System Wind-Tidal Power Generation [58]....41

Figure 31 Wind Emulator in GREAH 43
Figure 32 Tidal Emulator in GREAH 44
Figure 33 Effect of energy storage system in power generation and consumption [81] 47
Figure 34 Application of ESS in power system [81] 47
Figure 35 Utilization of Battery as ESS [82] 47
Figure 36 Installed Capacity of ESS [82] 48
Figure37 Thermal ESS [85] 48
Figure 38 Pumped Hydro Storage System 49
Figure39 Flywheel Energy Storage System FESS [71] 50
Figure 40 Compressed Air Energy Storage System CAES [71] 50
Figure 41 Battery Schematic [81] 51
Figure 42 Superconducting Magnetic Energy System SMES [90] 52
Figure 43 Hydrogen Storage and Fuel Cell [71] 52
Figure 44 Classification of EES 53
Figure 45 Wind and Solar Cells with Batteries [97] 53
Figure46 Thermal Station in France 54
Figure 47 Hybrid wind/tidal turbine energy conversion system [1] 69
Figure 48 Van der Hoven Spectrum 70
Figure 49 Wind Speed Probability Density Function [4] 71
Figure 50 Weibull Probability Density Function with Shape Parameter (K=1,2 and 3) and Scale Parameter C=8 72
Figure 51 Wind Profile 74
Figure 52 Variation of Tidal Currents High and Low Sea Level 75
Figure 53 Wind/Tidal Turbines Coupled On the Same Shaft 76
Figure 54 Cylindrical Volume Represents Energy Conversion in Wind Turbine 76
Figure 55 Graphical interface of 'Simtorque' Software 77
Figure 56 Constant wind speed VS variable Pitch Angle 78
Figure 57 Constant Pitch Angle VS Variable Wind Speed 79
Figure 58 Constant Wind Speed and Pitch Angle 79
Figure 59 One System Block Diagram of Wind/Tidal Turbine 80
Figure 60 Mathematical Modeling of Wind/Tidal Turbine 81

Figure 61 One-phase steady-state equivalent electric circuit of the DFIG 84
Figure 62 Phase steady-state equivalent electric circuit of the DFIG 85
Figure 63 Steady-State Equivalent Circuit of the DFIG Referred to Stator.....85
Figure 64 Four operating Modes of the DFIG 87
Figure 65 Different Reference Frames to Represent Space Vector of DFIG.....88
Figure 66 Model of DFIG in αβ Reference Frame.....90
Figure 67 Equivalent Circuit of DFIG Modeled in dq Frame.....92
Figure 68 Model of DFIG in dq Reference Frame.....93
Figure 69 Grid Side Converter.....94
Figure 70 Waveforms of Converter Output 95
Figure 71 Single Phase of Grid Inverter.....95
Figure 72 Single Phase Grid Side Converter 96
Figure 73 Inverter Grid Side Model.....97
Figure 74 Schematic of Power Converter Rotor Side (rectifier).....97
Figure 75 DC- link Power Converter.....98
Figure 76 DC-Link Model.....99
Figure 77 World's First Floating Wind-Current Turbine will be installed off Japanese's Coast 104
Figure 78 Electromechanical Coupling of Wind/Tidal Turbines.....105
Figure 79 Generated Power as Function of Wind Velocity 109
Figure 80Wind - Power Curve for low power wind turbine 110
Figure 81 Power as Function of Turbine Speed.....111
Figure 82 Schematic Diagram of Pitch Control System 113
Figure 83 Speed Control Scheme for Zones 1and 3.....114
Figure 84a 85b Stability and Maximum Power Curves 114
Figure 85Indirect Speed Control.....116
Figure 86 Direct Speed Control Block Diagram.....117
Figure 87 Steady State Analysis of DFIG.....118
Figure 88 Rotor & Stator Current (Ir & Is) MATLAB/SIMULINK.....119
Figure 89 Synchronous Rotating dq Reference Frame 120
Figure 90 Rotor Current Control Loop Block Diagram.....121
Figure 91 Equivalent Second Order System of Current Control Loop 122

Figure 92 Complete Vector Control Loop of DFIG 123
Figure 93 General Schema 3- Phase Inverter Connected Grid 124
Figure 94 Grid Side Control 124
Figure 95 Grid Voltage Oriented Vector Control Block Diagram 125
Figure 96 Diagram of DC-Bus 127
Figure 97 Voltage Control Loop 127
Figure 98 Wind Profile (18000 samples and 5 hours) 128
Figure 99 Reference Rotation Speed (rev/min) 129
Figure 100 (a) Mechanical Power “simulation” (b) Mechanical Power experimentally ... 130
Figure 101 Wind Profile of 300 samples 130
Figure 102a Rotation Speed Reference (rev. /min) 131
Figure 103 Bandwidths of Emulators 138
Figure 104 Hardware Simulator in GREAH Laboratory 139
Figure 105 dSPACE Interface Guild User 141
Figure 106 "Servo Machine" Interface Guild User 142
Figure 107 Schematic Diagram of DFIG Based Wind Turbine in MATLAB/Simulink 143
Figure 108 dq Synchronous Rotating Reference Frame Aligned with Stator Flux Vector 144
Figure 109 Current Loop Structure of Rotor Side Controller (RSC) 144
Figure 110 Fixed Speed Control (Rotor Simulation Results) 145
Figure 111 Fixed Speed Control (Rotor & Stator Simulation Results) 145
Figure 112 MPPT Control Strategy 146
Figure 113 Structure of MPPT in MATLAB/SIMULINK 146
Figure 114 Block Diagram of (RSG) and MPPT Control Strategy in MATLAB/SIMULINK ... 147
Figure 115 Variable Speed Control Rotor Simulation Results 148
Figure 116 Rotor & Stator' Voltages and Currents' 148
Figure 117 Control Block Diagram of Grid Voltage Oriented Vector Control. 150
Figure 118 Controlled Parameters of Grid Side Converter 151
Figure 119 Fixed Speed DFIG Rotor Side Based Tidal Turbine 152
Figure 120 Variable Speed Control of DFIG’s Rotor Side 152
Figure 121 Grid Side Converter of DFIG Based Tidal Turbine 153
Figure 122 Model of Wind Turbine and d-SPACE in MATLAB/SIMULINK 154

Figure 123 Interface User Guide of ControlDesk for Wind Turbine Hardware Emulator 155
Figure 124 Turbine Mechanical Power Simulated Experimentally [4-5] 155
Figure 125 Mechanical Power Simulated Experimentally; sampling every minute [4-5] 156
Figure 126 Mechanical Power Simulated Experimentally; sampling every 5 minutes 157
Figure 127 Mechanical Power Simulated Experimentally; Sampling Every 10 Minutes.....157
Figure 128 Simulation Results of Electro-Mechanical Coupling 159
Figure 129 Electrical Power Generated by Each Turbine.....159
Figure 130 Speed of DFIG Obtained Experimentally.....160
Figure 131 Generated Electrical Power, Supplied to Grid.....160
Figure 132 Electrical Power Generated by Hybrid System 162

TABLE OF TABLES

Table 1 Largest Tidal Power Generation Projects in the World 18
Table 2 Main Turbine Components 23
Table 3 Main Resources of Renewable Energy 28
Table 4 History of Batteries 46
Table 5 Main Advantages and Disadvantages of EES 55
Table 6 Comparison of Technical Characteristics of EES 56
Table 7 Operation Modes of an Electrical Machine (Generator/Motor/Break) 83
Table 8 Parameters of Power Conversion System Understudy 107

List of Abbreviations and Acronyms

AC	Alternative Current
AWS	Archimedes Wave Swing
CAES	Compressed Air Energy Storage
CO_2	Carbon Dioxide
CPP	Clean Power Plant
DC	Direct Current
DFIG	Doubly-Fed Induction Generator
DG	Distribution Generation
DQ0	Stationary Reference Frame
DSC	Direct Speed Control
EEA	European Environment Agency
EIA	Environmental Impact Assessment
ELF	Equivalent Losses Factor
ESS	Energy Storage System
EU	European Union
FESS	Flywheel Energy Storage System
GA	Genetic Algorithms
GHG	Green House Gaseous
GREAH	Group of Research Electro technique of Havre
GSC	Grid Side Control
HAWT	Horizontal Axis Wind Turbine
HFAC	High Frequency Alternative Current
HILS	Hardware In the Loop Simulation
HOMER	Hybrid Optimization Model for Electric Renewable
HOTT	Hybrid Offshore Tidal Turbine
HPG	Hybrid Power Generation
IEC	International Electro-technical Commission
IEO_{2016}	International Energy Outlook 2016
IGBT	Ideal Geat Bidirectional Transistors
ISC	Indirect Speed Control
MPPT	Maximum Power Point Tracking
MSFs	Multivariable Structure Functions
Mtoe	Million Tons of Oil Equivalents
MW	Mega watt
O&M	Operation and Maintenance
P^{-1}	Park Transformation (Invers)
PFAC	Power Frequency Alternative Current
PI	Proportional and Integral Regulator
PSO	Particle Swarm Optimization
PWM	Pulse Width Modulation
RE	Renewable Energy
RES	Renewable Energy Sources
RSC	Rotor Side Control
SEs	Storage Elements

SILS	Software In the Loop Simulation
SMES	Superconducting Magnetic Energy Storage
TES	Thermal Energy Storage
UPFC	Unit Power Flow Controller
VAWT	Vertical Axis Wind Turbine

Nomenclature

A	Area square-meter (m^2)
A	Electrical Current in Ampere (amp)
a,b,c	Three Phases
C	Capacitance Farad (F)
Cp	Power Coefficient
H	Inductance Hennery (L)
Hz	Frequency Hertz
Idq	Direct and Quadrature Current (Ampere)
i_g,v_g	Grid Current and Voltage
i_r,i_s,v_r,v_s	Rotor and Stator Currents and Voltages
J	Energy (E) Joule
k_p,k_i	Proportional and Integral Parameters
kWh	Kilowatt-hour Energy (E)
P	Pair of Pole
Pr	Electrical Power Watt W
Pw	Power of Wind Turbine
Q	Electric Charge Ampere-hour Ah
Qs	Reactive Power (VAR)
R	Radius (m)
S	Apparent Power (VA)
s	Second Time (t)
S	Slip
T_c	Torque Coefficient
T_{em}	Electromagnetic Torque
T_{em*}	Electromagnetic Torque Reference
T_m	Mechanical Torque N.m
V	Volt Voltage (V, E) Electromotive force (E), Potential difference (Δφ)
v^3	Wind Speed
Vdq	Direct and Quadrature Voltages (Volt)
αβ	Stationary Reference Frames
θ^0	Rotation Angle (degree)
θm	Rotor Rotation Mechanical Angle
θr	Rotor Rotation Electrical Angle
θs	Stator Rotation Electrical Angle
π	pi 3.14
πr2	Swept Area by Turbine Blades
ρ	Density of Air or Water
Ψ	Magnetic Flux (Weber)
Ω	Resistance (hom)
ωm	Electrical Rotor Speed (rad/sec)
Ωm	Rotation Mechanical Speed (rad/sec)
ωr	Frequencies and Voltages Speed of Rotor Winding (rad/sec)
ωs	Frequencies and voltages Speed of Stator Winding (rad/sec)
β	Pitch Angle (degree)
λ	Specific Speed Ratio

GENERAL INTRODUCTION

Recently, due to the pollution caused by greenhouse gas emission and consuming fossil fuels to produce electrical energy, it becomes very urgent to find an alternative renewable and safe energy resource. Among these renewable resources wind energy is the most important resource. So, a wind energy conversion system has been the subject of many industrial and scientific researchers. The main challenge of replacing conventional systems with more environmentally friendly alternatives is how to hybrid, control and optimize differ resources and deliver reliable energy with minimum cost. Hybridization of wind/tidal resource it becomes an important issue for reliable electrical networks. Thus, developed methodologies are highly needed to optimize the functionality of decentralized networks.

Due to functional similarity between wind and tidal turbines, thus make it possible to combine between these two resources. Therefore, the research team at GREAH Laboratory took the initiative to study and implement wind-tidal hybrid system using the multi-function emulator which is developed especially to study the hybridization of wind-tidal power conversion chain systems in real-time simulation.

Depending on what is mentioned previously, the main axis of this thesis can be summarized in the following points:

- As starting point, review in the previous studies in hybrid offshore wind-tidal power systems, as well as energy storage systems and its impact on power generation efficiency.
- Modeling, simulation and control for the suggested hybrid wind-tidal turbine power system, based on the hardware simulator available in the lab, using MATLAB/ SIMULINK.
- Studying what so-called “time acceleration “in a virtual time simulation to reduce analysis time of wind and tidal power generation systems.
- Developing real-time emulation structure of hybrid wind - tidal power generation system based electromechanical coupling.

Therefore, this thesis is mainly composed of four chapters:

Chapter one is devoted for wind and tidal as a source of renewable energy, explains the construction and operation principles of wind and tidal turbines, turbine types and its classification, includes state of the art of hybrid wind / tidal power generation systems, power storage units and real-time simulators available in the laboratory GREAH are introduced.

Chapter two proceeded to mathematical modeling of all elements of wind - tidal turbine conversion chain. This is a preliminary step in the implementation of the HIL real-time simulation, in order to study hybrid wind- tidal turbine system. In more details, mathematical modeling is carried out in order to have the possibility of modifying wind turbine characteristics to match with the real-time simulation.

This section begins with the mathematical modeling of tidal current and wind distribution. Then, present modeling of the wind and tidal turbine, based on the Final Element Theory using software developed at GREAH, in order to construct realistic characteristics of wind and tidal turbine. As mentioned previously, the wind energy conversion chain uses an asynchronous electric machine, doubly-fed induction generator, where two modes of modeling are presented, steady-state model and dynamic model, Power converter and DC-link are modeled as well. Power conversion system is completely simulated in MATLAB/SIMULINK environment.

Before designing any system it is essentially to carry out mathematical modeling, in order to study and understand that system. In energy conversion systems, wind and tidal resources and main power conversion system elements are need to be modeled.

Chapter Three is based on recently researches conducted in the field of hybrid wind-tidal power generation systems are mentioned in chapter one. As the majority of these researches and works concerns the electrical coupling only, we develop in this chapter the concept of Offshore Hybrid Wind/Tidal Power Conversion System electro-mechanical coupled on the same shaft of Double-Fed Induction Generator. We present different strategies of control used for a wind and tidal turbine systems highlighting their functional similarities. Two strategy modes are developed: fixed speed control called "Direct Speed Control" ('DSC'), and variable speed control based on Maximum Power Point Tracking, called "Indirect Speed Control" ('ISC').

In addition, we explain a methodology for the synthesis of regulators units to control rotor-side and grid-side power converters used in the conversion chain. At the end of this chapter a small scale wind - tidal turbine based Double-Fed Induction Generator are simulated and controlled in Matlab /Simulink environment.

Chapter Four, from the theories set out in previous chapters, and mathematical models developed in the laboratory, allows us to study a simulation approach of wind systems by introducing the concept of "time acceleration".

In this chapter, different sizes of wind profile are used in the simulation process; to study and analyze the impact accuracy of reducing the size of wind profile on the simulation of energy generation. The parameter used to study is the average power of the turbine over entire length of the selected sample. An analysis is carried out based on a software simulation, as well as experimentally. Tests were carried out over different periods of time (5 hours 1 hour and 1/2hour) with different sampling time. Parameters observed are: average speed of the wind turbine rotation and the average power.

Finally, the concept of electromechanical coupling (developed also by the Japanese company called MODEC) is implemented practically using the hardware simulator available at the laboratory GREAH, results are presented and discussed.

Finally, the **Conclusion** presents a summary of each chapter and our contributions of development a flexible real-time emulation system allowing to study wind turbine or tidal turbine conversion systems independently or in combination, in isolated mode or connected to the network

CHAPTER ONE

INTRODUCTION & STATE OF THE ART

1.1 Introduction

This chapter addresses the state of the art of hybrid offshore wind-tidal turbine power system. Thus, presents a definition of the system with its fundamental principles of operation. Subsequently, studying energy resource; history of wind and tidal turbines, construction of wind-tidal turbines, sizing of power units and configuration, and future trends of wind and tidal power and its contribution in global energy system, advantages and disadvantages of hybrid wind-tidal power generation systems.

Also, wind and tidal power simulators and its role in power investigation and study are addressed. Finally, power storage units and its impact on the power management and power grid in term of stability are presented.

1.2 Hydraulic Power Resources (Wind &Tidal)

1.2.1 Wind Rerource

Definition of Wind

Wind can be defined as the movement of the air. It yields from the variation of atmospheric pressure from place to another on the earth's surface, because of the non-homogenous of the earth surface and the difference in temperature according to time 'seasons' and the place, all this will cause the wind flow from regions of higher pressure to low pressure regions[1].

Wind Characteristics

The wind is characterized by the following main parameters:

A. Variation of height,

B. Its direction,

C. Its speed

D. Its statistics properties.

Wind Variation with Height

The speed variation of wind in the vertical position is called vertical wind profile; this is caused by the air convection in the atmospheric layer around the earth. Actually, wind data at various speeds are not accessible by measurement devices. Thus, mathematical equations are used to estimate the wind velocity, at a certain height, which is 10 meters above the surface of the earth.

The wind speed variation can be function of the height, which can be mathematically expressed as following [1]:

$$\frac{V}{V_{ref}} = \left(\frac{H}{H_{ref}} \right)^{\alpha} \qquad (1.1)$$

Where:

H_{ref} ; it is the height of the reference point which is generally taken at a height of 10 meters.

V_{ref} ; it is the wind speed corresponding to that height;

H; it is the point, at which the wind speeds need to be estimated;

α ; is the coefficient that must be chosen.

The coefficient α vary according to the altitude, time season and, nature of the terrain, wind velocity and temperature. Usually it is taken between 0, 1 and 0, 4.

Wind Direction

A specific diagram called ***wind rose*** is implemented to study the wind direction, as well as to find the best and more power wind direction.

The wind rose is a circle shape diagram which indicates wind distribution, and wind direction during measurement time, using this diagram; it is possible to determine direction of the wind, and its orientation mostly.

The wind rose can be used to trace the wind in multi directions and sectors. The figure shown below is an example of the wind rose for 16 sectors:

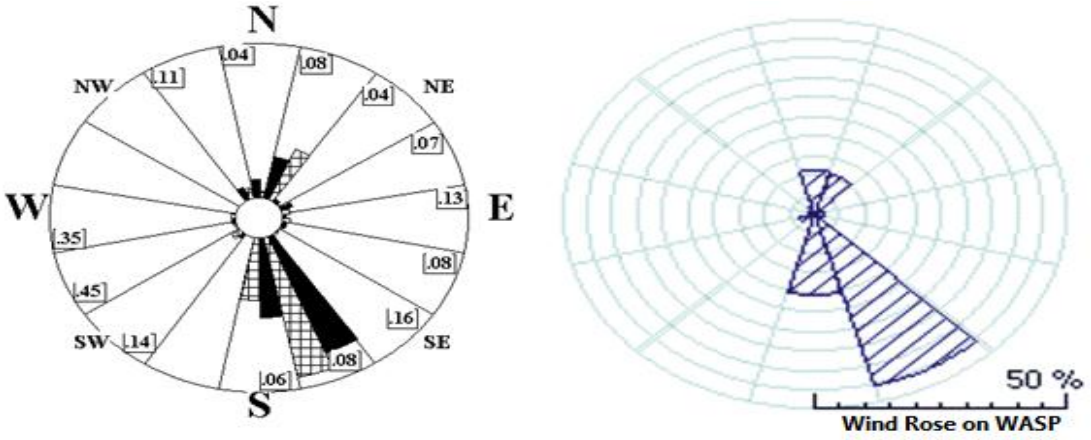

Figure 1 Wind Rose

Frequency of the wind speed represents the percentage of wind speed intervals for 1m /s registered in a given period of time in a certain site. Generally it is represented by a diagram as the one shown in figure 2:

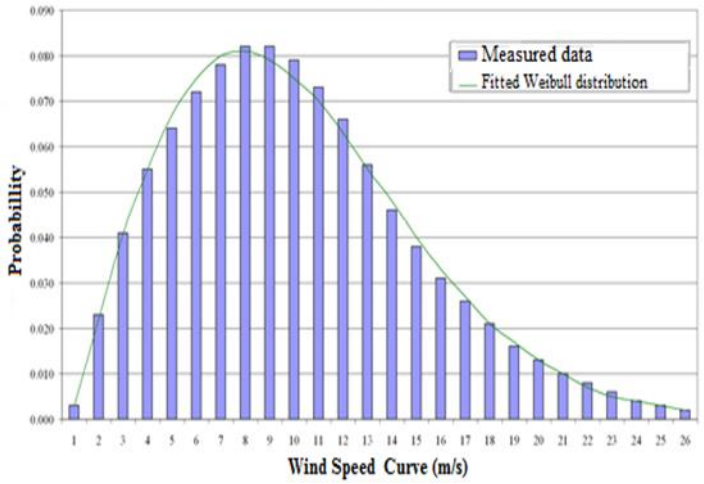

Figure 2 Wind Distribution Curve

Wind Distribution (Weibull)

The frequency of wind speed could be approximated with satisfactory accuracy by Weibull distribution. It is an especial case of the gamma distribution, and it is characterized by the probability density f(V), accumulation distribution function F(V), by the following equations:

$$f(v) = \left(\frac{k}{c}\right)\left(\frac{v}{c}\right)^{k-1} \exp\left[-\left(\frac{v}{c}\right)^{k}\right] \qquad (1.2)$$

$$F(v) = 1 - \exp\left(-\frac{v}{c}\right)^{k} \qquad (1.3)$$

(*k* and *c*) are Weibull parameters (*k* is a shape factor and c is a scale factor), this type of distribution is commonly used for engineering purposes; such as product lifetime analysis and reliability engineering, also it is the most fit to represent wind speed behavior at the designing stage of wind turbine farms, thus find out the most suitable location to install wind turbine unit. Therefore, helps to minimize generating costs as well as to optimize turbine design [2].

In the case where site data is not known, this function used to describe wind speed frequency, figure 3 illustrates Weibull distribution, where factor *C* is fixed and factor *K* is variable lift side figure, while the right side figure represents *K* is fixed and *C* is variable. Because of these two parameters k and c Weibull distribution curve has the capability to represent real data [3].

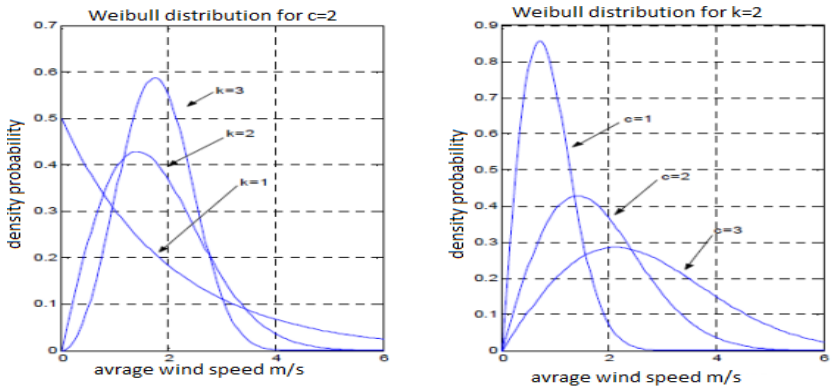

Figure 3 Weibull distribution curves

1.2.2 Tidal Resource

Definition of Tidal Stream

Tidal currents can be defined as the kinetic energy generated by the horizontal motion of water caused by the tide. Whereas, rotation of the earth, differences in temperatures degree, and gravitation associated between the sun and the moon, are the main causes of tidal phenomena in the sea [4]. Unlike other natural energy resources, tidal energy has an important advantage over the other natural energy resources, that it is a predictable source, continuous and stable [5]. On the other hand, the tidal source has some constraints, such as its impact on the environment, limitation of potential sites, and the high cost of power production [6].

Although, it is difficult to precise the potential, but in general it is estimated hundreds of TWh annually. In fact, in order to install a tidal turbine must research places where tidal streams are strong. Hereafter, the world tidal currents map is presented [7]:

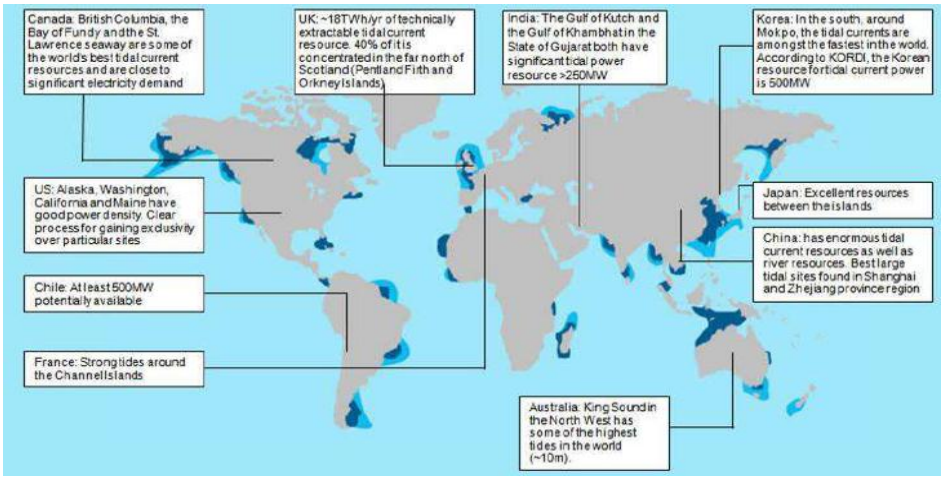

Figure 4 High Potential Areas for Tidal Resources

There are two types of tidal currents: linear waves, and random waves. [7]

Generally, currents are formed due to differences in temperature, salinity of adjacent water and wind speed. Also, tidal currents are classified into two categories: local windy tidal currents and, regular currents such as the Gulf Stream which provides alone a kinetic energy of 30 GW about 300 TWh annually. [6]

1.2.3 World Large Tidal Energy Projects

In the following table the recent large tidal projects all over the world [8]

Table 1 Largest Tidal Power Generation Projects in the World

Name of Project	Country	Total Cap.	No. of Turbines	Date of Project	Grid Connection
MeyGen	Scotland	398MW	265*15MW	2017	Yes
EDF	France	1MW	2*0.5MW	2016	Yes
AW Energy	Portugal	350kW	---	2017	Yes
Nova Innovation	Scotland	500kW	5*100kW	2017	Yes
Sabella	France	1MW	1*1MW	2015	Yes
ENEL Green Power	Italy	200kW	---	2016	Yes
Tocardo	Netherlands	1.2MW	5 x 240kW	2016	Yes
Wello	Scotland	3MW	3*1MW	2020	Yet
OpenHydro	Japan	2MW	1*1MW	2019	Yes
DP Energy	Canada	9MW	6 x 2.5MW	2018	Yes

1.3 History of Wind &Tidal Turbines

1.3.1 History of Wind Turbines

Since the time began, human being researched for power resources, wind was one of the early discovered power resources, it is used in navigation transport thousands of years ago by Egyptians[9], later it is developed to be used in day to day life as mills for grinding grain. The first windmills were conceived 2000 years ago by the Persians; and for water lift [10]. In [1846-1908] *Paul La COUR* - Danish meteorologist experimented wind turbine to rotate DC generator to generate electrical power [11]. During winter of [1887-1888] the American Charles Francis Brush constructed first wind turbine and electrical generator (12 kW) to supply his house by electric power using a battery as storage unite [12].

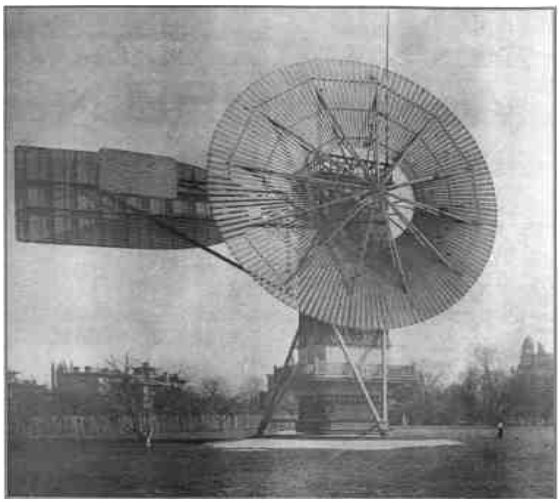

Figure 5 First Aerodynamic Generator Constructed by Charles F. Bruch [9]

In 1957, one of La COUR students 'Johannes JUUL', created the first wind turbine generates alternative current 200 kW (Gedser Turbine) [13-14].

Figure 6 Gedser Turbine [15]

1.3.2 History of Tidal Turbines

Centuries ago, tidal energy was exploited to produce mechanical energy by using a water wheel on the river's side or dams, these wheels are used as prime movers for mills to grind grains.

Tidal turbines sometimes called submersed wind turbines, due to the similarities between tidal and wind turbines, often tidal turbine compared to wind turbines [16].

Scientists have been interested in the phenomenon tides since long time ago. Pytheas and Euthymenes (in 4^{th} century BCE) discovered the influence of the moon on the tidal currents. However, mathematical question was adopted by many scientists in the followed centuries. Also, Pliny (writer and naturalist in 1^{st} century Roman) explained the influence of the sun and the moon

on the tidal currents. Centuries later, this theory was questioned by Johannes Kepler (1571-1630) and Galileo (1564-1642). In 1687, based on universal gravitation laws, Newton developed the static theory that constituted the real foundation of tidal theory. This theory explained that the surface of the water reacts instantly to the actions of stars by deforming according to an ellipsoid. But the theory of Newton failed because it assumed that the ocean surface was equipotential. Bernoulli supported Newton's theorem, but he could not prove it [17].

In his 4th book of celestial mechanics, Laplace examined the problem under its dynamic aspect and has formulated the first dynamic theory; this theory depends up on two principles: forced oscillations and the superposition of small movements. Lord Kelvin decomposed the potential of tide force in a sum of periodic terms, later he invented the "Tide Predictor" mechanical machine used to sum up all the terms and draw the tide curve. The basics Henri Poincaré also built up his dynamic theory and calculation methods to solve the problem of tides.

As the oceans are separated by continents, it would be easier to determine the period and the nature of the free oscillations of oceans tides.

Finally, the appearance of computers made it possible to accurately predict the evolution of tides.

1.4 Turbines Classification

Wind & tidal turbines are classified regarding to the point of view of the research area, for example in control point of view they are classified into two main categories:

- Fixed speed controlled wind and/or turbines
- Variable speed controlled wind and/or turbines

Also wind and tidal turbines are classified into three main categories according to mechanical power being generated:

1. Small scale: nominal power less than 40 kw
2. Medium scale: nominal power between 40 kw up to hundreds kw
3. Large scale: nominal power more than 1MW [18].

Whereas, in the position point of view turbines are classified into two main types:

- **Horizontal Turbines**
- **Vertical Turbines**

1.4.1 Horizontal Axis Turbines (HAT)

Horizontal turbines are the most commonly used type; it is composed of three blades usually, gear box, shaft and, electrical generator, all these elements are installed in the nacelle on the top of the tower.

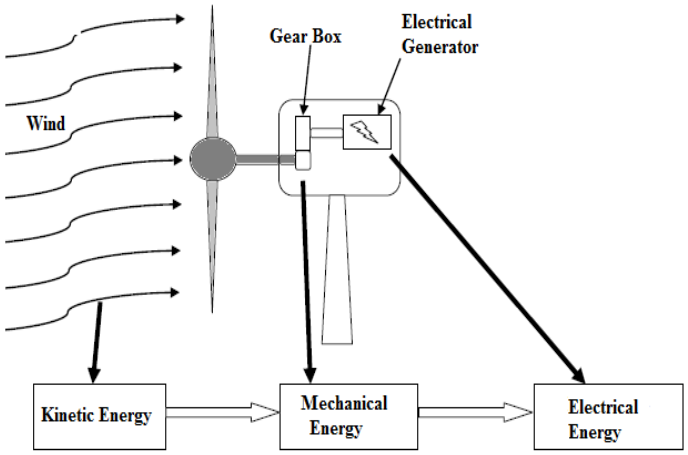

Figure 7 Wind Turbine Power System [18]

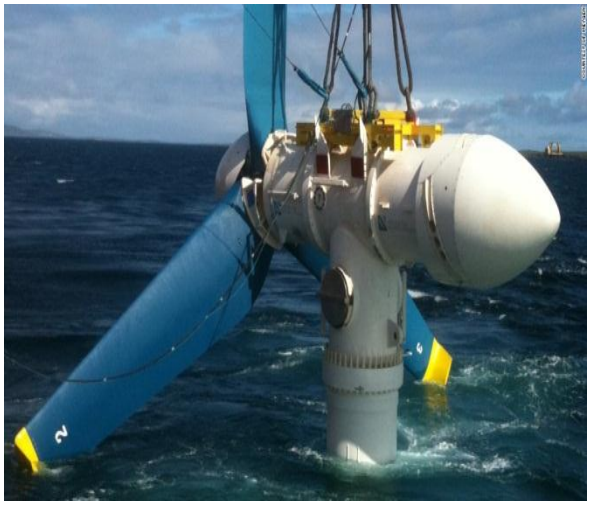

Figure 8 Horizontal Tidal Turbine [19]

1.4.2 Vertical Axis Turbines (VAWTT)

The most commonly used types are Darrieus and Savonius turbines.

Darrieus Wind Turbine

The Darrieus wind turbine is commonly called "Eggbeater" turbines because it looks like a giant eggbeater. It is one of the most successful vertical axis wind turbines. The most attractive feature of this type, that generator and transmission devices are located at ground level. In addition, it is able to capture winds from any direction. However, these advantages are counteracted by

reducing energy capture since winds intercepted by the rotor have less energy. Moreover, despite the fact that the generator and the transmission are located at ground level, the maintenance is not simply because it generally requires the removal of the rotor. Mainly for these reasons, the use of vertical axis wind turbines has declined considerably in recent decades [20].

Figure 9 Darrieus Wind Turbine at GREAH

Savonius Wind Turbine

This type of turbines works on the principle of differential drag force, indeed, the force exerted by the wind on each blade has different intensities. Thus, yields a torque causing rotation of the turbine [21].

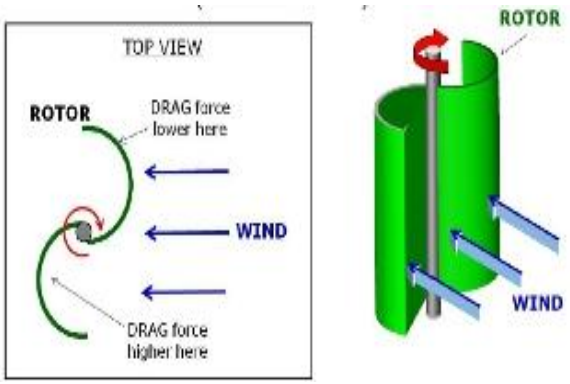

Figure 10 Drag-based wind turbine (Savonius Rotor) [21]

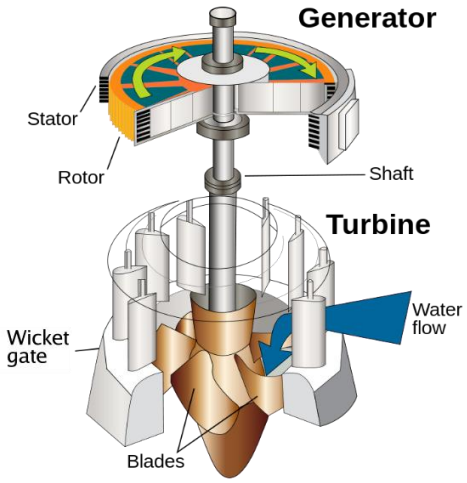

Figure 11 Swirling Turbine [22]

1.5 Wind/Tidal Turbines Construction and Operation Principle

Although, Wind and Tidal turbines are used in an environment totally different, but they have the same construction [23]:

Table 2 Main Turbine Components

Mechanical	*Primary*	Foundation, Tower, Nacelle, Rotor, Blades,
	Secondary	Gearbox, brake.
Electrical	*Primary*	Generator, transformer
	Secondary	Anemometer, vane, power converter

1.5.1 Mechanical Parts

1. **Foundation:** It is a large, heavy concrete immersed in the ground in order to hold up the tower and the other parts of the turbine figure 12.

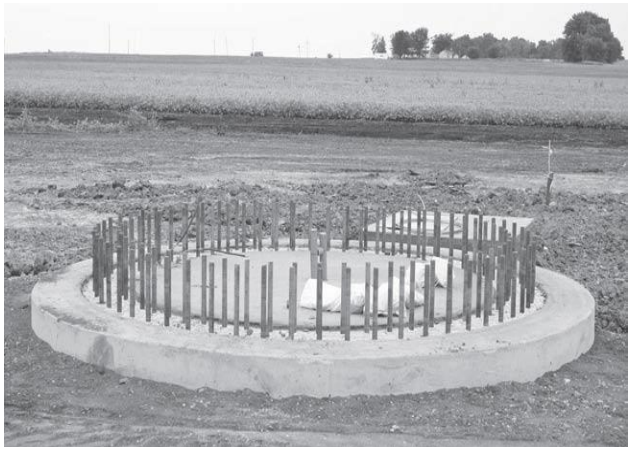

Figure 12 Wind Turbine Foundation [23]

2. **Tower:** It is used to supports and holds turbine's blades, rotor, gear box, and generator in the air (off the ground), see figure 13.
3. **Nacelle:** it is the chamber which contains and protects the electrical generator, high and low speed shaft, orientation control system Yaw, and control system, see figure 13.

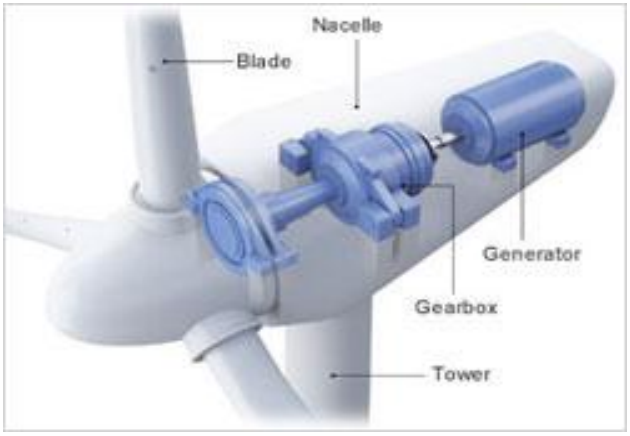

Figure13 Wind Turbine Nacelle [23]

4. **Rotor**: It is the connection part between the blades and generator, in some types of turbines when gear box is used there are two sides high speed side and low speed side rotor.
5. **Blades**: It is the main part responsible on transforming wind energy into mechanical energy, it represents the area of energy transformation, its length has a direct relationship with power generation, denoted in mathematical modeling by R^2, see figure 14 [23] [1].

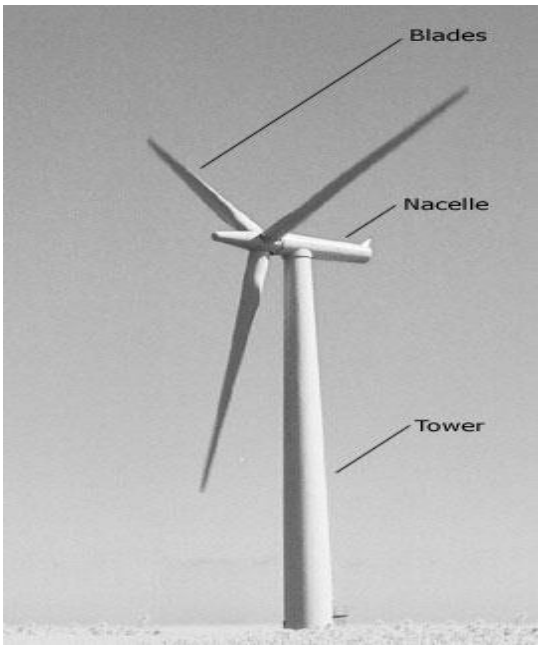

Figure 14 Main Mechanical Wind Turbine Components [24]

6. **Gear box:** It is used to step up the rotation speed of the electric generator's shaft, when the wind speed is not quite high enough to generate electrical power, see figure 15.

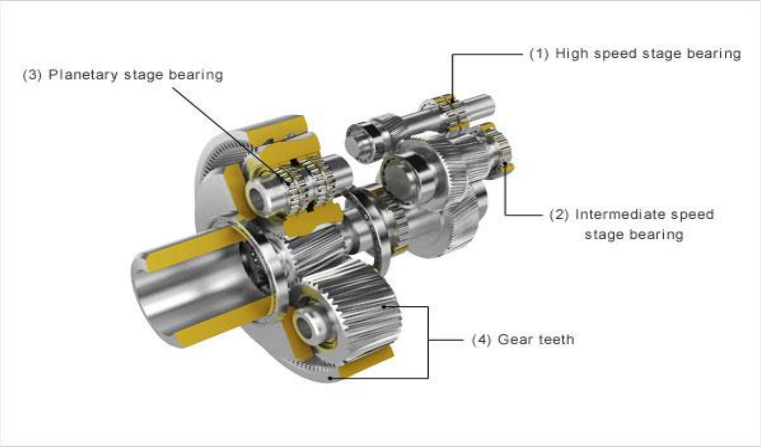

Figure 15 Wind Turbine Gearbox

1.5.2 Electrical Parts

1. **Electrical Generator**: It is used to convert mechanical energy into electrical energy, electrical generators usually used are synchronous or asynchronous machines.
2. **Power Converter**: It has two function to control the rotation speed of the generator, via pulse width modulation PMW, thus by altering the frequency of the rotor side, also to stabilize the output power by converting AC to DC and vice versa (rectifier and inverter) respectively.
3. **Transformer:** Transformers are used to adapt the generated tension to the gird side.

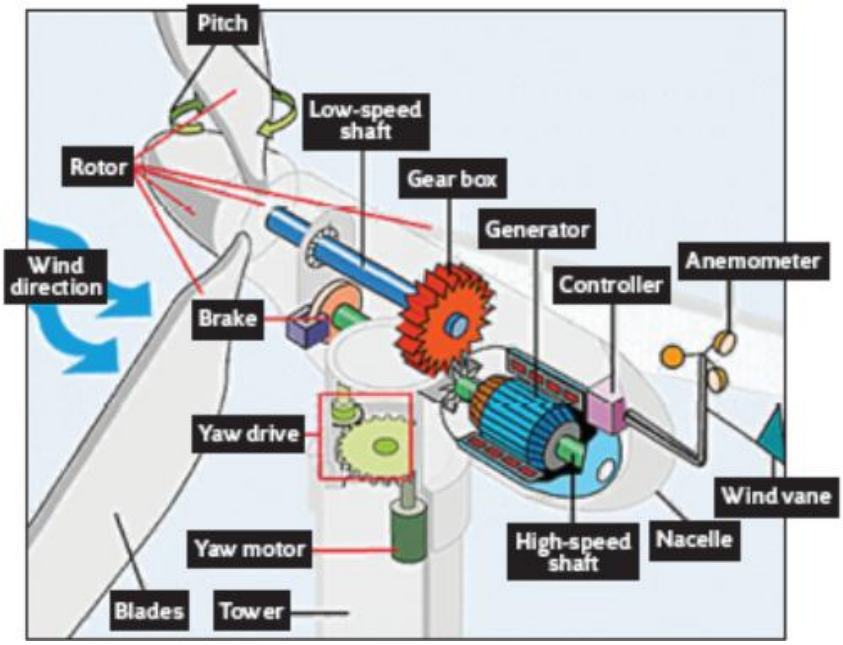

Figure16 Turbine Construction [25]

1.5.3 Operation Principle

The operating principle of an (aero/hydro) generator is practically the same as a windmill, the kinetic energy of the wind or water currents strike the surface of the blades, which turns the blades of the (aero/hydro) generator, blades are fixed on the rotor and coupled to an electrical generator that converts mechanical energy into electrical energy [18].

So, power generated by wind turbine depends up on certain factors that can be used to determine the power that can be extracted from the wind, these factors are expressed in the following mathematical expression:

$$P_w = \frac{1}{2}\rho\pi r^2 v^3 C_p(\lambda, \beta) \quad (1.4)$$

Where: ρ air or water density, πr^2 swept area, v^3 wind speed, C_p power coefficient.

Turbine efficiency is determined by how much power can be extracted by the turbine blades from the moving wind or water currents. Therefore, the power coefficient is a function of the turbine efficiency.

Energy produced by wind and /or tidal turbines is called wind or tidal energy; it is a clean energy, distributed geographically. Furthermore, it does not emit CO2 or waste nuclear materials. The captured and converted wind or tidal energy remains quite complex, because it alters with time and seasons [26].

1.6 Advantages & Disadvantages of Wind/Tidal Turbines

1.6.1 Horizental Axis Turbines

Advantages

1. High rotation speed comparing to vertical axis turbines
2. Can be oriented to track wind direction using Yaw control system.
3. Angle of attack can be remotely adjusted to extract maximum power available in the wind.
4. Horizontal axis turbines are Self-starting turbines.
5. Damage is minimized because of pitch system that can stop in high speed wind.
6. High efficiency of power generation the rotor blades [27].

Disadvantages

1. Complex control system is needed to achieve high performance.
2. Mechanical stress due to its perpendicular to the wind flow direction.
3. It needs to be at sufficient height.

4. Consuming large area of land and can be obstacle to navigation in offshore sites.
5. Vision and noise pollution.
6. Dangerous; kill birds [28].

1.6.2. Vertical Axis Turbines

Advantages

1. It bi-direction.
2. Generator, gearbox and other components are placed on the ground.
3. Low production cost compared to horizontal axis wind turbine.
4. It does not need to be oriented, so yaw drive and pitch mechanism is not needed.
5. Easy to install.
6. Low maintenance cost.
7. Low risk to human and birds, because blades moves at relatively low speed.

Disadvantages

1. Low efficiency compared to HAWTS.
2. Initial push to start is needed.
3. They have relative high vibration.
4. Because of vibration, bearing wear increases therefore increase of maintenance costs.
5. Pollution of noise.
6. Needs a guy wires to hold it up [29].

1.7 State of the Art-Hybrid Wind-Tidal Power Generation Systems

Recently many researches have been conducted in the field of hybrid wind and tidal power generation systems including; feasibility studies, computer modeling, control strategies, and experimental work as well as associated energy storage devices in order to improve their performance and reliability.

As mentioned previously, natural resources considered as unpredictable sources, means that, energy may be generated when it is not demanded and vice versa, so to overcome the problem of power intermittency, and thus improve the system performance, hybridization of two or more of renewable energy resources along with energy storage technology becomes an essential solution for power intermittency.

In general, the hybrid system operates in the following mode:

- When generation is more than the load demands, so generators supply the load and charge batteries in the same time.
- When load demand is greater than the generated power, tidal generator connected to make-up the power shortage in the system.
- Energy storage systems take the complete role, or partially participate when the load demand is higher than both sources. Tidal generator system has capacity factor of 30%–50% and that of wind generator is 25%–35%. If these two resources combined together renewable sources results in a system with overall good capacity. As system is located offshore, therefore there is no danger of pollution. Expected lifetime of such system is between 15–20 years [30] [31].

Hybrid power generation system can be defined as when two or more of power generation systems, sustainable or non-sustainable combined and controlled [32]. Figure17 illustrates schematic block diagram of typical hybrid wind/tidal power generation.

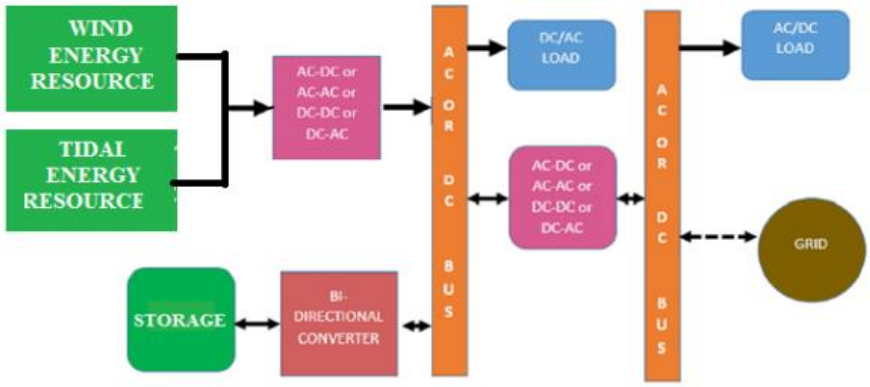

Figure 17 Basic components of hybrid system [33]

Selection of systems to be combined depends upon multiple factors such as: feasibility study, site location, technical features, socio-cultural, and economic considerations [33].

Main Renewable Energy Resources and Storage Devices are:

Table 3 Main Resources of Renewable Energy

Main renewable energy sources	**Storage devices**
Wind	Batteries
Solar cell/ thermal	Super-capacitors/SMES
Tidal waves	Flywheel / Compressed air
Biomass	Pumped hydro
Geothermal	Thermal

Investigation and analyzing of hybrid power generation systems is a complex process. Therefore, many software packages are used to find out unit sizing, efficiency, reliability, and feasibility of Hybrid Power Generation Systems (HPGS) and the associated Energy Storage Systems (ESS), some of these packages are listed hereafter:

I. MATLAB/Simulink and PSCAD/EMTDC

II. HOMER: it software used to simulate and size different model components energy sources and the hybrid alternative energy systems, based on the optimization of NPC.

III. HYBRID2: is used for the feasibility of hybrid alternative energy systems and performance.

IV. PVSOL: is used for both grid-on and grid-off connections performs analysis and cost estimation.

V. RAPSIM: is used for hybrid energy systems simulation PV, and DGs.

VI. TRANSYS: It is implemented for simulating solar PV, wind, solar thermal, and some other energy sources, but lacks the optimization feature [32-37].

1.7.1 Current Statistics and Future Trends of Renewable Power Generation

In EEA report addressed the *trends and projections* of actual and approximated recent progresses in RES at the EU level in the 28 EU Member States [38].

Analysis Show That:

- The contribution of renewable energy by EU-28 increased in 2013 by 0.7 % to reach 15% compared with 2012.
- As calculated in August 2015 — EEA approximation indicates that, the share of RES in EU is increased up to 15.2 % in 2014.
- EU achieved its target in both 2013 and 2014, compared with the trajectories in the RED and the NREAPs.

A gross positive impact of RES on GHG emissions has been estimated by the current report. In 2014 demand on renewable energy increased, compared with the level of gross final RES consumption in 2005, this leads to:

- Reduce GHG emissions by 380 Mega-ton of CO_2, equivalent to about 9 % of total EU GHG emissions;
- Fossil fuels consumption decreased by 114 Mtoe (Million Tons of Oil Equivalent), or roughly 10 % of total EU fossil fuel consumption;

• Primary energy consumption reduced by 32 Mtoe, which is equivalent to a 2 % reduction of primary energy consumption across the EU [38].

RE has been growing rapidly comparing with other source of electricity generation around the world, according to IEO2016 Reference case, electrical generation expected to increases 69% from 2012-2040.

Figure 18 illustrates that renewable energy resources are the fastest-growing source of energy for electricity production; with average increases of 2.9% per year from 2012 to 2040 the global prospects of Long-term continue to improve power generation from renewable energy sources, natural gas, and nuclear power, in the IEO2016 Reference case, with much of growth coming from wind power. After renewable energy sources, natural gas and nuclear power are the next fastest-growing sources of electricity generation. [38]

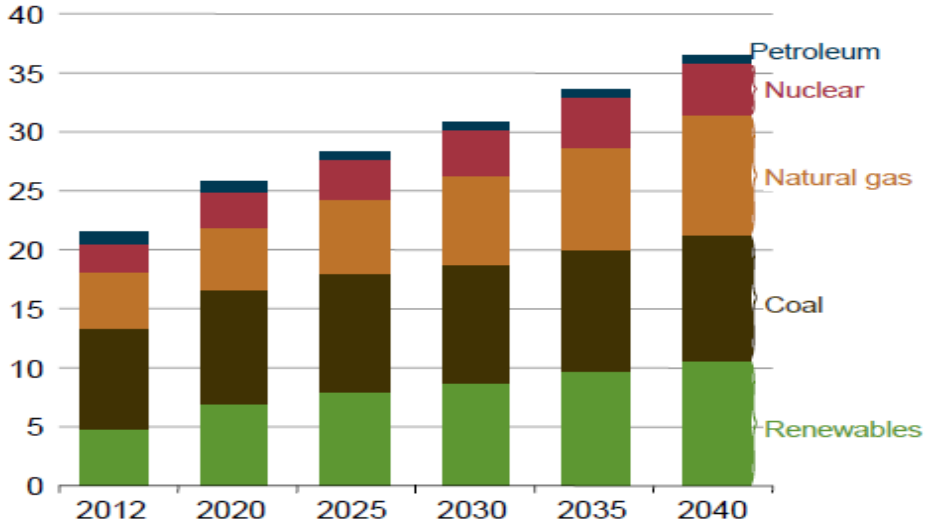

Figure18 World Net Electricity Generation by Energy Source, 2012– 40

According to EIA's analysis of the proposed Clean Power Plant (CPP) rule in figure 19, Solar energy is the world's fastest-growing form of renewable energy by an average of 8.3% per year, 859 billion kWh (15%), hydroelectric and wind each account for 2.9 trillion kWh (33%), for another renewables (mostly biomass and waste) for 856 billion kWh (14%) [39].

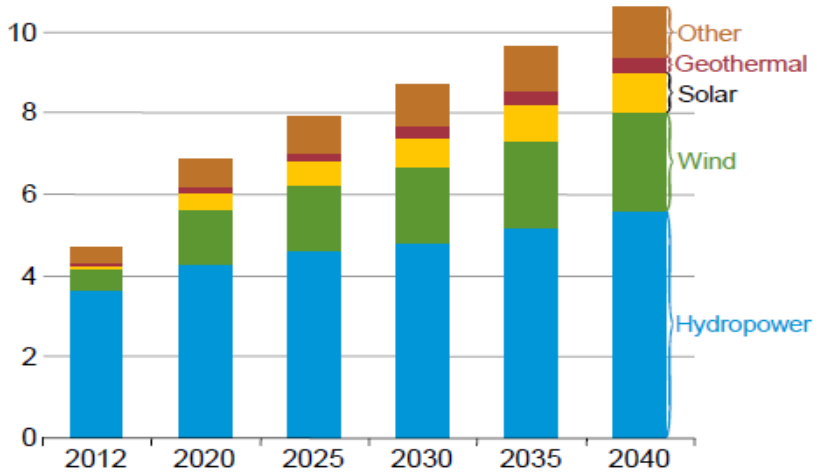

Figure19 World Net Electricity Generation from Renewable Resources 2012-2040

1.7.2 Configurations of Hybrid Energy Systems

Due to intermittent nature of renewable energy resources, Storage Elements (SEs) are essential parts to enable hybrid energy systems connected to power grid. However, Storage Elements SEs is divided into two categories:

- **Capacity-Oriented:** when long-term of energy storage and low response time are required for balancing power oscillation such as: Batteries, pumped hydroelectric systems, Compressed Air Energy Storage (CAES), and hydrogen storage.
- **Access-oriented:** when short-time of storage energy and fast response are demanded such as: Flywheels, super capacitors, and Superconducting Magnetic Energy Storage (SMES) are considered [40].

There are three possibilities for coupling hybrid renewable energy resources into power grid:

- **OFF-Grid Stand-Alone Connection:** Hybrid power resource connected to limited or isolated grid (micro-grid), such as island or farm in the country side.
- **ON-Grid Connection:** Hybrid power system is connected to open grid infinity or national electrical network.
- **Hybrid Connection:** Renewable hybrid systems can be connected with both types of grids isolated or non-isolated grid [41].

1.7.3 Integration Schemes

Hybrid renewable resources can be integrated with power grids in many different ways, generally classified into three categories [42]:

DC-Coupled: - As shown in figure20 in DC-coupled configuration, different distributed generators DG and storage energy SE can be connected to a DC-bus through power electronic (PE) converters. The DC source and DC loads may be connected to the DC-bus directly or through DC/DC converter, there are different types of DC–DC converters, but most commonly used are; buck, boost and buck–boost converters to achieve appropriate DC voltage for the DC loads. AC loads or grid utility also can be connected to DC-bus through an inverter. Although, DC-bus configuration is simple in construction and no synchronization is needed, but it has its own drawbacks that, low efficiency if DC/AC converter out of service AC loads cannot be supplied [42].

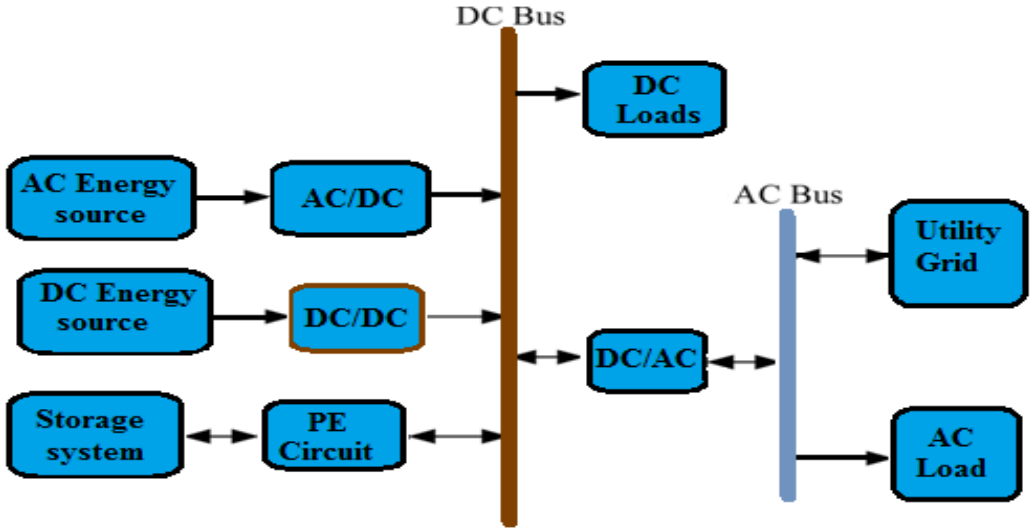

Figure 20 Schematic Diagram of a DC-Coupled Hybrid Energy System

1. AC-Coupled: Figure 21 demonstrates AC-bus is used for the integration of DG sources with ultimate AC outputs. DC sources need DC/AC converters (inverters) while those with AC outputs are connected to AC-buses either directly or through AC/AC converters (if required). DC-loads are connected to AC-buses by AC/DC converters (rectifiers) while AC loads are connected either directly or through AC/AC converters (if needed). There are two types of AC buses: (i) HFAC buses and (ii) PFAC buses.

High frequency (HF) AC Power generation systems and HF loads are connected to HFAC buses while those of Power frequency (PF) (i.e., 50–60 Hz) DG sources and PFAC loads are connected to PFAC buses. General hybridizations and energy flows of DG sources using HFAC Bus and PFAC Bus have been shown in figures 21(a-b), respectively. For obtaining DC power AC/DC rectification is needed, in case of both HFAC and PFAC configuration system. Utility grid can be

connected to HFAC through PFAC bus (through a DC/AC or an AC/DC converter), to which AC loads can be connected.

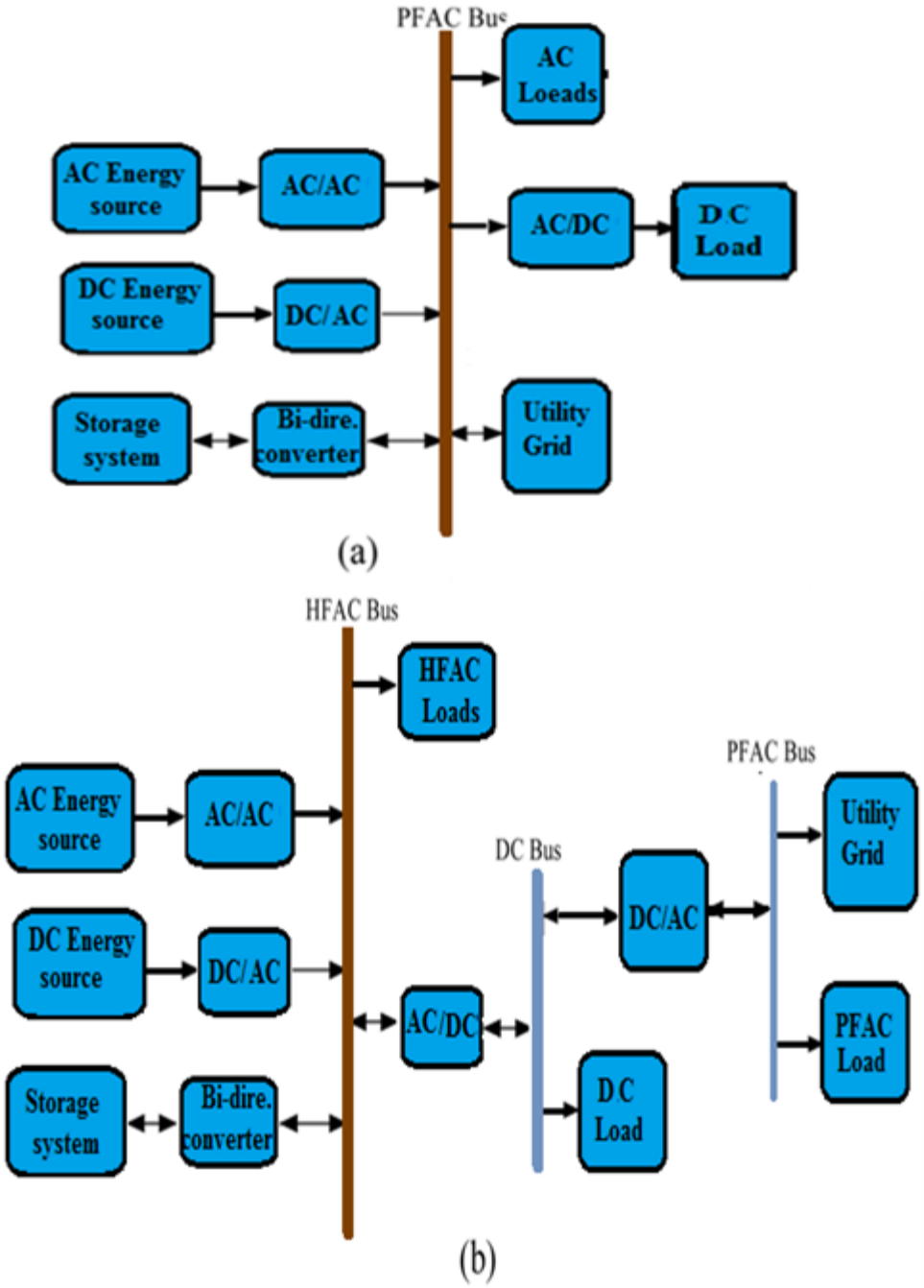

Figure 21 Schematic of AC-Coupled Hybrid Energy System: (a) PFAC; (b) HFAC

2. Hybrid-Coupled: Means that when AC and/or DC sources and loads are connected together as shown below in figure 22; such configuration has higher energy efficiency than the previous two types of configuration but it is more complex to control.

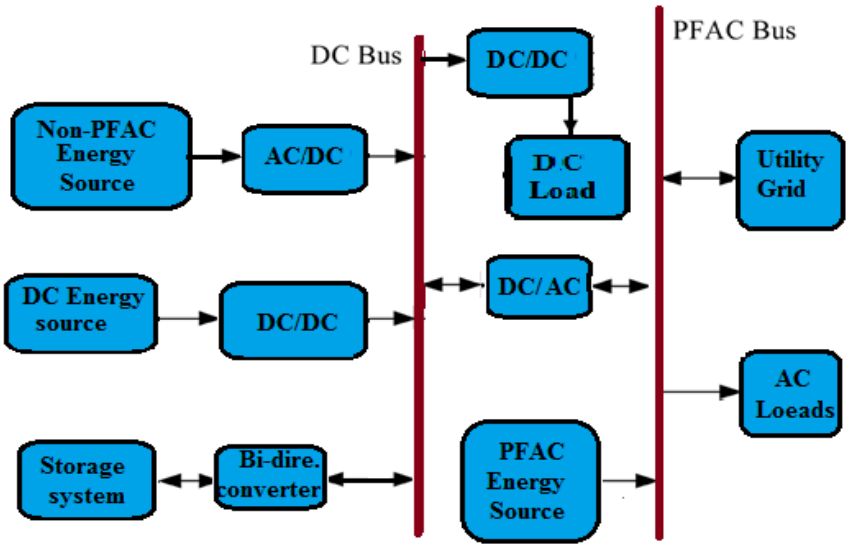

Figure 22 Schematic Diagram of Hybrid-Coupled Energy System [42]

1.7.4 Unit-Sizing and Hybrid Configuration Selection

At the designing stage of hybrid power generation system, it is important to select and size the right configuration. Unit sizing and technology election can be straightforward or complex according to the system requirements and conditions e.g., geographic factors, desired system reliability, and cost requirements. In addition, there are many software packages executed to evaluate and estimate unit size and efficiency of hybrid renewable and non-renewable resources, before realization real systems exist [37]. However, there are different technical methods used to figure out the best fit size, and the adequate configuration of the hybrid power system, many methods used for power system optimization; such as linear programming (LP), interior- point-method (IPM) and heuristic methods such as DIRECT search algorithm, genetic algorithms and particle swarm optimization (PSO) can be used for component sizing, and energy management of hybrid renewable energy systems [43-44].

Some very important questions need be answered, in order to determine the general configuration and unit size of hybrid system.

- What type of renewable energy system to be included?
- How many numbers of renewable energy units to be installed?

- How much the capacity of renewable energy units to be installed?
- Does a back-up unit, such as diesel generator, fuel cell etc. would be included in the system?
- Does energy storage would be integrated into the system?
- Is the system grid-off (stand-alone) or grid connected [36]?

1.8 Hybrid Wind-Tidal Power Generation Systems - Review

A prototype experimentally designed of hybrid system consists of offshore wind turbine as main power unit with 6-pulse diode rectifier used to convert the generated AC into DC, and tidal turbine (one way clutch system) flywheel generator/motor based as complementary, to guarantee the continuous supply availability to the grid power with IGBT bi-directional converter, as shown in figure 23. The wind power has been subjected into short time fluctuation, tidal turbine used to overcome power fluctuation. The MPPT algorithm and PWM used to maintain the DC bus voltage at level which gives maximum output power. The result shows that, tidal turbine is able to increase generation quickly in order to substitute power shortage in the power grid [45-46].

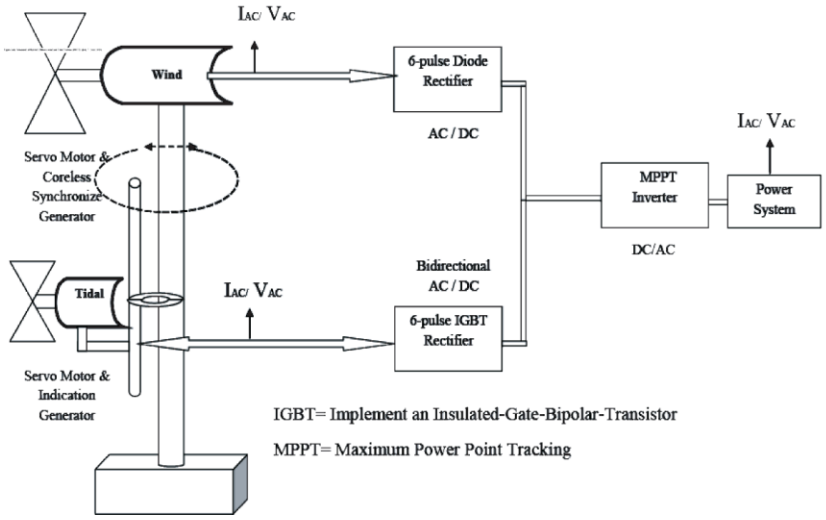

Figure 23 Hybrid Wind/Tidal Turbine Power Generation [46]

A hybrid Offshore Wind Farm (OWF) based doubly-fed induction generator (DFIG), and Tidal Farm (TF) based permanent magnetic generator (PMG) are connected to an Onshore power grid using a flywheel energy storage system (FESS) figure 24, the proposed system subjected to a wind-speed disturbance, the simulated result dynamic and steady-state characteristics were analyzed, and it can be concluded from that, FESS can be an effective solution for power stabilization in the power grid [47].

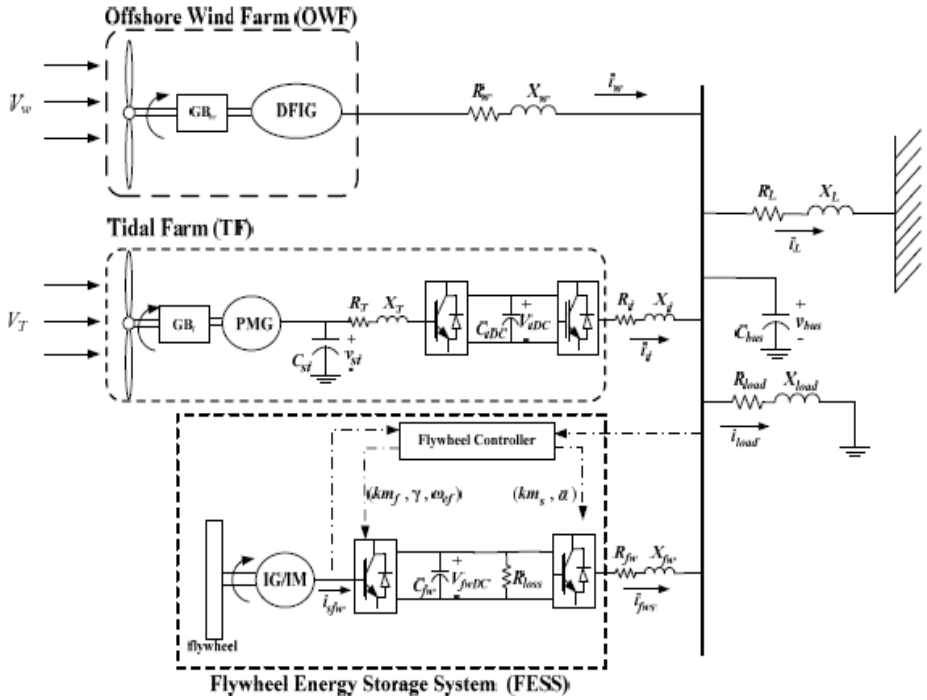

Figure 24 Configuration of Hybrid OWF and TF Connected to Power Grid Using FESS [47]

In this paper [48]control strategy is used to smooth power output fluctuation of a hybrid system figure 25 comprises of wind turbines based doubly-fed induction generator (DFIG), Archimedes wave swing (AWS) based linear permanent magnet generator (LPMG) and tidal turbine based DFIG (flywheel) as generator/motor system is used to smooth short time output power fluctuation. The tidal speed considered as set point of this control strategy, if the tidal speed is less than the cut-in speed tidal turbine disconnected mechanically and the DFIG operates as electrical motor by the bi-directional converter. The proposed system numerically simulated in MATLAB, the obtained result was satisfied to reduce the power fluctuation in the power system.

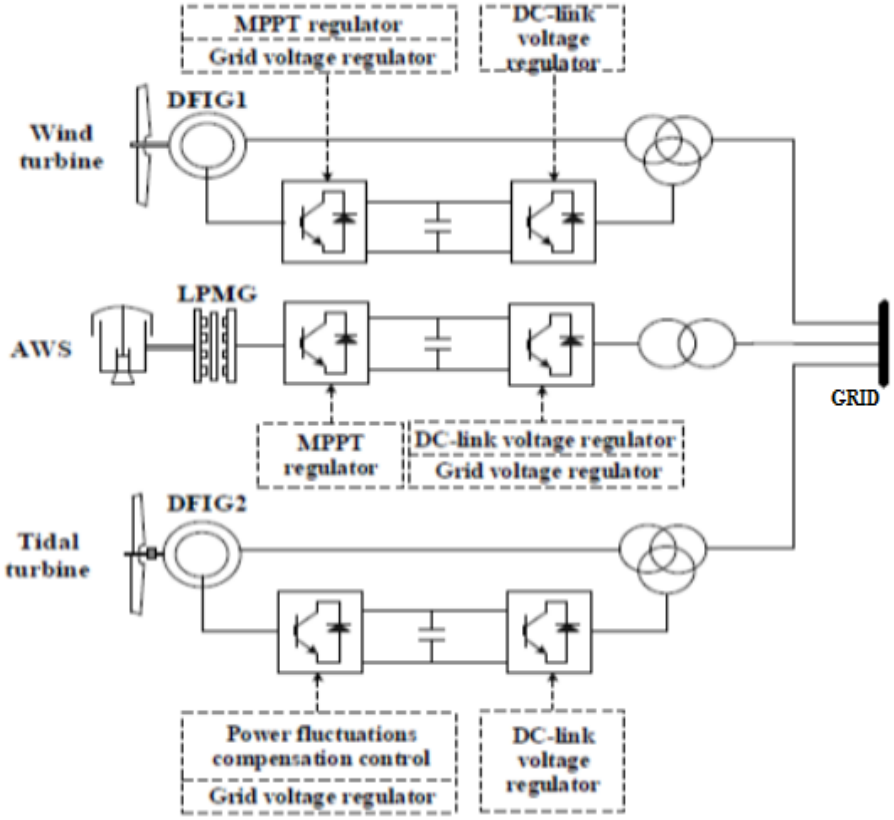

Figure25 Schematic Configuration of Hybrid Offshore Horizontal Axes Turbine [48]

The authors suggested in [49] dynamic modeling, simulation, control and energy management in an isolated integrated power generation system, consisting of (offshore wind turbine, tidal turbine, micro-turbine and battery storage). The feasibility of this system and optimal sizing is obtained based on genetic algorithms (GA) micro-turbine with a battery is suggested to be as back-up to the system, least square algorithm is implemented to estimate a model-power consumption of the micro-turbine. Adaptive feedback and space vector control is used to track the maximum power point in the wind speed, pitch angle zero, yaw system is not considered, supervisory controller is used to manage the power produced by the system and consumed by the load. Simulation and dynamic modeling are fulfilled using MATLAB Simulink^{TM}7.2 this system shows that, it can be used in the isolated rural and mountainous areas far from the power generation network.

Different electrical configurations of hybrid wind-tidal power system connected to DC-bus simulated in MATLAB, wind turbine based a (PMSM) and tidal turbine based a (DFIG) as shown in figure26. Two control strategies MPPT, PI Controller based oriented-field control are

used to extract the maximum power available in the wind, obtained results concluded that, more stability and easy to control the power variation in such configuration [50-51].

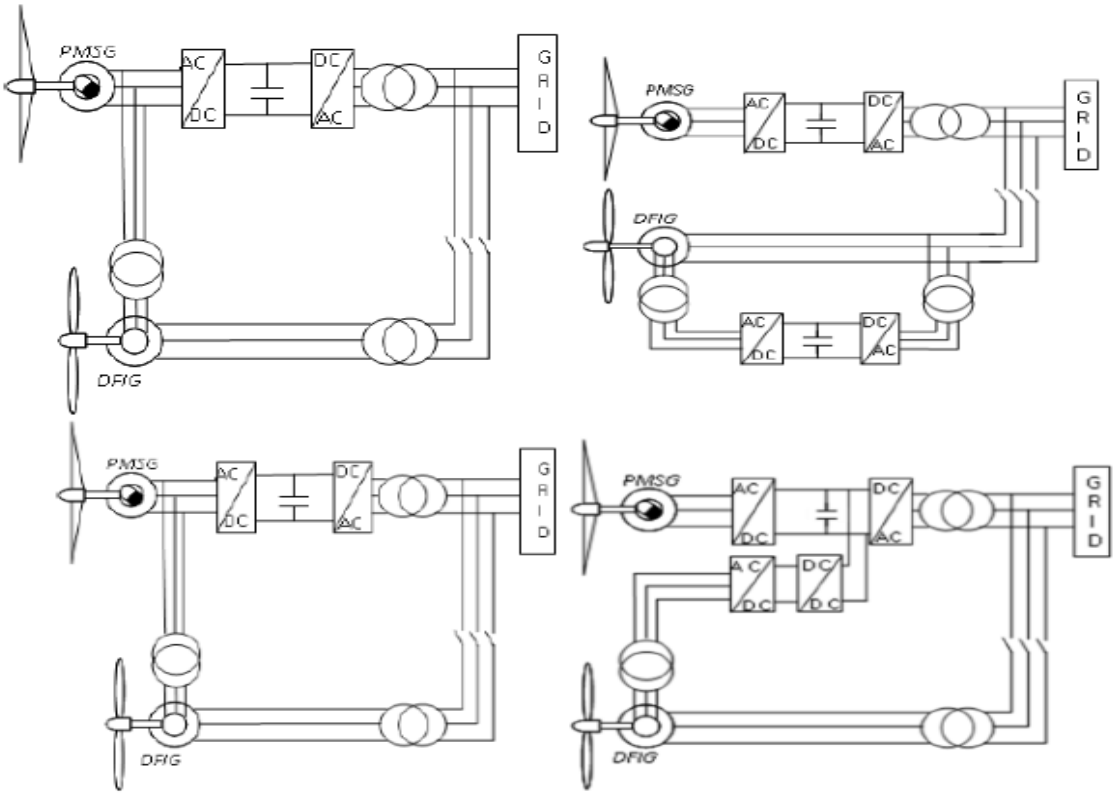

Figure 26 Different Configurations of Hybrid Wind/Tidal Turbines Connected to DC-bus

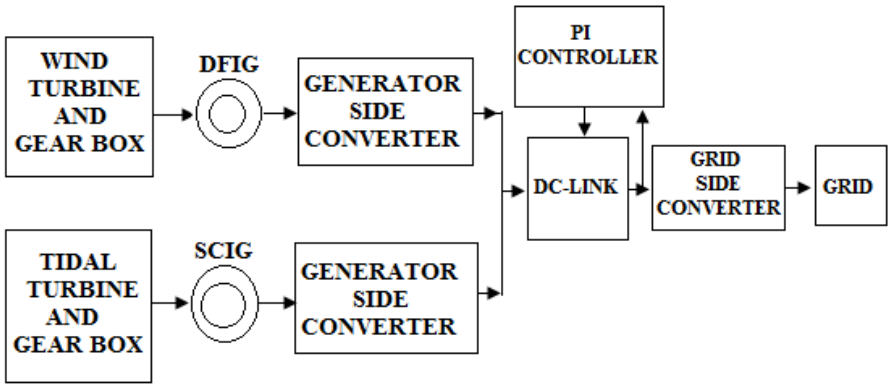

Figure 27 Block Diagram of Hybrid Wind/Tidal Turbines

This research [52] is devoted to propose a new method to stabilize the output power of hybrid wind-tidal system, by using Modulated Power Filter Compensator (MPFC) connected to the network figure27. The proposed MPFC is manipulated through a tri-loop dynamic error driven by PI controller; simulation results indicate a significant improvement of power quality.

In [53] authors proposed a dynamic model of offshore wind and tidal turbine system based different types of generators namely (DFIG, SCIG and DDPMSG), carried out to analyze system's stability. All models are validated using a common property of the generator for the validation. Obtained results indicate that, system stability is directly proportional with resistive loads, and inversely proportional with the inductive loads.

In this study [54] a dynamic model of hybrid offshore wind and tidal power system, based gearless (PMSG) simulated in MATLAB/Simulink®. MPPT and controlled rectifier are used to control the generator speed as shown in figure 28. Results prove that, the independent controlled rectifier is sufficient to adjust the rotation speed of the generator and extracts the maximum power of both turbines and improves system stability.

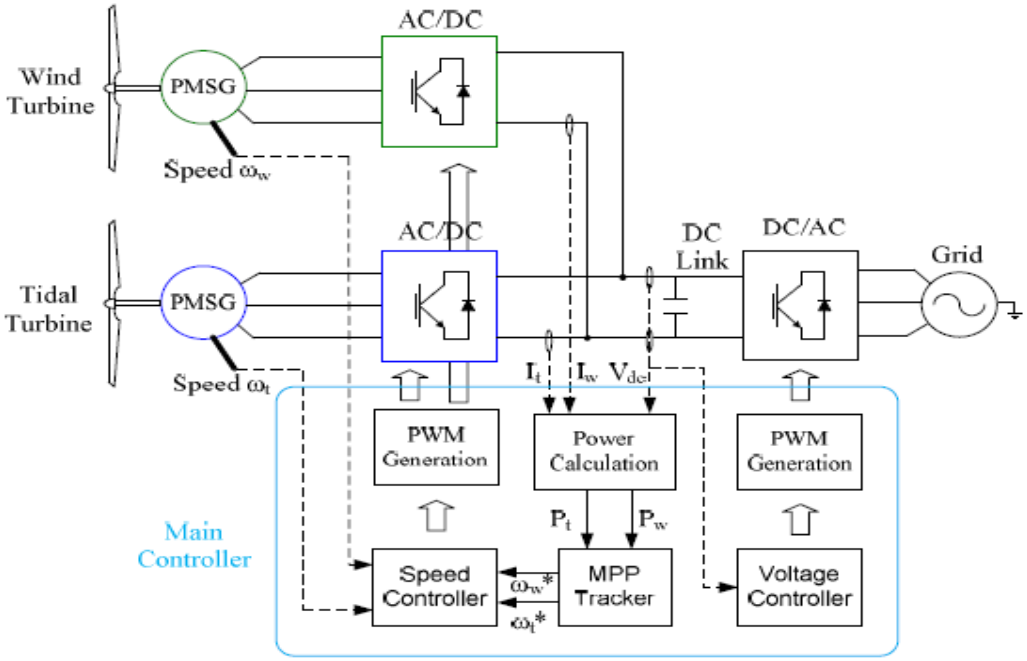

Figure 28 Hybrid Wind/Tidal Turbine based PMSG

In this paper[55], authors proposed four tidal turbine and one wind turbine combined together and connected to DC line, the proposed system modeled and simulated in PSCAD/EMTDC from the obtained results the control system maintained the DC voltage constant.

In figure 29 hybrid wind-tidal power system and hydraulic accumulator used as energy storage system are modeled and simulated in MATLAB. PID controller (standard torque controls) used to regulate hydraulic distribution between auxiliary pumps. Using such system demonstrates very high efficiency in terms of system stability and maximum power extraction [56].

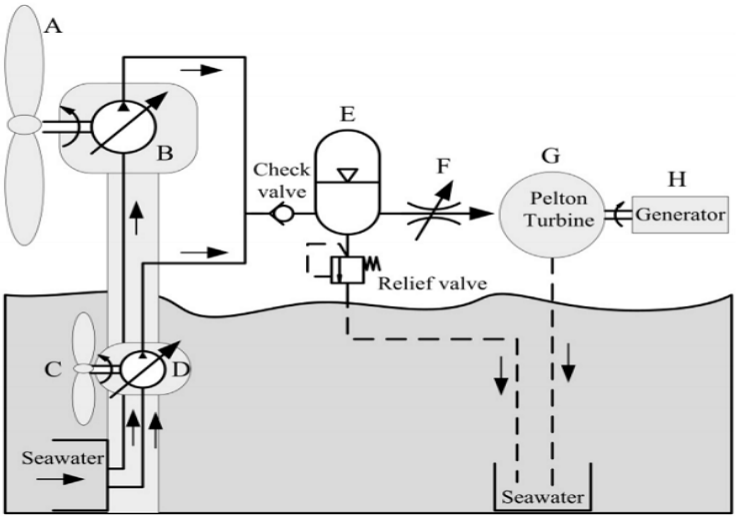

Figure 29 Schematic of Hybrid Wind-Tidal Turbine System [56]

Authors in [57] proposed an Individual Channel Analysis and Design (ICAD) – a frequency domain-oriented framework of multi-input multi-output (MIMO) are used, to analysis dynamic behavior of PMSG-based hybrid wind-tidal system, as well as the internal coupling evaluation and Multivariable Structure Functions (MSFs) is achieved, the suggested system simulated and assessed in MATLAB/Simulink. Obtained results of the control system based victor control strategy, focused on the generator-side converter shows that, it is not necessary decoupling loops in order to have sufficient control system design and performance.

The significant contribution of this work [58] is to reduce power fluctuation in the power grid due to the variation of wind speed, and the slow response of the tidal turbine to fast change, this problem can be eliminated by integrating a small-scale battery energy storage system (BESS) as shown in figure 30. Tidal turbine is connected to DC side via IGBT bi-directional converter, whereas, offshore-wind turbine is connected to DC side via diode rectifier, the proposed system simulated in PSCAD/EMTDC. Integration of BESS was successful accomplished and effective compensation achieved in the Hybrid Offshore wind Tidal generation system HOTT.

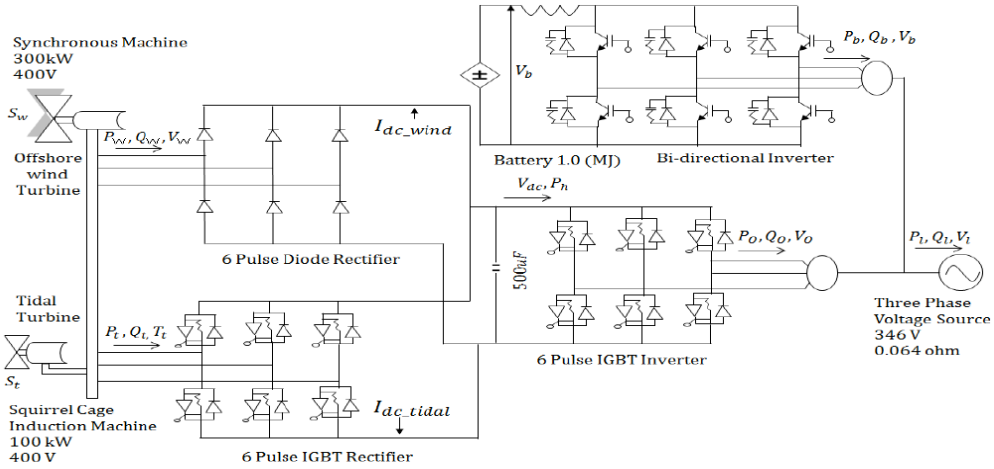

Figure 30 Hybrid System Wind-Tidal Power Generation [58]

The main objective of this study [59] is to investigate the feasibility and reliability of hybrid wind-tidal generation system with battery ESS, through analyzing its dynamic behavior and generated power using mathematical modeling approach. The suggested system under study supposed to be connected to isolated grid. The obtained results show that, the system efficiency depends on the rotor diameter and wind/tidal speed.

Authors in this paper [60] are discussed designing and optimal cost analysis of a hybrid wind and tidal power generation system, equipped with battery. The optimal design is performed using HOMER (Hybrid Optimization Model for Electric Renewable) software. According to results it is economically feasible as off-grid power connection.

This paper [61] is addressed the integration of wave energy into a conventional offshore wind farm. More specifically, to understand the effects of the co-location on both energies Depending on the following factors:

- Location and wave climate
- Co-located farms design,
- Wave propagation model.

The obtained results indicate what is called "shadow effect" yields to produce an area of lower wave height inside the offshore wind farm to increase the weather windows for O&M of the wind turbines.

A model of isolated hybrid offshore wind- diesel- tidal turbine based DFIG and DDMPMSG generators is discussed in [62] FACT device and STATCOM controller are used to manage

reactive power of the system. As a result, stability improvement, and efficiency is achieved in the prosed system.

In work [63] a standalone hybrid wind-diesel-tidal turbine based fuzzy control methodology and Unit Power Flow Controller UPFC are used to control the reactive power of the suggested systems, the proposed fuzzy controller shows better results in settling time and overshoot in the system.

Authors presented in this paper [64] steady state and dynamic performance analysis of hybrid wind/tidal farm turbines, based induction generator and superconducting magnetic storage unit (SMES), control method of frequency-domain approach, based on linearized system model, using Eigen Techniques and time-domain to control power flow, active and reactive power delivered to power grid. It can be concluded from the simulated results and under various conditions of wind and tidal speeds that PID controller has an effective power control improvement and achieved more stabilization in the system.

Authors presented in [62] a hybrid system composed of diesel-based generator, wind/PV/ battery, used to supply isolated network study focused on the dynamic performance, and effects of renewable energy sources on system stability. In plus, power generation quality simulation program called the RPM-Sim (Renewable-energy Power-system Modular Simulation) is implemented to investigate the case under study. An improvement is noted in the system stability and quality.

In this case study unit sizing [66] hybrid of wind, photovoltaic, tidal and battery as an auxiliary source simulated in MATLAB software. The main objective of this configuration is to minimize the annual cost of 20 years of operation. The Equivalent Loss Factor (ELF) has been used as an index to evaluate the system reliability level. Particle Swarm Optimization (PSO) is used for optimal sizing the system. Results shown that it has minimum cost and satisfy all constrains.

1.8.1 Advantages and Disadvantages of Hybrid Energy Systems

Advantages of Hybrid Systems

1. Some of power units can be installed very close to the end user without high risk issues, such as PV panels.
2. Reduce power cost.
3. Endless resources.

4. It is possible to be installed as a part of industrial process to exploit their wastes and used for power generation.
5. Reduce GHG emission.
6. Safe to environment.

Disadvantages of Hybrid Systems

Despite their significant benefits to the environment and great long-term potential for sustainable energy development, hybrid RE systems have some disadvantages, which make barriers to employ this source of energy; some inconvenient points are listed hereafter:

1. Not all resources available in everywhere, i.e. (in the north sun resources not available as in the south while wind resources available more in the north).
2. More complex to be controlled.
3. Generated unstable power according to the resources situation.
4. A storage system is essential for overcoming the problem of power fluctuation in the grid.
5. Sometimes one power unit is not sufficient to provide the required power so hybrid system is needed.
6. It is not easy to be integrated with the general electrical network.

1.9 Power Management Strategies Based on Energy Storage Technologies-Review For Future Implementations in Real –Time Emulators

In GREAH Laboratory researchers have developed real time emulators for wind system, figure 31, and for tidal hybrid systems figure 32 [67-68]. *More details in appendix A*

In order to optimize the generated power studies, energy storage units must be implemented.

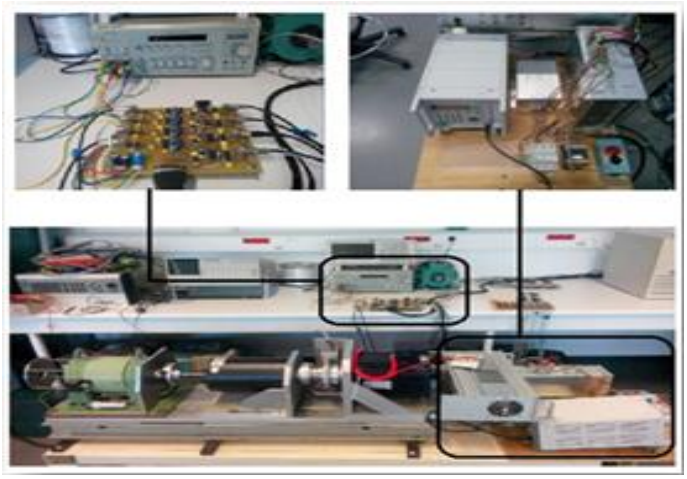

Figure 31 Wind Emulator in GREAH

It's considered that, this development should be done firstly by studying the new storage technologies that could be implemented in the emulator structure.

Figure 32 Tidal Emulator in GREAH

"Electrical Energy Storage project team" this "White" paper [69] has been prepared by Special Working Group on technology and market watch, in the IEC Market Strategy Board, with a contribution from the "*Fraunhofer Institut für Solare Energie systeme*". This paper treated the main three roles of ESS, in order to improve power quality by maintaining frequency and voltage, reduce electricity cost and improve the reliability of power supply, also this paper discussed in brief, present and future market needs for EES technologies, reviews their technological features.

While in [70] an up-to-date technical review for different types of ESS has been presented. Operation principle of each storage technology, advantages, disadvantages and main applications explained when integrated with power systems.

Authors in [71] addressed intensively ESS through the state-of-the-art technologies available, and where they would be most fit in a power generation and distribution system. As well as, an overview of the main operation principles, performance features the up-to-date research and development of most interesting EES technologies, and ESS classification based on the type of energy stored is illustrated. Finally, an overall comparison and potential analysis of reviewed application technologies are presented.

Another research [72] also discusses the multi types of storage technology, the development trend and the different applications of storage technology in the power system. Moreover, the need to store energy, various types of storage techniques and their field of application is described [73]. Nevertheless, characteristics and comparison is presented, in order to determine the most

appropriate technique for each type of application. Furthermore, integration of energy storage systems within renewable resources specifically wind resource is demonstrated in [74] 1MWh of time, 1 to 9 hours of high and low wind energy is simulated. However, the main objective of this research is to find characteristics and the most suitable type of energy storage system, which can be used with such power generation system. The final result of this work shows that, 67.80% of energy gained in high wind energy scenario, whereas 19% stored in low wind energy scenario.
Also, another research [75] in various energy storage technologies are analyzed and compared to marine application, emphasize is given to the role of energy storage systems for reducing power fluctuation in renewable energy sources.

1.9.1 History of Energy Storage Systems

Thermal energy storage system TESS is one of the oldest forms of energy storage systems in the world where ice is harvested for food preservation and cooling purposes, in China cold water was injected into an aquifer. Subsequently, it was noted that water had maintained it temperature for long period of time [76] Pumped hydro energy storage systems PHS has existed for a long time – the first pumped hydro storage plants were used in Italy and Switzerland in the 1890s.
The Wallace Dam Pumped Hydro Project was placed in full commercial operation in December 1980. In 1999 first seawater pumped hydro plant was built in Japan (Yanbaru, 30 MW) [69].
First fuel cell of about 2000 years old was discovered, near Baghdad, Iraq and it was first described by German archaeologist Wilhelm Koning. Then, the first step began when Emile Alphonse Faure invented and patented the so-called sticky plates in 1880; large scale production of lead-acid batteries was developed.
The next step was to increase storage capacity and electric power in battery. The most common used types of batteries Lead-acid battery invented by Gaston Plante in 1859 at France and it is the oldest and most widely used. Flow Battery FB invented by Lawrence Thaller in 1976 [77]. Hereafter summarized history of batteries in table 4 [78].

The first energy storage program was an integration of batteries with photovoltaic and wind energy systems in 1978, titled “Batteries for Specific Solar Applications” [79].

Table 4 History of Batteries

Developer / Inventor	Country	Year	Invention
Luigi Galvani	Italy	1786	Animal Electricity
Alessandro Volta	Italy	1800	Voltaic Pile
John F. Daniell	Britain	1836	Daniell Cell
Sir William Robert Grove	Britain	1839	Fuel Cell
Robert Bunsen	German	1842	Liquid electrodes to supply electricity
Gaston Plante	France	1859	Lead Acid Battery
Georges Leclanche	France	1868	Leclanche Cell
Thomas Alva Edison	United states	1901	Alkaline/Accumulator
T.A. Edison & Waldemar ungner	U.S.A & Sweden	1895-1905	Nickel-cadmium / nickel-iron
Andre		1930	Silver/oxide zinc cell

1.9.2 Role of Energy Storage Units in Power System

The Energy Storage Systems (ESS) is a key component in the electrical generation and stability, energy storage is one of the features of this century, where the need of energy increasing dramatically. Electrical interruption or its instability is one of the big challenges at all levels of life and may cause a death to a patient in Intensive Care Unit (ICU) or big losses in business. From this point of view, the need for storing energy becomes very essential to save lives and money. Also, using energy storage system will decrease the gas combustion hence the gas emission and reducing the environment pollution. The following sections show the contribution of energy storage systems in power demand and generation for different periods of time during the day [80].

As shown in Figures 33&34, using ESS will improve the performance of power generation system from first step of power generation, power transmission and finally the end user, these attractive vales that can be added by the ESS such as: i) reduce generation cost during peak demand periods, (ii) maintain continuous and flexible supply, (iii) management in power generation, (iv) improving power quality/ reliability, (v) help insertion of smart power grids.

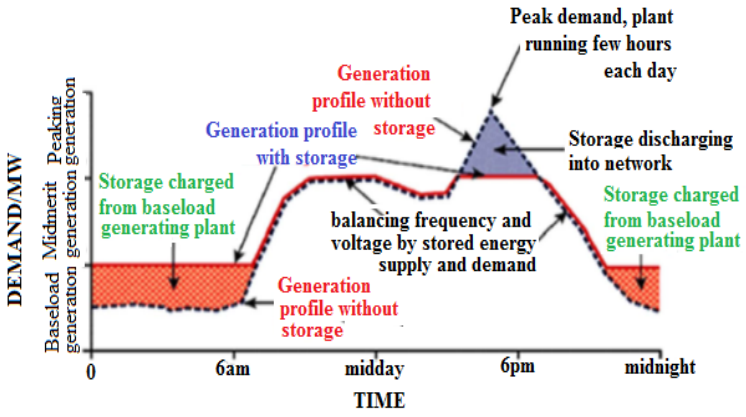

Figure 33 Effect of energy storage system in power generation and consumption [81]

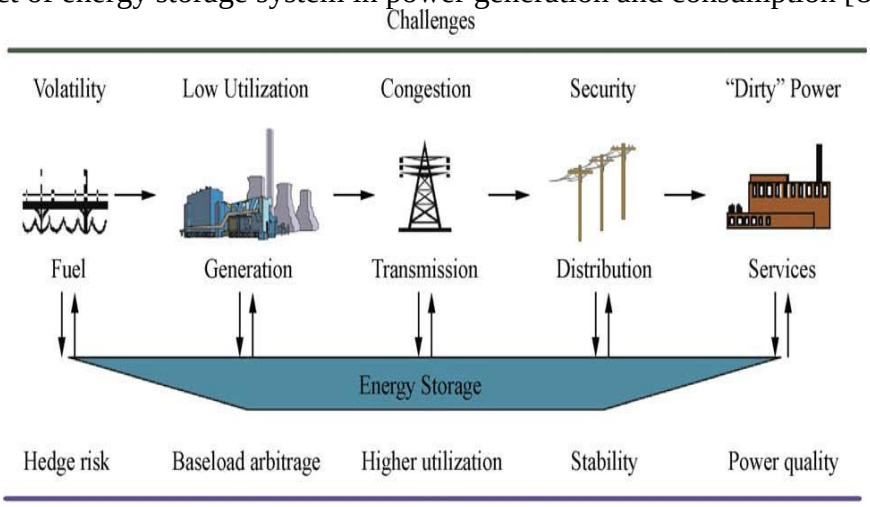

Figure 34 Application of ESS in power system [81]

Batteries are classified as small-scale storage systems in low distribution system. More than 64% of the utilized capacity of batteries is used is take place in the emergency units in the hospitals. Besides that, several battery systems (19%) are located in the office building as show in figure 35. With regard to the energy storage market, the high percentage (99%) capacity of installed storage is provided by plants of pumped hydroelectric as in figure 36 [82].

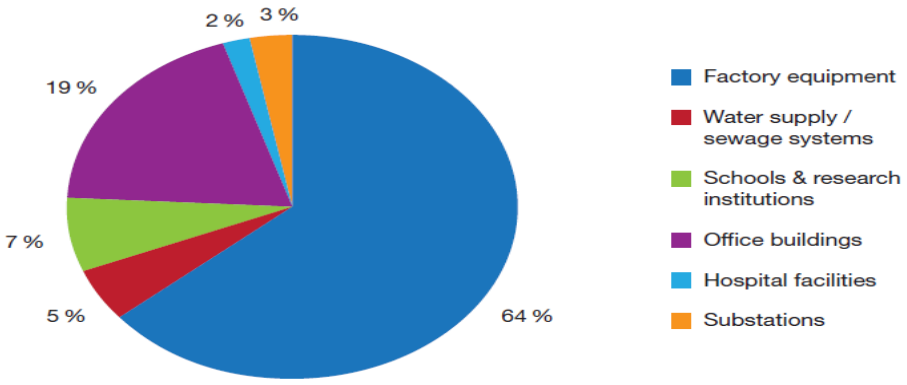

Figure 35 Utilization of Battery as ESS [82]

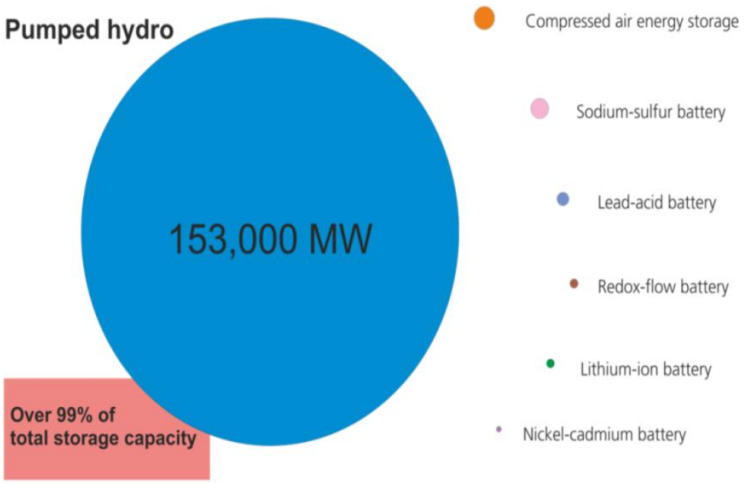

Figure 36 Installed Capacity of ESS [82]

1.9.3 Basic Theory of Energy Storage Systems

Thermal Energy Storage Systems TES

Thermal energy storage (TES) is process of stocking excessive energy in a form of heat, by heating or cooling a storage medium so that the stored energy can be used later for heating and cooling applications and power generation. TES systems are used particularly in buildings and industrial processes [83], energy can be stored by means of TES depends on two basic principle, sensible heat (e.g. water, rock) and latent (e.g. water/ice, salt hydrates) [84].

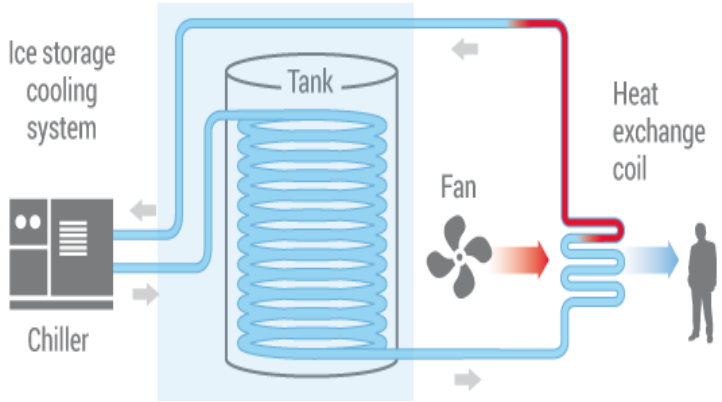

Figure37 Thermal ESS [85]

Main thermal storage techniques:

- Sensible Thermal Energy Storage
- Underground Thermal Energy Storage (UTES)
- Phase Change Materials for TES
- Thermal Energy Storage via Chemical Reactions[86]

Pumped Hydro Storage System PHESS

The PHS considered as a large scale storage unite represents about 99% of worldwide storage capacity, the main idea of PHES is to pump and store water at high levels during off-peak periods, and reuse it to operate power generation turbines during peak periods as shown in Figure 36. In another ward, store electric energy in another form of energy "hydraulic potential energy". Pumping and generating generally follow a daily cycle but weekly or even seasonal cycling is also possible with larger PHES plant [86].

The overall efficiency of this type of ESS can be determined by finding out the ratio of the energy used to pump up the water and produced energy. In addition, the period of storing and production is an important factor. The following two expressions used to find out the efficiency of the system: [87]

$$E_{pumping} = \frac{\rho.g.h.v}{\eta_p} \qquad (2.5)$$

$$E_{generator} = \rho.g.h.v.\eta_g \qquad (1.6)$$

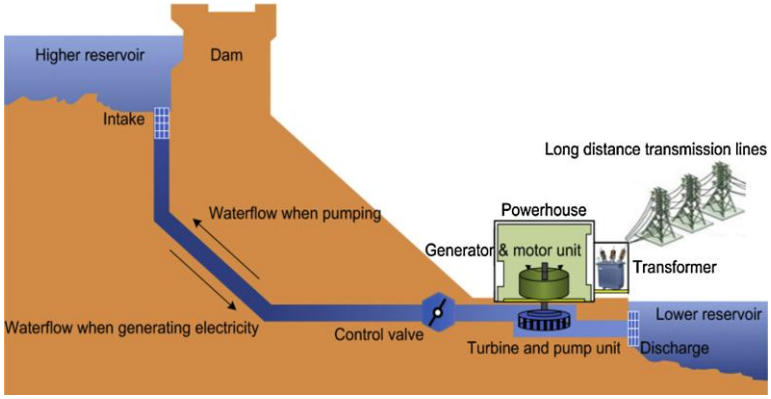

Figure 38 Pumped Hydro Storage System

Flywheel Energy Storage System FESS

In a very simple explanation the flywheel is made of a metal in cylindrical form, supported by magnetic bearing located in vacuum chamber to reduce friction losses and connected to a rotor of generator/motor as in figure39. Kinetic energy can be stored in the flywheel in rotation form [88]. The amount of stored energy depends on the inertia and speed rotation of the flywheel. The energy absorbed and released by a rotating flywheel rotor [89]. The kinetic energy that can be stored in flywheel according to the following equation:

$$E = \frac{1}{2} I.\omega^2 \qquad (1.7)$$

Where:

I: inertia momentum of the flywheel

Ω: angular speed

There are some factors affect the maximum energy that can be stored in flywheel system, these factors can be expressed in the following relation:

$$E_{sp} = K_s \frac{\sigma_m}{\rho} \qquad (1.8)$$

Where:

Esp: maximum specific energy density; σm: Maximum tensile strength of flywheel material

ks: Shape factor ; ρ: Density of the flywheel material [90]

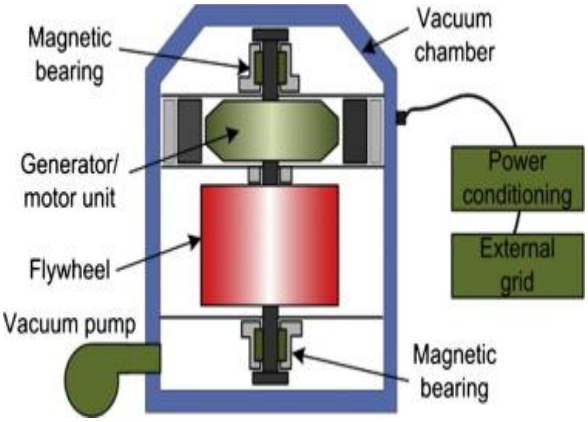

Figure39 Flywheel Energy Storage System FESS [71]

Compressed Air Energy Storage System (CAES)

The intermittency of wind is main reason to use this technology, the excessive electrical energy used to operate series of air compressors, to store electrical energy in a form of compressed air in reservoirs or over ground tanks, in order to reuse it later in peak demand figure 40.

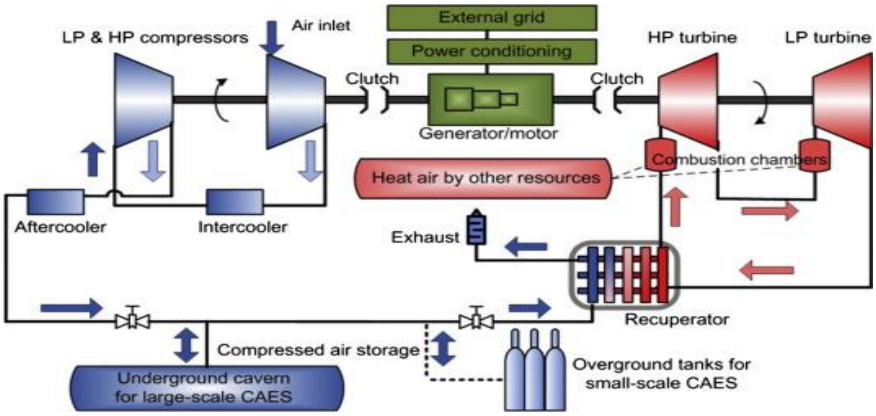

Figure 40 Compressed Air Energy Storage System CAES [71]

Batteries

A battery storage system mainly composed of electrode, anode and electrolyte figure 41 which can be at solid, liquid or ropy/viscous states, electrical energy can be stored in a form of controlled chemical reaction which reproduces electricity when it is needed "bi-directional convert of energy" [71]. In this category of ESS there are main common types of Batteries namely (Lead-acid battery, Sodium Sulfur battery, Lithium ion battery, Metal air battery, Flow battery) [91] [92].

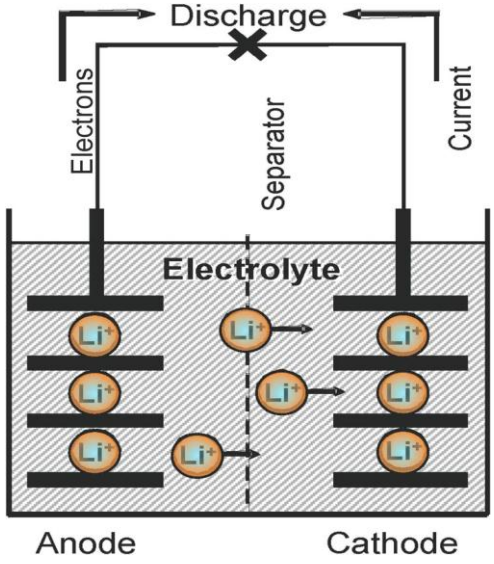

Figure 41 Battery Schematic [81]

Superconducting Magnetic Energy System SMES

An SMES device is a dc current device that stores energy in the magnetic field. The dc current flowing through a superconducting wire in a large magnet creates the magnetic field [93]. The coil is made of Niobiumtitane (NbTi) filaments and cooled below its superconducting critical temperature, one of the attractive properties of SMES that it can be fully charged and discharged in a very short of time, and high value of energy can be stored in figure 42. The energy stored in the coil, E, is given by expression [94].

$$E = \frac{1}{2} L.I^2 \qquad (1.9)$$

Where:

E: energy (W)

L: inductance (H), and

I: current (A).

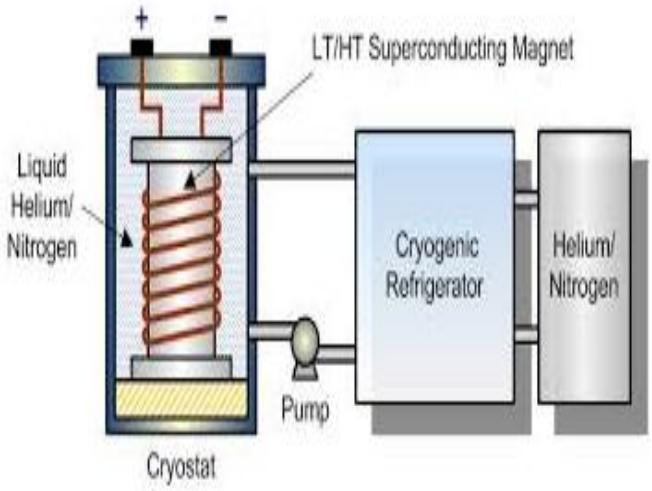

Figure 42 Superconducting Magnetic Energy System SMES [90]

Fuel Cell Energy Storage System FCESS

Fuel cell based on the separation of water into its original components Hydrogen and Oxygen, as shown in figure 43. Hydrogen is used to generate electricity; also it can be transported in portable cylinders or tanks and stored for long time [95].

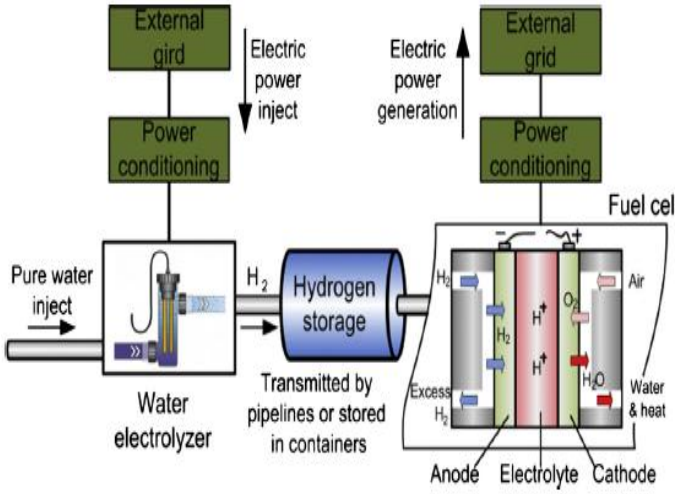

Figure 43 Hydrogen Storage and Fuel Cell [71]

1.9.4 Classification of Energy Storage Systems

Electrical energy storage systems are classified into five categories according to the energy storage principle as indicated in the following block diagram. Also, storage systems can be classified according to: the period of charging and discharging; long period and short period as high-energy batteries, like sodium sulfur battery, like super-capacitors respectively. In addition, another classification regarding their load capacity (low, medium and high storage capacity).

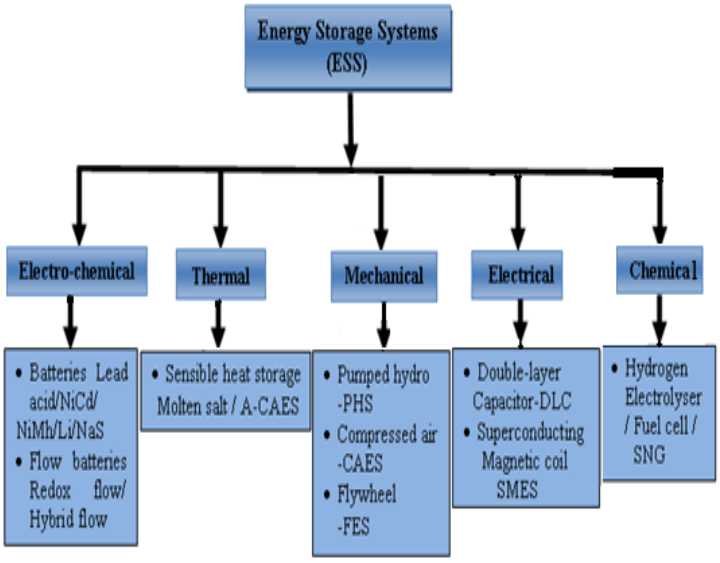

Figure 44 Classification of EES

1.10 Application of Energy Storage Systems

Electro-chemical Energy Storage Systems

Hereafter, review - papers [96-98] focused on types, uses and impact of energy storage systems on renewable energy systems, also addressed and evaluated some of drawbacks, facing the integration of energy storage units with the grid. Furthermore, provide perspectives on future directions. Found that, battery systems can offer a number of high-value opportunities and lower costs can be obtained.

Battery Storage System BSS in figure 45,considered as main part, for efficiency improvement of water desalination unite, supplied by renewable resource PV-wind turbine power generation system to eliminate the intermittently of required electrical power.

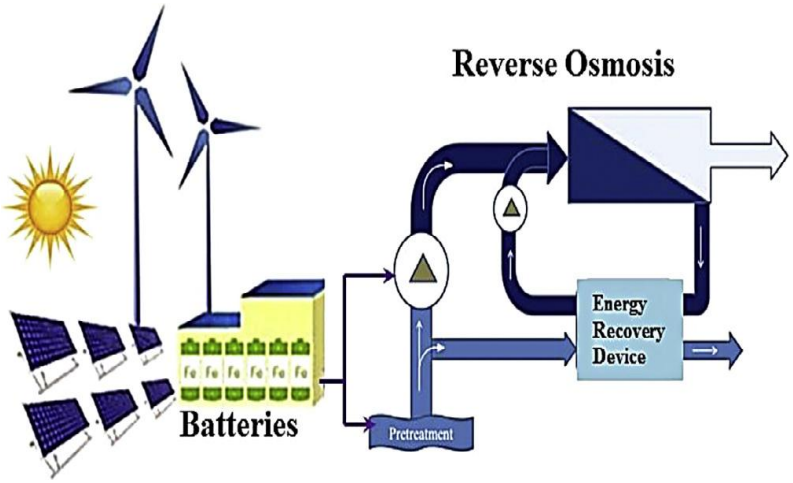

Figure 45 Wind and Solar Cells with Batteries [97]

Thermal Energy Storage Systems

Papers [99-101] devoted to study thermal properties of materials that can be used as storage energy units, i.e. storing energy in a form of heat or cold. Results show that, storing energy in this form is suitable for long-term, more efficient and less expensive than the other forms of energy storage systems. But, it is more complex to be implemented and expensive. Figure 46 demonstrates thermal energy storage systems in France, used to provide higher storage energy, Phase Changing Materials (PCMs).

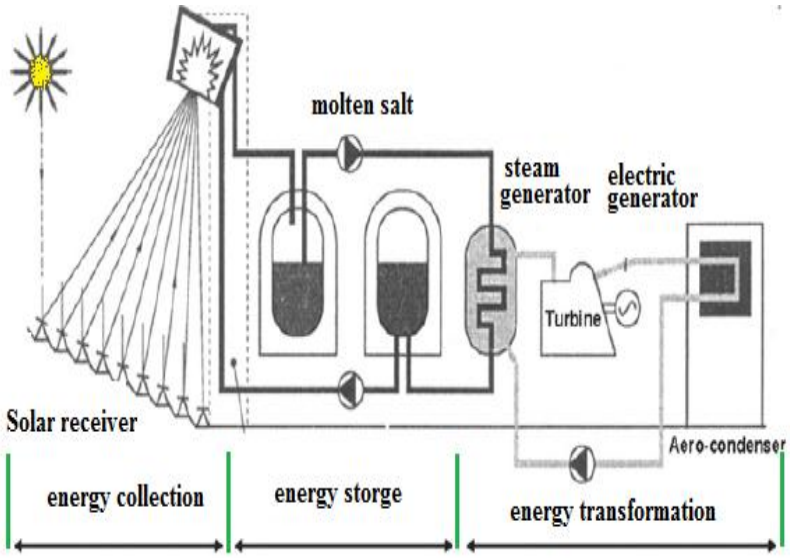

Figure46 Thermal Station in France

Mechanical Energy Storage System

Energy can be stored in a form of potential or kinetic energy. So, it can be reused later to operate turbines to produce electrical power. However, three main ways are used to store energy in mechanical form namely [102-107];

- Pumped Hydro Storage System (PHSS), used for long periods compensation.
- Flywheel Energy Storage System (FESS), used for short period compensation.
- Compressed Air Energy Storage System (CAESS), used for medium period compensation.

Cost is the main common disadvantage. Whereas, location and slow of response for pumped hydro storage system, but has long period of compensation.

Electrical Energy Storage Systems

Researches [108-110] provide an overview of Electrical Energy Storage Systems based Superconducting Magnetic Energy Storage and its applications in electrical energy systems. The electrical energy systems are classified into three main groups:

- Thyristor-based SMES,
- Voltage-source converter- based SMES, and
- Current-source-converter-based SMES.

Due to the instability of renewable energy resources, ESS is needed to be used in order to mitigate power fluctuation in power systems.

Chemical Energy Storage Systems

Two types of Chemical Energy Storage Systems (CESS), Fuel Cell (FC) and Ultra-Capacitor (UC) have been the subject of many papers and case studies [111-118]. In General, fuel cells are used as an energy resource hybrid with other resources to overcome the problem of power fluctuation in a micro-grid renewable power system, and to produce hydrogen gas when electrical energy is not demanded, thus store the generated gas in order to operate power units later. Whereas, Ultra-Capacitor used to store electrical energy in chemical reaction form

The common advantage of such an energy storage system it is portable and responds fast to power fluctuation. However, one notable disadvantage for a fuel cell that it is an explosive and flammable.

1.11 General Comparisons of Different Energy Storage Systems

The comparison between energy storage systems depends on the purpose of energy storage, and frequency of use as well as the location. Actually, it is difficult to find storage unit that meet all the power system requirements. Anyway, there are common factors to compare: Costs, density of energy, specific power, recyclability, Accessibility, durability energy efficiency [119].

Summary of advantages and disadvantages of energy storage technologies detailed in table 5.

Table 5 Main Advantages and Disadvantages of EES

Energy Storage System	Advantages	Disadvantages
Electrochemical	High efficiency	short storage period
Mechanical	High capacity and power	high costs (initial investment) and Special site requirement
Chemical	Long storage period	Low efficiency
Thermal	High efficiency and long lifetime	High production cost, Requires special charging circuit
Electrical	High efficiency and long lifetime	Low Energy Density

The intensive technical comparison for several EES systems has shown in table6.

Table 6 Comparison of Technical Characteristics of EES

ESS	Wh/kg	Power rating	Discharge time	Suitable storage duration	Life time (years)	Capital cost
PHES	0.5–1.5	100–5000 MW	1–24 h+	Hours–months	40–60	600–2000
CAES	30–60	5–300 MW	1–24 h+	Hours–months	20–40	400–800
Lead-acid	30–50	0–20 MW	Seconds – hours	Minutes–days	5–15	300–600
Fuel cell	800–10,000	0–50 MW	Seconds –24 h+	Hours–months	5–15	10,000+
Solar fuel	800–100,000	0–10 MW	1–24 h+	Hours–months	–	–
SMES	0.5–5	100 kW–10 MW	1 ms– 8 s	Minutes–hours	20+	200–300
Flywheel	10–30	0–250 kW	1 ms–15 min	Seconds–minutes	~15	250–350
Super capacitor	2.5–15	0–300 kW	1 ms – 60 min	Seconds–hours	20+	100–300

1.12 Research Objectives and Contributions

Throughout previous studies and researches conducted in renewable resources particularly in hybrid wind and tidal power systems and energy storage systems, it turns out that all the solutions proposed to overcome the problem of intermittency of the generated electrical power lies in two solutions:

1. Use the energy storage system to compensate for the shortage and overcome the interruption of electrical power in the network.
2. Hybridization of wind and tidal turbines electrically (electrical coupling only); in other words, the generated electrical power by the generators are combined, this connection is limited at two levels, electrical level connection, and DC-Link connection as its shown above.

Anyway, the analysis of the previous researches and studies show that these solutions are considered as conventional solutions. Therefore, in this thesis, we will study a new concept of hybridization called (electromechanical coupling), where both wind and tidal turbines are connected on the same axis with the electric generator. in addition, designing a control strategy to optimize the functional operation of both turbines based on the functional similarities between them. Using HIL simulation concept; along with time acceleration method to reduce the simulation time.

The objectives of the research and scientific contributions can be summarized as following:

Research Objectives

1. Development of software simulation for offshore hybrid wind/tidal power generation system :
   A- Electromechanical coupling design for hybrid wind and tidal systems horizontal axis.
   B- Designing unified control system adapted with the suggested system
2. Using HIL Simulation to:
   A- Execute and investigate the performance of hybrid wind-tidal power system based electromechanical concept
   B- Reducing simulation time based on time acceleration concept

Contributions

- Developed software simulation based on the concept of electromechanical coupling concept, adapted to the power level of the HIL simulator available in GREAH laboratory
- Utilize the acceleration time concept in software simulation
- Parameters of the Doubly-Fed Induction Generator are identified experimentally.
- Unified controller to control the two turbines (wind and tidal)

1.13 Conclusion

Finally, this chapter included: wind energy (speed and distribution), tidal resource, history of wind and tidal turbines, as well as, operation principle and construction of wind/tidal conversion chain, an intensive and comprehensive study of state of the art of hybrid power generation systems. Moreover, unit sizing and configuration are addressed. Energy storage systems and its impact on power generation, and how it can be integrated in power generation systems. Furthermore, the advantages and disadvantages of the hybrid power system, in addition to a comparison between energy storage systems. Last but not least, wind and tidal hardware simulators available in GREAH are presented.

References

[1] Pinson, Pierre. Estimation of the uncertainty in wind power forecasting. Paris : Ecole des Mines de Paris, 2006.

[2] Johnson, Gary L. Wind Energy Systems. Kansas State University: Prentice-Hall, 2001.

[3] RIOUCH, Tariq. "Commande d'un aérogénérateur en vue d'optimiser l'injection d'énergie au réseau électrique''. Fès, Maroc: University of Sidi Mohamed Ben Abdallah, 2014.

[4] Pugh, David T. Tides, Surges and Mean Sea - Level. New York: John Wiley & Sons, 1996. 0 471 91505 X.

[5] Caraiman G. "Etude de la transposition des similitudes éolien-hydrolien en vue de la conception et du développement d'un émulateur électromécanique de turbine hydrolienne, thesis Université du Havre, 2011.

[6] Deborah Greaves, Gregorio Iglesias. Wave and Tidal Energy. Wiley & Sons, 2018.

[7] T.K. Subramaniam, R. Premanand. A Device to Harness the Power of the Tides and Waves off Every Coast. Environmental Engineering and Science. 20, October,2015

[8] Ocean energy project spotlight Investing in tidal and wave energy.

[9] Camille D. "L'éolien offshore en Europe: état des lieux, politiques, impacts''. Lectures of seminars, University of Lyon, 2010, France.

[10] Trevor M. Letcher, Wind Energy Engineering a hand book for onshore and offshore wind turbines, Academic Press is an imprint of Elsevier, 2017, 525 B Street, Suite 1800, San Diego, CA 92101-4495, United States.

[11] http://www.europe-rhonealpes.eu/wordpress/wp-content/uploads/2010/12/expoeurope-science-reduit1.pdf

[12] http://tpeeoliennefoucauld20092010.wifeo.com/1-les-eoliennes-au-cours-dutemps.php

[13] http://www.europe-rhonealpes.eu/wordpress/wp-content/uploads/2010/12/expoeurope-science-reduit1.pdf

[14] http://tpeeoliennefoucauld20092010.wifeo.com/1-les-eoliennes-au-cours-dutemps. php

[15] http://www.info-eolien.com/historique.html

[16] R. H. Charlier and C. W. Finkl, Oceain Energy Tidal and Tidal Power, Berlin: Springre, 2009.

[17] Kiho S., Shiono M., Suzuki K., "The power generation from tidal currents by darrieus turbine" Renewable energy, 1996.

[18] Adaramola, Muyiwa. Wind Turbine Technology: Principles and Design. s.l.: Apple Academic Press, February 24, 2014. ISBN 9781771880152.

[19] https://upload.wikimedia.org/wikipedia/commons/thumb/0/09/Water_turbine_%28en_2%29.svg/560px-Water_turbine_%28en_2%29.svg.png

[20] Lift and Drag. http://people.bu.edu/dew11/liftanddrag.html. [Online] Boston University.

[21] Small Vertical Axis Wind Turbines for Energy Efficiency of Buildings. Casini, Marco. 10.7763/JOCET.254, Sapienza University of Rome, Italy: Journal of Clean Energy Technologies, 1, January 2016, Vol. 4.

[22] http://www.bluenergy.com/.

[23] Group, Planning and Environmental Policy. Draft Planning Policy Statement 18 Renewable Energy. Northern Ireland's Landscapes: Department of Environment, 23 November 2007. Draft PPS 18.

[24] Reinemann, Doug. Jenny Heinzen. How Do Wind Turbines Generate Electricity? University of Wisconsin-Madison: Midwest Rural Energy Council (MREC). 2014.

[25] Ross, D.A. Introduction to Oceanography. New York: HarperCollins, 1995. pp. 236-242.

[26] Meyers, C Bracken. Alternative energy. Centurion energy. [Online] 13 Dec. 2013. [Cited: 14 02 2018.] http://www.centurionenergy.net/types-of-wind-turbines.

[27] Magedi Moh. M. Saad, Norzelawati Asmuin, Comparison of Horizontal Axis Wind Turbines and Vertical Axis Wind Turbines, IOSR Journal of Engineering (IOSRJEN), ISSN (e): 2250-3021, ISSN (p): 2278-8719, Vol. 04, Issue 08 (August. 2014), ||V2|| PP 27-30.

[28] https://colortheearthturquoise.files.wordpress.com/2012/03/horizontal-and-vertical-axis-wind-turbines-1.pdf

[29] Matthew Burger, Sean Colella, Sean Quinlivan,Joel Rousseau. Construction of a Wind Turbine Project in the Town of Florida, MA. German: Worcester Polytechnic Institute, 2007.

[30] International Energy Outlook 2016 with Projections to 2040. 2016.

[31] Farzam Nejabatkhah, Yun Wei Li. Overview of Power Management Strategies of Hybrid AC/DC Microgrid. ieee transactions on power electronics. 22 Dec 2014, Vol. 30, pp. 7072 - 7089.

[32] Manfred Pochacker, Tamer Khatib, Wilfried Elmenreich. The Microgrid Simulation Tool RAPSim: Description and Case Study. 2014.

[33] Sunanda Sinha, S.S. Chandel. Review of software tools for hybrid renewable energy systems. Science Direct. Renewable and Sustainable Energy Reviews, 2014, Vol. 23.

[34] Muhammad Shahzad Aziz, Umair Saleem, Ehsan Ali, Khalid Siddiq. A review on bi-source, off-grid hybrid power generation systems based on alternative. Journal of Renewable and Sustainable Energy 7. 2015, AIP Publishing.

[35] K. ShivaramaKrishna, K.SathishKumar. A review on hybridr enewable energy systems. Renewable and Sustainable Energy Reviews. 2015, Elsevier, pp. 907–916.

[36] Md. Ibrahim, Abul Khair, Shaheer Ansari. A Review of Hybrid Renewable Energy Systems for Electric Power Generation. Journal of Engineering Research and Applications. 2015, Vol. 5, 8, pp. 42-48.

[37] M. H. Nehrir, C. Wang, K. Strunz, H. Aki, R. Ramakumar, J. Bing, Z. Miao, and Z. Salameh. A Review of Hybrid Renewable/Alternative Energy Systems for Electric Power Generation: Configurations, Control, and Applications. ieee transactions on sustainable energy, Vol. 2, NO. 4. Octorber 2011, pp. 392-403.

[38] Renewable energy in Europe 2016. Recent growth and knock-on effects. s.l.: European Environment Agency. 1977-8449.

[39] International Energy Outlook 2016 with Projections to 2040. 2016.

[40] Farzam Nejabatkhah, Yun Wei Li. Overview of Power Management Strategies of Hybrid AC/DC Microgrid. ieee transactions on power electronics. 22 Dec 2014, Vol. 30, pp. 7072 - 7089.

[41] Y. Jaganmohan Reddy, Y. V. Pavan Kumar, K. Padma Raju, and Anilkumar Ramsesh. Retrofitted Hybrid Power System Design With Renewable Energy Sources for Buildings. ieee transactions on smart grid. Vol. 03 April 2012.

[42] Changjie YIN, Manuela Sechilariu, ‘’Impact of diesel generator operating modes on standalone DC microgrid and control strategies implying supercapacitor’’,PhD thesis, university of Compiègne, avenues, 23 January 2018.

[43] Design and optimal sizing of hybrid PV/wind/diesel system with battery storage by using DIRECT search algorithm. Lu Zhang, George Barakat, Adnan Yassine. Novi Sad, Serbia: ieee, 2012. 13256238.

[44] Optimum sizing of wind-battery systems incorporating resource uncertainty, A. Roy, S. B. Kedare, and S. Bandyopadhyay, s.l.: Appl. Energy, 2010, Vol. 8, pp. 2712-2727.

[45] M.L.Rahman, S.Oka, andY.Shirai. Hybrid offshore wind and tidal turbine power system to compensate for fluctuation. T.Yaoed, Zero-Carbon Energy Kyoto 2010, Green Energy and Technology. Spriger-2011.

[46] Mohammad Lutfur Rahman, Yasuyuki Shirai. Design and analysis of a prototype HOTT, generation system. BUP JOURNAL. 2012.

[47] Li Wang, Chao-Nan Li, Yi-Ting Chen, Yi-Ting Kao, Vina, and Sheng-Wen Wang. Analysis of a Hybrid Offshore Wind and Tidal Farm Connected to a Power Grid Using a Flywheel Energy Storage System. ieee. 2011.

[48] Qin, Chuan, et al., et al. A Coordinated Control Method to Smooth Short-Term Power Fluctuations of Hybrid Offshore Renewable Energy Conversion System (HORECS). Power Tech, 2015 ieee Eindhoven / http://ieeexplore.ieee.org/. 2015, pp. 1 - 5.

[49] S.Mousavi, G. An autonomous hybrid energy system of wind/tidal/microturbine/battery storage. elsevier/ Electrical Power and Energy Sytems. 2012, pp. 1144-1154.

[50] Stevenson Pierre, Cristian Nichita, Jérome Brossard, Concept development of real time emulators for offshore wind power (OWP) and tidal current power (TCP) hybrid system. ieee. 2013.

[51] Caraiman George. Etude de la transposition des similitudes Eolien Hydrolien en vue de la Conception et du Développement D'un Emulateur Electromeanique de Turbine Hydrolienne. Le Havre : s.n. 2011.

[52] Sharaf, T. Aboul-Seoud A. M. Utilization of the Modulated Power Filter Compensator Scheme for a Grid Connected Rural Hybrid Wind/Tidal Energy Conversion Scheme. ieee Electrical Power & Energy Conference. 2010.

[53] El-Hawary, Hamed H. H. Aly and M. E. Modeling of Offshore Wind and Tidal Current Turbines for Stability Analysis. Proceedings of the World Congress on Engineering and Computer Science 2013 Vol I WCECS 2013, 23-25 October, 2013, San Francisco, USA. 2013.

[54] Yao Da, and Alireza Khaligh. Hybrid Offshore Wind and Tidal Turbine Energy Harvesting System with Independently Controlled Rectifiers. Industrial Electronics, 2009. IECON '09. 35th Annual Conference of ieee. 2009, pp. Pages: 4577 - 4582.

[55] Rahman, Mohammad Lutfur, and Yasuyuki Shirai. DC connected hybrid offshore-wind and tidal turbine generation system. Zero-Carbon Energy Kyoto 2009, 2010, Springer Japan, pp. 141-150.

[56] YaJun Fan, AnLe Mu,Tao Ma. Modeling and control of a hybrid wind-tidal turbine with hydraulic accumulator. Journal homepage: www.elsevier.com/locate/energy. 2016, pp. 188-199.

[57] Carlos E. Ugalde-Loo, Luis A. Amezquita-Brooks,Eduardo Liceaga-Castro,Jesus Lic eaga-Castro. Analysis and Efficient Control Design for Generator-side Converetrs of PMSG-Based Wnd and Tidal Turbines. Power Systems Computation Conference (PSCC). 2014, ieee Conference Publications, pp. 1-7.

[58] Mohammad Lutfur Rahman, Kazuki Nishimura, Kei Motobayashi, Shotaro Fujioka, Yasuyuki Shirai,. Characteristic analysis of small-scale BESS for HOTT generation system. Innovations in Technology Conference (InnoTek), ieee. 2014, pp. 1-9.

[59] 1M. G. Sobamowo, 2B.Y. Ogunmola, 3J. A. Ogbemhe. Analysis of dynamic behaviour and power generation of a wind-tidal system for marine environment. Nigeria: Sobamowo et al: Proc. ICCEM, 2012.

[60] Sikder, Amit Kumar, Khan, Nishat Anjum and Hoque, Aminul. Design and Optimal Cost Analysis of Hybrid Power System for Kutubdia Island of Bangladesh. 8th International Conference on Electrical and Computer Engineering. 2014, pp. 729 - 732.

[61] Perez Collazo, C., et al. Co-located wave and offshore wind farms: a preliminary case study of an hybrid array. International Conference in Coastal Engineering (ICCE). 2014.

[62] Asit Mohanty, Meera Viswavandya , Sthitapragyan Mohanty . reactive power Control and Optimisation of hybrid off shore tidal turbine with system uncertainties,. Ocean Engineering and Science. 2016.

[63] Asit Mohanty, Meera Viswavandya, Sthitapragyan Mohanty,Dillip K Mishra. Reactive Power Compensation in a Stand-alone Wind-diesel-tidal Hybrid System by a Fuzzy Logic Based UPFC. ScienceDirect / 3rd International Conference on Recent Trends in Computing. 2015, by Elsevier, pp. 1281 – 1288.

[64] Li Wang, Senior, Shiang-Shong Chen, Wei-Jen Lee,Zhe Chen,. Dynamic Stability Enhancement and Power Flow Control of a Hybrid Wind and Marine-Current Farm Using

smes. ieee transactions on energy conversion, Vol. 24, NO. 3. September 2009, pp. 626-637.

[65] Wenxia Pan, Wenzhong Gao, Eduard Muljadi, The dynamic performance and effect of hybrid renewable power system with diesel/wind/PV/battery. International Conference on Sustainable Power Generation and Supply. 2009, ieee, pp. 1-5.

[66] Sadeh, M. Bashir J. Size optimization of new hybrid stand-alone renewable energy system considering a reliability index. Environment and Electrical Engineering, 11th International Conference on. 2012, pp. 989 - 994.

[67] Cristian Nichita, Mohamed Ashglaf, Jerry Tekobon "Etude préliminaire d'un concept de couplage éolien-hydrolien utilisant des similitudes fonctionnelles d'emulation en temps réel". International Congress on Energy and Environment, 18-19 March 2018, Fez, Maroco.

[68] Jerry Tekobon, « Système multi physique de simulation pour l'étude des réseaux électriques intégrant la production distribuée de 'énergie basée sur le couplage éolien offshore – hydrolienne », Thèse de l'Université Le Havre Normandie, décembre 2016.

[69] Alamri B. R. and Alamri A. R., "Technical review of energy storage technologies when integrated with intermittent renewable energy," in International Conference on Sustainable Power Generation and Supply, Nanjing, 2009.

[70] Xing Luo,Jihong Wang, Mark Dooner, Jonathan Clarke "Overview of current development in electrical energy storage technologies and the application potential in power system operation," Applied Energy Volume 137, no. elsevier, p. 511–536, 2015.

[71] Xuesong Zhou, Yitong Lin, Youjie Ma "The overview of energy storage technology", ieee International Conference Mechatronics and Automation (ICMA), pp. 336-338, Aug 2014.

[72] H. Ibrahima, b, A. Ilincca, J. Perron "Energy storage systems—Characteristics and comparisons," Renewable and Sustainable Energy Reviews, p. 1221–1250, 2008.

[73] Andor Daniela, "Energy Storage Systems for Wind Energy Integration. Technology, Applications, and Benefit Analysis," university de la Rioja, 2015.

[74] Zhibin Zhou, Mohamed Benbouzid, Jean Frédéric Charpentier, Franck Scuiller and Tianhao Tang"Energy Storage Technologies for Smoothing Power Fluctuations in Marine Current Turbines," http://ieeexplore.ieee.org/, 2012.

[75] Morofsky, Edward, Thermal Energy Storage for Sustainable Energy Consumption, Quebec: Springer, 2007.

[76] Bent Sørensen- Roskilde University, Denmark- Roskilde University, Solar Energy Storage, Academic Press, Jun 3, 2015.

[77] Gogus, Yalcin, energy storage systems, vol. volum III, Oxford: EOLSS, 2009.

[78] «http://www.sandia.gov/ess/energy-storage-systems-history/,» [En ligne].

[79] Whittingham, M. Stanley, "History, Evolution, and Future Status of Energy Storage," vol. 100, pp. 1518-1534, 2012.

[80] Haisheng Chen, Thang Ngoc Cong, Wei Yang, Yongliang Li, Yulong Ding, "Progress in electrical energy storage system: A critical review," Progress in Natural Science, vol. 19, no. ScienceDirect, p. 291–312, 2009.

[81] Christian Doetsch, Bert Droste-Franke, Grietus Mulde, Yvonne Scholz, Marion Perrin, «Electrical Energy Storage Future Energy Storage Demand,» 2015.

[82] Andreas Hauer , Zae Bayern, "Thermal Energy Storage Technology Brief," IEA-ETSAP and IRENA© Technology Brief, E 17, January 2013.

[83] Ibrahim Dincer and Marc A.Rosen, thermal energy storage systems and Applications, West Sussex: John Willy & Sons, LTD, 2002.

[84] CALMAC, 2014. [Online].

[85] J.P. Deane, B.P. O´ Gallachoir, E.J. McKeogh "Techno-economic review of existing and new pumped hydro energy storage plant," Renewable and Sustainable Energy Reviews, p. 1293–1302, 2010.

[86] J.I. San Martín, I. Zamora, J.J. San Martín V. Aperribay, P. Eguía, "Energy Storage Technologies for Electric Applications," 2011.

[87] Bjorn Bolund, Hans Bernhoff, Mats Leijon, "Flywheel energy and power storage systems," Renewable and Sustainable Energy Reviews, p. 235–258, 2007.

[88] Qianzhi Shao, Yan Zhao, Shipeng Du and Yuanzhuo Du, "A Novel Hybrid Energy Storage Strategy Based on Flywheel and Lead-acid Battery in Wind Power Generation System," International Journal of Control and Automation Vol. 8, No. 7, pp. 1-12, 2015.

[89] Malte Krack1, Marc Secanell, and Pierre Mertiny, "Rotor Design for High-Speed Flywheel Energy Storage Systems," 2011.

[90] K.C. Divya∗, 1, Jacob Østergaard1 "Battery energy storage technology for power systems—An overview," Electric Power Systems Research 97, p. 511–520, (2009).

[91] S.Ould Amrouche, D.Rekioua, T.Rekioua, S.Bacha. "Overview of energy storage in renewable energy systems", International Journal of Hydrogen Energy, Volume 41, Issue 45. December 2016, Pages 20914-20927.

[92] Mohd. Hasan Ali, Bin Wu, and Roger A. Dougal, "An Overview of SMES Applications in Power and Energy Systems," ieee transactions on sustainable energy, pp. 38-47, APRIL 2010.

[93] Edward, Barbour, "Superconducting Magnetic Energy Storage (SMES)," Energy Storage Sense. [Online].

[94] Schiller, Mark, "Hydrogen Energy Storage: A New Solution To the Renewable Energy Intermittency Problem," 2016.

[95] Bruce Dunn, Haresh Kamath,Jean-Marie Tarascon, «Electrical Energy Storage for The grid: ABattery of Choices,» Science 334, pp. 928-935, 2011.

[96] Linas Gelažanskasa, Audrius Baranauskasb, Kelum A.A. Gamagea, Mindaugas Ažubalisb, "Hybrid wind power balance control strategy using thermal power, hydro power and flow batteries," International Journal of Electrical Power & Energy Systems, pp. 310-321, 2016.

[97] Gude, Veera Gnaneswar, "Energy storage for desalination processes powered by renewable energy and waste heat sources," Applied Energy, p. 877–898, 2015.

[98] NGÔ, Christian"Stockage de l'énergie," techniques de l'ingenieur, pp. 1-27, 10 juillet 2016.

[99] Atul Sharma, V.V. Tyagi, C.R. Chen, D. Buddhi, "Review on thermal energy storage with phase change materials and applications," Renewable and Sustainable Energy Reviews Volume 13, Issue 2, p. 318–345, 2009.

[100] Francis Agyenim, Neil Hewitt, Philip Eames, Mervyn Smyth, "A review of materials, heat transfer and phase change problem formulation for latent heat thermal energy storage systems (LHTESS)," Renewable and Sustainable Energy Reviews volume 14, p. 615–628, 2010.

[101] M.R.H.Asif, M.T.Iqbal, "Diesel consumption in a high penetration remote hybrid power system with a pumped hydro and battery storage," Electrical Power & Energy Conference (EPEC), 2013.

[102] Tao Ma, Hongxing Yang, Lin Lu, Jinqing Peng, "Technical feasibility study on a standalone hybrid solar-wind system with pumped hydro storage for a remote island in Hong Kong," Renewable Energy, pp. 7-15, 2014.

[103] S Ould Amrouche, Djamila Rekioua, Toufik Rekioua, Seddik Bacha "Overview of energy storage in renewable energy systems", International Journal of Hydrogen Energy, pages 20914-20927, 7 December 2016.

[104] Henrik Lund, Georges Salgi, "The role of compressed air energy storage (CAES) in future sustainable energy systems," Energy Conversion and Management, p. 1172–1179, 5 March 2009.

[105] Xing Luo, Jihong Wang, "Overview of current development in compressed air energy," European Energy Research Alliance, Coventry CV4 7AL, UK, 2013.

[106] Varin Vongmanee, Veerapol Monyakul, "A new concept of small-compressed air energy storage system integrated with induction generator," International Conference on Sustainable Energy Technologies, 2009.

[107] Marcelo Gustavo Molina, Pedro Enrique Mercado, "Power Flow Stabilization and Control of Microgrid with Wind Generation by Superconducting Magnetic Energy Storage," ieee transactions on power electronics, no. 3, pp. 910 - 922, 06 December 2010.

[108] Rajesh Joseph Abraham, D. Das, Amit Patra, "Automatic generation control of an interconnected hydrothermal power system considering superconducting magnetic energy storage," International Journal of Electrical Power & Energy Systems, vol. 29, 2007.

[109] Bhingare, D. K.; Virulkar, V. B., "Integration of energy storage technology and wind generator for power stabilization," Power, Automation and Communication (INPAC), International Conference, pp. 1-5, 2014.

[110] Sanjeev K Nayak, D. N. Gaonkar, "Modeling and performance analysis of hybrid fuel cell and microturbine based distributed generation system, "A review"," International Conference on Power, Energy and Control (ICPEC), ieee dconference, pp. 760-766, 2013.

[111] Dallia Ali, Ross Gazey,Daniel Aklil, "Developing a thermally compensated electrolyser model coupled with pressurised hydrogen storage for modelling the energy efficiency of hydrogen energy storage systems and identifying their operation performance issues," Renewable and Sustainable Energy Reviews, pp. 27-37, 2016.

[112] Fan Zhang, Pengcheng Zhao, Meng Niu, Jon Maddy, "The survey of key technologies in hydrogen energy storage," International Journal of Hydrogen Energy, vol. 41, p. 14535–14552, 2016.

[113] S. Tamalouzt, N. Benyahia, T. Rekioua, D. Rekioua, R. Abdessemed, "Performances analysis of WT-DFIG with PV and fuel cell hybrid power sources system associated with hydrogen storage hybrid energy system," International Journal of Hydrogen Energy, 2016.

[114] Ali, Dallia Morsi, "Energy capacity and economic viability assessment of the renewable hydrogen energy storage as a balancing mechanism in addressing the electric system integration issues inherent with variable renewable energy resources," in Reliability of Transmission and Distribution Networks (RTDN 2011), IET Conference on, London, 2011.

[115] Dante Fernando Recalde Melo, Le-Ren Chang-Chien, "Synergistic Control between Hydrogen Storage System and Offshore Wind Farm for Grid Operation," ieee transactions on sustainable energy, pp. 18-27, 2014.

[116] Milana Trifkovic, Mehdi Sheikhzadeh, Khaled Nigim, Prodromos Daoutidis, "Hierarchical control of a renewable hybrid energy system," 51st Annual Conference on Decision and Control (CDC), 2012.

[117] O.C. Onar, M. Uzunoglu, M.S. Alam, "Dynamic modeling, design and simulation of a wind/fuel cell/ultra-capacitor-based hybrid power generation system," Journal of Power Sources, no. Elsevier, pp. 707-722, 2006.

[118] Kuphaldt, Tony R., "Lessons In Electric Circuits Volumme I-DC," 2006. [Online].

[119] Casey, Tina, "Flow Battery Vs. Tesla Battery Smackdown Looming," 2015. [Online].

[120] Ionel Vechiu, Haritza Camblong, Octavian Curea, Gerardo Tapia, Brayima Dakyo. Analysis of Hybrid Power System Behavior under Renewable Resources and Load Variation Using a Dynamic Simulation Model. EWEC 2006, Feb 2006, Athens, Greece. Hal-00675536.

CHAPTER TWO

MODELING OF ENERGY CONVERSION SUBSYSTEMS

FOR HORIZONTAL AXIS WIND & TIDAL TURBINES

2.1 Introduction

Before designing any system it is essentially to carry out mathematical modeling, in order to study and understand that system. In energy conversion systems, wind and tidal resources and main power conversion system elements are need to be modeled.

In this chapter, mathematical modeling of wind resource as nonlinear signal, while tidal currents will be modeled as sinusoidal signal. Also, the main different elements that make up the hybrid wind and tidal conversion chains will be modeled namely: wind turbine, tidal turbine, electrical generator Doubly Fed Induction Generator DFIG, and power converter.

Wind and tidal systems, work on the same principle of energy conversion, and generally have the same construction of conversion chain.

Assumptions: Before modeling the proposed energy conversion chain, it is assumed that:

- The energy resource of each system has dynamic characteristics very different from each other; indeed, the wind resource (wind speed) is random, while the tidal resource (the marine current) is predictable most of the time.
- Both wind and tidal turbines forming the hybrid system are horizontal axis.
- Hybrid wind/tidal is based on 2 poles Doubly Fed Induction Generator coupled to both turbines on the same shaft.
- Gear box is used for both sides to adapt rotation speed and torque.

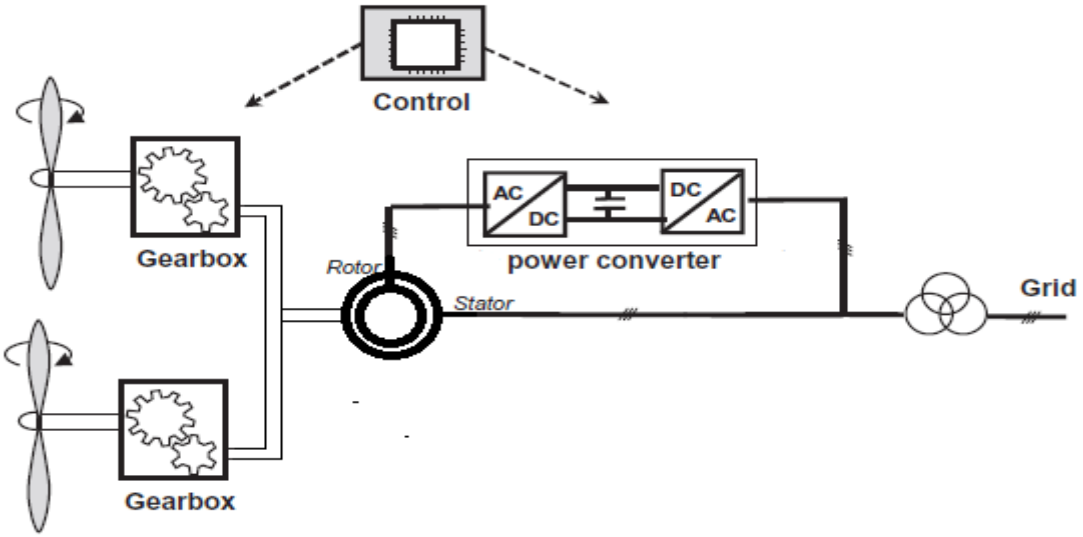

Figure 47 Hybrid wind/tidal turbine energy conversion system [1]

As shown in figure 47 the conversion chain includes two turbines, which convert the kinetic energy of the resource (wind and tidal current) into mechanical energy. This mechanical energy is

transmitted via a shaft to an electrical generator to generate electrical power. The latter is transmitted to the network through static converters that ensure the good quality of energy to provide the network. Very often, the speed of rotation of the generator is very large compared to that of the turbine. In this case, a gear box is provided.

2.2 Modeling of Wind Resource

Mathematical modeling is fundamental in order to fully understand, anticipate the behavior and control of resources, in case of the wind system the wind speed and in case of the tidal system, the tidal current, both being studied and modeled.

As well known that there is 8760 hour/year so it important to collect wind / tidal data and modeled mathematically as well as study the site location before designing process

2.2.1 Wind Speed

An important characterization of wind is its kinetic energy distribution in the frequency domain. Figure 48 shows a typical spectrum, the figure illustrates the power spectral density SV multiplied by the angular frequency ω [2]. It is noticed that, wind turbulence values (high wind frequency) change with a period of minutes and seconds. Whereas, the season value (low wind frequency), changes with a period of hours or days.

Also, it can be seen that two peaks of wind energy is concentrated in two different period of time a period of one minute corresponding to the scale of turbulent and a period of day corresponding to seasonal wind flow. It can be considered that, the wind speed is the sum of an average component and a fluctuating component.

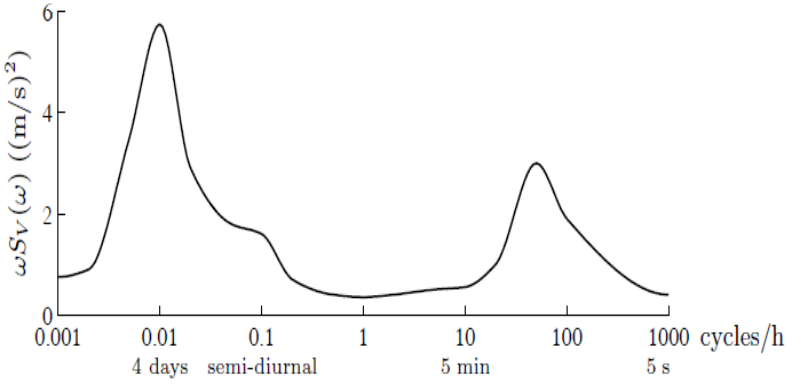

Figure 48 Van der Hoven Spectrum

So, we consider that wind speed is composed of two components [3]:

$$V_{wind}(t) = v_{avg}(t) + v_{turb}(t) \qquad (2.1)$$

Where $v_{avg\ (t)}$ is the (low-wind frequency) component and $v_{turb\ (t)}$ is wind turbulence (high wind frequency).

It is necessary to carry out statistics studies to find out the probability of exist enough wind speed to generate electrical power most of the time during the year.

There are two wind speed probabilities:

$$F(V) = (0 \le v \le \infty) = 1 \qquad (2.2)$$

This means that there is probability to have enough wind speed most of the time during the year.

$$F(V) = (V_1 \langle V \langle V_2) = 0 \qquad (2.3)$$

This means that it is impossible to have fixed or zero wind speed all the time during the year.

Thus;

$$F(V) = \int_0^v F(v)\, dv \qquad (2.4)$$

This equation above means that there is always wind speed, but must be assure that this wind speed is sufficient enough to produce power energy[4].

Average wind speed it is the wind speed at which the turbine been designed to operate at its optimum capacity. In other words, at which the turbine rotates at its nominal speed zone according to operation zones classification and curve of wind speed versus power generation as will be described later in wind turbine modeling.

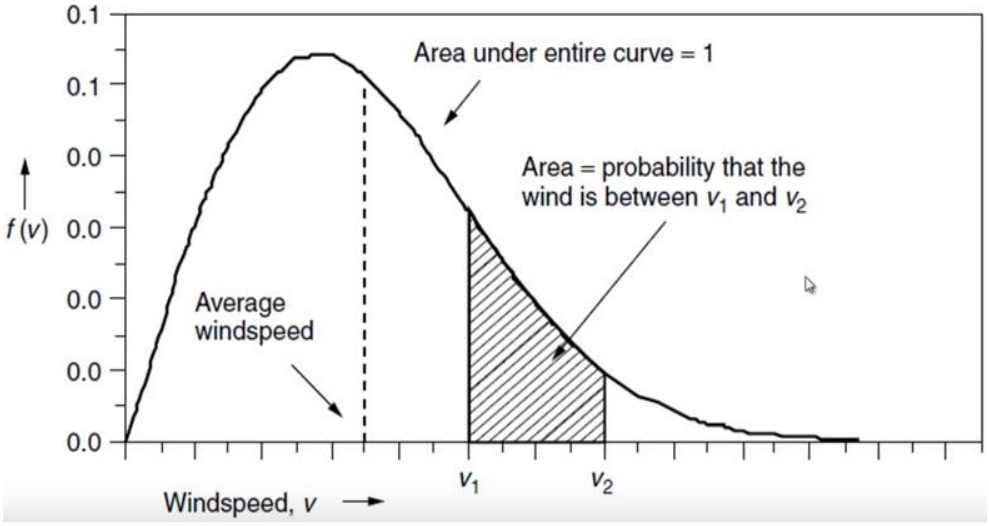

Figure 49 Wind Speed Probability Density Function [4]

2.2.2 Average Wind Speed (Weibull & Rayliegh)

The distribution of mean wind speed can be described by Weibull probability distribution, this distribution shows the average speed and, the average speed most likely, the following equation describes Weibull distribution [4-5]:

$$F(V) = \frac{K}{C}\left(\frac{V}{C}\right)^{K-1} e - \left(\frac{V}{C}\right)^{K} \qquad (2.5)$$

When K= 2; So Rayleigh equation:

$$F(v_{wind}) = \frac{2}{C}\left(\frac{V}{C}\right)^{2-1} e - \left(\frac{V}{C}\right)^{2} \qquad (2.6)$$

$$F(v_{wind}) = \frac{2V}{C}\ e^{-\frac{v^2}{c^2}} \text{.....} \ldots\ldots \qquad (2.7)$$

Note: Rayleigh is a special case of Weibull.

Where k is the shape parameter and C is the scale parameter.

The wind distribution is experimentally obtained, it can be approximated by Weibull distribution and Rayleigh as illustrated in figure 50. Studies prove that the best value of shape parameter is equal to *K* = 2 at which all wind speeds can be included under the curve. While the best value of scale parameter is equal to C= 8.

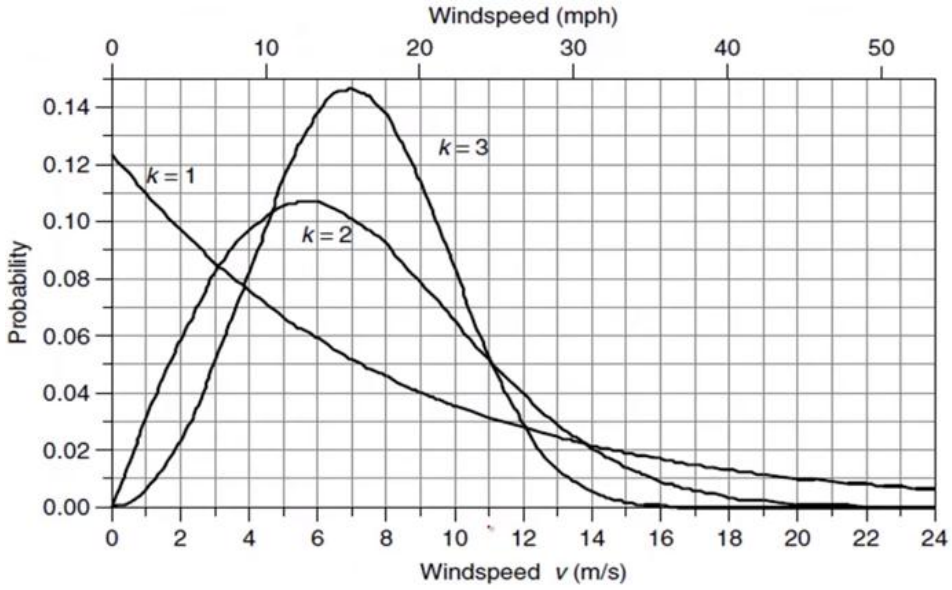

Figure 50 Weibull Probability Density Function with Shape Parameter (K=1,2 and 3) and Scale Parameter C=8

Average power in the wind can be calculated by:

$$P_{avg} = \frac{1}{2}\rho A\left(V^3\right)_{avg} \qquad (2.8)$$

Where average wind speed is equal:

$$\bar{V} = \int_0^{\infty} V\, f(v)\, dv \qquad (2.9)$$

$$= \int_0^{\infty} \frac{2V^2}{C^2} e^{-\left(\frac{v^2}{c}\right)} \Rightarrow = \sqrt{\frac{\pi}{2}} C \Rightarrow C = \frac{2\bar{V}}{\sqrt{\pi}} \qquad (2.10)$$

Substitute question (2.10) in question (2.5) to calculate the wind probability as function of wind speed average.

$$F(V) = \frac{\pi v^2}{2\bar{v}^2}\ e^{-\left(\frac{\pi v}{4v}\right)^2} \qquad (2.11)$$

By calculating cubic wind speed average from (2.8)

$$(V^3) = \int_0^{\infty} \left[V^3 \frac{\pi V^2}{2\bar{V}^2}\ e\left(\frac{\pi v}{4v}\right)^2 \right] dv \qquad (2.12)$$

So, the average wind speed will be equal to:

$$(V^3)_{avg} = \frac{6}{\pi}\bar{V}^3 \qquad (2.13)$$

And the wind power average can be calculated by:

$$P_{avg} = \frac{1}{2}\rho A\left(\frac{6}{\pi}\ \bar{V}^3\right) \qquad (2.14)$$

Collection of measured wind data during several years can be used to predict the probability distribution of the mean wind speed. All these data are usually arranged in a histogram.

The speed measured by an anemometer is different from the speed seen by the rotor of the turbine because of the aerodynamics of the blade, the inertia of the rotor and the influence of the blades on the air mass.

Modeling methodologies have been widely developed in [6-8] only the final result will be addressed. Two solutions emerged: one using a non-rational transfer function filter in the

modeling process of the turbulence component, and the other using a filter adaptation with a rational transfer function.

Modeling with non-rational filter is not adapted for the simulation in real time, because this algorithm it consumes time for calculation. However, a wind profile is generated using software program developed in GREAH as shown in figure 51 [9].

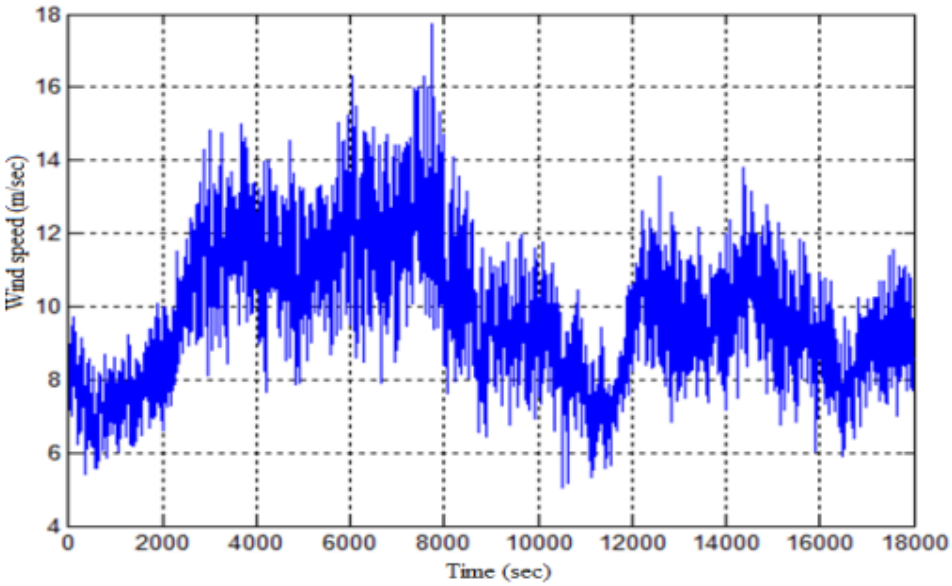

Figure 51 Wind Profile

2.3 Modeling of Tidal Current

Motioning water forms 70% of the geographical area of the earth and that water never remains to stand still steady.

There are two main types of marine currents:

- Spring tides (maximum or high tides) when earth sun and moon are aligned.
- Neap tides (minimum or low tides) when sun and moon are perpendicular to the earth.

When the earth and the moons gravity is aligned with each other, the influences of these two gravitational forces becomes very strong and causes water to flow towards the shore creating a "high tide" condition. In the other hand, when the earth and the moons gravity is perpendicular to each other, the influences of these two gravitational forces is weaker thus the water flows away from the shore as the water moves to another location, creating a "low tide" condition. This ebbing and flowing of the tides happens twice during each period of rotation of the earth with stronger weekly and annual lunar cycles superimposed onto these tides [10].

Tidal currents considering as the main sources of power, compared to other types of power sources it can be predicted (estimated) for most sites [11].

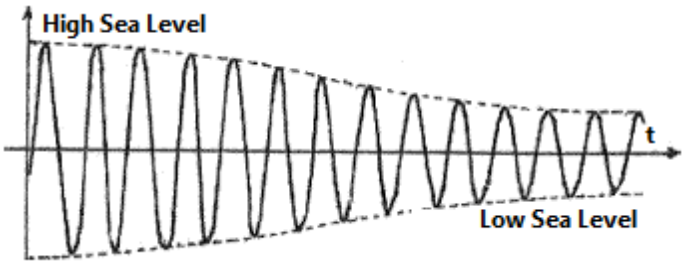

Figure 52 Variation of Tidal Currents High and Low Sea Level

According to its angular movement which almost regular most of the time in a form of a sine wave, therefore it can be modeled as a sinusoidal signal [12]:

$$V(t) = V_{max} \sin e\omega t \qquad (2.15)$$

With;

$$\omega = \frac{2\pi}{T} \qquad (2.16)$$

Where;

V_{max}: maximum velocity of tidal currents

ω: angular velocity of the tidal current

T: periodical cycle of the tidal current, normally 12h 25mints/day.

Therefore, this simple model of the tidal is considered for this work due to its periodic oscillation, where the tide can be represented by a long wave that spreads over oceans, seas and estuaries, and changes its length and amplitude periodically almost every half day.

The period of the tide, or time interval between two consecutive high waters, is approx. 12 h 25 min in the case of semidiurnal tides, and 24 h 50 min in the case of diurnal tides The terms semidiurnal and diurnal refer to the duration of one tide, approximately a half day or one day, respectively.

2.4 Modeling of Wind-Tidal Turbines

Wind and Tidal turbines are mechanical devices used to convert kinetic energy of a fluid (wind or water) into mechanical energy as shown in figure 53 when the kinetic energy of the fluid crossed the turbine blades causes a rotational movement, this movement then transformed into mechanical energy on a rotating shaft thus it can be coupled into different machines as prime mover in wind and tidal turbines its connected into electrical generator. However, modeling of

turbine is carried out in two ways: ideal modeling and practical modeling; ideal modeling at which all the energy available in the fluid is converted into energy, which does not exist in the reality, and the practical modeling, where only part of the energy is converted into mechanical energy, this will be explained further in the following section.

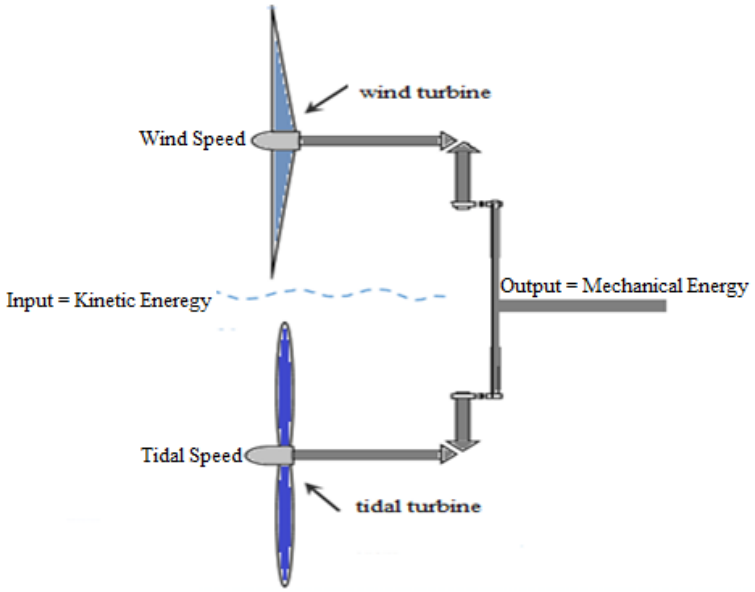

Figure 53 Wind/Tidal Turbines Coupled On the Same Shaft

The kinetic energy provided by mass of air or water ***m***, and moves at a velocity ***v***, is given by the formula:

$$E = \frac{1}{2} m \cdot V^2 \qquad (2.17)$$

Considering that air mass ***m*** passes through a cylinder whose base is the surface swept by the blades of a turbine of radius ***R***, by expressing this mass ***m*** as a function of the density ρ, some mechanical power of the fluid can be calculated by the expression presented below: [13]

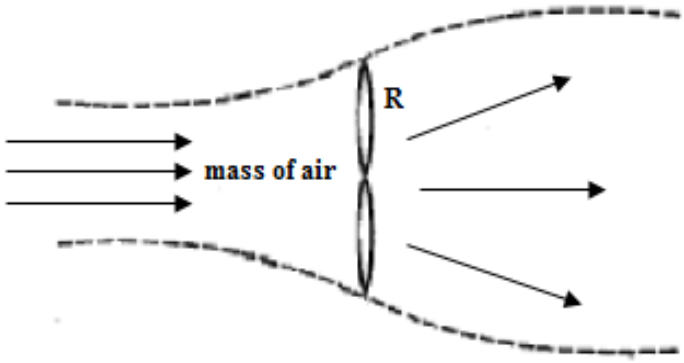

Figure 54 Cylindrical Volume Represents Energy Conversion in Wind Turbine

$$P_{mec} = \frac{1}{2}\rho\pi R^2 V^3 \qquad (2.18)$$

P_{mec}: the generated mechanical power of the wind / water received, by ideal turbine through its blades. However, since the speed of wind or water is not zero after passing through blades of the turbine, this means that only a part of the mechanical power been extracted [14].

The German physicist **Albert BETZ**, theoretically demonstrated in his book Wind Energy published in 1926, that the conversion efficiency achieved by any type of turbine in practice only fraction 16/27 of the mechanical power extracted by wind turbine which is equal to 59.3% of the power in the fluid, this percent is known as **Betz Limit**.

In general, the conversion efficiency of a wind turbine / tidal turbine is called the power coefficient and is noted C_p [13]. The coefficient power is a manufacturer variable that depends on the pitch angle β of the turbine's blade and the specific speed λ.

The actual mechanical power output can be written as:

$$P_{mec} = \frac{1}{2}\rho\pi R^2 V^3 \ . \ C_p(\lambda,\beta) \qquad (2.19)$$

Simtorque Software

There are several theories and methodologies implemented for determining the power coefficient C_p. The software "*Simtorque*", developed at the GREAH laboratory is based on the blade element method to determinate the power coefficient from the characteristic values of the cord of each blade of the turbine. Thus allows to model the static characteristics of any turbine, characteristics that generally are difficult to obtain from the manufacturer [15-16]. We need also for real time reasons specific models that could be implemented on the emulation devices.

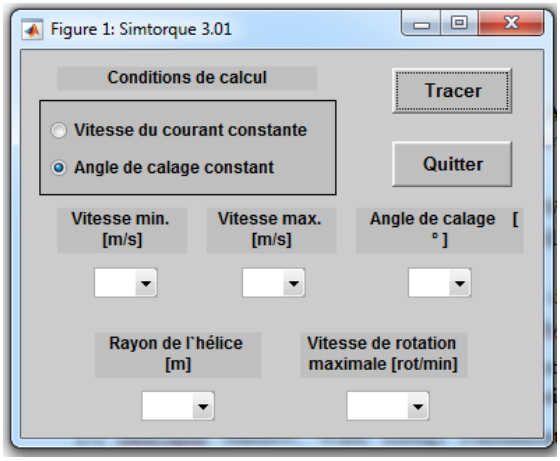

Figure 55 Graphical interface of 'Simtorque' Software

Using this software, it is possible to choose radius of the turbine's blades and maximum rotation, thus help to design our system. In addition to that, two modes of simulation can be carried out according to the designer needs:

- Constant wind speed versus variable pitch angle
- Constant pitch angle versus variable wind speed

Constant wind speed VS variable Pitch Angle

Regarding to the hardware simulator which is already available in the lab GREAH, where the electrical generator is a small scale power generator (1.5 kW), the wind and tidal turbines parameters have been chosen with this electrical generator installed in the simulator panel. As mentioned above this software is used to find out the power coefficient C_p, without need to know characteristics of the blade design which normally provided by the manufacturer. Also, specific speed λ and best pitch angle β can be obtained. In fact we can adapt the electrical parameters to a "designed" turbine optimized for this system.

Parameters of the proposed system are as follow:

- Radius length of the wind turbine blade is 1 m, and 0.5 m for tidal turbine
- Wind speed is 9 m/s, and 0.5m/s for the tidal speed
- Maximum rotation speed is 1500 revolutions/minute (rpm)
- Pitch angle vary between 0 to 6 degree

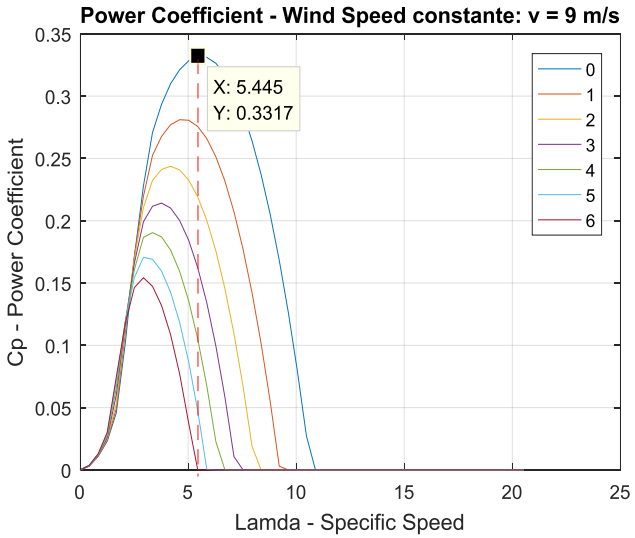

Figure 56 Constant wind speed VS variable Pitch Angle

Constant Pitch Angle VS Variable Wind Speed

- Radius length of the wind turbine blade is 1 m, and 0.5 m for tidal turbine
- Wind speed between 5 - 9 m/s.
- Maximum rotation speed is 1500 rpm
- Pitch angle constant 0^0.

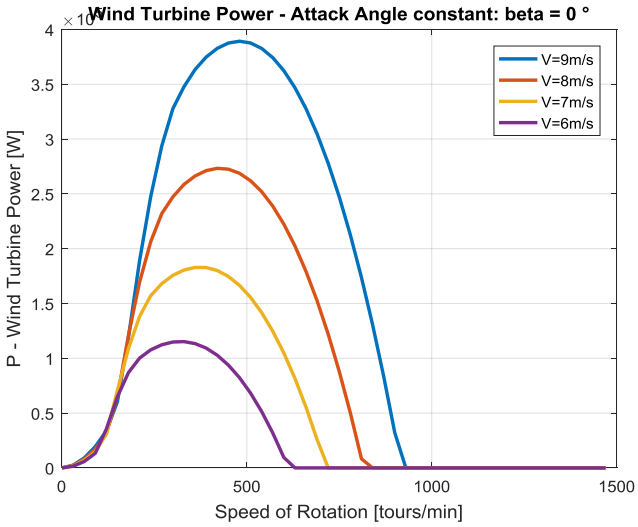

Figure 57 Constant Pitch Angle VS Variable Wind Speed

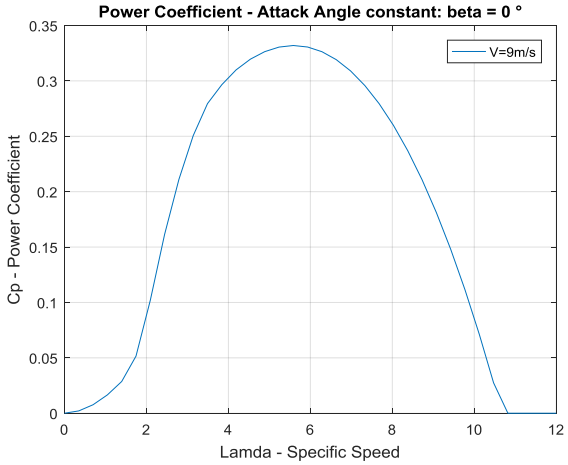

Figure 58 Constant Wind Speed and Pitch Angle

From figures above is noticed that, the pitch angle depends on the value of the power coefficient. For example, when = 0 ° (curve in blue), the maximum value of the power coefficient is 0.33 corresponding to a specific speed of 5.445; when = 1 ° (curve in green), we note that the maximum value of the power coefficient has decreased down to 0.28 for a specific speed of 4.78

The specific speed depends on *v*s peed of the fluid, and the angular velocity of rotation of the turbine Ω; it is expressed by the relation below:

$$\lambda = \frac{R\Omega}{V} \qquad (2.20)$$

The mechanical power captured by the wind or tidal turbine can be calculated as a function of the power coefficient C_p. From the following expression:

Ideal mechanical power extracted from the moving fluid as in equation:

$$P_{mec} = \frac{1}{2}\rho\pi R^2 V^3 \qquad (2.21)$$

The actual mechanical power extracted by the turbine from the moving fluid as in equation:

$$P_{mec} = \frac{1}{2}\rho\pi R^2 V^3 . C_p(\lambda,\beta) = P_{mec} . C_p(\lambda,\beta) \qquad (2.22)$$

Where the Pitch angle is considered at its optimum value (zero degree)

The rotational speed of the turbine is obtained from the equation below:

$$T_t - T_e = JFW.d\Omega \qquad (2.23)$$

$$\frac{d\Omega}{dt} = \frac{(T_t - T_e)}{J.FW} \qquad (2.24)$$

Where, *J.Fw* the inertia constant of the rotating mass, Ω is the rotor speed, T_t the input mechanical torque applied to the wind turbine rotor and T_e the electromagnetic torque of the electrical generator.

Due to the similarity between the function and characteristic of wind and tidal turbines, therefore, its mathematical modeling will be the same, except that the density of air and water will be different.

Wind or tidal turbine can be considered as a system having its input a non-linear fluid (air or water currents=, and its output, mechanical speed or mechanical torque, between the input and output there are other factors which play an important role in term of turbine efficiency.

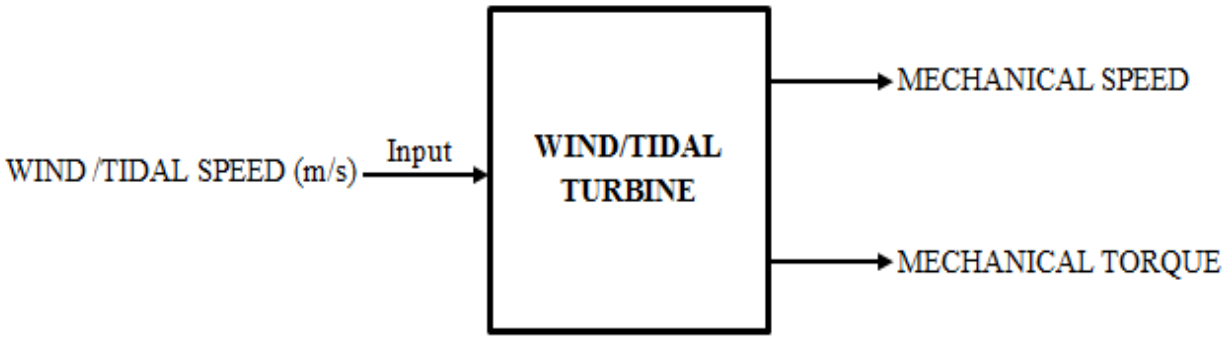

Figure 59 One System Block Diagram of Wind/Tidal Turbine

1. $P_{mec} = \frac{1}{2}\rho R^2 V^3$

2. $P_{mec} = \frac{1}{2}\rho R^2 V^3 C_p(\lambda,\beta) = P_{mec} C_p(\lambda,\beta)$

The coefficient power and torque can be provided by the manufacturer.

We presented below the power coefficient already used in the bibliography [17] [18].

3. $C_p(\lambda,\beta) = 0.5176\ (\frac{116}{\lambda_i} - 0.4\beta - 5)\ .\ e^{\frac{-21}{\lambda_i}} + 0.0068\lambda$ (2.25)

4. $\frac{1}{\lambda_i} = \frac{1}{\lambda + 0.08\beta} - \frac{0.035}{\beta^3 + 1}$ (2.26)

5. $\lambda = \frac{(R\,\Omega)}{v}$ (2.27)

6. $T_{mec} = \frac{P_{mec}}{\Omega}$ mechanical torque (2.28)

7. $T_{mec} - T_{Load} - F\Omega = J\frac{d\Omega}{dt}$ (2.29)

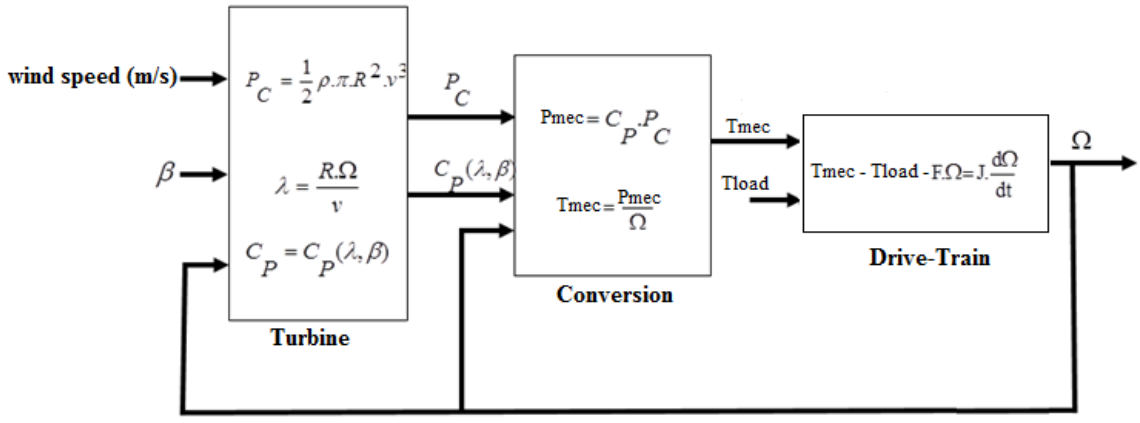

Figure 60 Mathematical Modeling of Wind/Tidal Turbine

Where;

P_c is the power captured by the turbine; C_p is the power coefficient; P_{mec} is the mechanical power; T_{mec} is the mechanical torque; T_{load} is the torque of the load; and F friction with air.

2.5 Modeling of Doubly-Fed Induction Generator DFIG

In electrical machines, it is useful to analyze and investigate main machine properties, in order to well understand its behavior in all conditions. In other words, steady state modeling which

focuses on the behavior of the machine in steady state conditions, and dynamic modeling concentrates on the transition behavior of the machine, and its response to changes in the network. Thus, two mathematical modeling will be explained in the following sections, but before that it would be better to have a simplified idea about the principle and construction of the doubly fed induction machine.

Basic Operation Principle and Structure of DFIG

The doubly fed induction generator (DFIG) or wound rotor induction generator (WRIG) are terms commonly used to describe an electrical machine, which has been used for long time in various applications, commonly in the range of megawatts of power less than in the range of a few kilowatts. This concept of the machine is as an alternative to more common asynchronous and synchronous machines [19].

Asynchrony machines composed of two main parts:

- **Stator winding:** a three-phase stator comprising ***p*** pairs of poles per phase, identical to that of a synchronous machine. The stator is connected directly into the grid with constant amplitude and frequency, and generates the stator magnetic field [20] [21].
- **Rotor;** there are two main configuration of the rotor part:
  - **Squirrel Cage Rotor**; the rotor consists of copper or aluminum bars connected at both ends by two conductive rings. This model (in the form of squirrel cage) is inexpensive and very robust and commonly used.
  - **Wound rotor winding**; the winding, similar to that of the stator, comprises ***p*** pairs of poles per phase; the three pairs are connected to three rings that allow to insert a rheostat in the rotor circuit [22].

Operation Principle of Doubly-Fed Induction Generator

Before studying the electric equations of DFIG, we introduce the well-known relationships between the different frequencies created in the stator and rotor of the machine. Therefore, frequency of voltages and currents generated in the stator ω_s is the sum of frequency of voltages and currents generated in the rotor ω_r and electrical rotor speed ω_m, as follows:

$$\omega_s = \omega_r + \omega_m \qquad (2.30)$$

Whereas, the mechanical speed of the rotor Ω_m is directly proportional to the number of pair pole *p* and the electrical speed of the rotor ω_m:

$$\Omega_m = P\omega_m \qquad (2.31)$$

Where; unites of these two equations are given in rad/sec.

While the slip ***s*** of the machine is defined as:

$$S = \frac{\omega_s - \omega_m}{\omega_s} \qquad (2.32)$$

In many applications, the stator windings are directly connected to the network and consequently, ωs is constant. This frequency is also known as the synchronous frequency. However, Depending on the sign of the slip, it is possible to distinguish three different operating modes for the machine as explained in table 7 presented below: [20]

Table 7 Operation Modes of an Electrical Machine (Generator/Motor/Break)

Conditions							Mode of operations
If	**ωm** *less than* **ωs**	⇒	**ωr** *more than* 0	⇒	s > 0	⇒	Sub-synchronous operation
If	**ωm** *more than* **ωs**	⇒	**ωr** *less than* 0	⇒	s < 0	⇒	Hyper-synchronous operation
If	**ωm** *equal* **ωs**	⇒	**ωr** *equal* 0	⇒	s = 0	⇒	Synchronous operation

2.5.1 Steady – State Modeling of DFIG

Equivalent Electric Circuit

The doubly fed induction machine like other induction machine can be represented in a simple form of electrical transformer connected into balanced three phase source. Modeling of DFIG is built up on the following assumptions: [19]

- Only one phase of the stator and rotor is represented, and the other two phases are modeled as essentially similar.
- The machine is symmetrical and balanced in structure.
- Magnetization is linear.
- The stator windings are supplied by three-phase voltages directly from the grid.

- The rotor windings are supplied by three-phase voltages but independent of the stator voltages.

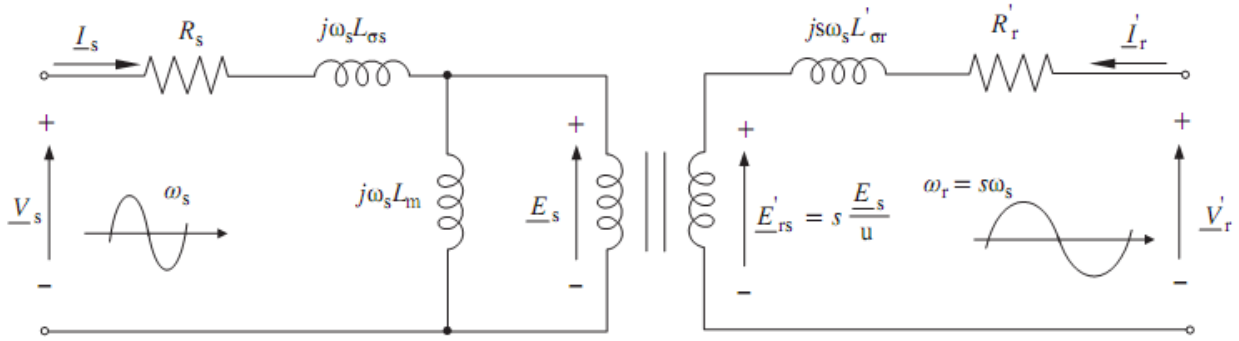

Figure 61 One-phase steady-state equivalent electric circuit of the DFIG

Where;

- $\underline{V}s$, $\underline{V'}r$: are supplied stator and rotor voltages respectively
- $\underline{I}s$, $\underline{I'}r$:are stator and rotor currents
- $\underline{E}s$, $\underline{E'}rs$: are induced e.m.f in the stator and rotor respectively
- Rs, R'_r: are stator and rotor resistances in (Ω)
- Lm, Lσs, L′σr: mutual, stator, and rotor leakage inductances respectively expressed in (H)
- Ns, Nr: are number of turns of the stator and rotor windings per phase

u, is the coefficient that indicates the relation between the stator and rotor turns per phase as follow:

$$u = \frac{N_s}{N_r} \qquad (2.33)$$

Therefore, the induced e.m.f in the stator and rotor calculated by:

$$E'_{rs} = \frac{E_s}{u} S \qquad (2.34)$$

NOTE; if the number of turns of the rotor and the stator and slip between them is equal 1 then the induced emf of both rotor and stator are the same.

In order to facilitate the analysis, the stator windings are reduced to be equivalent to that of the rotor winding. This provides us with the equivalent phase circuit of figure (61). [19]

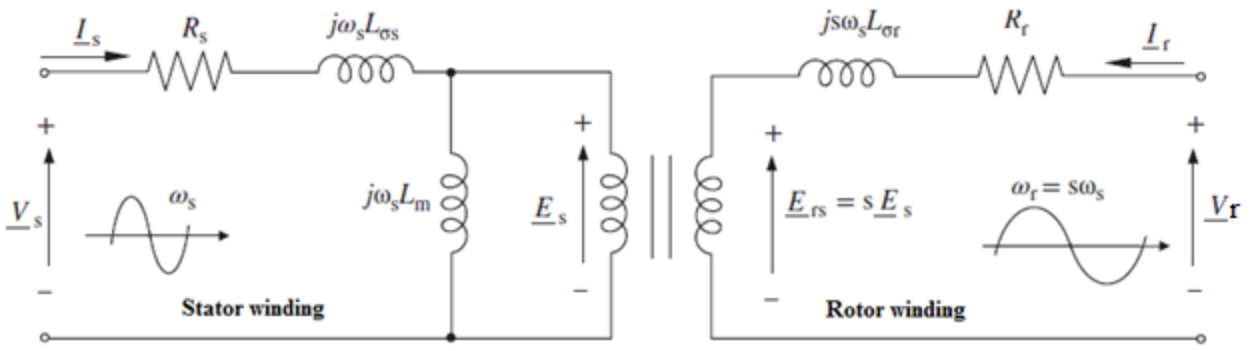

Figure 62 Phase steady-state equivalent electric circuit of the DFIG

To simplify the analysis of the equivalent circuit, it is recommended to subject both the stator and rotor circuits to the same frequencies. Thus, the rotor circuit is "converted" to the stator frequency ωs, by doing:

$$V_r - SE_s = \left(R_r + j_s\omega_s L\sigma r\right)I_r \Rightarrow \frac{V_r}{S} - E_s = \left(\frac{R_r}{S} + j\omega L\sigma r\right)I_r \qquad (2.35)$$

So, the final configuration of equivalent circuit will be as in figure (17)

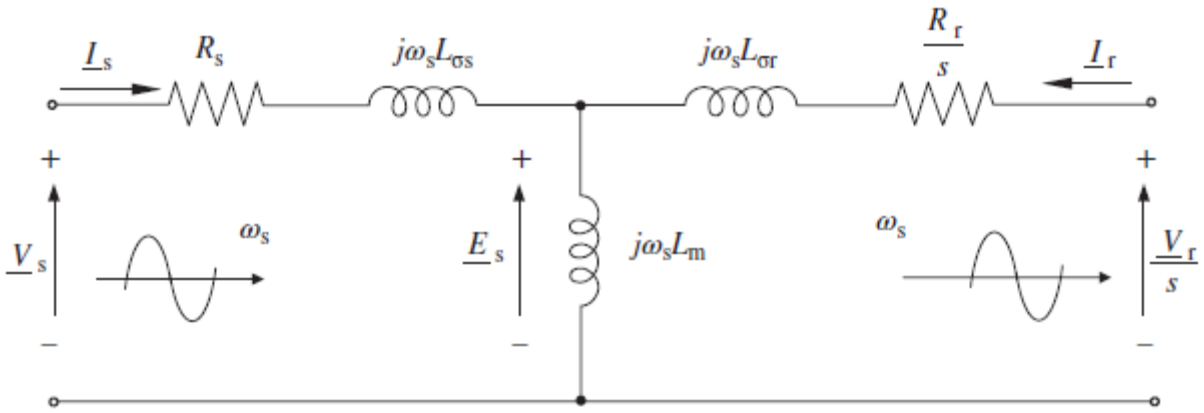

Figure 63 Steady-State Equivalent Circuit of the DFIG Referred to Stator

The final steady- state voltage and flux electric equations of the equivalent circuit of the DFIG are as follow:

- **Voltages :**

$$\begin{aligned} V_s &= R_s I_s + j\omega_s L\sigma_s I_s + j\omega_s L_m (I_s + I_r) \\ \frac{V_s}{S} &= \frac{R_r I_r}{S} + j\omega_s L\sigma_r I_r + j\omega_s L_m (I_s + I_r) \end{aligned} \qquad (2.36)$$

- **Fluxes:**

$$\begin{aligned} \psi_s &= L_m (I_s + I_r) + L\sigma_s I_s = L_s I_s + L_m I_r \\ \psi_r &= L_m (I_s + I_r) + L\sigma_r I_r = L_m I_r + L_r I_r \end{aligned} \qquad (2.37)$$

Where Ls = Lm + Lσs being the stator inductance and Lr = Lm + Lσs being the rotor inductance.
More explications are presented in appendix B

Power Equations and Operation Modes

In general two powers are developed in the stator and the rotor of the DFIG. namely; active and reactive power (P_r, P_s); these generated powers are due to the flow of electrical current in the machine coils which yields finally a mechanical power in the rotor side of the machine (motor operation mode). While the mechanical power (P_m) developed on the rotor side of the machine generates electrical power in the machine winding (generator operation mode).
However, in generator mode, active and reactive power (P_r,P_s) are function of mechanical power (P_m) mines cupper losses (P_{cu}) in the stator and rotor windings:

$$P_s + P_r = P_m - (P_{cur} + P_{cus}) \qquad (2.38)$$

As mentioned above that, the stator and rotor currents are calculated as in a perfect transformer:

$$\frac{i_r}{i_s} = \frac{N_s}{N_r} \qquad (2.39)$$

So, the ratio between the power P_r of the rotor and the power P_s of the stator is expressed by: [3]

$$\frac{P_r}{P_S} = \frac{i_r}{i_S}.\frac{E_r}{E_S} = s \qquad (2.40)$$

Equation (2.35) shows that in order to have a constant power transmitted to the stator, the power of the rotor and slip must be constant, and to increase power at the rotor, the slip must be increased. The stator pulsation (which is imposed by the network) is assumed constant; it is therefore possible to control the speed of the generator simply by acting on the power transmitted to the rotor via the slip *s*. Furthermore, for wind turbine operating at variable speed, the DFIG offers the possibility of operating at wide range of wind speeds.

Four modes of operation [23]

1. Hyper synchronous motor mode: when the DFIG receives power through the stator and the rotor windings, the electrical power it transforms into mechanical power;
2. Hyper synchronous generator mode: when the DFIG receives mechanical power, thus it is converted into electrical power and distributed to the network through the stator and the rotor windings.

3. Sub-synchronous generator mode: when the DFIG receives through its rotor, a mechanical power that will be converted into electrical power and distributed through the stator. However, some of this power will be absorbed by the rotor windings and the rest will be distributed to the network.
4. Sub-synchronous motor mode : when the DFIG receives electrical power through its stator winding, part of which is sent back to the network through the rotor windings, and the rest is converted into mechanical power;

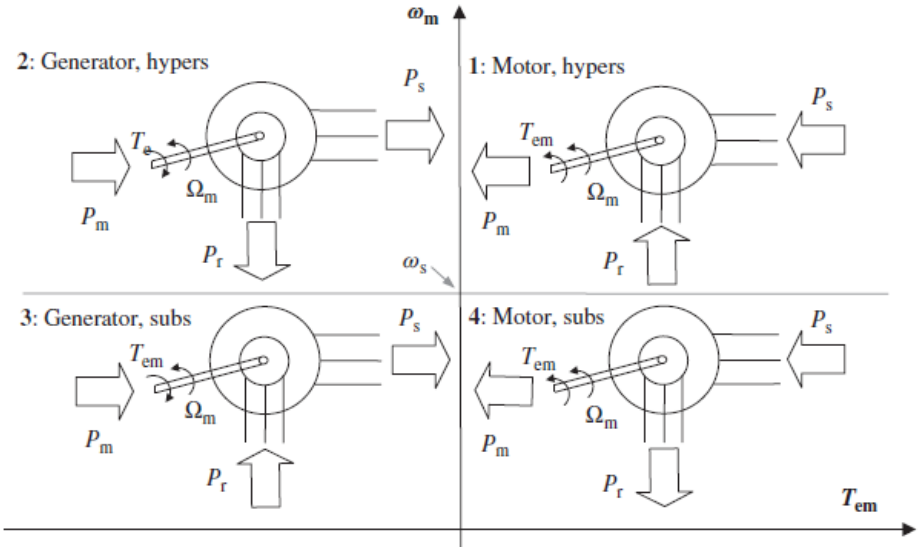

Figure 64 Four operating Modes of the DFIG

As illustrated in the figure 64, it is possible to differentiate four possible combinations of torque (positive motor mode or negative generator mode), and speed (sub-synchronism and hyper-synchronism), which yields four quadrant modes of operation of the DFIG [24].

2.5.2 Dynamic Modeling of DFIG

A hyper synchronous DFIG has been chosen to be modeled and used as part of this thesis.

DFIG is a poly-phase winding machine with stator and rotor. In this study, a three-phase windings DFIG is implemented. The stator is supplied by at constant frequency (fs) generates a rotating field at electric angular velocity ωs. The rotor windings are not short circuited. The rotor rotates at $\Omega = d\theta / dt$.θ is the angle between the stator and rotor axis [19] [25].

The following hypotheses have been taken in consideration for mathematical modeling of DFIG:

- The air gap is constant,

- Sinusoidal spatial air gap distribution of magnetic motive forces,
- The slot effect is neglected,
- Negligible iron losses,
- Unsaturated magnetic circuit with constant permeability,
- The influence of the skin effect and heating is not taken into account.
-

2.5.2.1 αβ Model

Space vector theory is applied to the electric equations of the machine for developing the dynamic α β model of the DFIG; it is assumed that, the machine is ideal and linear. Three different rotating reference frames are used to develop space vector-based models of the DFIG as shown in figure 19.

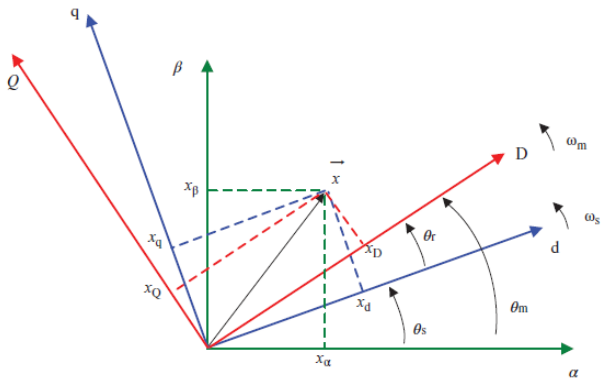

Figure 65 Different Reference Frames to Represent Space Vector of DFIG

Three reference frames are used to represent stator and rotor voltages and fluxes, the stationary stator reference frame (α–β)"s", the rotor reference frame (DQ) "r" rotates at ω_m and the synchronous reference frame (dq) "a" rotates at ω_s, are used to denote that one space vector is reference to the stator, rotor and synchronous reference frames, respectively. By using direct and inverse Park transformation, a space vector can be represented in any of these frames [25].

Thus, the three windings of the stator and rotor using space vector theory , can be represented separately, by two stationary α β coils for the stator and two rotating coils DQ for the rotor, yields the following voltage equations:

$$\vec{V}_s^s = R_s \vec{i}_s^s + \frac{d\vec{\psi}_s^s}{dt} \qquad \vec{V}_r^r = R_r \vec{i}_r^r + \frac{d\vec{\psi}_r^r}{dt} \qquad (2.41)$$

In case of both voltage equations need to be represented in stationary reference frame α β, then rotor equations must be multiplied by rotor electrical speed ω_m.

$$\vec{V}_s^s = R_s \vec{i}_s^s + \frac{d\vec{\psi}_s^s}{dt} \begin{cases} V_{\alpha s} = R_s i_{\alpha s} + \dfrac{d\psi_{\alpha s}}{dt} \\ V_{\beta s} = R_s i_{\beta s} + \dfrac{d\psi_{\beta s}}{dt} \end{cases} \qquad (2.42)$$

Rotor coils can be represented in stationary reference frame, by multiplying the rotor equations by ω_m, providing the following equations

$$\vec{V}_r^s = R_r \vec{i}_r^s + \frac{d\vec{\psi}_r^s}{dt} - j\omega m \vec{\psi}_r^s \begin{cases} V_{\alpha r} = R_r i_{\alpha r} + \dfrac{d\psi_{\alpha r}}{dt} \\ V_{\beta r} = R_r i_{\beta r} + \dfrac{d\psi_{\beta r}}{dt} \end{cases} \qquad (2.43)$$

Similarly, the flux equations of the stator and the rotor can be represented by space vector form as shown hereafter.

Stator and rotor flux equations:

$$\vec{\psi}_s^s = L_s \vec{i}_s^s + L_m \vec{i}_r^s \begin{cases} \psi_{s\alpha} = L_s I_{s\alpha} + L_m I_{\alpha s} \\ \psi_{s\beta} = L_m I_{s\beta} + L_s I_{\beta s} \end{cases} \qquad (2.44)$$

$$\vec{\psi}_r^s = L_m \vec{i}_s^s + L_r \vec{i}_r^s \begin{cases} \psi_{r\alpha} = L_r I_{r\alpha} + L_m I_{\alpha s} \\ \psi_{r\beta} = L_m I_{s\beta} + L_r I_{\beta r} \end{cases} \qquad (2.45)$$

Where:

R_s, R_r are stator and rotor resistances in Ω, i_s ,i_r are stator and rotor currents in A, L_m , Ls , Lr are mutual inductance, stator inductance, rotor inductance respectively, ψ_s, ψ_r are stator and rotor fluxes.

Electromagnetic torque and mechanical speed can be calculated by the following equations:

$$T_{em} = \frac{1}{2} p(I_{r\alpha}\psi_{r\beta} - I_{r\beta}\psi_{r\alpha}) \qquad (2.46)$$

$$J\frac{d\omega m}{dt} = T_{em} - T_{load} - F\Omega \qquad (2.47)$$

Where J is the inertia of the rotor and T is the load applied to the shaft in modeling.

In addition, the active and reactive powers (Pr,Ps & Qr,Qs) of the stator and rotor windings can be calculated using to the following expressions:

Power in the stator:

$$Ps = 1.5\ (v_{\alpha s} i_{\alpha s} + v_{\beta s} i_{\beta s})$$

$$Qs = 1.5\ (v_{\beta s} i_{\alpha s} + v_{\alpha s} i_{\beta s}) \qquad (2.48)$$

Power in the rotor:

$$Pr = 1.5\ (v_{\alpha r} i_{\alpha r} + v_{\beta r} i_{\beta r})$$

$$Qr = 1.5\ (v_{\beta r} i_{\alpha r} - v_{\alpha r} i_{\beta r}) \qquad (2.49)$$

Thus, from the equations above, the αβ equivalent circuit can be developed as illustrated in Figure 65. For each αβ coordinate there is one equivalent circuit, in which all the voltage, current and flux magnitudes are sinusoidal with a frequency of ω_s.

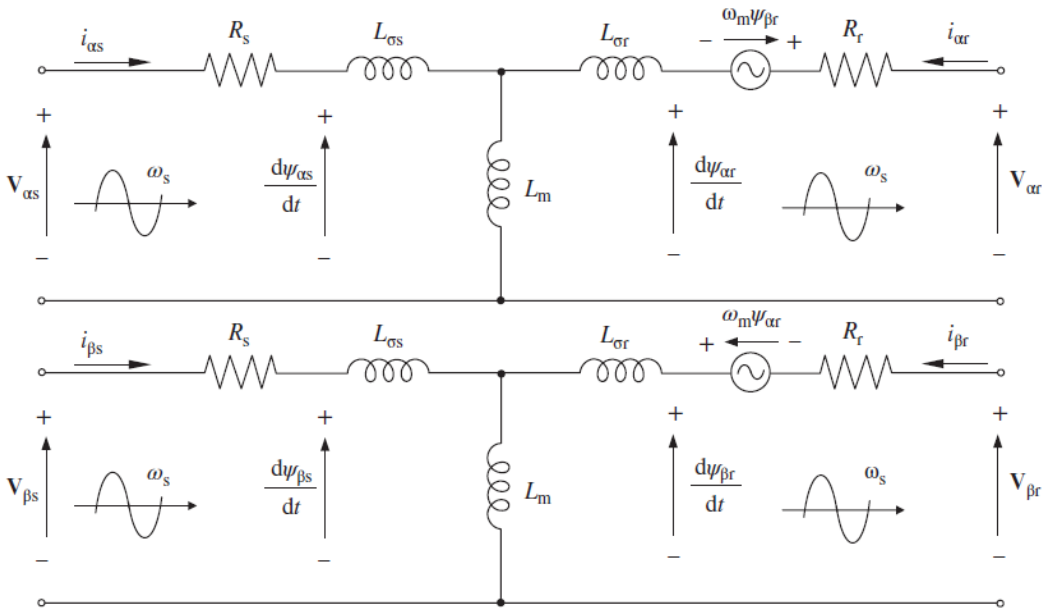

Figure 66 Model of DFIG in αβ Reference Frame

However, it is possible to develop several state-space representations of the DFIG, which are useful, hereafter, for simulation or analysis purposes an expression shows the state-space vector in which the DFIG model is composed of the stator and rotor fluxes:

$$\frac{d}{dt}\begin{bmatrix}\vec{\psi}_s^s \\ \vec{\psi}_r^s\end{bmatrix} = \begin{bmatrix}\frac{-R_s}{\sigma L_s L_r} & \frac{R_s L_m}{\sigma L_s L_r} \\ \frac{R_r L_m}{\sigma L_s L_r} & \frac{-R_r}{\sigma L_r} + j\omega_m\end{bmatrix}\begin{bmatrix}\vec{\psi}_s^s \\ \vec{\psi}_r^s\end{bmatrix} + \begin{bmatrix}\vec{V}_s^s \\ \vec{V}_r^s\end{bmatrix} \qquad (2.50)$$

Where; $\sigma = 1 - \frac{L_{m^2}}{L_s . L_r}$

2.5.2.2 dq Model

The space vector model of DFIG can be developed and presented in a synchronously rotating frame. Thus obtained by multiplying voltage expressions in ω_m, more detail of three-phase model is presented in Appendix B at the end of this thesis:

- **Stator Voltage Equations**

$$\begin{aligned} V_{sd} &= R_s I_{sd} + \frac{d\psi_{sd}}{dt} - \omega_s \psi_{sq} \\ V_{sq} &= R_s I_{sq} + \frac{d\psi_{sq}}{dt} + \omega_s \psi_{sd} \end{aligned} \tag{2.51}$$

- **Rotor Voltage Equations**

$$\begin{aligned} V_{rd} &= R_r I_{rd} + \frac{d\psi_{rd}}{dt} - \omega_r \psi_{rq} \\ V_{rq} &= R_r I_{rq} + \frac{d\psi_{rq}}{dt} + \omega_r \psi_{rd} \end{aligned} \tag{2.52}$$

- **Stator Flux Equations**

$$\begin{aligned} \psi_{sd} &= L_s I_{sd} + L_m I_{rd} \\ \psi_{sq} &= L_s I_{sq} + L_m I_{rq} \end{aligned} \tag{2.53}$$

- **Rotor Flux Equations**

$$\begin{aligned} \psi_{rd} &= L_r I_{rd} + L_m I_{sd} \\ \psi_{sq} &= L_r I_{rq} + L_m I_{sq} \end{aligned} \tag{2.54}$$

As previously a model of DFIG is represented by equivalent circuit in stationary α.β reference frame, also *dq* rotation frame can be used to represent a model of DFIG throughout an equivalent circuit as shown in the following figure 67.

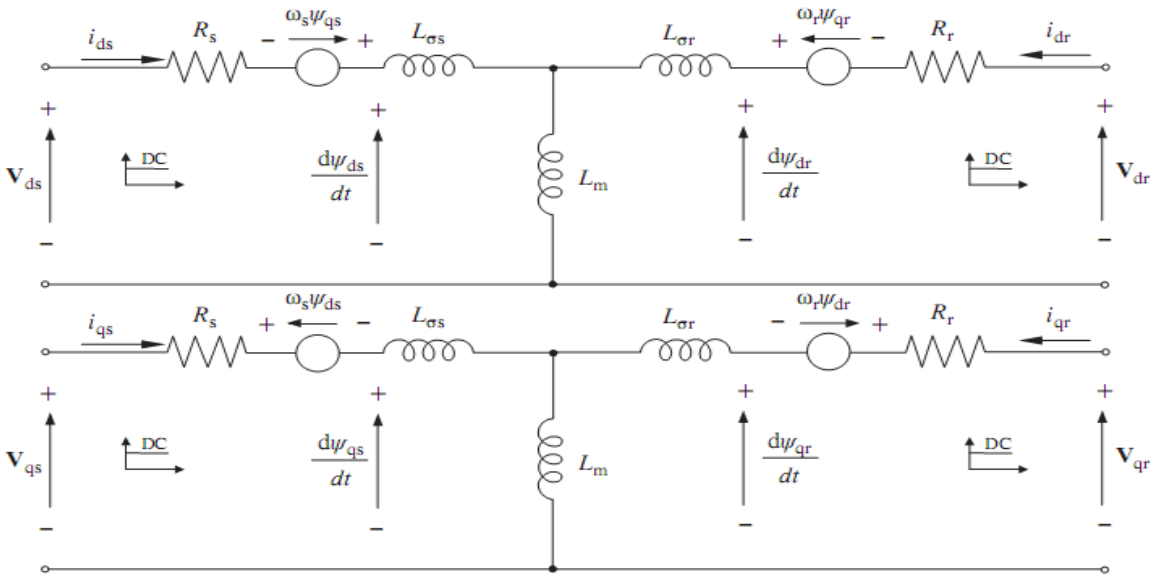

Figure 67 Equivalent Circuit of DFIG Modeled in dq Frame

Hereafter, block diagram demonstrates the main steps of DFIG mathematical modeling.

Step (1) Input supply conversion: the three phase input voltage (V_{sa}, V_{sb}, V_{sc}) and (V_{ra}, V_{rb}, V_{rc}) transformed into two phase (V_{sdq}, V_{rdq}) applying Park transformer.

Step (2) extraction of voltage equations: in this step four equations will be extracted for both stator and rotor windings in rotator reference frame (V_{sd}, V_{sq}) and (V_{rd}, V_{rq}) as indicated in the block diagram.

Step (3) extraction of flux equations: flux equations are extracted from voltage equations, the purpose of that is to find out current values of stator and rotor coils (I_{sdq}, I_{rdq}), which subsequently will be used for calculating electromagnetic torque or mechanical speed of the shaft.

Step (4) mechanical speed and electromagnetic torque equations: the extracted currents of stator and rotor coils will be used in the speed and torque equations in order to determine torque or speed needed.

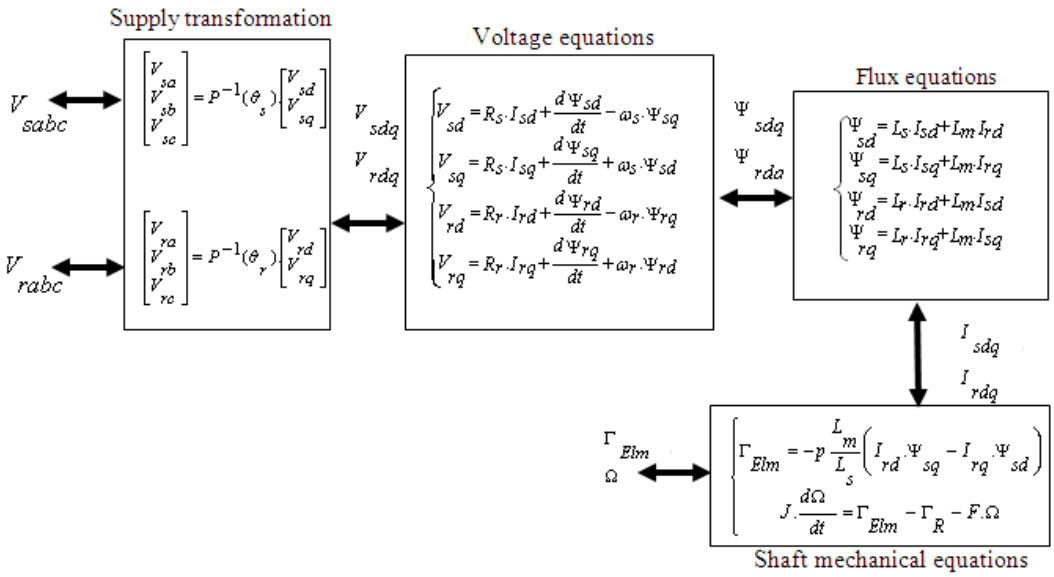

Figure 68 Model of DFIG in dq Reference Frame

2.6 Modeling of Power Converter

The power converter is implemented to supply the rotor of the DFIG. It is possible to control the wind turbine to operate at variable speed, delivering energy from the wind to the grid and meeting the grid code requirements. Recent developments in computer-aided design and semiconductors have enormous contribution to the modeling of power converters. Power converters are commonly used on the rotor side of DFIG. [26]

Power converter is composed of two main parts namely; rectifier and inverter, these two components are made up of power electronic devices such as diodes, transistors [27-28]. In addition to that DC-Link which is used as storage unit and point of decoupling and stabilization between the two main parts of the power converter. This configuration allows obviously bidirectional the flow of power i.e. from the machine to the grid and vice versa. Furthermore the three phase PWM boost rectifier has some advantages such as nearly sinusoidal waveform input currents, unity of input power factor, and low harmonic distortion of line currents, adjustment and stabilization of DC link voltage, reduced capacitor size and minimized pulsations of the torque [29-30].

The three-phase rectifiers and inverters used for this hybrid system are bidirectional and controlled power converters. This type of converter can therefore operate both inverter and rectifier, depending on the direction and type of electrical energy that passes through them.

Mathematical Modeling of Power Converter

It is considered as modeling hypothesis that the IGBT and diode are all ideal: zero resistance in closed and infinite resistance in open position, and instantaneous response to control signals.

2.6.1 Grid Side Converter Model

The grid side system is composed of converter, filter, and grid voltage. As illustrated in figure (69).

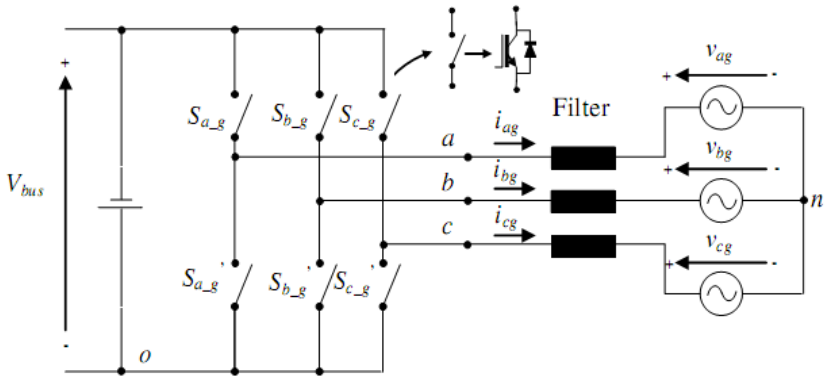

Figure 69 Grid Side Converter

Two-level converter is modeled with ideal switches, where the current can flow in both directions. Switches are commanded by triggers denoted by S_{a_g}, S_{b_g}, and S_{c_g}, which are generated by Pulse Width Modulation (PWM) method.

Under ideal situation, the converter switches hold this command condition:

$$\begin{aligned} S^{\bullet}_{a\_g} &= \bar{S}_{a\_g} \\ S^{\bullet}_{b\_g} &= \bar{S}_{b\_g} \\ S^{\bullet}_{c\_g} &= \bar{S}_{c\_g} \end{aligned} \qquad (2.55)$$

For instance, the voltage V_o referenced to the zero point of the DC bus:

$$\begin{aligned} V_{jo} &= V_{bus} S_{j\_g} \\ S_{j\_g} &= \in \{0,1\} \\ j &= a,b,c \end{aligned} \qquad (2.56)$$

Note that, it is not possible to have two switches connected in the same time on the same leg.

Also, by manipulating switch positions it possible to have different wave forms and amplitudes at the output of the converter.

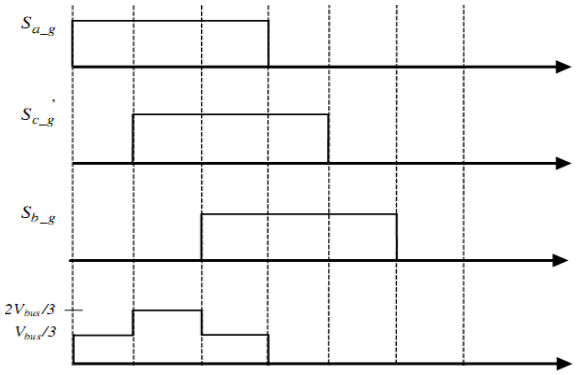

Figure 70 Waveforms of Converter Output

Figure 71 illustrates the relationship between inverter output voltage and neutral point of the grid (*n*) [30].

$$V_{jn} = V_{jo} - V_{no} \text{ with j } = a,b,c \qquad (2.57)$$

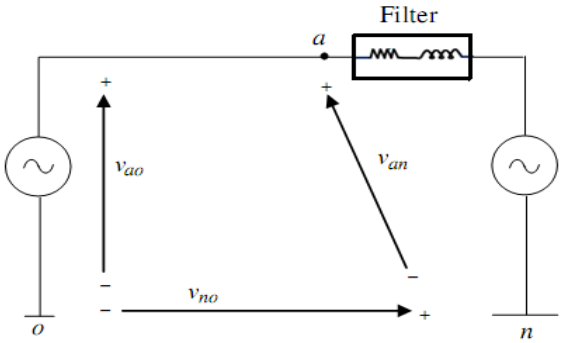

Figure 71 Single Phase of Grid Inverter

Therefore, it is essential to know the voltage between the neutral point (*n*) and the negative point of the DC bus (o), by assuming the following expression of a three-phase grid system that holds:

$$V_{an} + V_{bn} + V_{cn} = 0 \qquad (2.58)$$

V_{no} will be equal to the third of the sum of the three phases:

$$V_{n0} = \frac{1}{3}(V_{a0} + V_{b0} + V_{c0}) \qquad (2.59)$$

Also, by substit1uting equation $v_{jn} = v_{jo} - v_{no}$ with $j = a,\ b,\ c$ into last expression, yields

$$\begin{aligned} V_{an} &= \frac{2}{3}V_{a0} - \left(\frac{V_{b0} + V_{c0}}{3}\right) \\ V_{bn} &= \frac{2}{3}V_{b0} - \left(\frac{V_{a0} + V_{c0}}{3}\right) \\ V_{cn} &= \frac{2}{3}V_{c0} - \left(\frac{V_{b0} + V_{a0}}{3}\right) \\ V_{an} &= \left(\frac{V_{af} - R_f i_{ag} - V_{ag}}{L_f}\right) \end{aligned} \qquad (2.60)$$

Or more simply, directly from the order commands,

$$V_{an} = V_{bus}\left(\frac{2S_{ag} - S_{bg} - S_{cg}}{3}\right)$$
$$V_{bn} = V_{bus}\left(\frac{2S_{bg} - S_{ag} - S_{cg}}{3}\right) \qquad (2.61)$$
$$V_{cn} = V_{bus}\left(\frac{2S_{cg} - S_{ag} - S_{bg}}{3}\right)$$

Converter Model with Inductive Filter

The same as the previous system but in this case an inductive filter will be taken in consideration for system modeling as shown in figure 72.

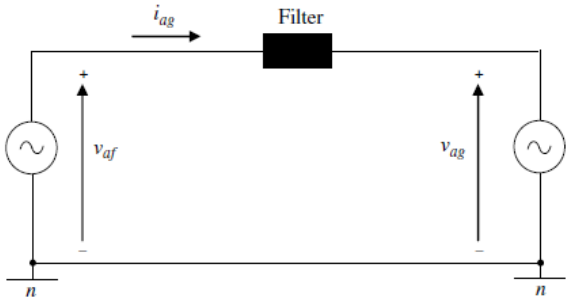

Figure 72 Single Phase Grid Side Converter

So, the voltage output of the converter will be expressed as:

$$V_{af} = R_f i_{ag} + L_f \frac{di_{ag}}{dt} + V_{ag}$$
$$V_{bf} = R_f i_{bg} + L_f \frac{di_{bg}}{dt} + V_{bg} \qquad (2.62)$$
$$V_{cf} = R_f i_{cg} + L_f \frac{di_{cg}}{dt} + V_{cg}$$

Also, current in three - phases can be derived as:

$$\frac{di_{ag}}{dt} = \left(\frac{v_{af} - R_f i_{ag} - v_{ag}}{L_f}\right)$$
$$\frac{di_{bg}}{dt} = \left(\frac{v_{bf} - R_f i_{bg} - v_{bg}}{L_f}\right) \qquad (2.63)$$
$$\frac{di_{cg}}{dt} = \left(\frac{v_{cf} - R_f i_{cg} - v_{cg}}{L_f}\right)$$

Where;

Lf ; inductance of the grid side filter (H)

Rf ; resistive part of the grid side filter (Ω)

vag, vbg, vcg; grid voltages (V), with *ωs* electric angular speed in (rad/s)

iag, ibg, icg; currents flowing thorough the grid side inverter's output (A)

vaf, vbf, vcf; output voltages of the converter referred to the neutral point of the load *n* (V).

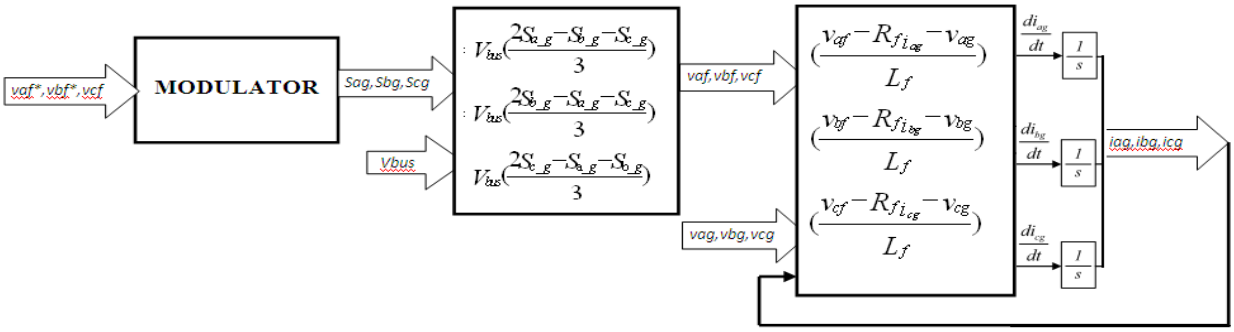

Figure 73 Inverter Grid Side Model

As illustrated above, the model of the grid side system is represented in figure 73. The inverter voltage outputs are formed with the help of a modulator. The grid ideal sinusoidal voltages are generated at constant amplitude and frequency. Then the currents exchanged with the grid are calculated, taking into consideration the filter, according to expressions listed above.

2.6..2 Rotor Side Converter Model

Each phase of the DFIG's rotor coils can be represented by an electromotive force (e.m.f) in series with an inductance and resistance. Denoted by e_{r_i} phase induced voltage, v_{r_i} three-phase voltages at the input of the rectifier and, i_{r_i} currents crossing each phase with $i = a, c, b$.

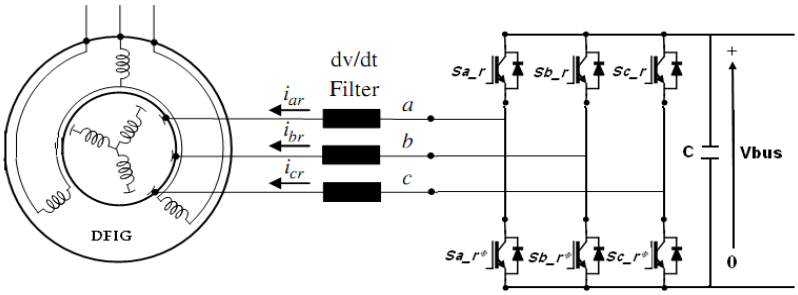

Figure 74 Schematic of Power Converter Rotor Side (rectifier)

Figure74 demonstrates schematic of rotor side converter used to supply rotor of the DFIG, in term of components and basics; the rotor side converter is similar to the grid side converter shown in the previous section. The main objective of this filter installed between the rotor and converter is to protect the generator from unexpected dips in the electrical grid.[26]

The rotor side converter is connected to the grid side converter via the DC link.

2.7 DC - Link

It is the linkage between the grid side and rotor side converters. It is a capacitor used to minimize power fluctuation, its function to maintain a constant voltage in the terminals of the grid side converter. Figure 75 shows a simplified model of a DC link [30].

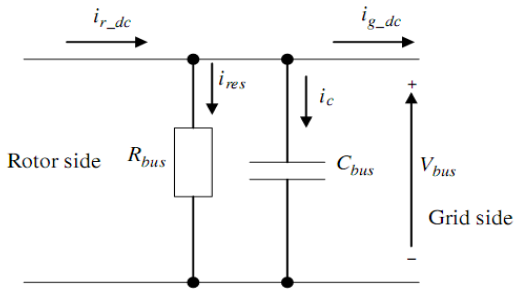

Figure 75 DC- link Power Converter

The DC bus voltage can be calculated.

$$V_{bus} = \frac{1}{C_{bus}} \int i_c dt \qquad (2.64)$$

The DC currents can be calculated as follows from the output AC currents of the converters:

$$\begin{aligned} i_{g\_dc} &= S_{a\_g} i_{ag} + S_{b\_g} i_{bg} + S_{c\_g} i_{cg} \\ i_{r\_dc} &= S_{a\_r} i_{ar} - S_{b\_r} i_{br} - S_{c\_r} i_{cr} \end{aligned} \qquad (2.65)$$

The current through the capacitor can be found as

$$i_c = i_{r\_dc} - i_{g\_dc} - i_{r\_res} \qquad (2.66)$$

Where

i_{res} : current through the resistance (A)

i_g_dc : DC current flowing from the DC link to the grid (A)

i_r_dc: DC current flowing from the rotor to the DC link (A)

The current through the resistance is

$$i_{res} = \frac{V_{bus}}{R_{bus}} \qquad (2.67)$$

Hereafter, the model of the DC link system illustrated in Figure 76.

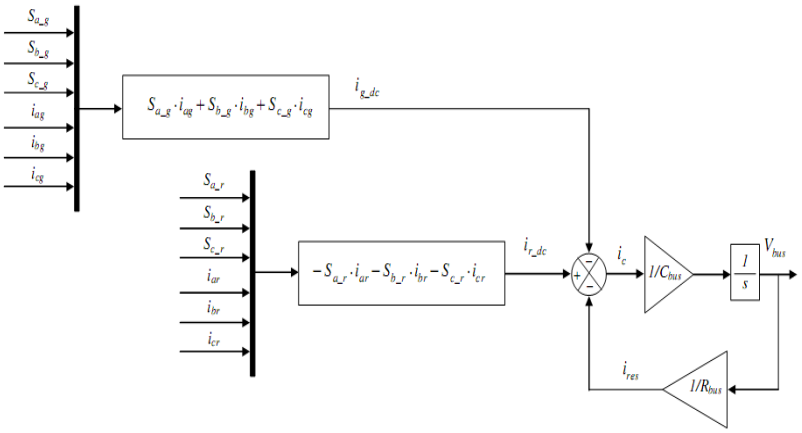

Figure 76 DC-Link Model

2.8 Conclusion

This chapter presents static and dynamic modeling of different elements of the wind and tidal conversion system. The wind energy conversion chain been studied includes: wind turbine that converts the kinetic energy of the wind into mechanical energy on its shaft, Doubly-Fed Induction Generator (DFIG), a PWM-controlled rectifier and a PWM-controlled inverter. The DFIG is connected to the network directly via its stator, and its rotor is connected via the converter. Different models of power conversion system are presented.

Both turbines function on the same principles, the only difference lies in the density of resources (Air and Water). The model of the electrical machines is presented in the natural coordinate system (a, b, c) then in the two-phase Park transformer is used. This transformation is very important for modeling and control complexity, i.e. instead of having a command on three axes, only two axes will be treated.

References

[1] Trevor M. Letcher, Wind Energy Engineering hand book for onshore and offshore wind turbines, Academic Press of Elsevier, 2017, 525 B Street, Suite 1800, San Diego, CA 92101-4495, United States.

[2] Bianchi, F.D.; Battista, H.; Mantz, R.J, Wind Turbine Control Systems Principles, Modelling and Gain Scheduling Design, 105 illus., 2007, 207p. Hardcover ISBIN: 978-1-84628-492-2.

[3] Jerry Tekobon, Système multi physique de simulation pour l'étude de la production de l'énergie basée sur le couplage éolien offshore-hydrolien, Thèse de doctorat, Le havre, 2016

[4] Tom Overbye, ECE 333 Renewable Energy Systems, lecture 10: Wind Power System, Dept. of Electrical and Computer Engineering, university of Illinois at Urbana-Champaign

[5] Sathyajith Mathew, Wind Energy Fundamentals, Resources Analysis and Economics, Springer- Verlage Berlin Heidelberg 2006, ISBN-13 978-3-540-30905-5 Springer Berlin Heidelberg NewYork.

[6] S. Pierre, C. Nichita, M.B. Camara, B. Dakyo, "Control strategy of a wind turbine simulation system designed fora hybrid wind-tidal real time emulator", 3rd Renewable Power Generation Conference (RPGTM), 24-25 September 2014, Naples, Italy.

[7] K. Kerrouche, A. Mezouar, K. Belgacem, "Decoupled control of double fed induction generator by vector control for wind energy conversion system." Energy procedia42 (2013) 239-248.

[8] Baoling Guo ; Seddik Bacha ; Mazen Alamir , A review on ADRC based PMSM control designs IECON 2017 - 43rd Annual Conference of the IEEE Industrial Electronics Society,2017.

[9] M. Singh, S. Santoso, "Dynamic models for wind turbines and wind power plants", NREL/SR-5500-52780, October 2011.

[10] Mohmed Ashglaf, Cristian Nichita, Tekbon Jerry, Study of an electromechanical coupling of a wind - tidal turbines hybrid system using the functional similarities of a real-time emulation system, SGE national conference 3-5 juillet 2018, Nancy France.

[11] Roger H. Charlier, Charles W. Finkl Ocean Energy: Tide and Tidal Power Publisher: Springer-Verlag Berlin Heidelberg, Year: 2009 ISBN: 3540779310,978-3-540-77931-5,978-3-540-77932-2

[12] Baker, A. Clive. Tidal Power, Published by the Institution of Engineering and Technology, London, United Kingdom 1991 Peter Peregrinusm Ltd.

[13] G. Caraiman - "Etude de la transposition des similitudes éolien-hydrolien en vue de la conception et du développement d'un émulateur électromécanique de turbine hydrolienne. " thèse de Doctorat, Université du Havre, Décembre 2011.

[14] Muyeen, S.M; Tamura, J; Murata, T. Stability Augmentation of a Grid-connected Wind Farm 2009, XIV, 248 p. Springer, ISBN: 978-1-84800-315-6.

[15] K. Kerrouche, A. Mezouar, K. Belgacem, "Decoupled control of double fed induction generator by vector control for wind energy conversion system." Energy procedia42 (2013) 239-248.

[16] Cristian Nichita, Mohmed Ashglaf, Jerry Tekbon, Preliminary study of a concept of wind-turbine coupling using functional similarities and systems emulation in real time, International Congress of Energy and Environment 28-29-mars-2018 Fes, Marco.

[17] D. Ikni, M.B Camara, A. Payman, B. Dakyo, "Dynamic control of wind energy conversion system", Ecological vehicles and renewable energies (EVER), 8thinternational conference and exhibition on, Monaco, 2013.

[18] S. Pierre, «Contribution au développement d'un concept d'hybridation énergétique: structures de commande d'un système intégré éolien-hydrolien» Thèse de doctorat, Université du Havre, 2015.

[19] Abobkr Hamida Abobkr, M. E. El-Hawary, Evaluation of Wind Turbine Characteristics Built-in Model in Matlab Simulink, Electrical Power and Energy Conference (EPEC), 2016.

[20] Haitham Abu-Rub,Mariusz Malinowski, Kamal Al-Haddad. Power Electronics For Renewable Energy Systems, Transportation and Industrial Applications.A co-publication of ieee Press and John Wiley & Sons Ltd 2014, ISBN: 978-1-118-63403-5 (cloth).

[21] Abad, G., López, J., Rodríguez, M.A. et al. (2011) Doubly Fed Induction Machine: Modeling and Control for Wind Energy Generation, John Wiley & Sons, Inc.

[22] Pena, R., Clare, J.C., and Asher, G.M. (1996) doubly fed induction generator using back-to-back PWM converters and its application to variable-speed wind energy generation. iee Proceedings - Electric Power Applications, 143, 231–241.

[23] C. Chevassu, "Electrical Machines, Courses and Problems", Course Paper, Ecole Nationale Supérieure Maritime, July 2012 edition.

[24] Subramanian Chandrasekaran" Grid Connected Doubly Fed Induction Generator Based Wind Turbine under LVRT" Alma Mater Studiorum – University of Bologna, Italy 2014.

[25] Salma El Aimani «Modeling different technologies of integrated wind turbines in a medium voltage network. PhD Thesis, Ecole Centrale de Lille, 2004.

[26] Wu, B., Lang, Y., Zargari, N., and Kouro, S. (2011) Power Conversion and Control of Wind Energy Systems, John Wiley & Sons, Inc.

[27] Seddik Bacha, Iulian Munteanu, Antoneta Iuliana Bratcu. (2014) General Control Principles of Power Electronic Converters. In: Power Electronic Converters Modeling and Control. Advanced Textbooks in Control and Signal Processing. Springer, London

[28] Octavian Curea, Brayima Dakyo, "Research and validation of knowledge models of a converter fed synchronous machine for diagnostic: conception of a virtual instrumentation", PhD thesis, university of Le Havre, 2001.

[29] S. Müller et al., Doubly fed induction generator systems. ieee Industry Applications Magazine, 2002. 8(3): p. 26-33.

[30] B. K. Bose, Power Electronics and Drives. Elsevier, 2006.

[31] B. Wu, High Power Converters and AC Drives. John Willy & Sons. Inc., 2006.

CHAPTER THREE

CONTROL METHODS FOR POWER CONVERSION SYSTEM BASED ON WIND/TIDAL TURBINES SIMILARITIES

3.1 Introduction

In order to optimize the functionality of a renewable energy conversion system, a specific control is essential to extract as much as possible of energy available in the wind or tidal current. In other words, the control of a renewable energy system is very important to exploit the system ideally during its lifetime.

Recently researches conducted in the field of hybrid wind-tidal power generation systems are mentioned in chapter one. But the majority of these researches and works concerns the electrical coupling only. In this chapter the concept of Offshore Hybrid Wind/Tidal Power Conversion System electro-mechanical coupled on the same shaft is treated and developed. The specific control strategy of doubly fed induction generator is presented. As well as, the concept of time acceleration called also "virtual time" is addressed in order to improve the HILS emulator's performances.

3.2 Offshore Hybrid Wind/Tidal Power Conversion System

3.2.1 Concept of Electro-mechanical Coupling

This work focused on coupling two resources of energy specifically (wind and tidal), and due to the similarity between these resources (wind-water) and the possibility of such combination is investigated. This is new concept of offshore hybrid wind-tidal turbine, what so-called "electro-mechanical coupling", where a wind turbine and a tidal turbine are coupled to the same shaft with a Doubly-Fed Induction Generator (DFIG).

A similar study is conducted by Japan Company called Mitsui Ocean Development &Engineering Company (MODEC), where the scientists and researchers expected that, such combination will produce energy two times more than the conventional wind turbine [1].

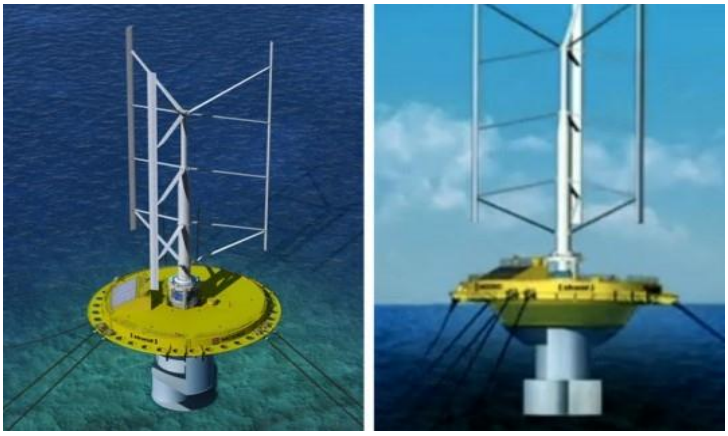

Figure 77 World's First Floating Wind-Current Turbine will be installed off Japanese's Coast

In electro-mechanical coupling, it is possible to have several scenarios of operation:

1. Single operation mode, where only one turbine is connected to the generator, while the other turbine is disconnected, according to certain conditions (wind – tidal speed), in this type of coupling an automatic clutch system is used to connect and disconnect turbines as needed.
2. Simultaneous operation mode, when two turbines are coupled mechanically at the same time (wind and tidal) to the generator's shaft.

3.2.2 Assumptions for Simulation of Electro-Mechanical Coupling

The functional concepts of horizontal tidal turbine are close to those of a wind turbine. So, fast development could be expected for tidal power generation system, depending on the already developed technologies of wind power systems [2] [3].

Both wind and tidal horizontal turbines operate based on the same principle of energy conversion. In other words, convert the kinetic energy of a fluid into mechanical energy then transforms this later into electrical energy. Despite some differences in the properties of both resources (water and air), but the tidal energy conversion system is very similar to the wind energy conversion system i.e. (have the same structure). Due to the intermittency of the natural resources, these resources can be modeled as nonlinear input with different statistical properties [4].

Figure 78 presents synoptic diagram of electro-mechanical coupling of wind/tidal turbines.

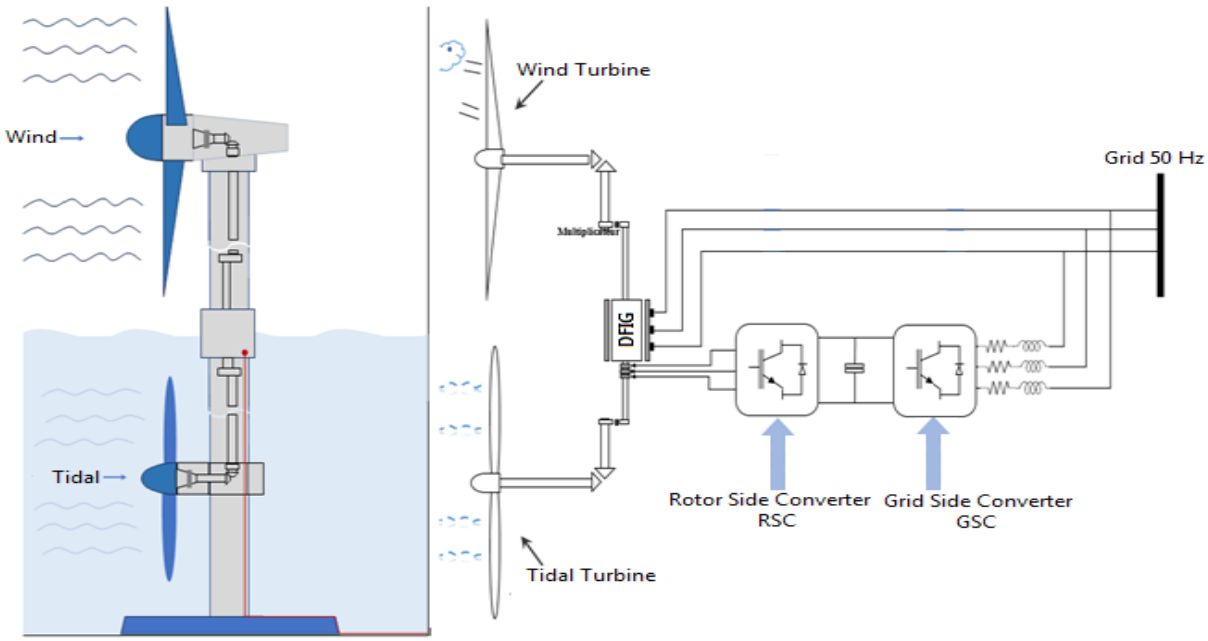

Figure 78 Electromechanical Coupling of Wind/Tidal Turbines

The suggested system that we studied is composed of the following elements

- 2- Poles asynchronous electrical generator (DFIG), 1200W.
- 3- Blades horizontal wind turbine.
- 3- Blades horizontal tidal turbine.
- Wind and tidal profiles (7.8-11.8 m/s and 0.2-1.9m/s) respectively.
- Actual rotation speed maintained at 1550 revolution /minute.
- Simulation period 30 minutes.

As the power coefficient Cp represents the efficiency of the turbine, to convert fluid energy into mechanical energy. In this work, the estimation of this coefficient is based on the theory of Rankine – Froude. Considering incompressible fluids, thus simplify modeling resources to be implemented as input in real time emulator and in control system [5]. Based on these approaches [6], we have developed simulation software that makes it possible to obtain mechanical power as function of rotation speed and some other static characteristics of a hybrid system.

It is supposed that static characteristics of the turbine to be simulated are unknown, turbine static characteristics are obtained using the simulation approach that developed at GREAH lab and are tested at the Inha University (South Korea). These results are validated with real ocean turbine installed in Circulating Water Channel of Inha University Ocean Engineering Laboratory [7].

The qualitative analyses takes into account the wind speed vector in respect to the turbine blades in horizontal axe, for a section of blade at a distance r from the axes of rotated propeller as we presentd in chapter 2.

The used adopted approach is based on specific methods and modelling algorithms of wind turbine, through which the pitch angle can be changed, starting from its constructive characteristics. These algorithms allow generating the main characteristics of the turbine:

- Power coefficient $C_p = C_p(\lambda, \beta)$
- Torque coefficient $C_\Gamma = C_\Gamma(\Omega, v, \beta)$

These results will be discussed in chapter 4.

3.3 Turbine Control System

Control system of a wind or tidal turbine is composed of different elements that interact together in order to guide the whole system to function as required and in the same time safely. So, wind or tidal turbine control system is composed of a wind speed and wind direction sensors (anemometer) to measure wind speed and its direction, then transmit to the comparator or controller to compare and find out the correction value, thus the correction value will be send to the actuator which will manipulate the final control element which could be turbine's blade to adjust the angle of blades according to wind speed or re-orients the turbine to face the wind direction. In addition, some important variables need to be observed and manipulated, so that the turbine performance will be improved and riches its objective to control the system [8].

These parameters are indicated in table 8.

Table 8 Parameters of Power Conversion System Understudy

1. Turbine	2. Electrical Generator	3. Electrical Grid
Speed	Speed	Power
Torque	Load	Power factor
Efficiency	Voltage	Voltage
Mechanical Power	Frequency	Frequency
	Efficiency	

3.3.1 Control Strategies of Wind/Tidal Turbines

Considering the functional characteristics and similarities between the wind and tidal horizontal axis turbines highlighting in the 1st chapter, we develop control strategies for one "generically" turbine based on experience of wind engineering control.

In fact, controlling the speed of the generator and the angle of attack (pitch angle) are the most effective methods to adjust rotation speed of the turbine, hence the power output of the system. Pitch and generator speed control are main control elements used to regulate turbine functionality throughout the power curve. The strategies are divided into two parts as following below [8].

Fixed-Speed Control

a- Fixed-Pitch

b- Variable-Pitch

Variable-Speed Control

a- Fixed-Pitch

b- Variable-Pitch

Fixed-Speed & Fixed-Pitch Control Method

In this configuration, the turbine's generators are directly connected to the power grid, the generator rotational speed is limited by the power line frequency (the rotational speed is fixed). Passive stall methods are usually used to regulate turbines at high wind speeds. The gearbox ratio selection becomes essential for this passive control thus it ensures that the rated power is not exceeded [9].

Fixed-Speed & Variable-Pitch Control Method

This configuration leads to fix the pitch angle below the rated wind speed, and keeps changing continuously the pitch angle above the rated wind speed. However, fixed-speed operation implies a maximum output power at only one wind speed. It is possible to use feather and stall pitch control methods in this configuration to limit power. Keep in mind that both, feathering and stalling have some disadvantages (takes a significant amount of control design and increases unwanted thrust force as stall increases) respectively [9].

Variable-Speed & Fixed-Pitch Control Method

In this configuration power electronics are used to control the synchronous speed of the generator by adjusting continuously the rotor speed relative to the wind speed. Fixed angle of attack relies heavily on the blade design to limit power through passive stalling. The power efficiency is maximized at low wind speeds, and rated turbine power can be achieved only at one wind speed. Passive stall regulation plays an important role in not achieving the rated power and leads to poor power regulation above the rated wind speed. In lower wind speed cases, this method can extract more energy and improve power quality [10].

Variable-Speed & Variable-pitch method

This design is a derivation of (variable speed – fixed pitch and fixed speed – variable pitch). Operating below the nominal speed, variation of speed and angle of attack is used to maximize energy capture hence increasing power quality. Operating above the nominal speed, fixed speed and variable pitch allows efficient power regulation at the rated power [10].

Variable Speed Control

Turbine Speed Control Zones

There are four stages of power/wind development on the turbine shaft as presented in figure 80. We considered that the tidal turbine is a horizontal axis and three blades designed in order to take advantage of the functional similarities with the wind turbine. Therefore, we consider in principle that the operating zones are the same as those of a wind turbine.

In each stage there is limit must not be over ride and certain control action must be taken, these stages are determined as follows [11]:

1. Minimum operation speed limit
2. Extraction of maximum power from variable speed operation with partial load.
3. Limit the maximum speed at partial load operation.
4. Limit the maximum operating speed at rated power output.

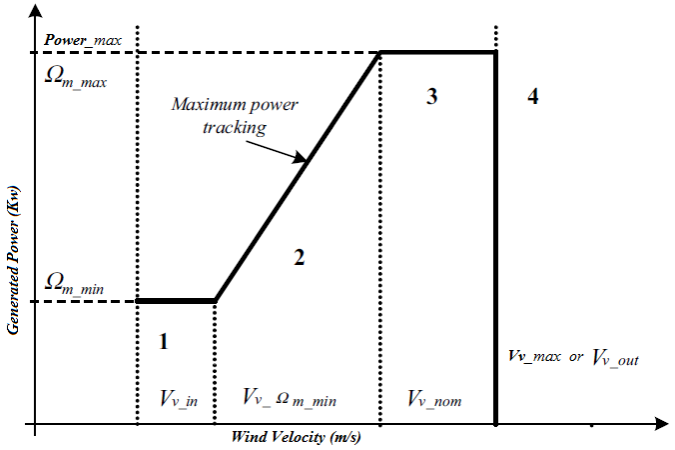

Figure 79 Generated Power as Function of Wind Velocity

- **Zone 1:** it is the starting zone of the turbine. Indeed, below a minimum wind speed required for starting, the turbine does not work (P = 0)
- **Zone 2:** it can be noted that the power of the turbine increases according to the wind speed until reaching its nominal value. In this zone, the control will make it possible to extract the maximum power for a given wind speed.
- **Zone 3:** whatever the wind speed between V_{nom} and V_{max}, the power must remain at its nominal value. So, the turbine must run at speed constant.

- **Zone 4:** beyond the maximum speed, a safety device (operating safety system) must be activated to protect the turbine from being damaged [12].

  According to the simulation methodologies presented in chapter 2, we obtained the power curve - wind speed, for a low power wind turbine that we had chosen for the study for reasons of implementation then on the real-time emulators. This curve corresponds to the power domains of emulators limited to kilowatts. This figure shows the three different zones of operation, cut-in wind speed zone, maximum power point tracking zone, and cut-off zone.

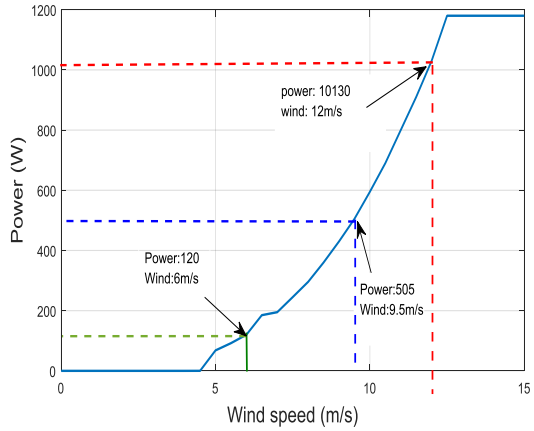

Figure 80Wind - Power Curve for low power wind turbine

Maximum Power Point Tracking MPPT

The optimization of energy conversion systems (extraction as possible as it could be the power available in the air by the system) is a very important issue for renewable power generation systems, among these energy sources, wind and tidal energy systems. In fact, this optimization is necessary not only to maximize the efficiency of the wind turbine, but also to minimize the time of the investment during its installation and operation [10].

The extracted power characteristic is considered as a function of the rotation speed and the wind speed P (Ω, v). Figure 82 shows that, for every wind speed, there is a maximum power point of mechanical power can be extracted by the turbine [11]. The optimization method used must keep the turbine rotate at its optimal operation condition.

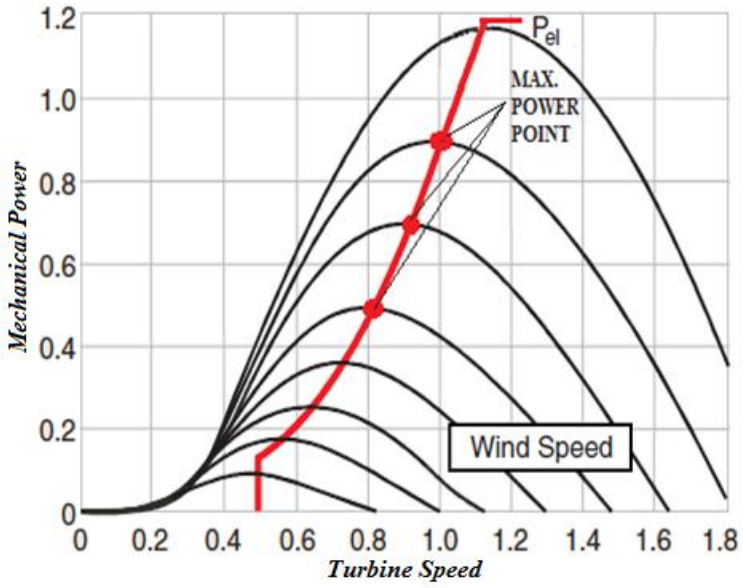

Figure 81 Power as Function of Turbine Speed

Depending on the designing control strategy, different methodologies of tracking the maximum power point Tracking are used. Therefore, Maximum Power Point Tracking (MPPT) can be classified into four categories.

i. "Look-up table" Technique

ii. The disruptive-observer Technique (P & O)

iii. The optimal specific speed Technique

iv. Optimal Torque Technique

The first two methods mentioned above are used in cases where the static characteristic of the wind power is not known; while the last two methods are based on the knowledge of the static characteristic [12].

Each of these methods has its advantages and disadvantages.

i. "Look-up Table" Technique

It is a commonly used method. It requires a rotation speed sensor or observer for the generator and a pre-registration table which contains the values of the generator's optimal speed of rotation which corresponding to each wind speed so the maximum power is extracted.[13]

ii. Perturbation - Observation Techniques (P & O)

Disruption –Observation, it is a method based on simple algorithms. It does not require prior knowledge of the characteristics of the wind turbine. Nevertheless, it is inefficient for a system with great dynamics like a wind turbine. It is mainly used for slower dynamics such as photovoltaic systems [14].

iii. The Optimal Specific Speed Technique

This method based on finding the optimal specific speed (Tip Speed Ratio) (TSR) it is commonly used in the industry. It requires an anemometer and pre-knowledge of the optimum specific turbine speed to achieve the correspondence between each value of the wind speed and the respective reference speed of the generator. It responses fast, so more wind energy is expected to be captured by this method more than other methods. [15]

iv. Optimal Torque Technique

The optimal torque search method is an alternative to the TSR method that uses the torque characteristic. It is simple method where it depends up on the optimal torque that evolving as a quadratic function of the wind turbine speed. Thus, the variation of turbine rotation speed depends on the dynamics of the mechanical coupling [16].

3.3.2 Operation Zones & Maximum Power Point Tracking MPPT

Lower and Upper Speed Control Limits: Regions 1 and 3:

The main objective of speed control in this operation zone is to maintain a constant rotation speed of the turbine at its minimum value in Zone 1 and its nominal value in Zone 3. As shown above in figure 80.

Concerning energy efficiency, optimization is not as important as in Zone 2, where the speed of the turbine may vary to maintain a specific speed λ_opt corresponding to the maximum power coefficient Cp_max. In these two zones (1, 3) the generator operates at constant speed [17-19].

Power Optimization: Region 2

In this operation zone, the aim of the speed control is to track the trajectory of maximum power extraction. In the literature, different methods are suggested to regulate the wind turbine at partial load following the maximum power extraction path.

Power Control: Region 3

As shown previously in figure 80, at a certain wind speed ($V_{\_nom}$), the power extracted by the wind turbine must held constant even though the wind speed increases; this is because the electric machine coupled to the wind turbine cannot exceed a certain speed of rotation. That's why; control system is needed to limit the power of the wind turbine for safety reasons. [20-22]

Two control systems are used to limit the power extracted by the generator to its nominal value:

- An aerodynamic stall system: in this system blades are designed with a shape to increase the lift losses at a certain wind speed.
- Pitch control system: modify the pitch angle of the blades according to the wind speed in order to maintain the power extracted by the generator at its nominal value.

The aerodynamic stall system is generally used for small-scale wind turbines at fixed speed. Constructers justify this choice that this system is more economical. [18]

The blade orientation system "Pitch Control" is mainly used for high variable speed control systems. In the latter, the blade is rotated around its axis to change the angle of attack according to the reference speed or power compared to the wind speed. [19] [20].The most common control structure for controlling the wind turbine in this region is illustrated in figure 82; this structure leads to good regulation of electric power.

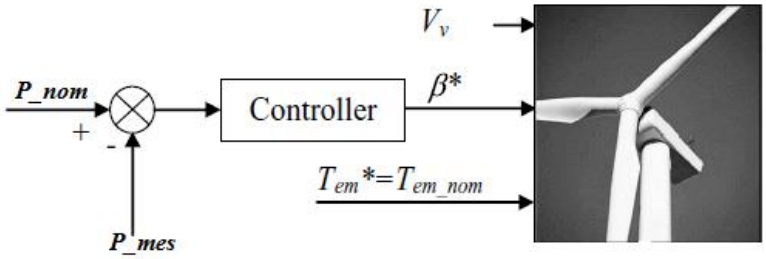

Figure 82 Schematic Diagram of Pitch Control System

Here most of the generated electrical power by the stator, that is, the electromagnetic torque produced by the electrical stator pulsation ω_s; thus the flicker emission is low with this configuration. The electromagnetic torque does not, nevertheless, use to regulate the rotation speed [8]. The pitch control uses two control loops: the power control and the control of the positioning of the blades. The purpose of the power control is to generate the reference pitch angle.

By controlling the positioning of the blades, we obtain the speed of the blades around their axis [21] [22]. This structure is associated with a speed regulation whose schematic diagram is given in the figure 83.

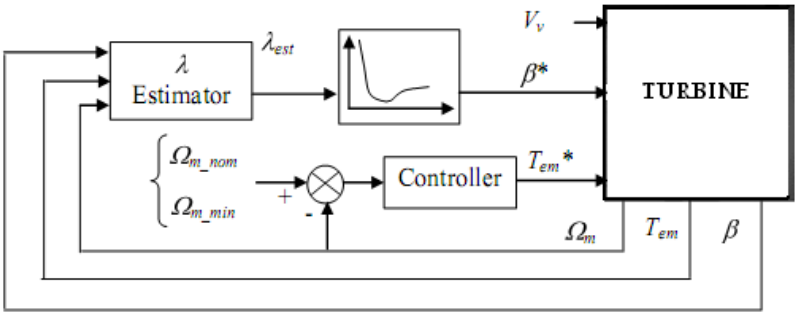

Figure 83 Speed Control Scheme for Zones 1and 3

Power Cut off: Region 4: if the wind speed exceeds the operating limit imposed by the manufacturer, the turbine must stop, either by stall or by pitch.

3.4 Speed Controller (ISC) Strategies

Two different types of strategies have been considered that will be described and developed below.

3.4.1 Indirect Speed Controller (ISC) Strategy

From Zone 2 of figure 80 the turbine operates at a point around the optimal power point of the turbine. This means that for any rotational speed variation around a point in the maximum power curve.

Suppose that a wind turbine is operating at point (a) of the curve in figure 84a, the wind speed and the electromagnetic torque being fixed. If the turbine rotational speed is decreased, and the electromagnetic torque is fixed, then the turbine torque increased and the operating point will be moved to point (b), thus the turbine speed increases to get back the operating point to the preceding point (a) [8].

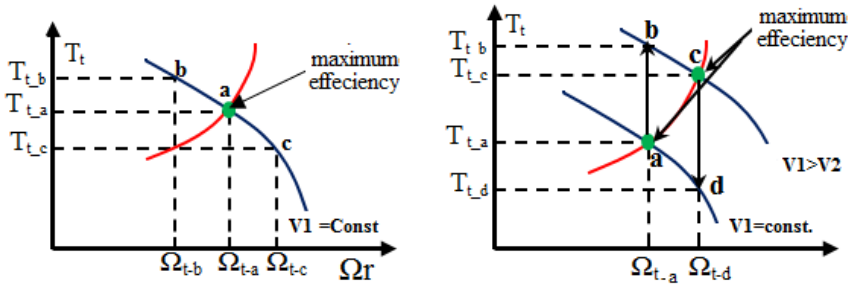

Figure 84a 85b Stability and Maximum Power Curves

If the wind speed is changed as in figure 85b then the operating point will change from point (a) to point (b), as result the turbine torque becomes $T_{t\_b.\ the\ controller}$ will provide electromagnetic torque corresponding to the maximum power curve point (c), thus will reduce the turbine torque T_{t_c} , hence the rotation speed of the turbine will be increased until reaches the adequate operating point (c).[8]

When the turbine is working on the maximum power point,

$$\lambda_{opt} = \frac{R\Omega_t}{V_v},\ C_p = C_{p\_max}\ ,\ \text{and}\ C_t = C_{t\_opt} \qquad (3.1)$$

The aerodynamic torque extracted by the turbine is then given by

$$T_t = \frac{1}{2}\rho\pi R^3 \frac{R^2\Omega_t^2}{\lambda_{opt}^2}\frac{C_{p\_max}}{\lambda_{opt}} \qquad (3.2)$$

That is,

$$T_t = \frac{1}{2}\rho\pi\frac{R^5}{\lambda_{opt}^3}C_{p\_max}\Omega_t^2 = k_{opt\_t}\Omega_t^2 \qquad (3.3)$$

Where

$$K_{opt\_t} = \frac{1}{2}\rho\pi\frac{R^5}{\lambda_{opt}^3}C_{p\_max} \qquad (3.4)$$

$$(D_{tm} = D_t + D_m)$$
$$\Omega_m = N\Omega_t \qquad (3.5)$$

Where,

$$T_{em} = -\frac{T_t}{N} + (D_t + D_m)\Omega_m \qquad (3.6)$$

Where D_t , D_m are damping coefficients of the turbine and the machine.

Replacing T_t in Equation (3.6) by the expression (3.4), we have

$$T_{em} = -k_{opt}\Omega_m^2 + (D_t + D_m)\Omega_m \qquad (3.7)$$

Where,

$$k_{opt} = \frac{1}{2}\rho\pi\frac{R^5}{\lambda_{opt}^3 N^3}C_{p\_max} \qquad (3.8)$$

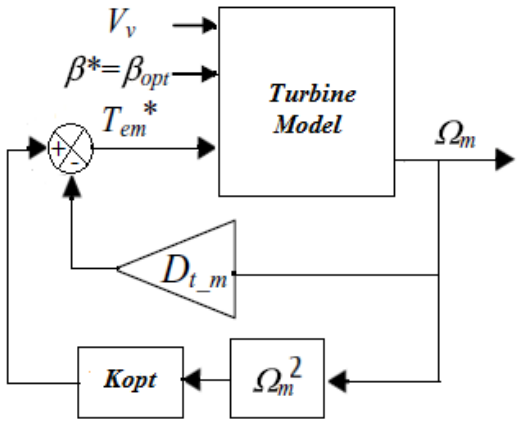

Figure 85Indirect Speed Control

Figure 86 demonstrates the indirect speed control method. As in Equation (3.7); the variation of the rotational speed Ω_t, depends on the dynamics of the mechanical coupling. With the ISC method, the behavior of the electromagnetic torque T_{em} and that of Ω_t is the same, as long as the relation between Ω_t and T_{em} has no dynamics. The electromagnetic torque is not used to increase the Ω_t dynamics as it could be if it were the output of a regulator. Therefore, the main disadvantage of the ISC is that the mechanical coupling dynamics is not cancelled out, leading to a fixed soft response of the system [8].

3.4.2 Direct Speed Controller (DSC) Strategy

With faster dynamics the DSC follows the maximum power curve more closely. From the definition of the specific speed ratio λ, the optimal wind turbine rotational speed Ω_{t_opt} could be found from the wind speed (v_v). But unfortunately, v_v cannot be measured because it is a fictitious wind speed; it does not exist.

However, the optimal rotational speed value can be achieved by using an aerodynamic torque estimator. Based on equation (3.9) an observer is built and using magnitudes such as the electromagnetic torque T_{em} and the turbine rotational speed Ωt, directly linked to measured signals, can easily be designed to estimate the turbine aerodynamic torque Tt_est. [8]

$$J_t = \frac{d\Omega_{t\_ar}}{dt} = T_{t\_ar} - D_t\Omega_{t\_ar} - T_{em}$$

$$J_m = \frac{d\Omega_m}{dt} = T_{em} - D_m\Omega_m - T_{em} \qquad (3.9)$$

$$\frac{dT_{em}}{dt} = K_{tm}(\Omega_{t\_ar} - \Omega_m) + D_{tm}\left(\frac{d\Omega_{t\_ar}}{dt} - \frac{d\Omega_m}{dt}\right)$$

Thus, from Equation (3.3), in the optimal operating point

$$\Omega_m^* = N\sqrt{\frac{T_{t\_est}}{K_{opt\_t}}} \qquad (3.10)$$

The diagram of the DSC from figure 86 shows that, the reference electromagnetic torque value T_{em} is regulated using the difference between the obtained rotational speed reference and the actual turbine rotation speed. [8]

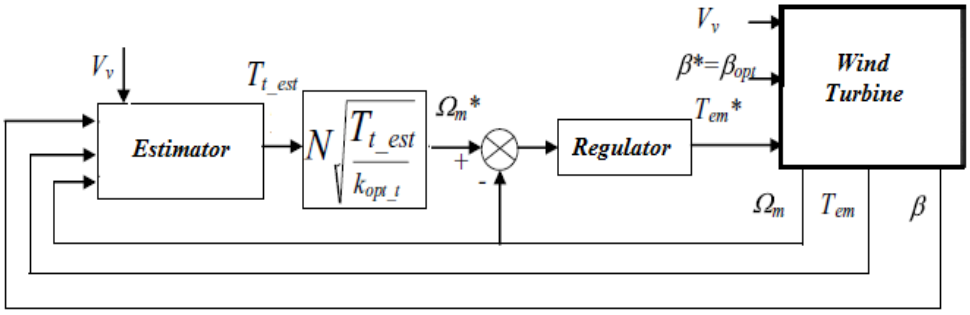

Figure 86 Direct Speed Control Block Diagram

3.5 Specific Approaches for Field - Oriented Control of DFIG

3.5.1 Steady State Analysis of Doubly Fed Induction Generator (DFIG)

Firstly, we introduce the concepts underlying steady state analysis showing how this analysis is more instructional for using it later in dynamic models. The DFIG is represented by equations through which the essential magnitudes of the machine such as: power current voltages and torque can be calculated. Equations were written as MATLAB function-file. Therefore, different steady state points of the DFIG can be obtained, this depends on how the machine being controlled, in this work, two different control strategies (magnetizing levels) are implemented, stator reactive power reference equal zero (Q_s=0), and direct rotor current equal zero (I_{dr}=0). Results are presented in figure 87.

It is noticed that, there are some variables in which two control strategies are almost the same, and in some other variable are very contrasted as in stator I_s and rotor currents I_r, and stator reactive power Q_s.

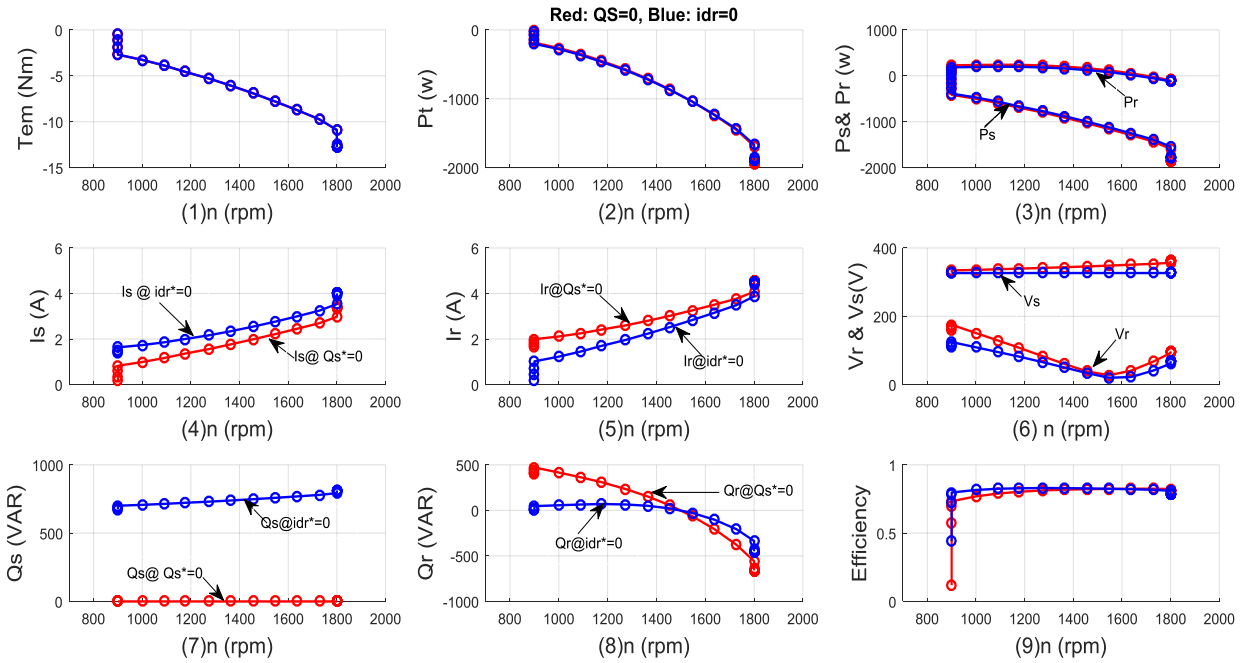

Figure 87 Steady State Analysis of DFIG

Figure 87-1 shows the input torque in function of rotation speed, as long as the torque is negative this means that, the machine operates in generator mode. Figure 87-2 represents the output mechanical power. Figure 88-3 illustrates the rotor and stator active power of the generator; we can see that the stator active power is much bigger than the rotor active power; also the active power of the rotor can be negative or positive depending on the rotation speed while the stator power is always negative.

Figure 87-4 represents the stator currents, the blue curve when the reactive power is equal to zero, and the red curve when the I_{dr} equal to zero. So, obviously when the reactive power equal to zero the maximum value of I_s is less than when the I_{dr} equal to zero.

Contrarily, in figure 87-5 we can see that with I_{dr} equal to zero makes rotor currents a little bit smaller. Figure 87-6 shows stator and rotor voltages, as the stator windings are directly connected to the grid, thus the voltage is always constant, whereas, rotor voltage depends on the synchronous speed. Figure 87-7 demonstrates reactive power generated by the stator, a clear difference between the two strategies of control high reactive power is generated where Idr equal zero, while reactive power is at minimum when Qs equal to zero. Finally, in figures 87-8 and 9 explains the rotor reactive power in both cases of control strategies and the operating efficiency of the DFIG respectively.

Figure 88 illustrates rotor and stator currents match figures 87-4 and 87-5, thus validate results of the Simulink simulation, considered that the generator model is verified for this case.

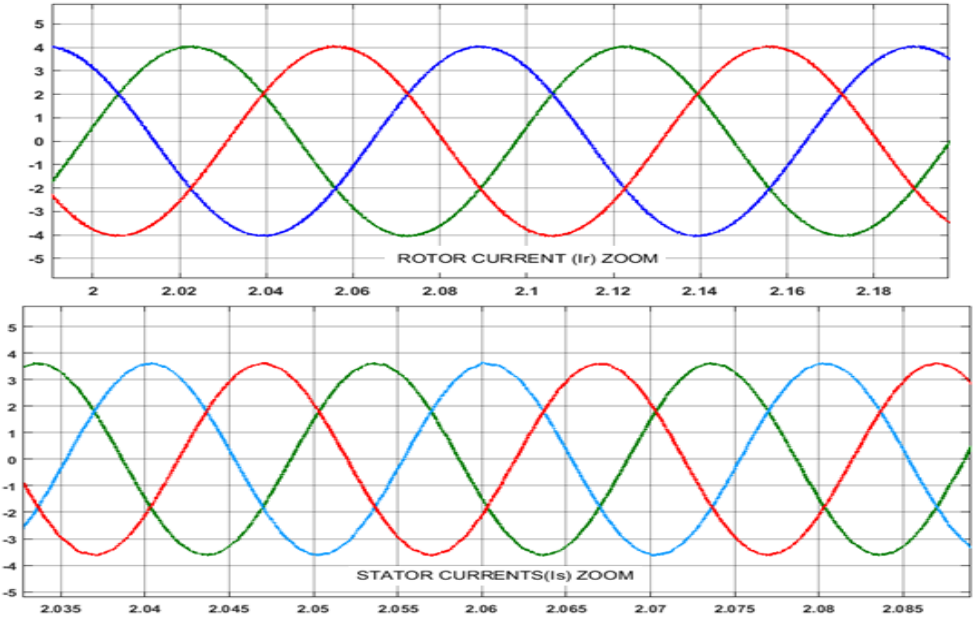

Figure 88 Rotor & Stator Current (Ir & Is) MATLAB/SIMULINK

3.5.2 Control of Rotor Side Converter (AC/DC)

As mentioned previously, doubly fed induction generators can be operated in different modes. In this work, we are interested in the hyper-synchronous generator mode; where the generated power by the stator and rotor of the DFIG is transferred simultaneously to the network.

Control of the DFIG is based on the field - oriented control of the machine's rotor voltages. There are several ways of field-oriented control classified according to the orientation of two-axis (*d*,*q*) reference frames. [11]. *for more details see appendix C*

- The rotor flux
- The stator flux
- The air gap flux.

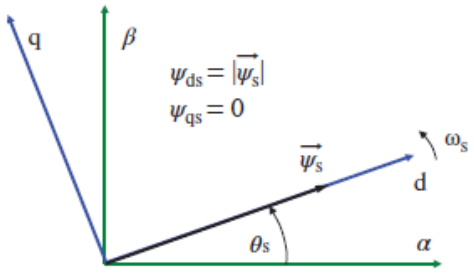

Figure 89 Synchronous Rotating dq Reference Frame

In this case, the d-axis is aligned with the stator flux space vector, as shown in figure 89. Having this alignment will lead to proportional relation between the direct rotor current and the stator reactive power, and that the quadrature rotor current will be proportional to the torque or active stator power. Therefore, the following implications are obtained: [23]

$$\Psi_{sq} = 0 \text{ and } \Psi_{sd} = \Psi_s \quad (3.11)$$

Therefore, the quadratic component of the stator flux is zero. So, equations of the DFIG model in the reference (d, q) frame will be as following:

$$\begin{aligned} V_{ds} &= R_s I_{ds} + \frac{d\Psi_{ds}}{dt} \\ V_{qs} &= R_s I_{qs} + \omega_s \Psi_{ds} \\ V_{dr} &= R_r I_{dr} + \frac{d\Psi_{dr}}{dt} - \omega_r \Psi_{qr} \\ V_{qr} &= R_r I_{qr} + \frac{d\Psi_{dr}}{dt} + \omega_r \Psi_{dr} \end{aligned} \quad (3.12)$$

Where ψ;

$$\begin{aligned} \Psi_{ds} &= L_s I_{dr} + L_m I_{dr} \\ 0 &= L_s I_{qs} + L_m I_{qr} \\ \Psi_{rd} &= L_r I_{rd} + L_m I_{sd} \\ \Psi_{rq} &= L_r I_{rq} + L_m I_{sq} \end{aligned} \quad (3.13)$$

Where electromagnetic torque can be controlled via the following expression:

$$T_{em} = P \frac{L_m}{L_s} I_{qr} \Psi_{ds} \quad (3.14)$$

From equation 3.13 the rotor flux equation can be re-written as:

$$\Psi_{dr} = \left(L_r - \frac{L_m^2}{L_s} \right) I_{dr} + \frac{L_m}{L_s} \Psi_{ds} = \sigma L_r I_{dr} + \frac{L_m}{L_s} \Psi_{ds} \quad (3.14)$$

$$\Psi_{qr} = \left(L_r - \frac{L_m^2}{L_s} \right) I_{qr} = \sigma L_r I_{qr} \qquad (3.15)$$

With ; $\sigma = 1 - \frac{L_m^2}{L_s L_r}$

By substituting rotor flux equations 3.13 in voltage rotor equations 3.12 the final rotor voltage can be written:

$$\begin{aligned} V_{dr} &= R_r I_{dr} + \sigma L_r \frac{d}{dt} I_{dr} - \omega_r \sigma L_r I_{qr} + \frac{L_m}{L_s} \frac{d}{dt} \left| \overrightarrow{\Psi_s} \right| \\ V_{qr} &= R_r I_{qr} + \sigma L_r \frac{d}{dt} I_{qr} + \omega_r \sigma L_r I_{dr} + \omega_r \frac{L_m}{L_s} \frac{d}{dt} \left| \overrightarrow{\Psi_s} \right| \end{aligned} \qquad (3.16)$$

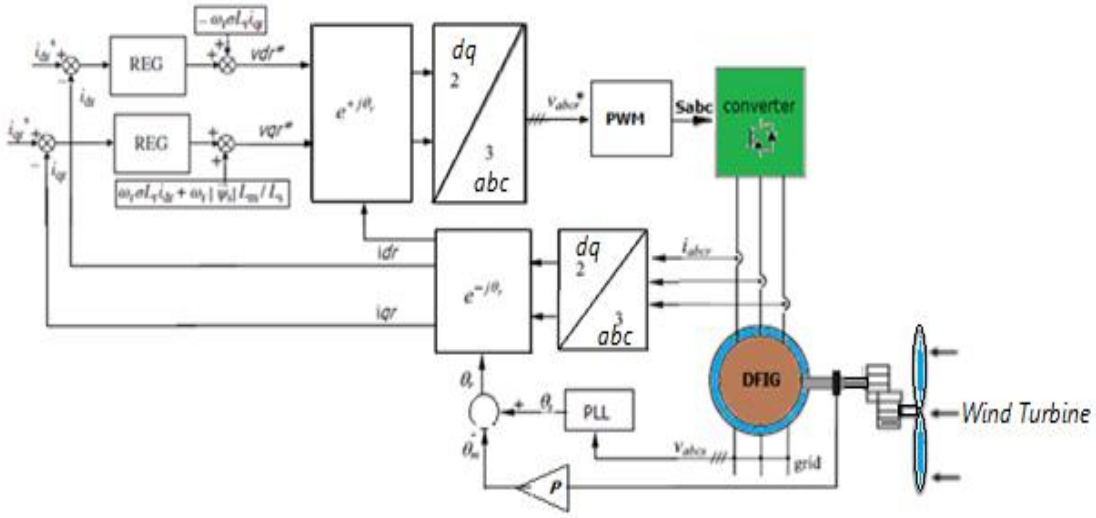

Figure 90 Rotor Current Control Loop Block Diagram

From Equation (2.42), for instance, supposing that the voltage drop in the stator resistance is small, the stator flux is constant because it is connected directly to the grid at constant AC voltage; as result, the term is zero. These last two equations reveal that it is possible to control dq rotor currents, by using a simple regulator for each current component, as shown in Figure 91. Cross terms of Equation (3.16) can be added at the output of each regulator in order to assist the regulator. Note that the stator flux and ωr must be estimated for that purpose; however, the angle θr must be estimated for the reference frame transformation. The control must be executed in dq coordinates, so the rotor currents and voltage must be transformed into rotary frame. Therefore, it is possible to calculate the angle of the stator voltage space vector, then subtract 90 ∘ from this estimated angle, and thus, obtain θs. A simple phase-locked loop (PLL) can be used to perform

the stator voltage grid synchronization, providing robustness to the estimation and a rejection of small disturbances or harmonics. Note that if the DFIG employed presents a different turn's ratio at the stator and rotor, it must be considered at the control stage. In the control block diagram presented in figure 90, the current loops work with the rotor currents referred to the stator side, while the conversion to rotor-referred quantities is performed at the measurement stage for the currents and before the creation of the pulses for the converter for the voltages. [24]

Equivalent Current Control Loop

However, system shown in figure 90 can be represented by an equivalent second order system for both current loops as illustrated in figure 91, two equal proportional-integral (PI) regulators are chosen for both loops, by neglecting the effect of the voltage source converter and using compensation of the cross terms, and the possible delays in computation or measurements, thus the two second order equations have two pols and a zero can be repositioned using classical control theory [25, 29].

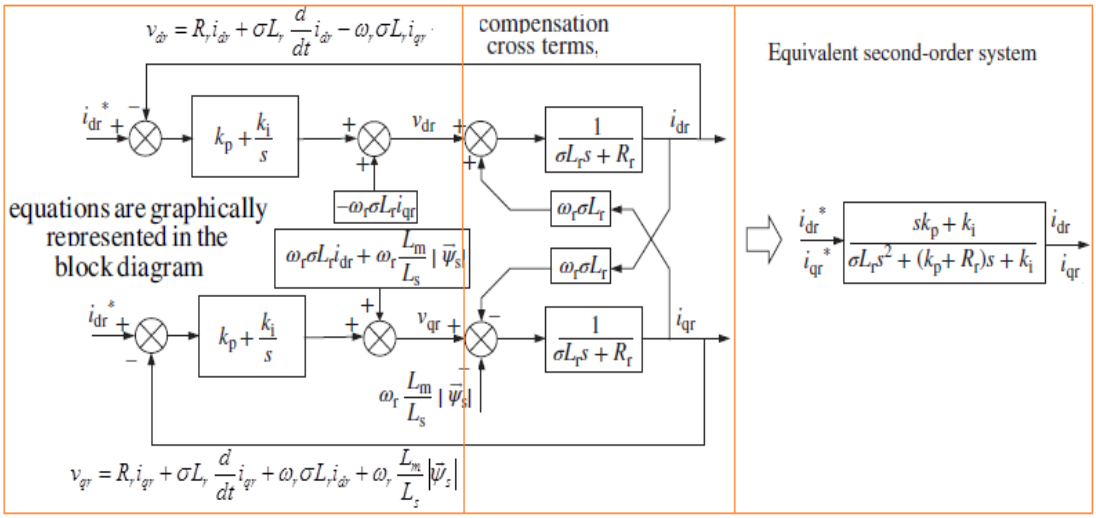

Figure 91 Equivalent Second Order System of Current Control Loop

3.5.3 Power and Speed Control

As the current and flux angle are calculated and figured out, the complete control system can be introduced. Due to the alignment of d-axis of the reference frame with the stator flux space vector, the torque equation in the *dq* frame can be re-written as follows: [29]

$$T_{em} = 1.5P\frac{L_m}{L_s}(\Psi_{qs} I_{dr} - \Psi_{ds} I_{qr}) \qquad (3.17)$$

Where ; $\Psi_{qs} I_{dr} = 0$

$$T_{em} = 1.5P\frac{L_m}{L_s}\left|\overrightarrow{\Psi_s}\right| I_{qr} \Rightarrow T_{em} = K_T I_{qr} \qquad (3.18)$$

Noticed from the equation above that the i_{qr} is proportional to the torque, which means it is possible to control the torque by controlling i_{qr}, and as result, the speed of the machine if needed. In a similar way, stator reactive power can be controlled in the *dq* frame, as shown in the following expression, which gives the possibility to manage Qs by controlling i_{dr}.[8,29,30]

$$\left|\overrightarrow{\Psi_s}\right| = \Psi_{ds} = L_s I_{ds} + L_m I_{dr} \qquad \Psi_{qs} = 0 = L_s I_{qs} + L_m I_{qr} \qquad (3.19)$$

Therefore, it is possible to control the reactive power of the stator and torque by controlling rotor currents (i_{qr},i_{dr}) independently, based on these expressions, figure 92 illustrates the complete vector control of the DFIG. Therefore, it is possible to control the magnetization of the machine by the Qs loop as long as, the stator of the machine is connected directly to the grid, as in such case the stator flux amplitude is constant, which means that $\left|\vec{\psi}_s\right| \cong \left|\vec{v}_s\right| / \omega_s$, so the following equations can be extracted. [20-23]

$$\left|\overrightarrow{\Psi_s}\right| = \Psi_{ds} = L_s I_{ds} + L_m I_{dr} \qquad \Psi_{qs} = 0 = L_s I_{qs} + L_m + I_{qr} \qquad (3.21)$$

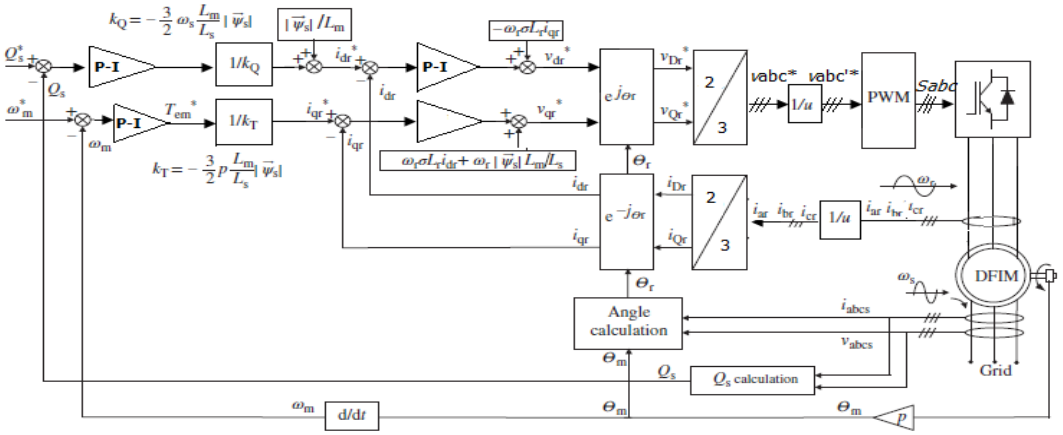

Figure 92 Complete Vector Control Loop of DFIG

3.5.4 Control of Gird Side Converter (Inverter) DC/AC

The inverter is connected to the grid via RL filter; it is positioned after the DC bus, it has two basic functions: to maintain constant DC bus voltage whatever the magnitude and direction of power flow through it, and to maintain a stable power factor at the connection point to the power grid.

Figure 93 illustrates three phase inverter of the grid side converter connected to the network via RL filter.

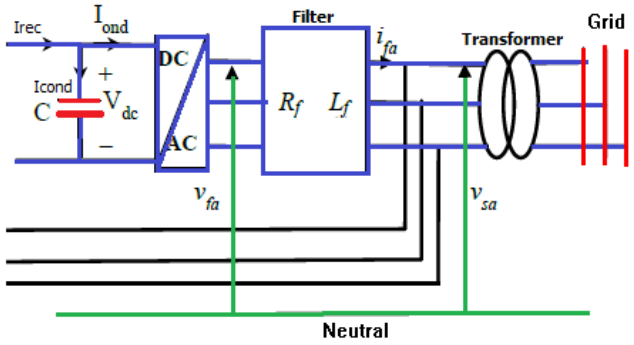

Figure 93 General Schema 3- Phase Inverter Connected Grid

The basic control principles of the grid side converter is very similar to that of the rotor side converter, where *abc* voltages are measured and transformed form three phase to two phase in the *dq* reference frame.

For simplicity a 2L-VSC topology is used. Anyway, from a vector control point of view, using multilevel or two-level topology converter the same procedure will be followed [29].

In order to keep DC bus voltage and the reactive power of the gird constant and at the required rang for both network and DFIG, as illustrated in figure 94, currents and voltages of the grid (i_{ag} i_{bg} i_{cg}), (v_{ag} v_{bg} v_{cg}), as well as the voltage of the DC bus (V_{bus}) are measured and compared to the DC bus voltage reference (V_{bus}*) and reactive power reference (Q_g*), then pulses are generated by the modulator to the converter switches or transistors to open or close accordingly. [8]

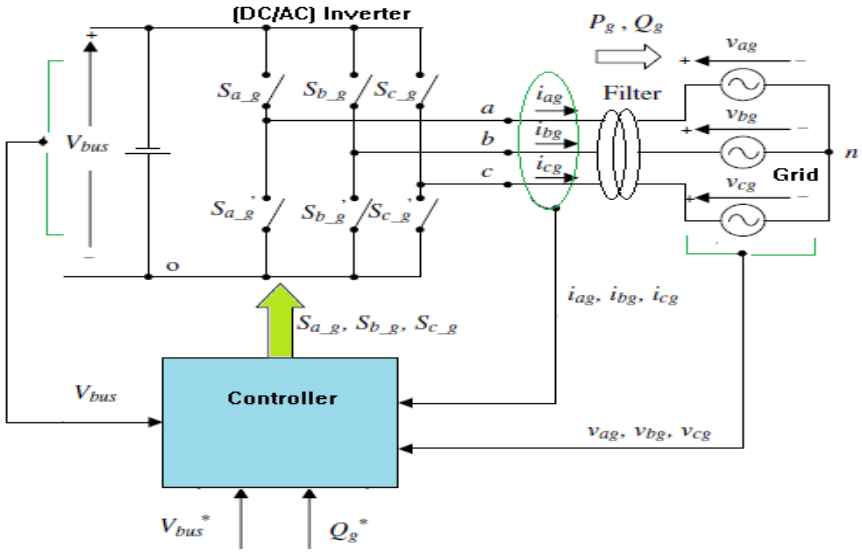

Figure 94 Grid Side Control

Figure 95 illustrates basics of control method in more details. Hence the pulses Sa_g, Sb_g, Sc_g are generated by the modulator from the *abc* voltage references for the grid side converter: *vaf**, *vbf**, and *vcf**. Whereas, these *abc* voltage references are first transformed in *dq* coordinates (*vdf**,*vqf**), then transformed to αβ coordinates (*vαf**, *vβf**), and finally generate the *abc* voltage references.

Then, the *dq* voltage references (*vdf**, *vqf**) are independently created by the *dq* current (*idg**, *iqg**) controllers. As in the following expressions: [8, 29, and 32].

$$V_{df} = R_f I_{dg} + L_f \frac{dI_{dg}}{dt} + V_{dg} - \omega_s L_f I_{qg} \qquad (3.22)$$

$$V_{qf} = R_f I_{qg} + L_f \frac{dI_{qg}}{dt} + \omega_s L_f I_{dg} \qquad (3.23)$$

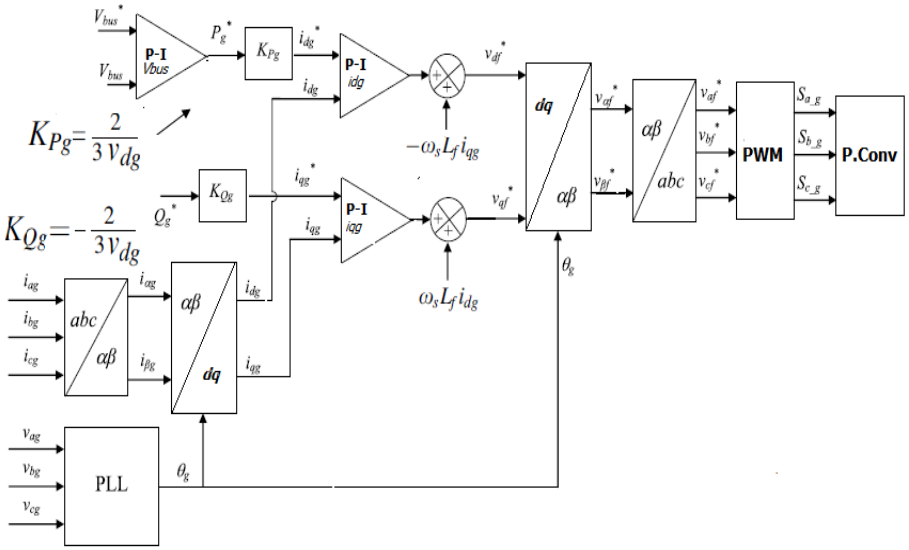

Figure 95 Grid Voltage Oriented Vector Control Block Diagram

The power at the converter output is calculated as follows:

$$P_f = 1.5\,\mathrm{Re}\left\{\overrightarrow{V_f} \,.\, \overrightarrow{I_g^*}\right\} = 1.5(V_{df} I_{dg} + V_{qf} I_{qg}) \qquad (3.24)$$

$$Q_f = 1.5\,\mathrm{Im}\left\{\overrightarrow{V_f} \,.\, \overrightarrow{I_g}^*\right\} = 1.5(V_{qf} I_{dg} - V_{df} I_{qg}) \qquad (3.25)$$

Substituting the voltage expression (3.22) and (3.23) into these last two equations, we find

$$P_f = 1.5\left(R_f \left|\overrightarrow{I_g}\right|^2 + L_f \frac{dI_{dg}}{dt} I_{dg} + L_f \frac{dI_{qg}}{dt} I_{qg} + V_{dg} I_{dg} \right) \qquad (3.26)$$

$$Q_f = 1.5\left(L_f \omega_s \left|\vec{I}_g\right|^2 - L_f \frac{dI_{qg}}{dt} I_{dg} - V_{dg} I_{qg} \right) \qquad (3.27)$$

In ideal conditions the grid active and reactive power can be calculated by the simplified expressions:

$$P_g = 1.5 V_{dg} I_{dg} = 1.5 \left|\overrightarrow{V_g^a}\right| I_{dg} \qquad (3.28)$$

$$Q_g = 1.5 V_{dg} I_{qg} = 1.5 \left|\overrightarrow{V_g^a}\right| I_{qg} \qquad (3.29)$$

However, considering that the inverter is ideal and neglecting losses in the capacitor, the inverter and the RL filter, the power supplied to the grid is identical to the power at the input of the DC bus:

$$P_f = P_{rec.} = V_{dc} I_{rec.} = V_{dc} I_{cond.} + V_{dc} I_{inv} = P_{cond.} + P_{inv.} \qquad (3.30)$$

From last equation (3.30), it is possible to control the power factor PF by regulating the DC bus voltage *Vdc*. The reference value of the continuous bus is given by the relation: [7, 27]

$$V_{dc\_ref} = \frac{3\sqrt{3V_{seff}}}{2} \qquad (3.31)$$

Where Vseff: the rms value of the mains voltage.

3.6 DC-Link (C-Bus)

If loss of power in the inverter is neglected, then the power can be expressed by the relation (3.32).

$$V_{dc} I_{dc} = \frac{3}{2} V_{dr} I_{dr} \qquad (3.32)$$

$$I_{dr} = \frac{2V_{dc}}{3V_{dr}} I_{dc} \qquad (3.33)$$

$$\text{Let} \quad \frac{2V_{dc}}{3V_{dr}} = D$$

Figure 96 illustrates the electrical model of the DC bus. The relationship between currents and the bus voltage is given by the equation (3.34) [13].

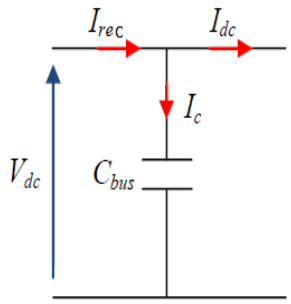

Figure 96 Diagram of DC-Bus

$$I_{dc} = I_{rec} - I_c$$
$$I_{cc} = C_{bus}\frac{d}{dt}(V_{dc}) \qquad (3.34)$$

Using both expressions, the voltage control loop can be defined as a function of the I_{dr} current, as shown in figure 97.

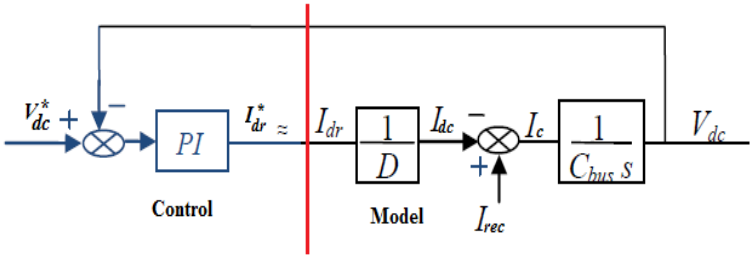

Figure 97 Voltage Control Loop

3.7 Concept of "time acceleration" in Wind Turbine Power Generation

It is important to simulate and analyses in short time, thus will save time and money, as well as reduce the risk of long time operation , and term of saving data will reduce the volume of saving data , as in wind data profiles may takes very large volume of storing data collected during days ,months and even years[10]. In this suggested method '*Time Acceleration*' wind data profile of 5 hours contains 18000 samples of wind are used to simulate and analyses electrical power that can be generated for a given site.

The basic principle of time acceleration method depends on finding out the average of the collected wind data and then standard deviation, this process will be repeated several times, each time number of samples is reduced, and consequently time of simulation will be reduced as well. We will study the effect of accelerated time simulation on the energy potential of a given site, using the same sample of data in numerical and experimental simulations.

Transition from the initial sample to a new sample is a difficult inference problem, because should specify the conditions that make it possible to say, what if the observed reduced sample is valid for the whole samples or not. This rises up the question: what size must be given to the sample, or in other words, what criteria need to be taken into account when setting the sample size?

We have chosen as criteria for setting the size of a sample two parameters: the average speed of rotation of the wind turbine (which serves as a reference for the control of the conversion chain, according to the strategy described above), and the average power that is obtained with the wind turbine for each wind profile.

3.7.1 Time Acceleration Method

In this section in virtual time a wind profile composed of variety of low and high frequencies will be generated using MATLAB program called 'sim –vent' and Simulink. It is supposed that, samples are taken every second and every minute so like this the simulation time will be reduced every time when the average of the previous wind profile is calculated.

3.7.1.1 Wind Profile Data (18000) Samples

Figure 99 presents a wind profile of 18000 samples, with average speed of 9.8m/s generated by software developed at GREAH; specifically for the HILS emulation of wind turbines. Wind turbine used in this simulation has nominal power of 1 kW, radius of 1m, power coefficient C_p 0.33, specific speed ratio λ= 5.45, and pitch angle = 0.

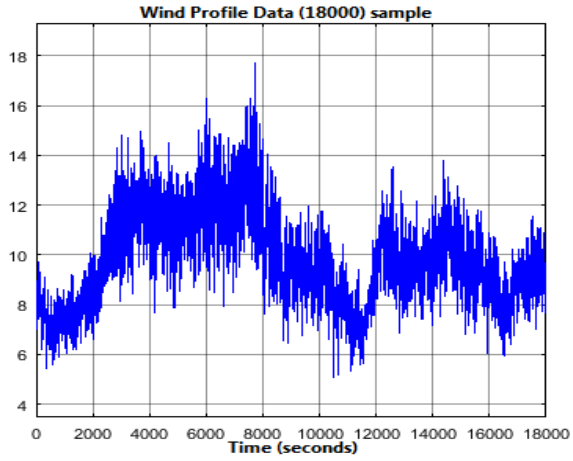

Figure 98 Wind Profile (18000 samples and 5 hours)

Figure 99 shows the rotation speed generated by the admitted wind profile; the average speed is 505 revolutions per minute.

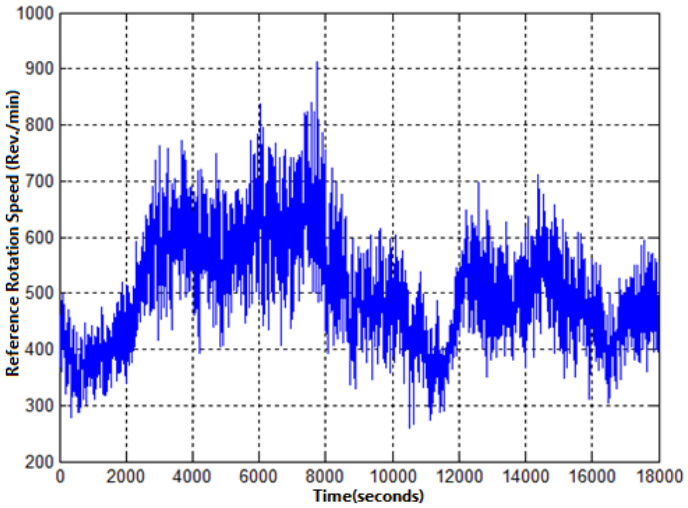

Figure 99 Reference Rotation Speed (rev/min)

Software In the Loop" (SIL) and experimentally Hardware In the Loop (HIL), used the same wind profile data (18000 samples). Figure (100 a, b) illustrates the obtained results of the Software In the Loop SIL and the Hardware In the Loop (HIL).

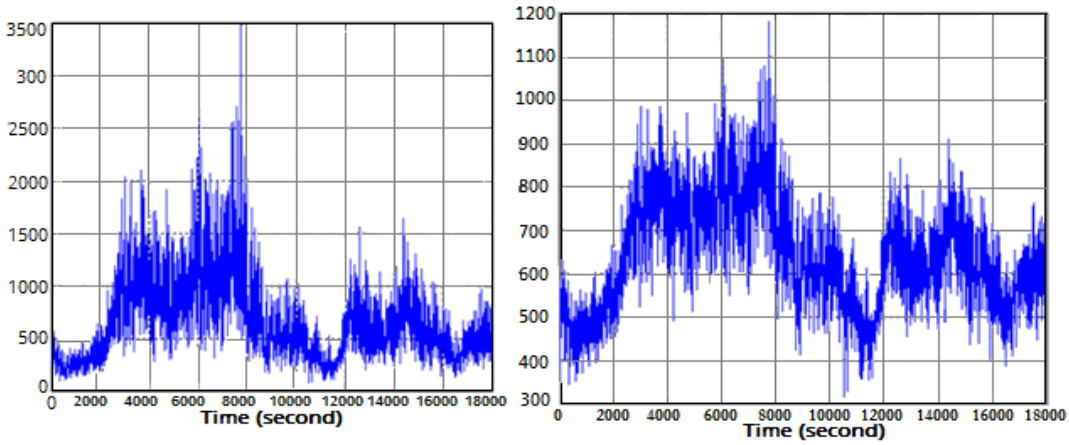

Figure 100 (a) Mechanical Power "simulation" (b) Mechanical Power experimentally

While the average mechanical power generated is 641 W; figure 100-b by the emulator.

There is measurement difference between simulation and experiment results, because it was possible to take one sample every second in the software simulation, while in the emulator, samples are taken every 1.2 second. Results obtained are still reasonable, although there is about 2% difference between hardware emulator and software simulation.

3.7.1.2 Wind Profile Data (300) Samples

Figure 101, by calculating the average of 18000 samples wind profile every minute, a new wind profile of 300 samples is generated, with the same average wind speed of the original profile 9.8 m/s. Therefore, simulation is carried out on 300 samples and instead of 18000 samples.

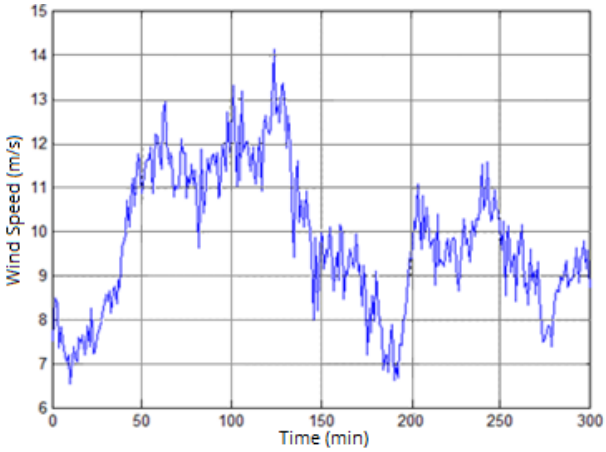

Figure 101 Wind Profile of 300 samples

Hereafter, simulation is carried out with reducing sampling time .i.e. number of samples is reduced. It is clear from figure 102 that the rotation speed generated by the wind profile of 300 samples is smoother and more stable, compared to that generated in the previous wind profile 18000 samples per second. In addition, the average rotation speed is 504.4 rev. /min; with only a difference of 0.1% from the average of rotation speed generated by the previous wind profile (18000); where the sampling time is not reduced.

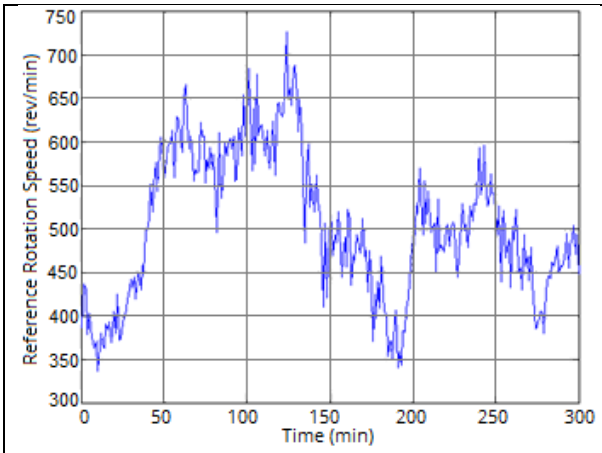

Figure 102a Rotation Speed Reference (rev. /min)

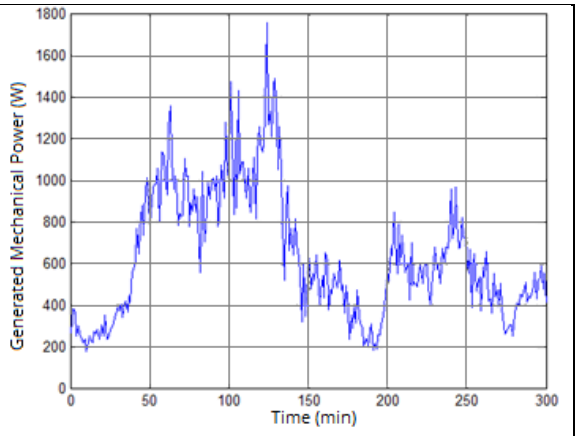

Figure 102b Wind Turbine Mechanical Power

It can be observed from figure 102b that, the maximum power obtained is much less than that generated when samples are taken every second which is 3500W; whereas in every minute, the highest power does not reach 1800W. The average mechanical power is 638W. This average power therefore, has a difference of about 2.5% compared to the non-accelerated sampling time simulation. This is due to reducing the effects of high-frequency components in the wind spectrum; this may lead to reducing the powers exchanged during the simulation.

More samples are presented in appendix D.

3.8 Conclusion

Finally, concluded that the concept of hybrid offshore wind tidal turbines 'electro-mechanical coupling' is good enough when the speed of wind and tidal are sufficient so that, the speed of the machine is greater than its synchronization speed.

If the rotation speed of one turbine is lower and the generator speed is inferior to the synchronous speed then this turbine acts as load and drag down the system. Consequently the generator speed

is much lower, therefore in this case the decoupling is necessary in order to keep the system generate electrical power.

Also, a steady state analysis and control strategy are discussed; it includes the control of the wind turbine, control of Doubly-Fed Induction Generator (DFIG), Rotor-Side Converter (RSC), and Grid-Side Converter. Two different control strategies are used to control power conversion systems: variable speed; and fixed speed control. In addition, the concept of virtual time or what so called time acceleration is described, obtained results show that time acceleration is efficient to reduce simulation time with very reasonable results, also this method is useful to decreases data size of wind profiles.

References

[1] https://inhabitat.com/worlds-first-floating-wind-current-turbine-to-be-installed-off-japanese - coast.

[2] Jerry Tekobon, Ferhat Chabour, Cristian Nichita, "Hardware-In-the-Loop Simulation of a Hybrid Wind - Tidal Energy System, 2016, Maroc, 2016.

[3] P.J. Moriarty, A.C. Hansen. AeroDyn Theory Manual. Golden, Colorado: National Renewable Energy Laboratory, 2005.

[4] Jai N. Goundar, M. Rafiuddin Ahmed. Design of a horizontal axis tidal current turbine. Applied Energy. 2013.

[5] C. Nichita, B. Dakyo, Chapitre 6. Chaines de conversion des éoliennes offshore, "Energies marines renouvelables aspects généraux, éolien, marémoteur et hydrolien", coordinateur Bernard Multon, Editions Hermes / Lavoisier (versions en français), 2011.

[6] Wind Energy Systems Electronic Edition, by Gary L. Johnson, December 10, 2001.

[7] George Caraiman , Cristian Nichita , Viorel Mînzu , Brayma Dakyo , and Chul-Hee Jo, Simulation Platform for Real Time Ocean Current Energy Emulator", International Journal of Ocean System Engineering 2(1) (2012) 16-24

[8] Brahim Metidji, Nabil Taib, Lotfi Baghli, Toufik Rekioua, Seddik Bacha, Low-cost direct torque control algorithm for induction motor without AC phase current sensors, ieee transactions on power electronics, volume 27, pages 4132-4139, September 2012.

[9] Gonzalo Abad, Jesus Lopez, Miguel A. Rodrıguez, Luis Marroyo, Grzegorz Iwanski. Doubly Fed Induction Machine Modeling and Control for Wind Energy Generation, John Wiley & Sons, 2011 Canada.

[10] Xiang, D. and Ran, L. and Tavner, P. J. and Yang, S. 'Control of a doubly fed induction generator in a wind turbine during grid fault ride-through. ieee transactions on energy conversion. 21, 2006, Vol. 3, pp. 651-662.

[11] Hongliang LIU, Fabrice Locment, Manuela Sechilariu Contribution for integrating urban wind turbine into electrical microgrid: modeling and control, PhD thesis, university of Compiègne Avenuse, 27 February 2017.

[12] Munteanu I.; Bratcu I.A, Cutululis N.A; Ceanga E. "Optimal Control of Wind Energy Systems towards a Global Approach", London: Springer-Verlag, 2008.

[13] Freris L. L. "Wind Energy Conversion System". England: Prentice Hall International Ltd,

1990.

[14] Djamel Ikni, "Production d'énergie marine: Intégration de la production éolienne offshore dans un bouquet énergétique décentralisé". Thesis, University of Le Havre, 2014.

[15] Pan C.T, Juan Y.-L. "A Novel Sensor less MPPT Controller for a High-Efficiency Micro-scale Wind Power Generation System" ieee transactions on energy conversion, 2010 (25) 207-216.

[16] Kazmi S.M.R., Goto H., Guo H., Ichinokura O. "A Novel Algorithm for Fast and Efficient Speed-Sensor less Maximum Power Point Tracking in Wind Energy Conversion Systems". ieee transactions on industrial electronics, 2011(1).29 – 36.

[17] Datta R., Ranganathan V. T. "A method of tracking the peak power points for a variable speed wind energy conversion system". ieee transactions on energy conversion 2003(18).163 – 168

[18] Haidar Islam, Saad Mekhilef, Noraisyah Binti Mohamed Shah, Tey Kok Soon, Mehdi Seyed mahmousian, Ben Horan, Alex Stojcevski. Performance Evaluation of Maximum Power Point Tracking Approaches and Photovoltaic Systems. Energies 2018, 11, 365.

[19] Mohammad Mahdi Rezaei 'A nonlinear maximum power point tracking technique for DFIG-based wind energy conversion systems wind energy conversion systems', Engineering Science and Technology, an International Journal 25 July 2018 P. 901–908.

[20] Zakariya M. Dalala, Zaka Ullah Zahid, Wensong Yu, Member, Younghoon Cho, Jih-Sheng (Jason) Lai. Design and Analysis of an MPPT Technique for Small-Scale Wind Energy Conversion Systems. ieee transactions on energy conversion, vol.28, No.3, September 2013.

[21] Hamzaoui I. "Improvement of the performances MPPT system of wind generation". Electronics, communication and photonics conference, Saudi international, 2011.

[22] M. EL mokadem, C. Nichita, B. Dakyo, W. Kocraza, «Maximum wind power control using torque characteristic in a Wind diesel system with battery storage», Recent Developments of Electrical Drives, Springer Engineering, DOI10.1007/978-1-4020-4535-6, ISBN978-1-4020-4534-9 (Print) 978-1-4020-4535-6 (Online), 2006.

[23] Wai Hou Lioa, Bryn LI. Jones, Qian Lu and J.A. Rossiter. "Fundamental performance similarities between individual pitch control strategies for wind turbines". International Journal of Control. ISSBN 1366-5820, 07 September, 2015.

[24] Adel Merabet, Khandker Tawfique Ahmed, Hussein Ibrahim, Rachid Beguenane, and

Amer Ghias. “Energy Management and Control System for Laboratory Scale Micro-grid based Wind-PV-Battery”. ieee transactions on sustainable energy. 24 June 2016.

[25] Santiago Arnaltes, Jose Luis Rodriguez-Amenedo and Miguel E. Montilla-DJesus “Control of Variable Speed Wind Turbines with Doubly Fed Asynchronous Generators for Stand-Alone Applications”. Energies. 23 December 2017.

[26] H. Abouobaida, M. Cherkaoui, Modeling and Control of Doubly Fed Induction (DFIG) Wind energy conversion system, Journal of Electrical Engineering 2015.

[27] Ibtissam Kharchouf, Ahmed Essadki, Tamou Nasser, Wind System Based on a Doubly Fed Induction Generator: Contribution to the Study of Electrical Energy Quality and Continuity of Service in the Voltage Dips Event, International Journal of Renewable Energy Research, vol.7, No,4. 2017.

[28] Ibtissam Kharchouf , Ahmed Essadki, Tamou Nasse , Wind System Based on a Doubly Fed Induction Generator: Contribution to the Study of Electrical Energy Quality and Continuity of Service in the Voltage Dips Event, International Journal of Renewable Energy Research, Vol.7, No.4, 2017.

[29] Moussa Reddak, Abdelmajid Berdai,Anass Gourma, Jamal Boukherouaa, An Improved Control Strategy using RSC of the Wind Turbine Based on DFIG for Grid Harmonic Currents Mitigation, International Journal of Renewable Energy Research, Vol.18,No.1,march 2018.

[30] Haitham Abu-Rub, Mariusz Malinowski, Kamal Al-Haddad, Power Electronics for Renewable Energy Systems Transportation and Industrial Applications, ieee Press and John Wiley & Sons Ltd, 2014.

[31] Tony Tawil. On Sizing and Control of a Renewables-based Hybrid Power Supply System for Stand Alone Applications in an Island Context. Electric power. Université de Bretagne Occidentale (UBO); Université de Bretagne Loire, 2018. English.

[32] Li Wang, Chun-Yu Lin, Hong-Yi Wu, Anton Victorovich Prokhorov, "Stability Analysis of a Micro-grid System With a Hybrid Offshore Wind and Ocean Energy Farm Fed to a Power Grid Through an HVDC Link", Industry Applications ieee transactions, vol. 54, no. 3, pp. 2012-2022, 2018.

[33] Mouna Ben Smida, Anis Sakly, A Comparative Study of Different MPPT Methods for Grid-Connected Partially Shaded Photovoltaic Systems , International Journal of

Renewable Energy Research,vol.6 no.3, 2016.

[34] Mohmed Ashglaf, Cristian Nichita, Jerry Tekobon, Study of an electromechanical coupling of a wind - tidal turbines hybrid system using the functional similarities of a real-time emulation system, Symposium de Génie Electrique", France, Nancy 3-5 July 2018.

[35] Baoling Guo ; Amgad Mohamed ; Seddik Bacha ; Mäzen Alamir. Variable Speed micro-hydro power plant: Modeling, losses analysis, and experimental validation. International Conference on Industrial Technology (ICIT), ieee 2018.

CHAPTER FOUR

NUMERICAL SIMULATION & EXPERIMENTAL RESULTS ON REAL TIME EMULATORS

4.1 Introduction

The previous chapter addressed modeling of each element of the offshore wind - tidal turbine system. This chapter is focused on the numerical simulation completed and followed by the implementation of the hardware emulators of the wind system and the tidal system the proposed methods and hybrid power conversion system are investigated numerically and validated experimentally on emulators. As well as, control strategies are used in order to optimize the functionality of the proposed system. We develop particularly on the simulation of power generation in a virtual time approach what-so-called "accelerated time"; impact of time simulation on the estimation of energy potential for a given site is studied, using the same sample of data in numerical and experimental simulations.

4.2 Principles of Real-Time Emulation of Actuators

Emulator components are chosen with very small time constant comparing with the simulated actuators. Speed and torque variation on the actuator's shaft vary slower than the corresponding variables of the servo-motor which follows with the smallest possible errors the references (set point) given by the software subsystem. Therefore, errors in the servo loops must be negligible. Most servomotors have small time constant and that is why many actuator types can be simulated and extended. Figure 103 represents the frequency characteristics As (ω) with the bandwidth Bs corresponding to the several simulated actuators under investigation and emulation control. The emulator bandwidth is defined as the frequency range (0, ω_{cs}), in which the attenuation does not exceed a given limit, for example 3 dB (where ω_{cs}; the cut-off frequency of the subsystem). Consequently, it can be consider that the hardware system to be investigated is a wind turbine ATE (ω), a diesel motor AD (ω), some hydraulic motors AH1 (ω); AH2 (ω) or some electrical motors AE1 (ω); AE2 (ω) [1].

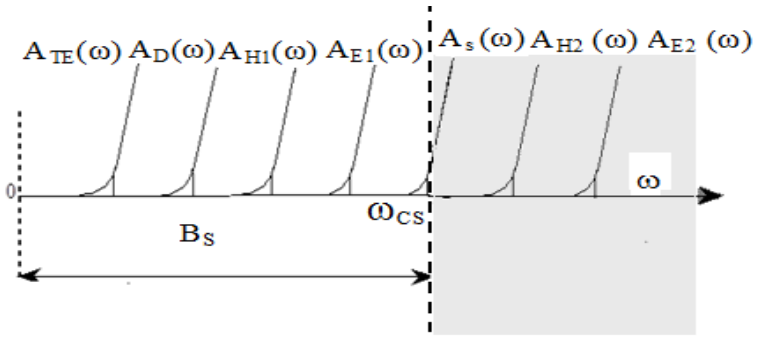

Figure 103 Bandwidths of Emulators

In addition, a new concept of "electro-mechanical coupling" in which an offshore wind-tidal turbines are coupled together on the same shaft with Doubly-Fed Induction Generator (DFIG); this proposed system is implemented experimentally.

4.2.1 Structure of Hardware Simulator

The GREAH laboratory, in addition to the wind energy emulator already available, has also developed recently a hardware simulator of small wind/tidal power generation system (2.2 kW); figure 104 shows the structure of the hardware simulator [2].

Figure 104 Hardware Simulator in GREAH Laboratory

The hardware simulator is composed of two mean parts:

Hardware System

- **Electrical Generator**: It is a 4-pole Doubly-Fed Induction Generator (DFIG), with a nominal power of 2 kW and a power factor of 0.63. Its rotor can be short-circuited to operate as an asynchronous cage generator. The generator is driven by controlled electrical motor, and the generated electrical power is delivered to the grid via AC/DC power converter.
- **Power Converter AC/DC**: it is a power converter of type TRANSOMIK U2 (see Appendix). Its function is to adjust the generated power as grid requirements, by rectifying the AC generated power to DC then inverting DC to adequate AC. It is a frequency inverter suitable for starting, braking, speed variation, closed-loop control and positioning of three-phase induction motors. It is considered as bidirectional inverter with a constant voltage and a pulse width modulation block.

- **Vector-Controlled Electrical Motor**: It is a 4-poles adjustable speed asynchronous electrical motor with nominal power 2.2kW, used to drive the Doubly-Fed Induction Generator (DFIG). It is powered by an integrated frequency converter, type MOTEC 8200 (see Appendix). It represents wind or tidal turbine by reproducing on its shaft the static characteristics of the studied turbine.
- **Mechanical Load "Break"**: It is a controlled synchronous electrical motor with nominal power 2.6kW used to generate a variable moment of inertia on the turbine's shaft. It is a self-winding, self-cooling motor able to provide the rated torque over the entire rotational speed range required for the experiment.
- **Load Control Unit**: it is used as measurement device to measure generated torque and speed, as well as an interface between a specific designed software program and mechanical load 'electrical motor'
- **Measurement Instruments**: digital and analog measurement devices used to measure and visualize process variables namely: generated active and reactive power, power factor, stator and rotor voltage and current.
- **Electrical Transformer**: It is used to equalize rotor voltages with stator voltages, and to protect rotor windings.
- **Emergency Stop Unit**: used to disconnect and isolate completely the simulator from power supply in case of emergencies.
- **Computer Connection Port:** USB connection used to connect the simulator to computer to recover the measurements digitally, and to connect oscilloscope to visualize some variable parameters and curves.
- **dSPACE Input /Output Card**: it is used as interface between the hardware and software simulator parts, and through which reference signals and feedback signals transmit.
- **Safety Guarding Cover**: it installed on the shaft coupling between the electrical motor and generator, thus the system will not start up if this part is not installed and well tied up.

Software System

The function of software system is to simulate digitally wind or tidal resources and wind or tidal turbines. Also, error correction signals are generated by regulators and reference points are given.

In addition, parameters of the system such as speed and torque can be presented in form of curves.

The software system is composed of the following items:

- **MATLAB/SIMULINK**: it is used to design wind turbines and regulators and also to present system variables such as torque –speed relationship in a form of curve hence it can be studied and analyzed.
- **dSPACE Control Disk**: It is a software program provided by dSPACE GmbH. compatible with MATLAB program via a platform : DS1103 , this program generates a configuration code which allows to communicate with hardware simulator part. Also, it has software interface 'blocks', through which input and output signals can be sent and received between soft and hard ware simulator parts figure 105.

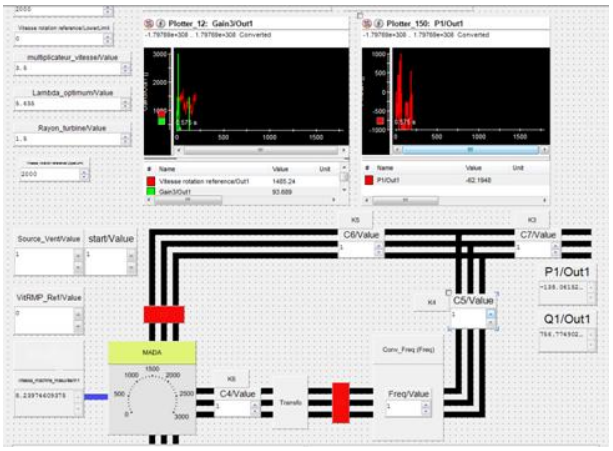

Figure 105 dSPACE Interface Guild User

- **Software "Servo Machine"**: Figure 106 the control unit used to drive the synchronizing servo machine and to measure the engine speed and torque. The already integrated interface RS232, together with the Windows® compatible software "Servo Machines", allows for an easy operation, data recording and analysis of DC-, AC- and three-phase-machine parameters, as well as a standard characteristic display and archiving on the PC. Besides the known operating functions of the Servo Drive and Brake System, such as speed control, engine torque control and automatic characteristic recording, the simulation of the gyrating masses is also possible. The moment of inertia can be set up within a large range.

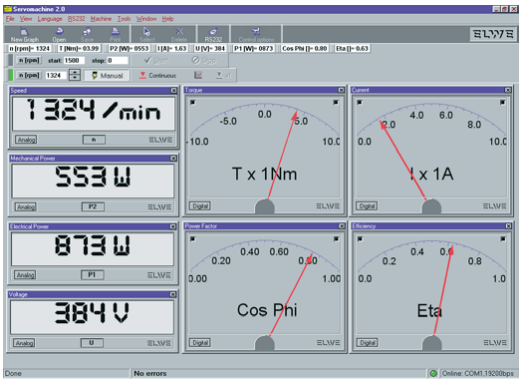

Figure 106 "Servo Machine" Interface Guild User

4.3 Simulation and Control of Power Conversion System

It is very important to simulate and control of wind and tidal power conversion system. In the following sections wind-tidal power conversion system will be simulated and controlled using MATLAB/SIMULINK simulation environment, this helps to study, investigate and exploit these resources of energy as possible as it could be, with minimum possible of risk.

Both wind and tidal horizontal turbines operate based on the same principle of energy conversion. In other words, convert the kinetic energy of a fluid into mechanical energy then transforms this later into electrical energy. Despite some differences in the properties of both resources (water and air), but the tidal energy conversion system is very similar to the wind energy conversion system i.e. (have the same structure).

4.3.1 Simulation and Control of Doubly-Fed Induction Generator Based Wind Turbine

Hereafter, the hardware simulation is modeled and simulated in MATLAB/SIMULINK as demonstrated in figure 107, where parameters of the doubly-fed induction generator are identified experimentally; while the wind turbine is configured according to the nominal power of the generator, PI regulator is used to control generator's output. The sampling time is (5µ second).

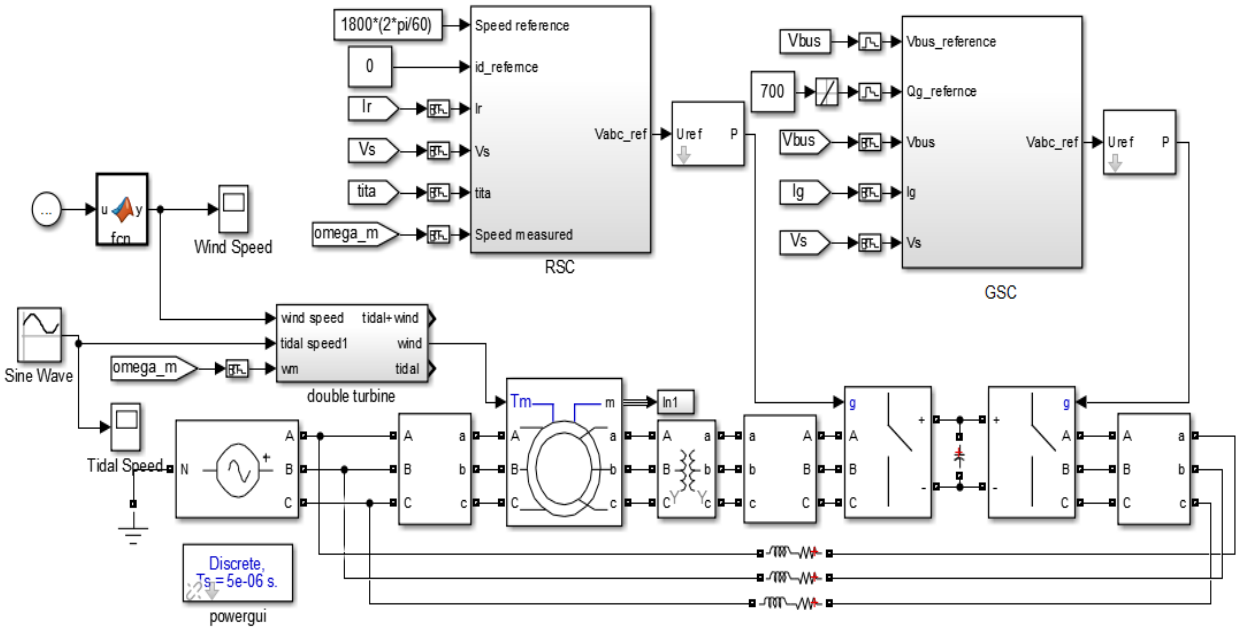

Figure 107 Schematic Diagram of DFIG Based Wind Turbine in MATLAB/Simulink

4.3.1.1 Control of Rotor Side Converter (RSC)

The generator's rotor side is an important part in the electrical machine; it includes two movements, mechanical movement and electrical movement, each of which has its effect on the mode of operation of the machine. And as result on its behavior and characteristics, thus, will determine the best way to control its actions and reactions according to the operation's need. In the following two sections two different strategies of control (**Fixed Speed and Variable Speed**) will be used to control the power productivity of DFIG using MATLAB/Simulink the '*Simscape*' model already exist in MATLAB is used. Only the rotor-side converter is addressed in this section, assuming that the DC bus voltage of the power converter is set by the grid-side converter with any dc voltage resource.

Fixed Speed Control

The classic vector control techniques is performed in a synchronously rotating *dq* frame to control the DFIM, where the d-axis is aligned, with the stator flux space vector, as illustrated in Figure 108. Having this alignment choice leads to the fact that, the direct rotor current (Idr) is proportional to the stator reactive power (Qs), and that the quadrature rotor current (Iqr) is proportional to the torque or active stator power (Tem). Therefore, from the model of the DFIM in a stationary reference frame (αβ), by substituting rotor flux equations ($\vec{\psi}_s^{\,a}$ and $\vec{\psi}_r^{\,a}$) into the

rotor voltage equation ($\vec{v}_r^a$), the obtained rotor voltage will be a function of the rotor currents and stator flux (note that ψqs = 0):

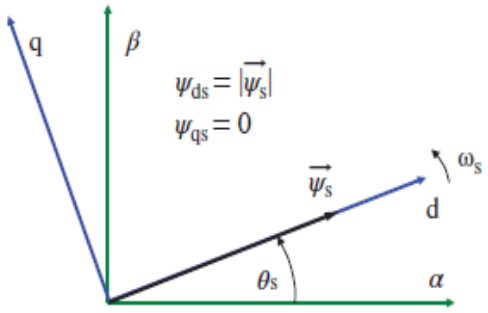

Figure 108 dq Synchronous Rotating Reference Frame Aligned with Stator Flux Vector

The control strategies are carried out under the following assumptions:

- Stator windings are connected to a stable gird, so flux is constant; and its variation to time equal zero.
- From dq rotor voltage equations, the direct and quadrature rotor currents will be controlled separately, using simple PI regulator.
- Electrical rotation angle (θr) must be calculated for the sake of frame transformations stationary to rotary frames.
- The conversion to rotor-referred quantities is performed at the measurement stage for the currents and before the generation of the pulses by PWM to the power rotor side converter. [3]

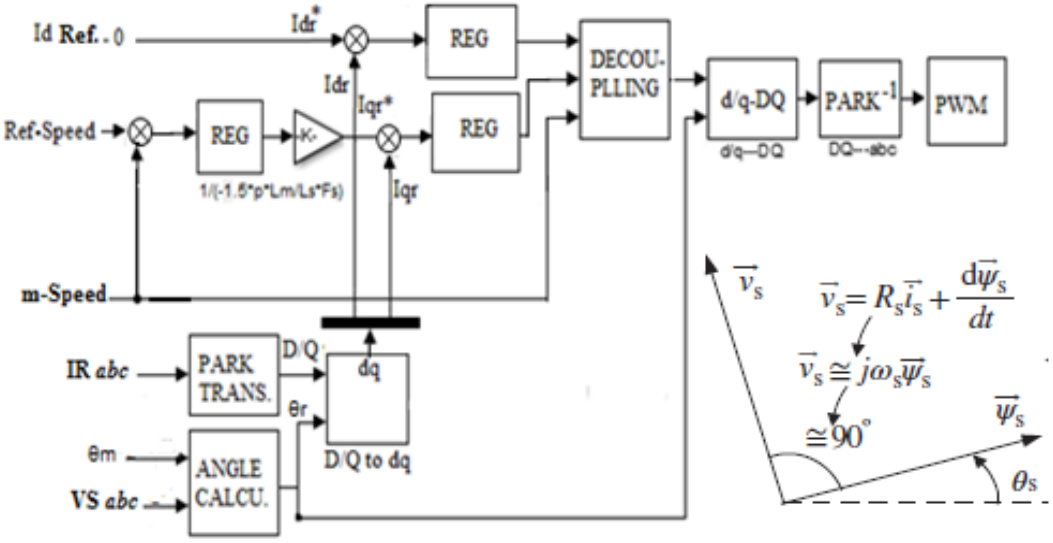

Figure 109 Current Loop Structure of Rotor Side Controller (RSC)

Figure 109 illustrates current loop structure of the rotor side and frame transformations, where the measured speed is compared to the reference speed the output of the regulator will be quadrature rotor current Iqr* thus the error will be regulated via PI regulator then the correction value transformed from frame to another after decoupling unite, finally the PWM will generates pulses to the power converter according to the result of controller output.

Hereafter, fixed speed control simulation results are presented in figures 110-111.

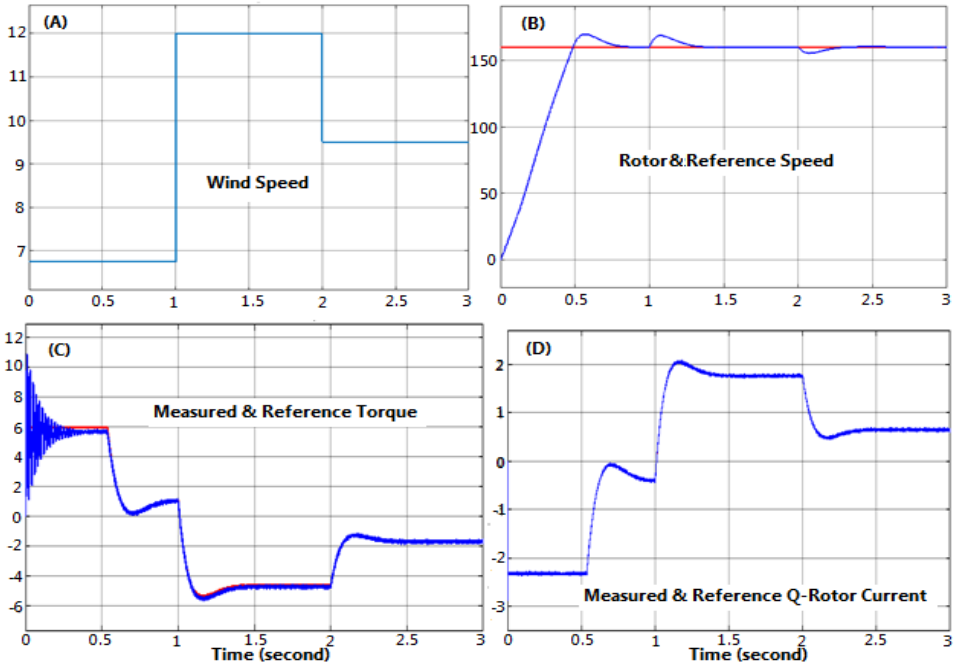

Figure 110 Fixed Speed Control (Rotor Simulation Results)

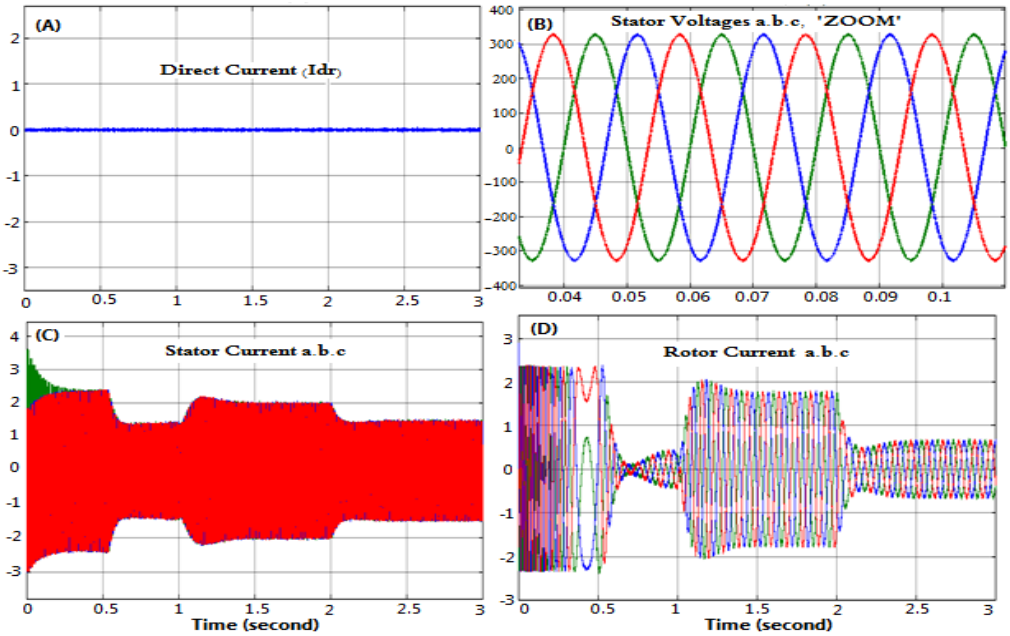

Figure 111 Fixed Speed Control (Rotor & Stator Simulation Results)

It can be noticed from figures shown above that; stator voltage figure 111-B is constant; because it is connected into the grid which supposed to be constant in this simulation. On the other hand, all other parameters are variable according to the wind speed except the rotation speed figure 110-B maintained constant by PI regulator. In addition, quadrature rotor current I_{qr} figure 110-D has direct proportional relationship with electromagnetic torque Tem figure 111-C.

Variable Speed Control

In this section, the maximum power point tracking **MPPT** strategy or "indirect speed control" will be used to extract the maximum power and optimizing the operation of the power system. This MPPT functions on the principle of measuring and squaring the rotation speed of the rotor and multiplied by K_{opt} constant as shown in figure112, hence optimizing the electromagnetic torque T_{em*}.[3] [4]

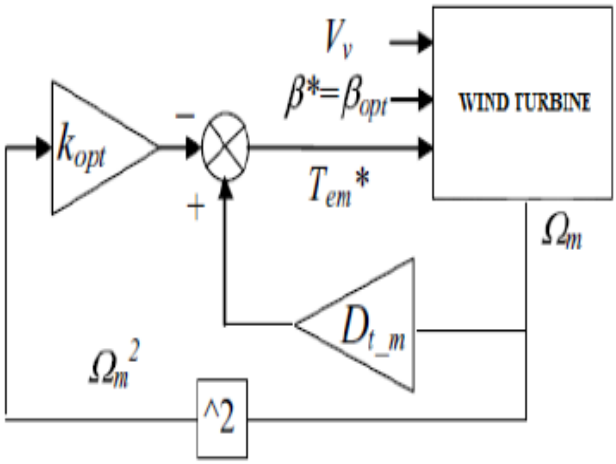

Figure 112 MPPT Control Strategy

$$T_{em}^{*} = K_{opt.}\Omega m^2 \qquad (4.1)$$

$$\text{With } K_{opt} = \frac{1}{2}\pi\rho R^5 \frac{C_{p\,max}}{\lambda_{opt}^3} \qquad (4.2)$$

Note: - The model can be simplified by neglecting the damping coefficients (D_{t_m}), because it is very small.

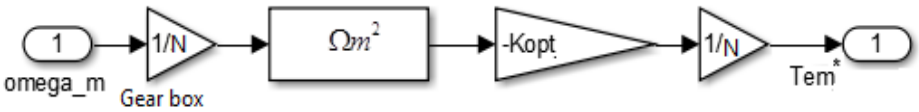

Figure 113 Structure of MPPT in MATLAB/SIMULINK

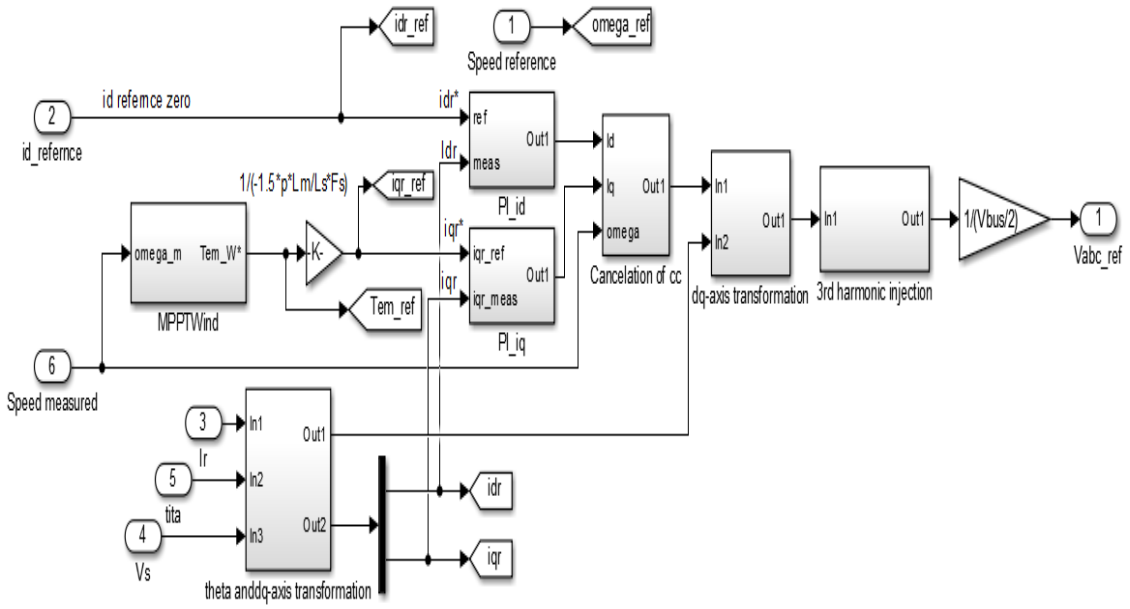

Figure 114 Block Diagram of (RSG) and MPPT Control Strategy in MATLAB/SIMULINK

Maximum power point tracking MPPT or Indirect Speed Control (ISC) in figure114 demonstrates the structure of the rotor side converter, it is controlled by measuring rotation speed to obtain the reference torque T_{em*}. In general, the main structure of the RSC is the same as that, in fixed speed control the only difference is that, the reference speed is not needed in controller structure.

Figure 115-A shows that, the actual speed of the rotor is proportional to the wind speed. In other words, turbine and generator rotates at the optimum speed regarding to the equation used in the MPPT, hence extracts the maximum power 'torque' available in the wind.

Figure 115-B presents the relationship between wind speed and mechanical power generations of the proposed system. Also, this figure shows the three different zones of operation, cut-in wind speed zone, maximum power point tracking zone, and cut-off zone.

Figure 115-C illustrates the generated mechanical power increases and decreases according to the wind variation. Thus confirm the robustness of the MPPT controls strategy, and how well the system responses in to the variations of wind speed. As mentioned previously in the control strategy, that I_{qr} of the rotor is proportional to the generator's rotor speed, while the I_{dr} axis is set to zero, as shown in figure 115-D.

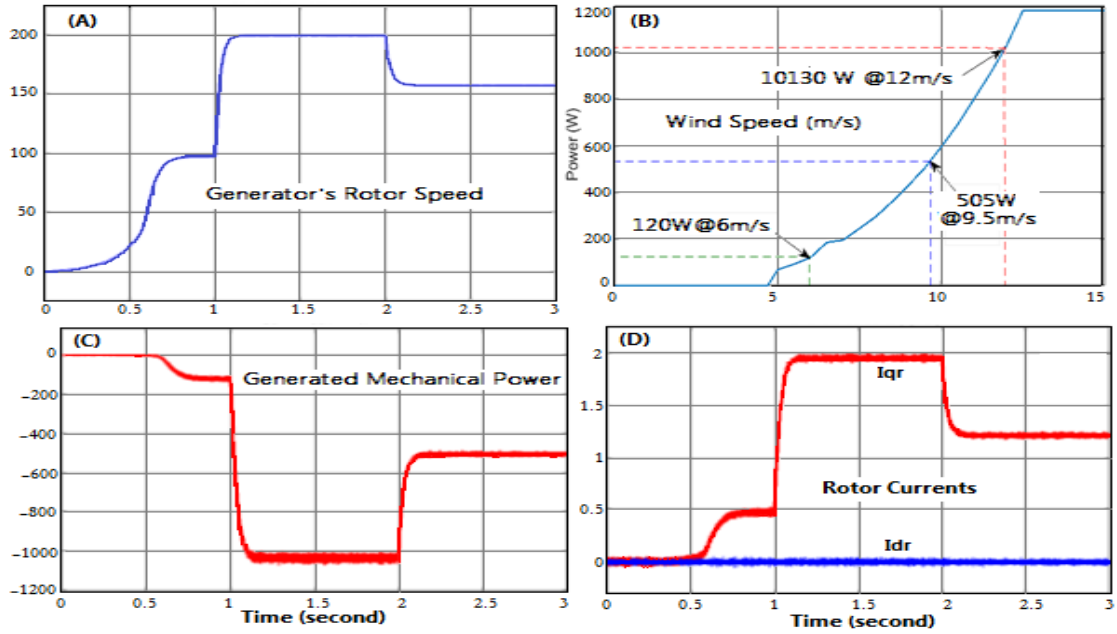

Figure 115 Variable Speed Control Rotor Simulation Results

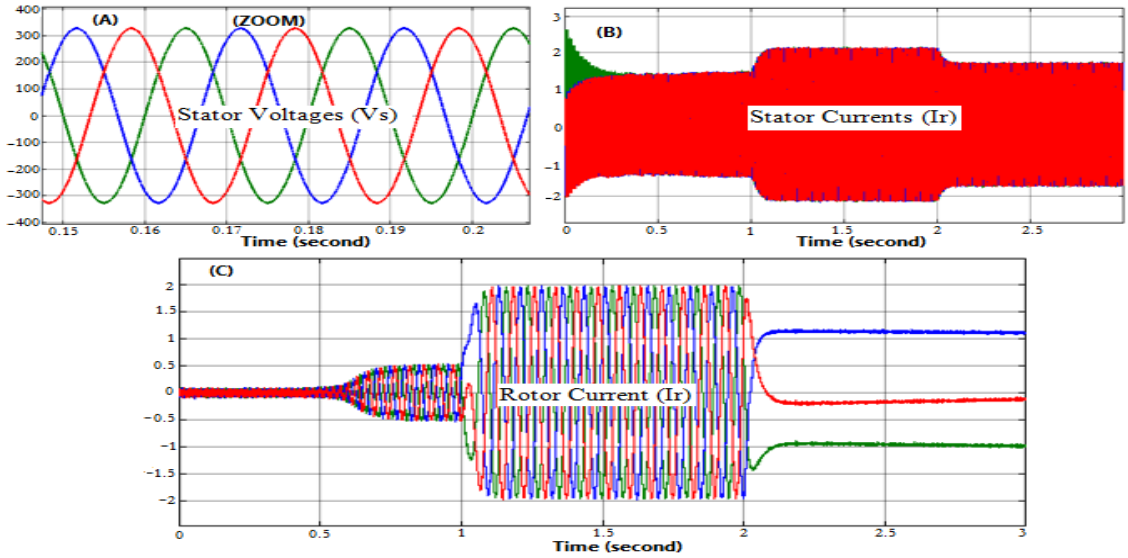

Figure 116 Rotor & Stator' Voltages and Currents'

It is noticed from figure 116-A-B-C that, stator and rotor currents are directly affected by the wind speed, whereas the stator voltages are constant because it is connected directly to stable electrical network.

The GSC (Grid Side Converter) is installed before the DC bus and connected into the electrical grid via a RL filter. This converter has two functions:

- Keeps the DC bus voltage constant, whatever the magnitude and direction of flow of the rotor power of the DFIG.
- Maintain a unity power factor at the point of connection to the electrical network.

Finally, this study an intensive attention was given to the control strategies constant and variable speed control, an indirect (MPPT) and direct control methods are used to control the rotation speed of the rotor. We present hereafter a comparison between the proposed methods:

- Fixed speed control has an advantage that stable frequency can be achieved so, it can be connected directly to the grid or load if needed. On the other hand, maximum power cannot be extracted from the wind as well as the turbine will be exposed to high mechanical stress due to the speed limitation, also winding temperature will be increased in case where there is high wind speed due to the high currents pass in the windings.
- Variable speed control has main advantage that maximum power can be extracted from the wind, less stress on the turbine side. But the frequency will be unstable, which imposes to use AC/DC converter, over speed due to high speed wind may cause damage to the turbine.

4.3.1.2 Control of Grid Side Converter (GSC)

In this part of the system the power converter can be controlled independently form the rotor side converter as long as it is supplied by the DC-Link. Anyway, a Grid Side Converter (GSC) will be simulated, implemented and controlled in MATLAB/SIMULINK to manage exchange of the output reactive power of the generator with the electrical grid.

The main components of the grid side system are: the grid side converter, the grid side filter, and the grid voltage. Figure 117 illustrates simplified model of the grid side system. We can distinguish the following elements.

- An ideal bidirectional switches (IGBT) are used in to model the grid side converter. It must be noticed that, the controlled switches ideally, not considering real characteristics such as switching time or voltage drops.
- The grid side filter is normally composed of inductances and capacitors (LC), which are the link between each output phase of the converter and the grid voltage.
- In order to operate with real voltages in the rotor side converter and grid side converter; and due to the fact that, the rotor winding is 1/3 of the stator windings, thus an electrical transformer need to be installed in series with the rotor side converter, and directly connected into the rotor of the generator.

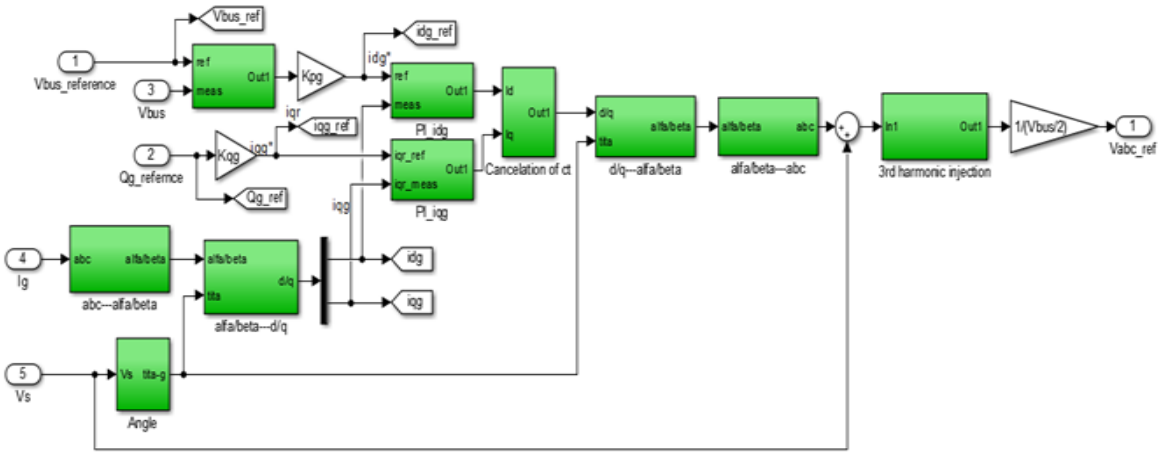

Figure 117 Control Block Diagram of Grid Voltage Oriented Vector Control.

Block control loops of dq axes current scheme is described in figures 117. PI regulators are used. In this block diagram control shows the compensation terms and dq axis decoupling and GSC model. The reference dq-axis currents Igd* and Igq* are respectively provided from the block of the DC bus voltage control and reactive power control at the connection point of the GSC to the grid.

Note: The Idg current is used to control the reactive power at the connection point of the GSC with the grid; while Iqg current is used to regulate the DC bus voltage.

Simulation Results of Grid Side Converter (GSC)

Figure 118 illustrates the output reactive generated power of 3 kW DFIG connected via 2L-VSC, back-to-back converter into power grid of 400 V and 50 Hz: (a) DC-bus voltage, it is maintained constant due to the PI regulator, (b)and (c) dq grid side converter currents, (d) and (h) abc zoom of grid side converter output voltage, (e) measured current transmitted to the grid with the desired current (f) reactive power exchange with the grid as demanded by the grid side.

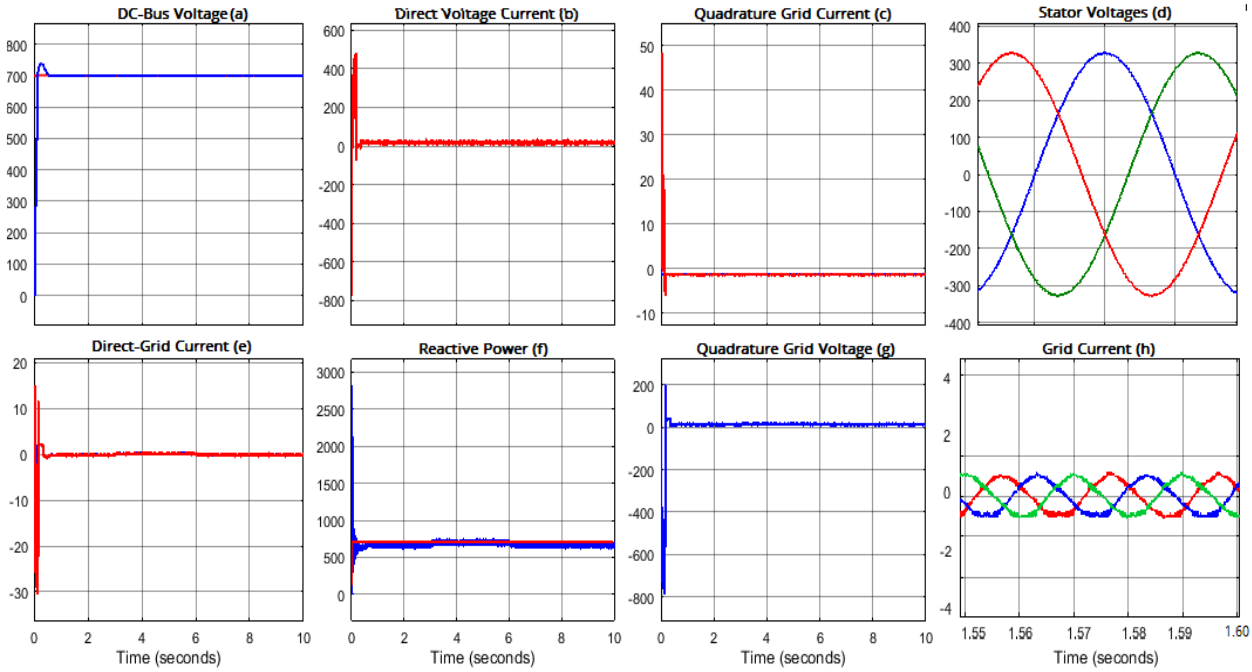

Figure 118 Controlled Parameters of Grid Side Converter

4.3.2 Simulation and Control of Doubly-Fed Induction Generator Based Tidal Turbine

To avoid repetition and due to the similarity between wind and tidal turbines, in terms of design and operation principles are very similar. Although the water speeds is low. However, the density difference between fluids, where the water density is much greater than the density of the air, which creates the real difference in production between the turbines. In this part, only some variables will be highlighted and presented.

4.3.2.1 Control of Rotor Side Converter (RSC)

Fixed Speed Control

From figure 119 we can see that the rotation speed of the rotor is constant although the wind speed is altered, also the robustness of the PI regulator, that let the actual values track the set point, generated mechanical power and mechanical torque increase and decrease according to the wind speed.

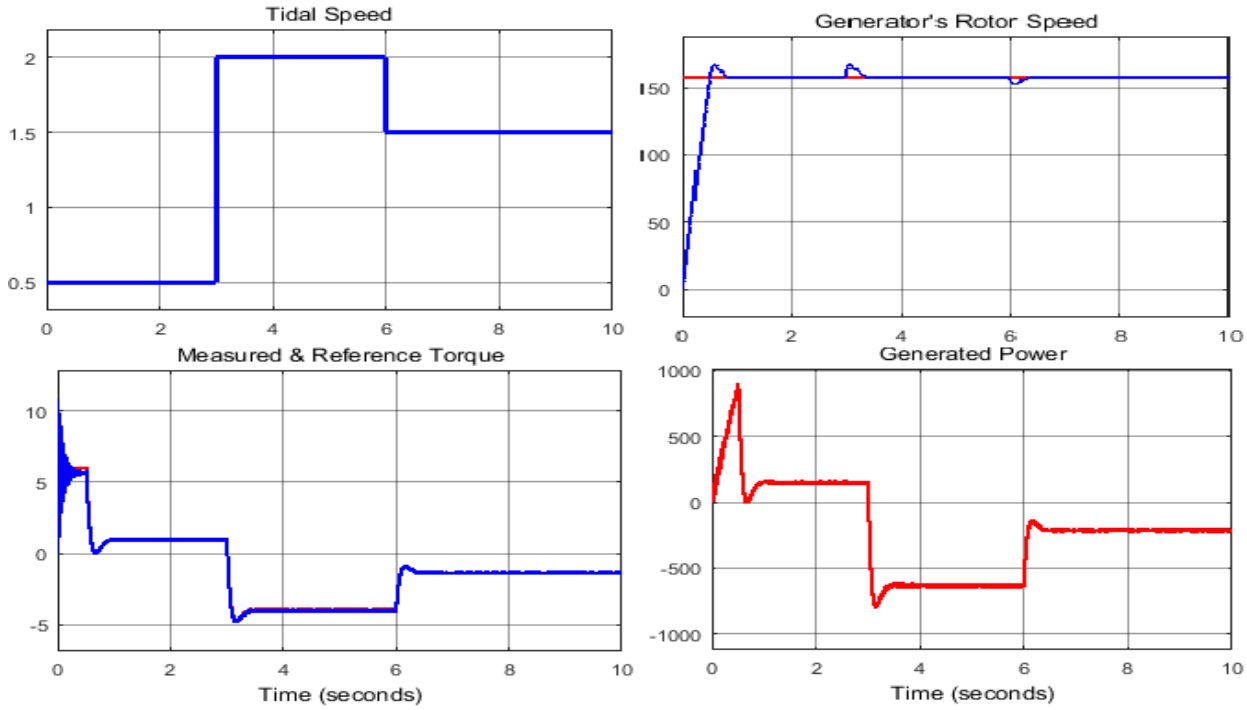

Figure 119 Fixed Speed DFIG Rotor Side Based Tidal Turbine

Variable Speed Control

In figure 120 we can observe the response of the rotor speed to the wind speed change, as well as the other variables; such as rotor currents (Ir) and mechanical torque, also the robustness of the PI regulator.

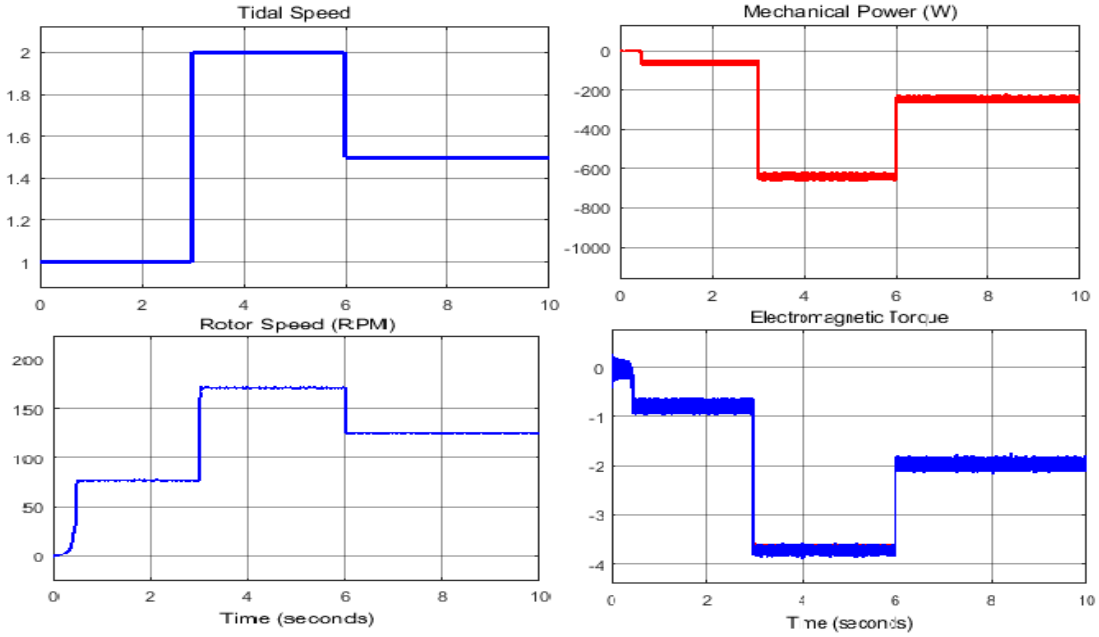

Figure 120 Variable Speed Control of DFIG Rotor Side Tidal Turbine

4.3.2.2 Control of Grid Side Converter (Simulation Results)

As mentioned before that, the designed power of this turbine should be in the range of the nominal power of the DFIG in the laboratory. Figure 121 illustrates the robustness of the PI regulator, where it is not affected by the sudden change of the simulated tidal turbine, thus prove also, that the grid side converter can function properly independently form the rotor side converter.

Finally, in the previous sections, modeling and simulation of almost each part of the wind and tidal turbine coupled to doubly-fed induction generator, and power converters are carried out in MATLAB/SIMULINK environment. All this has been done in order to investigate, prove and assure that, the system has been well designed and the control strategy functions well in most situations.

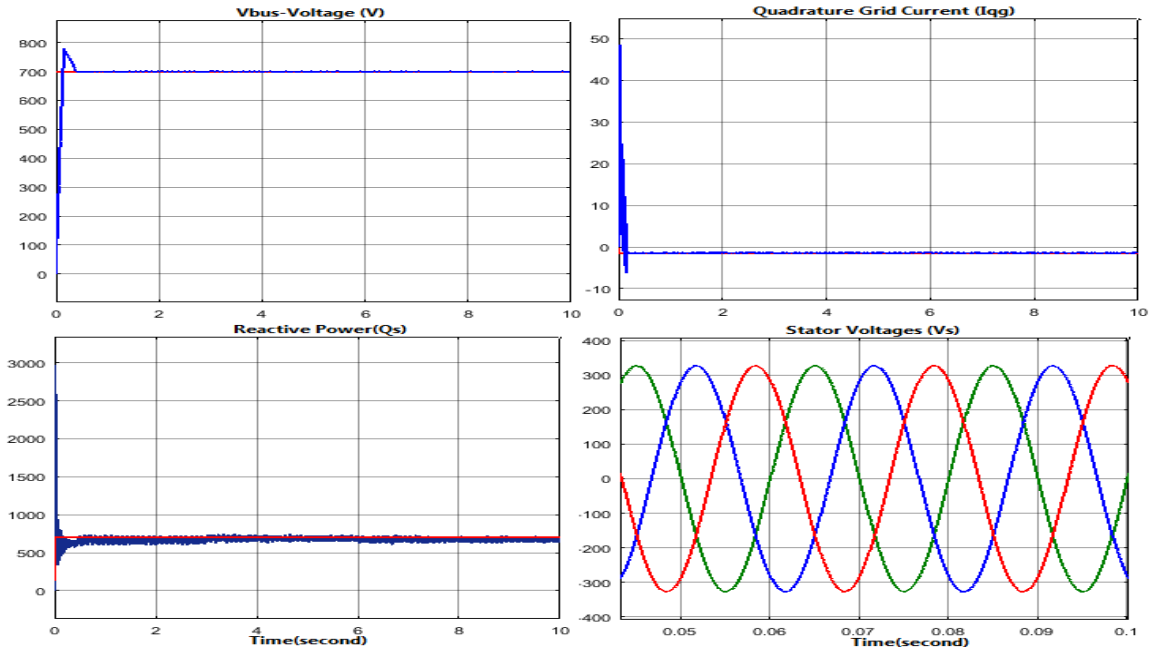

Figure 121 Grid Side Converter of DFIG Based Tidal Turbine

4.4 Application of "time acceleration" Concept in Wind Turbine Power Generation

In this section in virtual time a wind profile composed of variety of low and high frequencies will be generated using MATLAB program called 'sim –vent' and Simulink. It is supposed that, samples are taken every second and every minute, subsequently the simulation time will be reduced every time, when the average of the previous wind profile is calculated.

4.4.1 Impact of "Time Acceleration Method" on Power Simulation

Hereafter, the time acceleration method will be implemented experimentally, in order to prove its validation for reducing the simulation time, using hardware in the loop simulation available in the lab, and with aid of d-SPACE.

However, using the hardware emulator, presented previously, and software simulation represented by MATLAB/SIMULINK, in addition to d-SPACE. All these are used to implement practically the suggested method, of time acceleration, which will be used to decrease the simulation time of wind turbine coupled to doubly-fed induction generator, which is connected to the electrical grid.

Furthermore, the wind turbine is modeled and simulated in MATLAB/SIMULINK environment, along with d-SPACE (DS1103) ,"ControlDesk"; software blocks as shown in figure 122; Digital to Analog Converters (DAC); and Analog to Digital Converters (ADC) are used to transmitter signals, between software and hardware simulation.

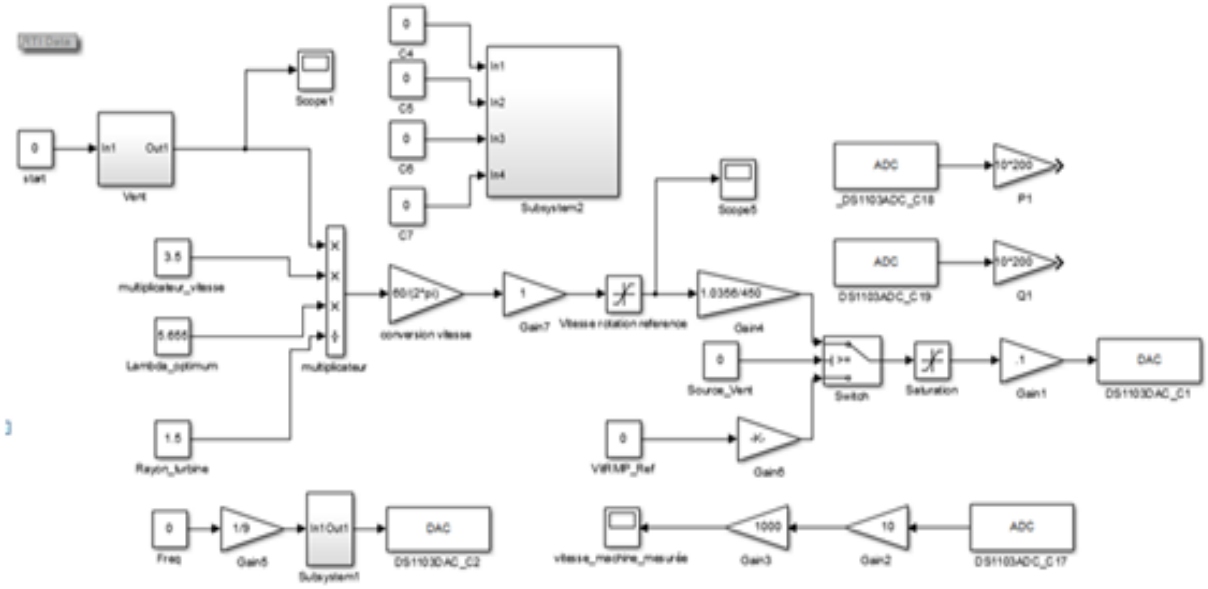

Figure 122 Model of Wind Turbine and d-SPACE in MATLAB/SIMULINK

Figure 123 illustrates the Interface User Guide (IUG) of "ControlDesk" used to simulate and communicate interactively with the hardware simulator.

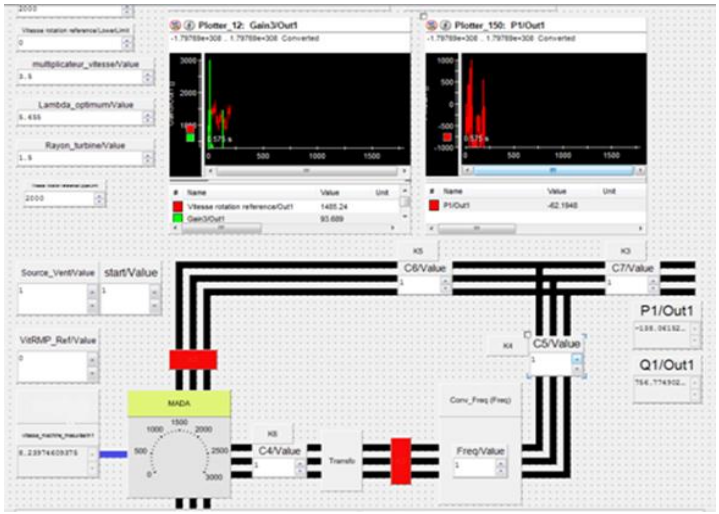

Figure 123 Interface User Guide of ControlDesk for Wind Turbine Hardware Emulator

In this part of the work, the time acceleration method is implemented experimentally on the Hardware In the Loop Simulator, HILS; Furthermore, different wind profiles (18000 samples, 300 samples, 60 samples, and 30 samples) are used as input to the wind turbine 1 kW, simulated in MATLAB/SIMULINK. In order to investigate and prove the validity of the proposed method, the generated mechanical power of every wind profile is presented and compared to the previous result.

Simulation of 18000 Seconds

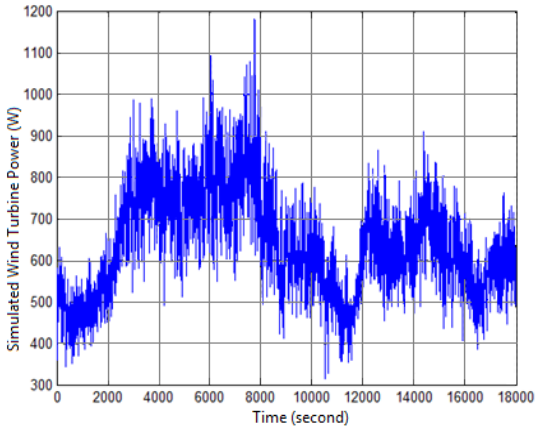

Figure 124 Turbine Mechanical Power Simulated Experimentally [4-5]

As mentioned previously the average of power generated by the software simulation is about 654W; while the average of the power generated by hardware simulator is about 641W; which

yields a difference of about 2%, this is considered as an acceptable difference between both simulations.

Figure 124 shows the maximum mechanical power generated by hardware simulator is smaller than the mechanical power generated by software simulation in the previous chapter figure100-a, this is mainly due to the fact that, the measurement of mechanical power in the emulator is taken every 1.2 second; whereas every second in software simulation. Although, there is a difference in term of the generated power average, but the general form of the resulted curves are very similar.

4.4.2 Simulation in accelerated time of 300, 60 and 30 Minutes

Simulation of 300 Minutes

In this experimental test, the wind profile of 300 minutes is used instead of the wind profile of 18000 seconds. In other words, the sampling time will be carried out in minutes, and not in seconds. The average mechanical power generated experimentally figure 125 is about 619 W, while 638 W the average mechanical power generated by software simulation see figure 103 in chapter 3. Thus, yields a difference of about 3% between both simulations, although the difference has increased by 1%, it is still a good result.

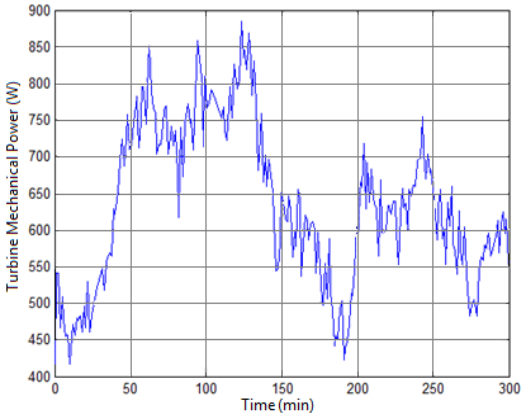

Figure 125 Mechanical Power Simulated Experimentally; sampling every minute [4-5]

On the other hand, from an experimental point of view, the simulation in sampling reduction time (every minute), produces an average mechanical power of about 619 W, whereas in the previous simulation 18000 seconds, produces an average mechanical power of 641 W, which yields a difference about 3.4%, between both wind profiles.

Simulation of 60 Minutes

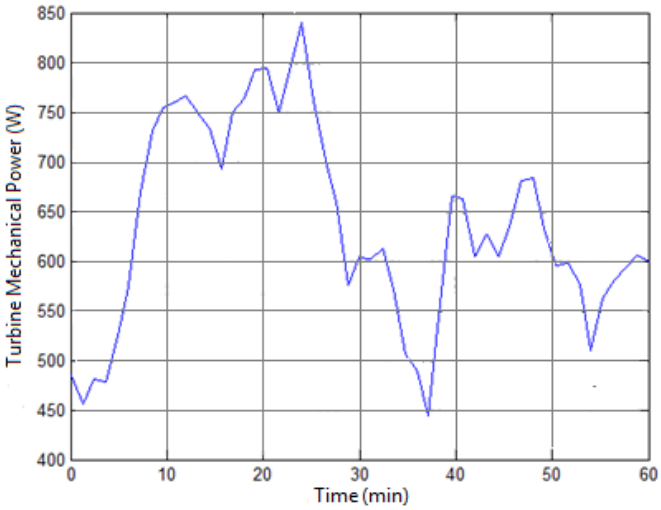

Figure 126 Mechanical Power Simulated Experimentally; sampling every 5 minutes

Time acceleration method is applied; where samples are calculated every 5 minutes, figure 126 shows the average mechanical power generated experimentally is about 626 W, while the mechanical power generated by software simulation is about 632W; which yields a difference of about 1%.

Moreover, simulation in accelerated time (every 5 minutes), generates an average mechanical power of about 626 W. whereas, simulation using 18000 samples, generates an average mechanical power of 641W, which yields a difference about 2.3%.

Simulation 30 Minutes

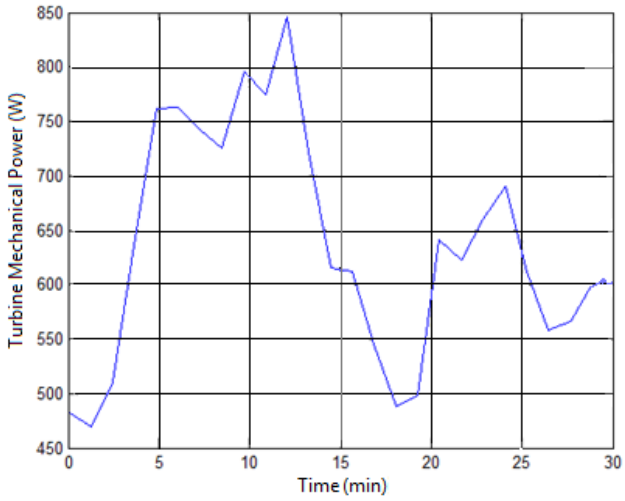

Figure 127 Mechanical Power Simulated Experimentally; Sampling Every 10 Minutes

Figure 127 shows the average experimental power is about 637 W, while the average power by software simulation is about 622W; which yields a difference of about 2.4%.

Throughout the comparison between simulations in time acceleration, with sampling time every 10 minutes, the average of the generated power is about 637W, while the average mechanical power generated without time acceleration 18000 samples 641W. So, the difference between accelerated and non-accelerated simulation is about 0.6%. Therefore, this simulation is considered to be the best approximation of all previous simulations.

Two major remarks emerge from these experiments:

1. Accelerated time simulation, either software or experimental, give a good approximation for variable sampling periods, in addition the system modeling is well defined;
2. In experimental simulation, compromise is essential between the choice of sampling time and results precision.

4.5 Electro-Mechanical Coupling Simulation Results

The concept of electromechanical coupling is simulated and controlled in MATLAB environment, where the wind profile is generated from the original 18000 samples presented previously, this new profile is composed of 30 samples i.e. samples are taken every 10 minutes, thus yields 30 minute wind profile, and tidal profile represented by a sinusoidal waveform. Subsequently, these two turbines are connected to the same shaft of the DFIG; simulation results are presented and discussed.

Figure 128 demonstrates the simulation results of electro-mechanical coupling, figure 128-A, represents wind speed variation between 7.9 and 11.7m/s. While figure 128-B illustrates tidal current represented by sine waveform altered between 1.9 and 0.2 m/s .Whereas, in figure 128-C indicates the dependence between generated electrical power, and wind-tidal speeds, and figure 128-D demonstrates actual rotation speed tracking the reference rotation speed (1550 revolution /minute).

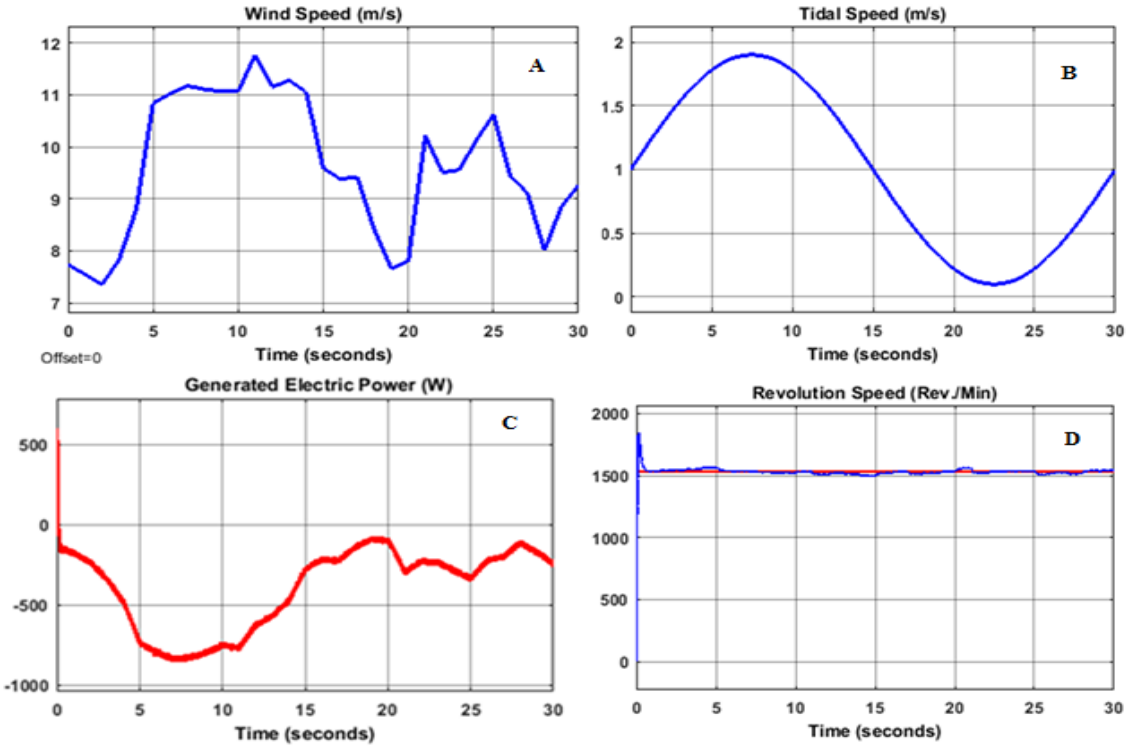

Figure 128 Simulation Results of Electro-Mechanical Coupling

4.6 Electro-Mechanical Coupling Experimental Results

As part of this thesis, the proposed electro-mechanical coupling is simulated experimentally on the hardware simulator. Wind turbine is emulated by the vector-controlled servo-motor, while tidal turbine is emulated by the permanent magnet synchronous machine. These two turbines are coupled on the same shaft with the DFIG mentioned previously. Stochastic profiles of wind and tidal current are used; figure 129 illustrates the electrical power generated by each turbine.

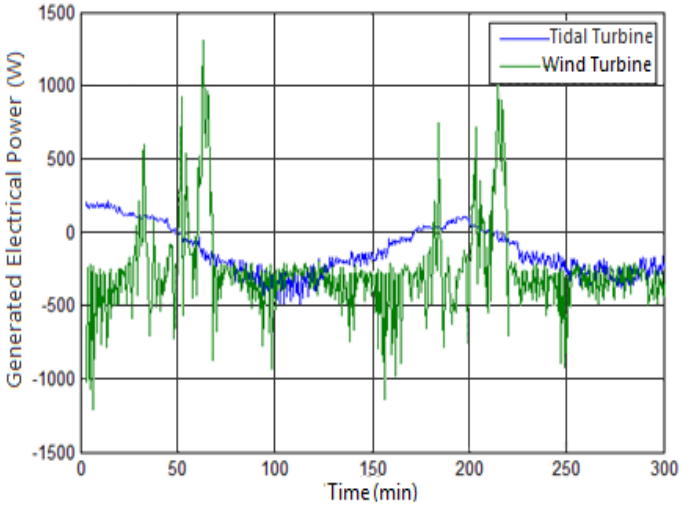

Figure 129 Electrical Power Generated by Each Turbine

4.6.1 DFIG Modes of Operation: (Motor / Generator)

Figures 130 and 131 shows measured and reference rotation speed of the DFIG, and the electric power supplied to the network. However, this experiment proves that, the DFIG functions as an electrical motor or generator depends on the rotation speed. Figures 130 and131 demonstrate that, when the speed is less than the synchronous speed, the machine function in electrical motor mode, vice versa when the reference speed is more than the synchronous speed (1500 rpm), the electric machine function in generator mode, and when the reference speed is lower than the synchronous speed the electric machine function in motor mode.

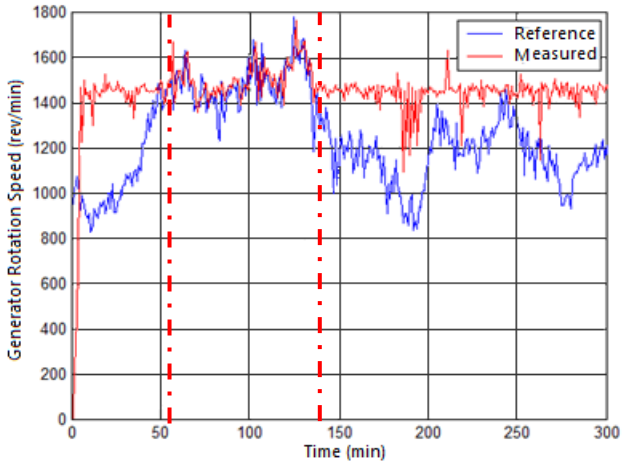

Figure 130 Speed of DFIG Obtained Experimentally

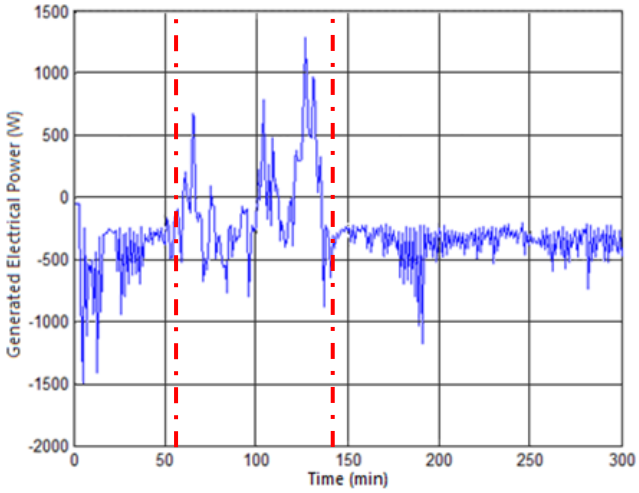

Figure 131 Generated Electrical Power, Supplied to Grid

Interval [53; 147] measured rotation speed and reference speed in figure 130 are more than (1500 rpm) so electrical machine function in generator mode, and generates electrical power as indicated in figure 131 interval [53; 147], whereas the interval [147; 300] when the reference

speed is lower than the generation speed, the rotation speed of the DFIG is imposed by electrical grid, so the generator function as electrical motor.

4.6.2 Operations modes of Simultaneous coupling of wind and tidal turbine

Simultaneous coupling of wind and tidal turbine requires the presence of precise and fast tracking control system, to control rotation speeds of each turbine according to wind speed and tidal speed. Indeed, if the wind speed at certain moment is just quite enough to let the wind turbine functions at speed very close to the generation speed, and the rotation speed of the tidal turbine is lower than the generation speed, then it would be better to decoupling tidal turbine, because it will act as mechanical load, and will slow down the rotation speed of the wind turbine and vice versa. This scenario can be approached also by exchanging the roles of the wind turbine and the tidal turbine.

- Intervals [30; 40], [50; 70], [170; 180] and [200; 230] **wind turbine** generates electrical power.
- Intervals [0; 50] and [140; 210] **tidal turbine** generates electrical power.

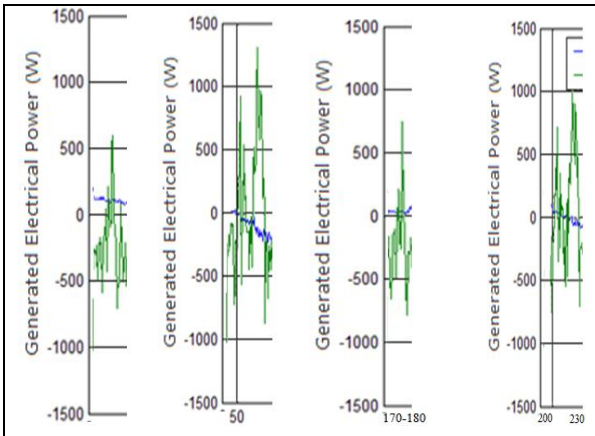

Figure 129A Electrical power generated by Wind turbine

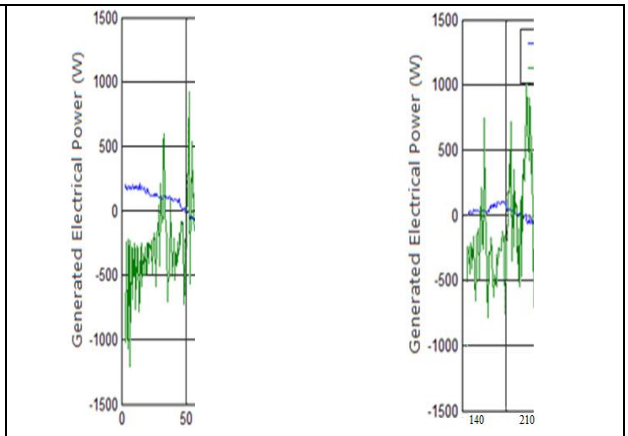

Figure 129B Electrical power generated by Tidal turbine

- Intervals [70; 170], and [220; 300] minutes, both turbines do not generate electrical power, because wind and tidal speeds are lower than the generation speed, consequently the DFIG functions as an electrical motor.

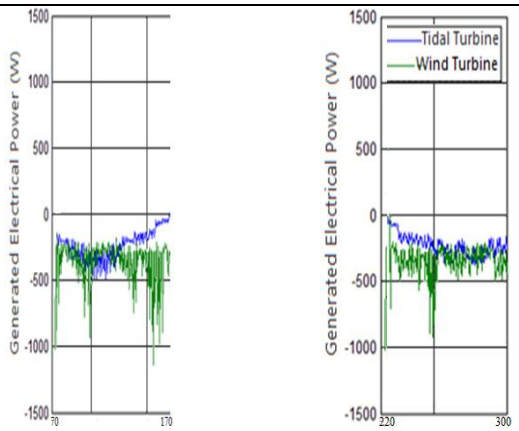

Figure 129C

Both turbines do not generate electrical power

On the other hand, in the intervals where the reference rotational speed is greater than the synchronism speed, the electric machine operates in generator mod. In Figure 132 that illustrates below the electrical power generated experimentally by electro-mechanical coupling wind –tidal turbine system, we can observe the power injected in the grid (positive curve) [4-5].

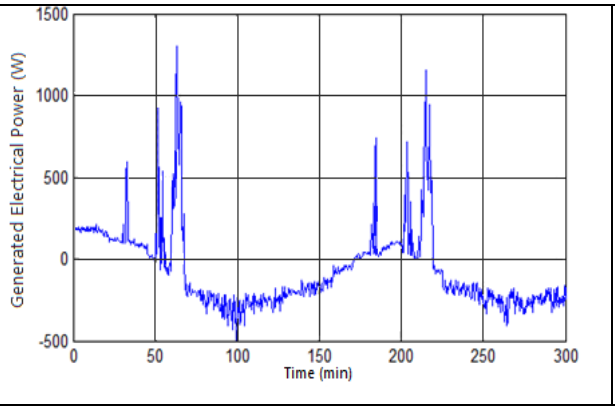

Figure 132 Electrical Power Generated by Hybrid System

Figure 132 also illustrates intervals where the reference speed of rotation is lower than the speed of synchronism of i.e. 1500 revolutions / min the machine operates in motor mode. Intervals where the energy provided to the grid by each turbine is insufficient, thus electrical machine will function in motor mode rather than generator mode; in this case, decoupling electrical machine from the network to avoid motor mode, or add an energy storage unit to overcome these production declines.

4.7Conclusion

The objective of this chapter is to present, on one hand, a methodology called "accelerated" time simulation, and its experimental validation, and on the other hand to present multi-hardware flexibility, through which various emulation architectures could be developed: wind turbine, tidal turbine, and wind-tidal turbines.

First part of this work presented the architecture of hydraulic emulator, available in the GREAH laboratory. Furthermore, the hydraulic emulator is developed to simulate hybrid and separate wind and tidal power conversion system, based on the HILS concept.

In the second part, a wind profile data is recorded every second, for a total period of 5 hours. This later used in software and experimental simulations. Subsequently, instead of using a wind profile of 18000 samples, it is possible to express wind profile, by reducing the number of samples. Thus simulation time will be reduced as well. Results obtained practically have the same average values of power and speed of rotation, with differences not exceeding 5%. This allowed decreasing simulation and time of calculation.

Subsequently, an experimental simulation of a wind-turbine hybrid system is carried out, based on an electromechanical coupling on the same shaft along with a single generator. Hence, the DFIG is used as a generator of the hybrid system. Stochastic profiles of wind and ocean current are selected so that their energy potentialities are complementary. Additionally, highlighted the need for an energy storage system to ensure power generation, when one of the main energy sources is declining or suddenly cut off.

Concluded that, in order to generate electrical power must be both two resources higher than the generation speed or one of them is high enough to lead the other and keep the system function in generation mode. Otherwise, the system could consume electrical energy rather than generates. In addition, when one of the resources is lower than the generation speed it would be better to disconnect it or substitute this shortage of energy by using energy storage unites.

On the other hand, if one of the resources overrides the nominal speed up to cut- off speed then in this case, it is advised to keep two turbines coupled thus slow down the rotation speed and acts as mechanical load or breaks for system’s safety.

References

[1] Cristian Nichita, Mohmed Ashglaf, Yacine Amara, 'Preliminary study of a concept of wind-tidal turbine coupling using functional similarities of real time emulation'. International Conference on Renewable Energies and Power Quality (ICREPQ'19), 10-12 April, 2019, Tenerife (Spain).

[2] ELWE TechniK: Training systems for future oriented vocational training and further education in all fields of technology.

[3] Haitham Abu-Rub, Mariusz Malinowski, Kamal Al-Haddad, "Power Electronics for Renewable Energy Systems Transportation and Industrial Applications" ieee Press Wily and Sons, 2014.

[4] Gonzalo Abad, Jesu´s Lo´pez, Miguel A. Rodrı´guez, Luis Marroyo ,Grzegorz Iwanski, Doubly Fed Induction Machine Modeling and Control for Wind Energy Generation, Copyright _ 2011 by the Institute of Electrical and Electronics Engineers, Inc. Published by John Wiley & Sons, Inc., Hoboken, New Jersey. All rights reserved. Published simultaneously in Canada

[5] Jerry Tekobon, Système multi physique de simulation pour l'étude de la production de l'énergie basée sur le couplage éolien offshore-hydrolien thesis, university of Havre, 2016.

CHAPTER FIVE

GENERAL CONCLUSIONS

5.1 General Conclusions

The main objective of this thesis is to study the concept of offshore wind / tidal turbine hybridization based on the flexibility of a multi-function emulator that allows various emulation architectures: wind turbines, tidal turbines, and hybrid wind - tidal turbines systems. We analyze its impact on the output power of the system; the obtained results are correlated with wind and tidal speed profiles, in which statistical properties impacting global power chains could be complementary and in particular in function of the given sites.

In order to reduce real-time simulation with minimum distortion in output results we develop a methodology called "accelerated simulation time" by simulation method followed its experimental validation on emulators systems.

.

Power systems is composed of three blades horizontal axes wind turbine and horizontal axis tidal turbine, coupled to the same shaft of a Doubly-Fed Induction Generator. The choice of this type of electrical machine is motivated by sizing reduction, low cost of the static converters, as well as its efficiency to control in active and reactive power, and its speed range in ± 30% of the speed of synchronism.

This work started by presenting an up to date state of the art on wind energy (speed and distribution), tidal resource, history of wind and tidal turbines, as well as, operations principles of wind/tidal conversion chain based on their similarities. Even if we did not develop in the thesis the absolutely necessary storage, the problem being extremely complex, we present a state of the art on the impact of energy storage units on power stability in the network. Furthermore, the advantages and disadvantages of the hybrid power system, in addition to a comparison between energy storage systems.

Finally yet importantly, wind and tidal hardware simulators available in GREAH are presented.

Dynamic and steady state modeling of different elements of offshore wind-tidal turbine system are conducted, since this is the preliminary step for the HIL simulation. Therefore, proceeded to mathematical modeling of each element of the global system namely:

- Wind and tidal turbines
- Asynchronous machine Doubly-Fed Induction Machine DFIM
- Three-phase rectifier
- Three-phase controlled inverter and DC bus.

The modeling of both turbines is based on their functional similarities, the main difference lies in the density of resources (Air and Water).

The model of the electrical machines is presented in the natural coordinate system (a, b, c) then in the two-phase Park transformer is used. This transformation is very important for modeling and reducing control complexity, i.e. instead of having a command on three axes, only two axes will be treated.

We introduce the concept of hybrid offshore wind /tidal turbines based on an electro-mechanical coupling and the methodology of a virtual time called “time acceleration”.
Optimal speed control is achieved by designing two control strategies, fixed and variable speed, where a low power wind/tidal hybrid system is mechanically coupled on the DFIG shaft.

Also, control strategies are discussed; it includes the control of the wind or tidal turbine, control of Doubly-Fed Induction Generator, control of Rotor-Side Converter and Grid-Side Converter Units.

In addition, the concept of time acceleration is described, methodology introduced for reducing simulation time with reasonable results, also this method is useful to decreases data size of wind/tidal profiles.

We present HILS flexibility, through which various emulation architectures could be developed: wind turbine, tidal turbine, and wind-tidal turbines. Furthermore, the hydraulic emulator is developed to simulate hybrid and separate wind and tidal power conversion system, based on the HILS concept.

The wind-tidal emulator system includes the following elements:

- A computer that simulates the static characteristics of a wind turbine
- A Dspace card used to control and data transmission, between real-time emulator, and software simulator.
- A vector controlled asynchronous motor is used to drive a Doubly-Fed Induction Generator (DFIG). This electrical drive emulates the wind turbine by reproducing on its shaft the turbine static characteristics.
- A Synchronous motor emulates tidal turbine if it is needed. This electrical drive is used also as a mechanical load when single turbine is simulated. Also to generate different magnitude of mechanical torque, thus different operating points can be obtained.
- Doubly-Fed Induction Generator (DFIG) 2-poles is used to generate electrical power ≈1.2 kW.
- Compacted power converter AC / DC and DC / AC are connected into the rotor side of the DFIG.

An experimental simulation of a hybrid offshore wind-tidal turbine system is carried out, using a new architecture of the emulator system that we developed as part of collaboration with a team of Korean researchers. However, the vector-controlled servomotor is used to emulate the wind turbine, while the synchronous machine is used to simulate a tidal turbine. The generator's shaft serves as a mechanical coupling between both turbines. We have highlighted in this experiment, the hybridization of two different resources to generate electrical, and also the importance of adding a storage system to overcome the problem of voltage drop when there is not enough wind or tidal to generate sufficient electrical power.

The simulation results concerning "accelerated" time methodology are discussed, following by experimental validation. A wind profile data is recorded every second, for a total period of 5 hours. This later used in software and experimental simulations. Subsequently, instead of using a wind profile of 18000 samples, it is possible to express wind profile, by reducing the number of samples. Thus simulation time will be reduced as well. Results obtained practically have the same average values of power and speed of rotation, with differences not exceeding 5%. This allowed decreasing simulation and time of calculation.

Subsequently, an experimental simulation of a wind-turbine hybrid system is carried out, based on an electromechanical coupling on the same shaft along with a single generator. Hence, the DFIG is used as a generator of the hybrid system. Stochastic profiles of wind and ocean current are selected so that their energy potentialities are complementary. Additionally, highlighted the need for an energy storage system to ensure power generation, when one of the main energy sources is declining or suddenly cut off.

Concluded that, in order to generate electrical power must be both two resources higher than the generation speed or one of them is high enough to lead the other and keep the system function in generation mode. Otherwise, the system could consume electrical energy rather than generates. In addition, when one of the resources is lower than the generation speed it would be better to disconnect it or substitute this shortage of energy by using energy storage unites.

On the other hand, if one of the resources overrides the nominal speed up to cut- off speed then in this case, it is advised to keep two turbines coupled thus slow down the rotation speed and acts as mechanical load or breaks for system's safety.

By analyzing results of software and experimental simulations of a wind turbine based on the concept of "accelerated time", it is observed that, the concept of accelerated time simulation lead to reduce simulation time; using for example 300 samples of wind speed instead of 18000 samples. The transition to the new sample is an inference problem, which makes it difficult to conduct; because it must specify the conditions that make it possible to say, what is observed in the sample is valid for the entire sample.

This is partially answered the question: what size need to be given to the sample? In other words, what criteria should be taken into account, when setting the sample size?

Two parameters were chosen as criteria for setting the sample's size:
-the average speed of rotation of the wind turbine (which serves as a reference for the control of the conversion chain, according to the variable speed control strategy used in our work), and -the

average power obtained by the software or experimental simulation systems, for different samples of wind profiles.

Applying this concept reduces the simulation time from 5 hours to just 30 minutes; moreover, the percentage of error on obtaining the average speed and the average power, is very low, the same observation is made by using experimental simulation. However, it is observed also that, there is a relationship between reducing the number of samples and decreasing the simulation time.

This work contributed also in the development of the emulator systems (wind - tidal turbines systems) by using in particular, the physical similarities between both systems based on a common HILS concept.

5.2 Future Work and perspectives

-Carry out an in-depth analysis of the concept of "accelerated" time simulation based on an inverse procedure: start from a reduced sample to expanded sample, a procedure which is a problem of difficult inference but which could be verified with the system emulator;

-Improve control and supervisory structures for wind and tidal turbine emulation systems;

-Develop a software simulation, which is partially proved in this thesis. Therefore, an emulation system of a hybrid wind-tidal-electric system, in which turbines are electrically coupled;

-Develop the concept of the emulation system of a hybrid wind-turbine system, where turbines are coupled and decoupled automatically via clutch system;

- Study and develop the concept of electric shaft regime:

If the electromechanical coupling is difficult to achieve from the mechanical point of view and the single shaft decouples are too frequent so high mechanical stress, one can study the electric shaft regime with two DFIG induction machines.

There is a regime in which the ratios between the speeds of the different machines are rigorously constant. The system operates in synchronous mode. Their speeds may differ from their own synchronous speeds.

There is a similar function to that of a single machine where in the rotor circuit you have connected a resistor or an equivalent static converter.

Appendix A

Chapter One: Wind System – Hardware Simulator

Recently, the GREAH laboratory has developed a test bench, to simulate and study experimentally small wind power systems limited to 3kW. Hereafter, the wind turbine simulator is presented, main components of the wind system simulator are:

- A computer that simulates static characteristics of the wind turbine.
- A Dspace card (the DS1102) for real-time control and supervision the simulator automatically.
- A galvanic isolation card to control and protect circuit devices from overvoltage.
- A brushless servomotor, used to reproduce on its shaft the characteristics of a given wind turbine.
- An AC / AC converter integrated in an electronic module called PARVEX DIGIVEX, used to control the rotation speed of the brushless servomotor.
- Permanent Magnets Synchronous Generator PMSG to generate electrical energy.
- Data acquisition card
- An AC / DC converter connected the generator to the continuous bus
- A DC / DC converter connected the DC bus to the data acquisition card
- A powder brake for mechanically loading the servomotor

Components listed above, which are part of the real-time simulator of the wind system, are classified into two systems: the simulator software subsystem of the wind turbine and the hardware subsystem:

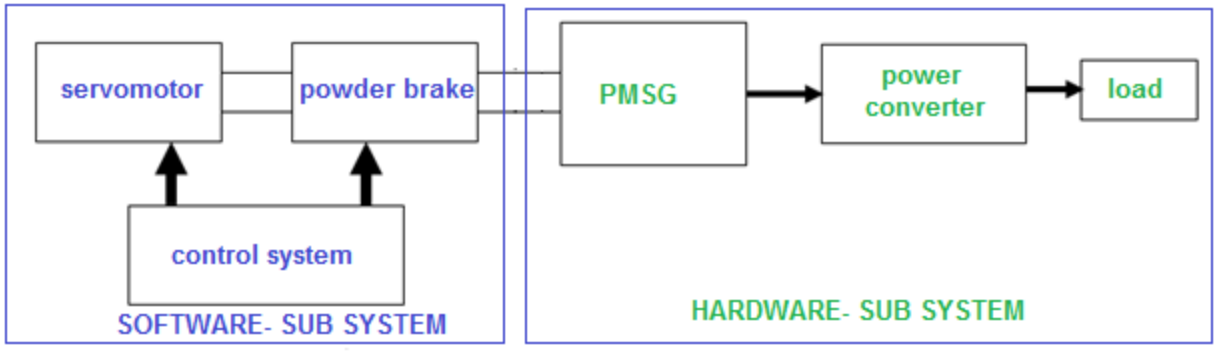

Subdivisions Wind System Simulator

The software subsystem consists of the following elements:

- A **PC** in which software simulation of the wind turbine's characteristic is programmed. Also, the speed set-point values of the servomotor and the torque of the powder brake are calculated and controlled.
- **DSPACE card:** This is the DS1102 card connected directly to the host PC's motherboard through an ISA bus. It serves as a calculator and communication interface between the PC and the rest of the system.

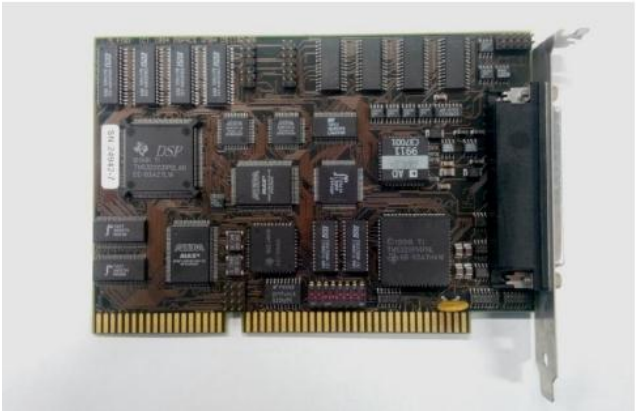

Card dSPACE DS1102

- **Processor:**
  - Texas Instrument TMS 320C31 Floating-point DSP;
  - The frequency - 60 MHz and time cycles of 33.33 ns;
  - 232-bit chip chronometer;
  - A DMA chip
  - 4 interruptive lines.
- **16-bit ADC:**
  - (±) 10 V input voltage;
  - 4 μs conversion time;
  - (±) 5 mV offset voltage;
  - (±) 0.25% error.
- **Memory :**
  - 128K - 32 bits;
  - 2K - 32 bits for each memory part;
- **DAC:**
  - (±) 10 V output voltage;
  - 4 μs adjustment time;
  - (±) 5 mV offset voltage;
  - 5 mA output current.

- **Acquisition and transmission data card:** it is an electronic card allowing communication between the DS1102 card and the control units of the servomotor and the brake. It performs the following functions:
    - Acquisition speed and torque measurements on the powder brake shaft.
    - Acquisition speed measurement on the servomotor shaft.
    - Transmits speed and torque references from Dspace card to the system and vice versa.

Acquisition Card

The hardware subsystem consists of the following elements:

- **A brushless servomotor:** it is a small power asynchronous machine, used as a speed-controlled servomotor whose function is to reproduce on its mechanical shaft, torque-speed characteristic of a given wind turbine.

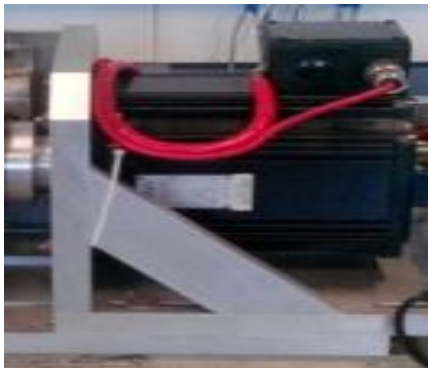

Servomotor

Servomotor characteristics:

Slow turning couple	31	N.m	Mo
Maximum speed	900	Rev./min	N
Continuous supply voltage under load	540	V	U
Steady current slow rotation	7,51	A	I
Pulse current	16	A	Imax.
emf per 1000 rpm (25 ° C) *	546	V	Ke
Electromagnetic torque coefficient	4,13	N.m/A	Kt
Winding resistance (25 ° C) *	5,77	Ω	Rb
Inductance of winding *	97,3	mH	L
Rotor inertia	1200	kg.m².10-5	J
Thermal time constant	55	min	Tth
Motor mass	25,2	kg	M

- **Brushless Permanent Magnetic Synchronous Generator:** It is a brushless synchronous machine with permanent magnets type Alxion 170 FC H1 6-pairs of poles.

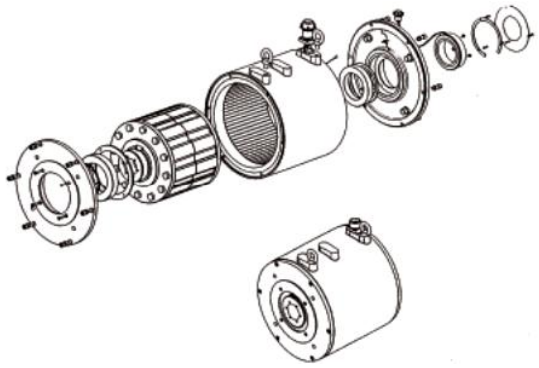

Generator Type Alxion 170 FC H1

Generator characteristics:

Permanent torque locked rotor	Nm	26
Permanent power torque	A	2.9
Maximum torque	Nm	83
Current at maximum torque	A	10.2
Rated speed	$Tr.mn^{-1}$	420
Nominal power	W	1147
Inertia	$Kg.m^2$	0.0136
Mass	Kg	20
Thermal time constant ambient carcass	s	4270
Ambient heat resistance	C^0 /W	0.225
Resistance phase at 20 ° C	Ω	11.68
Inductance phase at nominal I	mH	75.24
Electric time constant	ms	6.4
Emf by vacuum phase at 60 min^{-1}	V	21.6
Number of Poles		12

- **Powder Brake:** it is used to reproduce on its mechanical shaft, a load torque resistant.

  Thus makes it possible to vary operation point of wind system.

Powder Brake

Powder Brake characteristics:

Rated braking torque	25N.m
Rated braking power	1.5kW
Rated speed	570 min^{-1}
Maximum speed: excited	3000 min^{-1}
Maximum speed: not excited	6000 min^{-1}
Moment of mass inertia J	0,92. $10^{-3}Kgm^2$
Residual torque measured (brake not excited)% full scale	2N.m
Current / voltage excitation	2,5/12 A/V
Weight	55 Kg

- **Frequency converter:** it is inserted inside a PARVEX DIGIVEX type box; it enables to control servomotor speed. The static frequency converter is composed of a three-phase bridge rectifier (semiconductor diodes) and a three-phase voltage inverter realized with Insulated Gate Bipolar Transistors (IGBTs) with reverse current diodes. On the DC bus is installed a capacitive filter (the CF filter capacitor) and an ultrafast fuse (SU) or a DC switch. The system is connected to low voltage supply network 380 / 220 V, 50 Hz.

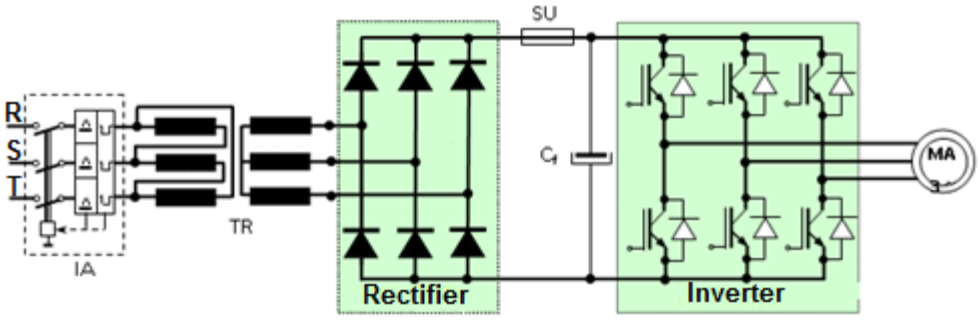

Power Converter

- **Control Unit of Powder Brake:** this device is called Vibro-meter, whose role is to control torque of the powder brake. It offers the possibility to control the powder brake manually or automatically, thanks to a selection button on the front panel.

Front and Back side of Vibre-meter

Appendix B

Doubly-Fed Induction Generator

Nominal Tension U_N	230 V Δ / Y 400 V, 50 Hz
Nominal Courent I_N	4.22 A Δ / 2.44 A Y
Power Factor cosφ	0.63
Apparent Power nominal S_N	1600 VA
Nominal active Power P_N	1000 W
Rotor Tension U_R	130 V
Rotor Courent I_R	5.7 A
Nominale Speed	1385 tour/min
Germany Standard	DIN EN 60034
Dimensions in mm	380 x 235 x 280 (W x H x D)
Weight	23,6 kg

Servo Drive and Brake System

The illustration shows the control unit for the servo drives and brake system mounted to an experimental frame and the servo machine connected to a tested three-phase squirrel-cage induction machine.

The already integrated interface RS232, together with the Windows® compatible software "Servo Machines", allows for an easy operation, data recording and analysis of DC-, AC- and three-phase-machine parameters, as well as a standard characteristic display and archiving on the PC. Besides the known operating functions of the Servo Drive and Brake System, such as speed

control, engine torque control and automatic characteristic recording, the simulation of the gyrating masses is also possible. The moment of inertia can be set up within a large range.

At present, an optional software is being developed. With its aid the Servo Drive and Brake System can simulate the characteristic behavior of different loads, such as working machines e.g. of centrifugal pumps, fans, cranes, compressors, winders, centrifuges etc.

The Control Unit for the Servo Machine

The control unit is used to drive the synchronizing servo machine and to measure the engine speed and torque, as well as the voltage and current of the electrical test machine. The speed and torque are indicated by two 270 degrees circular measuring dials with center neutral positions. A four quadrant monitor with large LEDs is used as an operating status indicator, for operator guidance and to diagnose faults.

The clear design, a digital potentiometer with a push button switch, a tachometric switch and an integrated operational module guarantee simple, intuitive operation of the control unit. Alternatively the operation, measured value indicators and evaluation can be implemented by a PC and the optional software "Servo Machine" (for DC/AC and 3 phase machines). The required inter-face RS232 is already integrated.

Control unit	**100-W class**	**300-W class**	**1000-W class**
Art. no.	**10 05 000**	**10 15 000**	**24 05 000**
Type of construction	Experimental panel	Experimental panel	Portable equipment *
Dimensions in mm (W x H x D)	440 x 297 x 190	440 x 297 x 190	480 x 310 x 315
Mass	11.3 kg	12.9 kg	15.0 kg
Experimental panel available in a table-top house-ing * (equipped at factory)	•	•	–
Color of table unit	RAL 5014, pigeon blue	RAL 5014, pigeon blue	–

Servo Machine

The small compact AC synchronized servo machine for driving, stopping and braking on the ELWE machines, is equipped with an integrated resolver which supplies the precise values of the speed and the rotor bearing. The self-cooling servo machine, which is mounted onto an aluminum profile, supplies the rated load torque over the whole speed range required for the test. It can be connected to the control unit using two multi-wire cables over robust plug-in connections, which are protected against polarity reversal.

Servo machine	**100-W class**	**300-W class**	**1000-W class**
Art. no.	**30 07 001 01**	**30 17 001 01**	**30 27 001 01**
Power output in kW	P_N = 0.54 kW	P_N = 1.8 kW	P_N = 2.6 kW
Speed in rpm	n_N = 4000, n_{max} = 5500	n_N = 4000, n_{max} = 5500	n_N = 2300, n_{max} = 6000
Engine torque in Nm	M_N = 1.3, M_{max} = 2.7	M_N = 4.2, M_{max} = 12.5	M_N = 10.8, M_{max} = 24.4
Current in A	I_N = 1.1	I_N = 3.6	I_N = 5.5
Color	black	black	black
Dimensions in mm (l x w x h)	220 x 210 x 170	305 x 210 x 265	400 x 210 x 300
Mass in kg	5.0	9.2	26.0

Options for the Servo Drive and Brake System

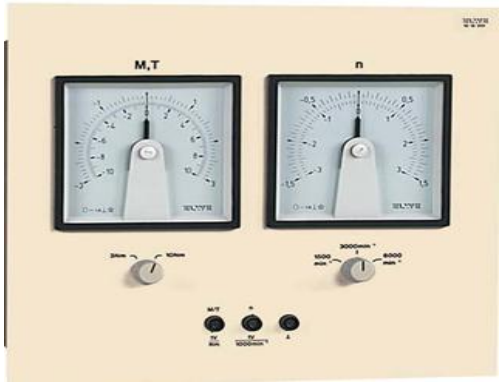

Display panel n, M

The "Display Panel n, M" with its extra-large moving-coil instruments is very suitable for displaying the machine speed and torque to a large group of people, e.g. when demonstrating an experiment. The panel is mounted to the top row of an experimental frame and connected to the 4-mm safety sockets on control unit for the servo machine with 4-mm safety cables. Moving-coil instruments: 270° circular scale, pointer at center position, class 1.5

Display panel n, M	300-W class	1000-W class
Art. no.	**10 15 001**	**10 25 001**
for control unit	10 15 000	24 05 000
Engine torque ranges in Nm	–3 ... 0 ... +3 –10 ... 0 ... +10	–10 ... 0 ... +10 –30 ... 0 ... +30
Speed ranges in rpm	–1500 ... 0 ... + 1500 –3000 ... 0 ... + 3000 –6000 ... 0 ... + 6000	
Dimensions in mm	319 x 297 x 115 (w x h x d)	
Mass	2.0 kg	


31 00 000


31 00 003


31 00 005

Coupling collar **31 00 000**
for all power classes.

Coupling covers
100-W class **31 00 002**
300/1000-W class **31 00 003**

Shaft end cover
100-W class **31 00 004**
300/1000-W class **31 00 005**

Technical data of 8200 vector frequency inverter

Types, mains voltage range and dimensions

Type	Rated power [kW]	Increased rated power [kW]	Supply voltage [V] (45 ... 65 Hz)	Dimensions (H x W x D) [mm]
E82xV251K2C	0.25	0.37	230/240 V 1 x 180 ... 264 V ± 0%	120 x 60 x 140
E82xV371K2C	0.37	–		
E82xV551K2C	0.55	0.75	230/240 V 1 x 180 ... 264 V ± 0% 3 x 100 ... 264 V ± 0%	180 x 60 x 140
E82xV751K2C	0.75	1.1		
E82xV152K2C	1.5	2.2		240 x 60 x 140
E82xV222K2C	2.2	–		
E82xV302K2C	3.0	4.0	230/240 V 3 x 100 ... 264 V ± 0%	240 x 100 x 140
E82xV402K2C	4.0	–		
E82xV552K2C	5.5	7.5		240 x 125 x 140
E82xV752K2C	7.5	–		
E82xV551K4C	0.55	0.75	400/500 V 3 x 320 ... 550 V ± 0%	180 x 60 x 140
E82xV751K4C	0.75	1.1		
E82xV152K4C	1.5	–		240 x 60 x 140
E82xV222K4C	2.2	3.0		
E82xV302K4C	3.0	4.0		240 x 100 x 140
E82xV402K4C	4.0	5.5		
E82xV552K4C	5.5	–		
E82xV752K4C	7.5	11		240 x 125 x 140
E82xV113K4C	11	–		
E82xV153K4B	15	22	400 V 3 x 320 ... 550 V ± 0%	350 x 250 x 250
E82xV223K4B	22	30		
E82xV303K4B	30	37		
E82xV453K4B	45	55		510 x 340 x 285
E82xV553K4B	55	75		591 x 340 x 285
E82xV753K4B	75	90		680 x 450 x 285
E82xV903K4B	90	110		

Functions and features

Degree of protection	IP 20					
Interference suppression limit value classes A and B in accordance with EN55011	Integrated in power range up to 11 kW, optional as compact footprint filter					
Environment temperature range	0 ... +50°C (with power reduction above +40°C)					
Approvals	CE, UL/cUL					
Switching frequencies	2, 4, 8, 16 kHz					
Standard functions	PTC input, PID controller, motor parameter identification and adaptation, 1 programmable relay output, S ramps, level inversion, skip frequencies, fixed speeds, four parameter sets (switchable online), password protection, bipolar setpoint processing, etc.					
Open-loop and closed-loop control methods	vector control, V/f characteristic control (linear, quadratic), torque control					
Drive characteristics	1.8 x M_{rated} (60 s), torque setting range 1:10 for 3 ... 50 Hz, speed setting range 1:50 with M_{rated} (50 Hz), concentricity ± 0.1 Hz					
Function modules		Analog IN	Analog OUT	Digital IN	Digital OUT	Freq. OUT
I/O modules	Standard I/O (PT)	1	1	4*	1	-
	Application I/O (PT)	2	2	6*	2	1
	* With option of 1 frequency input					
Bus modules	INTERBUS PT, PROFIBUS-DP PT, LECOM-B (RS 485) PT, CAN PT (system bus), DeviceNet PT, CANopen PT, AS-Interface PT, CAN-I/O (system bus) PT					
Options	Keypad, LECOM-A/B (RS232/485), LECOM-LI (optical fibre), brake control module, external brake resistor					

Chapters Two and Four: Steady- State Modeling and Analysis

Equations Used for DFIG.

Therefore, firstly, it is necessary to calculate the stator flux amplitude of the machine. By assuming a steady state and a stator flux alignment with the *d*-axis, it is possible to obtain the following set of five equations. From these five exact equations, it is easy to compute the stator flux:

$$\left.\begin{aligned} v_{ds} &= R_s i_{ds} \\ v_{qs} &= R_s i_{qs} + \omega_s \left|\vec{\psi}_s\right| \\ Q_s &= \frac{3}{2}\omega_s |\vec{\psi}_s| i_{ds} \\ T_{em} &= \frac{3}{2} p |\vec{\psi}_s| i_{qs} \\ |\vec{v}_s|^2 &= v_{ds}^2 + v_{qs}^2 \end{aligned}\right\} \Rightarrow |\vec{\psi}_s| = \sqrt{\frac{-B \pm \sqrt{B^2 - 4AC}}{2A}} \Rightarrow \begin{cases} A = {\omega_s}^2 \\ B = \frac{4}{3} R_s T_{em} \omega_s - \left|\vec{v}_s\right|^2 \\ C = \left[\frac{2}{3}\frac{R_s}{L_m}\right]^2 \left[\left(\frac{Q_s}{\omega_s}\right)^2 + \left(\frac{T_{em}}{p}\right)^2\right] \end{cases}$$

In an alternative way, if instead of the *Q*s reference *i*dr = 0 is imposed, minimizing the rotor current; the steady-state computation procedure is slightly modified:

$$\left.\begin{aligned} i_{ds} &= \frac{\left|\vec{\psi}_s\right|}{L_s}, i_{qs} = -\frac{L_m}{L_s} i_{qr} \\ v_{ds} &= R_s i_{ds} \\ v_{qs} &= R_s i_{qs} + \omega_s |\vec{\psi}_s| \\ T_{em} &= -\frac{3}{2} p \frac{L_m}{L_s} |\vec{\psi}_s| i_{qr} \\ |\vec{v}_s|^2 &= v_{ds}^2 + v_{qs}^2 \end{aligned}\right\} \Rightarrow |\vec{\psi}_s| = \sqrt{\frac{-B \pm \sqrt{B^2 - 4AC}}{2A}} \Rightarrow \begin{cases} A = \left(\frac{R_s}{L_s}\right)^2 + \omega_s^2 \\ B = \frac{4}{3}\frac{R_s T_{em} \omega_s}{p} - |\vec{v}_s|^2 \\ C = \left(\frac{2}{3}\frac{R_s T_{em}}{p L_m}\right)^2 \end{cases}$$

Table 1, Procedure to derive the steady-state magnitudes with Qs reference, theses equations were written in MATLAB M-file, to calculate and represent all the necessary magnitudes in steady-state.

Procedure to derive the steady-state magnitudes with Q_s reference

Given grid voltage: ω_s $|\vec{v}_s|$ **Given operating point:** Q_s ω_m T_{em}

Stator flux	$\lvert\vec{\psi}_s\rvert = \sqrt{\frac{-B \pm \sqrt{B^2 - 4AC}}{2A}}$	$C = \left[\frac{2}{3}\frac{R_s}{L_m}\right]^2 \left[\left(\frac{Q_s}{\omega_s}\right)^2 + \left(\frac{T_{em}}{p}\right)^2\right]$	$B = \frac{4}{3} R_s T_{em} \omega_s - \lvert\vec{v}_s\rvert^2$	$A = \omega_s^2$
Stator currents	$i_{ds} = \frac{Q_s}{\frac{3}{2}\omega_s \lvert\vec{\psi}_s\rvert}$	$i_{qs} = \frac{T_{em}}{\frac{3}{2} p \lvert\vec{\psi}_s\rvert}$	$\lvert\vec{i}_s\rvert^2 = i_{ds}^2 + i_{qs}^2$	$\theta_{i_s} = a\tan\left(\frac{i_{qs}}{i_{ds}}\right)$
Rotor currents	$i_{dr} = \frac{\lvert\vec{\psi}_s\rvert - L_s i_{ds}}{L_m}$	$i_{qr} = -\frac{L_s}{L_m} i_{qs}$	$\lvert\vec{i}_r\rvert^2 = i_{dr}^2 + i_{qr}^2$	$\theta_{i_s} = a\tan\left(\frac{i_{qs}}{i_{ds}}\right)$
Stator voltages	$v_{ds} = R_s i_{ds}$	$v_{qs} = R_s i_{qs} + \omega_s \lvert\vec{\psi}_s\rvert$	$\lvert\vec{v}_s\rvert^2 = v_{ds}^2 + v_{qs}^2$	$\theta_{v_s} = a\tan\left(\frac{v_{qs}}{v_{ds}}\right)$
Slip	$\omega_r = \omega_s - \omega_m$		$s = \omega_r / \omega_s$	
Rotor voltages	$v_{dr} = R_r i_{dr} - \omega_r \sigma L_r i_{qr}$	$v_{qr} = R_r i_{qr} + \omega_r \sigma L_r i_{dr} + \omega_r \frac{L_m}{L_s} \lvert\vec{\psi}_s\rvert$	$\lvert\vec{v}_r\rvert^2 = v_{dr}^2 + v_{qr}^2$	$\theta_{v_r} = a\tan\left(\frac{v_{qr}}{v_{dr}}\right)$
Rotor fluxes	$\psi_{dr} = L_m i_{ds} + L_r i_{dr}$	$\psi_{qr} = L_m i_{qs} + L_r i_{qr}$	$\lvert\vec{\psi}_r\rvert^2 = \psi_{dr}^2 + \psi_{qr}^2$	$\theta_{\psi_r} = a\tan\left(\frac{\psi_{qr}}{\psi_{dr}}\right)$
Active powers	$P_m = T_{em}\frac{\omega_m}{p}$	$P_s = \frac{3}{2}(v_{ds} i_{ds} + v_{qs} i_{qs})$	$P_r = \frac{3}{2}(v_{dr} i_{dr} + v_{qr} i_{qr})$	
Reactive powers	$Q_s = \frac{3}{2}(v_{qs} i_{ds} - v_{ds} i_{qs})$	$PF_s = \cos(a\tan(Q_s / P_s))$	$Q_r = \frac{3}{2}(v_{qr} i_{dr} - v_{dr} i_{qr})$	$PF_r = \cos(a\tan(Q_r / P_r))$
Efficiency	$\eta = \frac{P_m}{P_s + P_r}$ if $P_m > 0$		$\eta = \frac{P_s + P_r}{P_m}$ if $P_m < 0$	

Appendix C

Chapter Three: Park Transformer

The PARK transformer is used to pass from three-phase reference to two-phase reference, while the PARK^{-1} transformer is used to reverse the process of transformation from two-phase to three-phase.

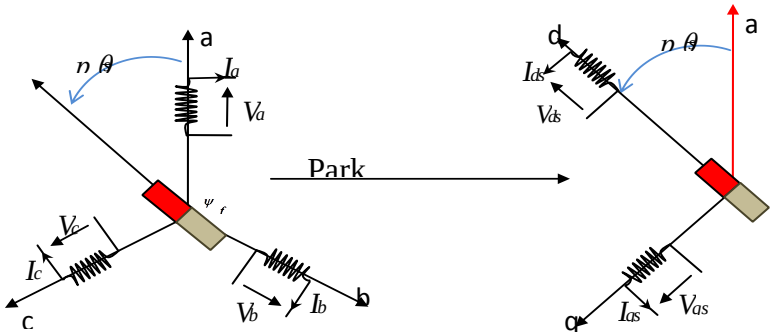

The PARK transform is explained by the equation below:

$$\begin{bmatrix} V_{ds} \\ V_{qs} \end{bmatrix} = [P(\theta_s)] . \begin{bmatrix} V_{as} \\ V_{bs} \\ V_{cs} \end{bmatrix}$$

&

$$\begin{bmatrix} V_{dr} \\ V_{qr} \end{bmatrix} = [P(\theta_r)] . \begin{bmatrix} V_{ar} \\ V_{br} \\ V_{cr} \end{bmatrix}$$

$$[P(\theta_s)] = \begin{bmatrix} \cos(\theta_s) & \cos(\theta_s - \frac{2\pi}{3}) & \cos(\theta_s + \frac{2\pi}{3}) \\ -\sin(\theta_s) & -\sin(\theta_s - \frac{2\pi}{3}) & -\sin(\theta_s + \frac{2\pi}{3}) \end{bmatrix}$$

&

$$[P(\theta_r)] = \begin{bmatrix} \cos(\theta_r) & \cos(\theta_r - \frac{2\pi}{3}) & \cos(\theta_r + \frac{2\pi}{3}) \\ -\sin(\theta_r) & -\sin(\theta_r - \frac{2\pi}{3}) & -\sin(\theta_r + \frac{2\pi}{3}) \end{bmatrix}$$

Where:

θ_s : The phase shift between the stator reference and the rotating reference dq

θ_r : The phase shift between the rotor reference and the rotating reference dq

Chapter Three: PI- Regulator calculations:

A PI regulator has proportional and integral actions. Thus, the transfer function of such a regulator is:

$$Kp + \frac{Ki}{S}$$

With:

kp: Proportional constant

ki: Integral constant

S: Laplace variable

Suppose current need to be regulated such as:

$$i = \frac{V}{R + Ls}$$

With:

V: Supply voltage

R and L: Respectively resistance and inductance

The regulation loop is described as:

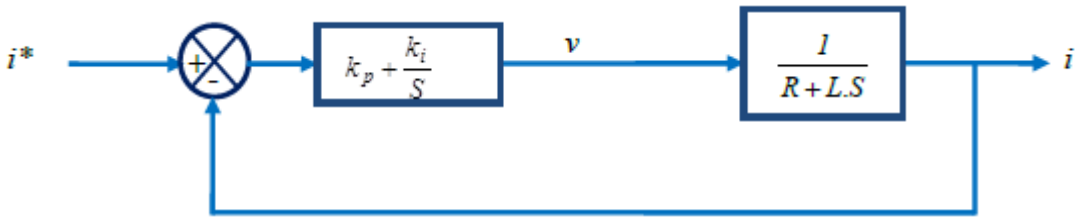

Open loop transfer function is:

$$G_0 = \left[kp + \frac{ki}{S}\right].\left[\frac{1}{R + LS}\right]$$

Closed loop transfer function is:

$$G_C = \frac{\left[kp + \frac{ki}{S}\right].\left[\frac{1}{R + LS}\right]}{1 + \left[kp + \frac{ki}{S}\right].\left[\frac{1}{R + LS}\right]}$$

Multiple and divide the previous expression by:

$$\left[\frac{S}{R + L.S}\right]$$

Then it becomes:

$$G_c = \frac{kp.S + ki}{LS^2 + [R + kp].S + ki}$$

Multiply and divide by $\frac{1}{ki}$ then previous expression becomes:

$$G_o = \frac{\frac{kp}{ki}.S + 1}{\frac{1}{L}S^2 + \left[\frac{R + kp}{ki}\right].S + 1}$$

If filter is used at the input of the system then its transfer function is:

$$\frac{1}{\frac{kp}{ki}S + 1}$$

Then closed loop transfer function becomes:

$$G_c = \frac{1}{\frac{L}{ki}S^2 + \left[\frac{R + kp}{ki}\right]S + 1}$$

It's noticed from the above transfer function that it is a second degree. Indeed, the transfer function of second degree system is written in the following formula:

$$\frac{1}{\frac{1}{\omega_n^2}S^2 + \frac{2.\varepsilon}{\omega_n}.S + 1}$$

With:

ω_n: Natural pulsation

ε: Damping.

By identification, we can determine the parameters of the PI regulator.

$$\frac{L}{ki} = \frac{1}{\omega_n^2} \rightarrow ki = \omega_n^2.L$$

$$\frac{R + kp}{ki} = \frac{2.\varepsilon}{\omega_n} \rightarrow kp = \frac{2.\varepsilon}{\omega_n}.ki - R \rightarrow kp = 2.\varepsilon.\omega_n.L - R$$

We considered:

$$\omega_n = \frac{2.\pi}{T} \text{ Where} \leq \frac{\tau}{10} \text{ ; with } \tau = \frac{L}{R}$$

$$\varepsilon = 0.707$$

Appendix D

Sampling every 5 minutes:

The average wind speed is calculated using samples taken every 5 min from the original wind profile. Thus, obtain a new wind profile of 60 samples; the simulation is therefore carried out on 60 samples and no more on 18000:

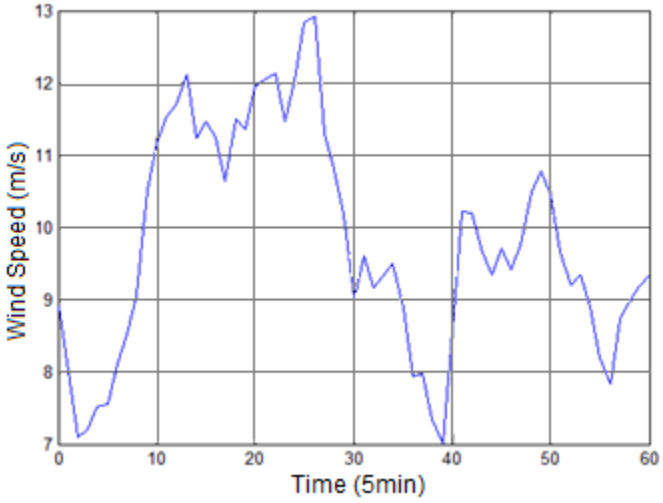

Wind Profile Every 5 Minutes

As before, noted here that the time interval is 5 minutes, and the wind profile is much smoother than the previous one. This corresponds to the reference rotational speed variation below:

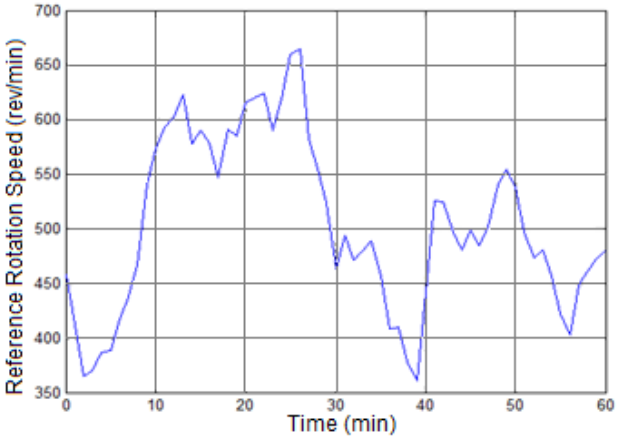

Reference Rotation Speed Every 5 Minutes

The average reference rotational speed is Nmoy_5min = 504rpm.

Time-acceleration simulation every 5 minutes instead of every second produces an average speed of rotation with a difference of only 0.2% of that calculated in non-accelerated time simulation. The error increased slightly compared to the simulation with sampling every minute; however, this error remains very low.

Hereafter, we observe the variation of the wind turbine power:

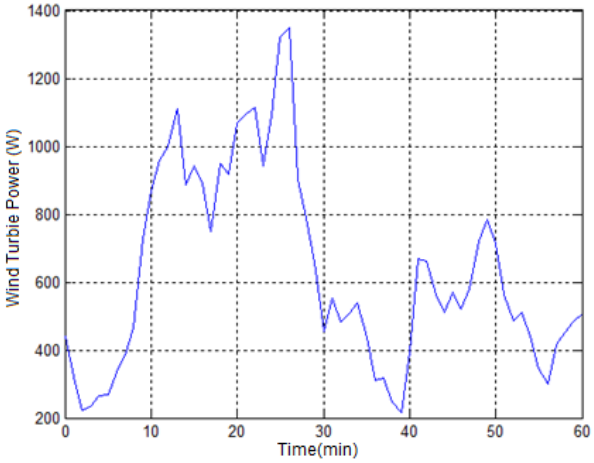

Wind Turbine Mechanical Power

It can be seen from the figure above, that the maximum power achieved by the turbine is decreased. With sampling every minute, we had powers that are close to 1800W whereas at present, the highest power does not reach 1400W. The average power of the turbine for this type of simulation is Pmoy_5min = 631.6W. This average power has a difference of about 3.5% with that calculated in non-accelerated time simulation.

It is therefore found that, the more the number of samples is reduced, the more the error on the power as on the speed of rotation increases. This can be explained by the fact that, the influence of turbulence components of the wind speed decreases with the number of samples taken for the simulation. Their effects are therefore much more felt for much smaller sampling periods.

We will confirm this observation by conducting a new sampling every 10min:

Sampling Every 10 minutes:

As before, we calculate the average wind speed every 10 min from the original wind profile. We obtain a new wind profile of 30 samples; the simulation is therefore performed on 30 samples and no longer on 18000:

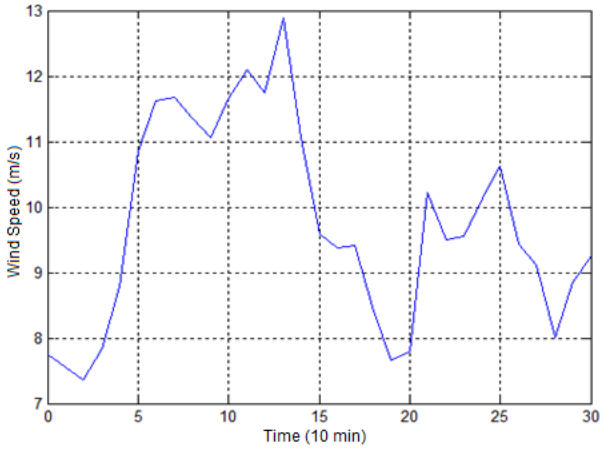

Wind Profile Sampling Every 10 minutes

As before, note here that the sampling time is in 10 minutes and not in seconds, and the profile of the wind is much smoother than the previous one. This corresponds to the reference rotational speed variation below:

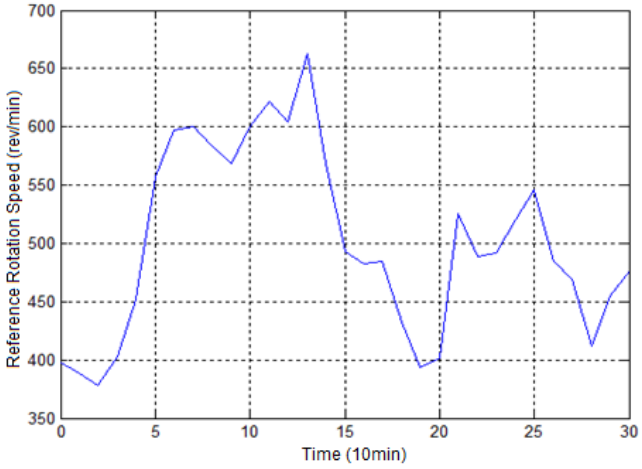

Reference Rotation Speed Sampling Every 10 minutes

The average rotational speed of reference is Nmoy_10min = 501rpm.

Time-acceleration simulation every 10 minutes instead of every second produces an average speed of rotation with a difference of 0.8% from that calculated in non-accelerated time simulation. The error went from 0.2% every 5 minutes to 0.8% every 10 minutes; even if it remains it is very weak, it is only a 4-times increase in the error, which is not a very good approximation.

Below we observe the variation of the power of the wind turbine:

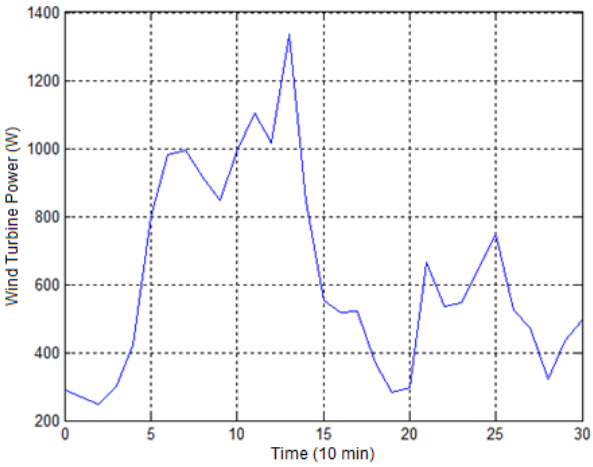

Wind Turbine Mechanical Power

The average power of the turbine for this type of simulation is Pmoy_10min = 622W. As we mentioned above, this average power has a difference of about 5% with that calculated in non-accelerated time simulation. Thus more we reduce the number of samples for the simulation, and the more we lose precision in the results obtained.